



HAL
open science

Involvement of dorsomedial prefrontal projections pathways to the basolateral amygdala and ventrolateral periaqueductal grey matter in conditioned fear expression

Fabrice Chaudun

► **To cite this version:**

Fabrice Chaudun. Involvement of dorsomedial prefrontal projections pathways to the basolateral amygdala and ventrolateral periaqueductal grey matter in conditioned fear expression. *Neurons and Cognition [q-bio.NC]*. Université de Bordeaux, 2016. English. NNT : 2016BORD0118 . tel-01412296

HAL Id: tel-01412296

<https://theses.hal.science/tel-01412296>

Submitted on 8 Dec 2016

HAL is a multi-disciplinary open access archive for the deposit and dissemination of scientific research documents, whether they are published or not. The documents may come from teaching and research institutions in France or abroad, or from public or private research centers.

L'archive ouverte pluridisciplinaire **HAL**, est destinée au dépôt et à la diffusion de documents scientifiques de niveau recherche, publiés ou non, émanant des établissements d'enseignement et de recherche français ou étrangers, des laboratoires publics ou privés.

THÈSE PRÉSENTÉE

POUR OBTENIR LE GRADE DE

**DOCTEUR DE
L'UNIVERSITÉ DE BORDEAUX**

Ecole doctorale
Mention : **Sciences, Technologie, Santé**
Option : **Neurosciences**

Par FABRICE CHAUDUN

**Implication des voies de projection du
cortex préfrontal dorso-médian vers
l'amygdale et la substance grise
periaqueducale dans l'expression des
réponses conditionnées de peur**

Soutenue le *27 septembre 2016*

Membres du Jury

M. Georges Di Scala (DR-CNRS Bordeaux)	Président
Mme Thérèse Jay (DR-INSERM Paris)	Rapporteur
Mme. Nadine Ravel (CR-CNRS Lyon)	Rapporteur
M. Yann Humeau (CR-CNRS Bordeaux).....	Membre invité
M. Sidney Wiener (DR-CNRS Paris)	Examinateur
M. François Georges (DR-CNRS Bordeaux).....	Examinateur
M. Cyril Herry (DR-INSERM Bordeaux).....	Directeur de thèse

THÈSE PRÉSENTÉE

POUR OBTENIR LE GRADE DE

**DOCTEUR DE
L'UNIVERSITÉ DE BORDEAUX**

Ecole doctorale
Mention : **Sciences, Technologie, Santé**
Option : **Neurosciences**

Par FABRICE CHAUDUN

**Involvement of dorsomedial prefrontal
projections pathways to the basolateral
amygdala and ventrolateral
periaqueductal grey matter in
conditioned fear expression**

Soutenue le *27 septembre 2016*

Membres du Jury

M. Georges Di Scala (DR-CNRS Bordeaux)	Président
Mme Thérèse Jay (DR-INSERM Paris)	Rapporteur
Mme. Nadine Ravel (CR-CNRS Lyon)	Rapporteur
M. Yann Humeau (CR-CNRS Bordeaux).....	Membre invité
M. Sidney Wiener (DR-CNRS Paris)	Examineur
M. François Georges (DR-CNRS Bordeaux).....	Examineur
M. Cyril Herry (DR-INSERM Bordeaux).....	Directeur de thèse

Remerciements

L'ensemble des travaux de thèse présenté dans ce manuscrit a été réalisé au sein du Neurocentre Magendie, dans le laboratoire INSERM U1215 du docteur Pier-Vincenzo Piazza sous la direction du docteur Cyril Herry.

Je tiens à commencer ces remerciements en exprimant toute ma gratitude à Cyril Herry. Tout d'abord je souhaite te remercier de m'avoir ouvert les portes de ton laboratoire à mon arrivé en master 1, de m'avoir formé minutieusement pour finalement m'avoir donné la chance de réaliser cette thèse au sein de ton équipe. Je te remercie pour ta grande disponibilité et pour l'autonomie que tu m'as accordée au cours de ces 4 années de thèse. Travailler dans ton équipe m'a permis de bénéficier de tes qualités scientifiques et humaines que j'espère arriver à retranscrire dans ma future carrière avec autant d'enthousiasme. Je te remercie de m'avoir permis de confirmer mon intérêt pour la recherche et surtout ma passion pour l'électrophysiologie qui sans nul doute me suivra tout au long de ma carrière. Travailler avec toi a été un plaisir immense et j'espère que nos relations perdureront.

Je remercie également le docteur Pier-Vincenzo Piazza de m'avoir accueilli au sein de l'institut qui est un lieu propice à l'élaboration de thèses.

Je voudrais également remercier l'ensemble des membres du jury. Tout d'abord les docteurs Thérèse Jay et Nadine Ravell, pour avoir accepté la tâche d'évaluer mon manuscrit. Je remercie aussi les docteurs François Georges, Sidney Wiener et Yann Humeau qui ont bien voulu examiner mon travail. Enfin, je remercie le docteur Georges Di Scala pour avoir accepté de présider ce jury.

Je tiens à remercier l'ensemble des membres de l'équipe, tant pour leurs qualités personnelles que scientifiques, qui au cours de longues discussions animées lors de l'élaboration de ces travaux ont contribué à l'avancement de ces projets et à leurs publications dans des journaux de hautes qualités. Enfin je remercie tout particulièrement Julien, Sophie, Robert, Helene, Nikolas, Cyril, Suzana et Thomas pour leur aide qui ont permis de publier ces recherches.

Je remercie les docteurs Andreas Lüthi et Philippe Tovote de m'avoir proposé de collaborer avec eux. Cette collaboration fructueuse m'a appris l'importance de ne jamais baisser les bras face aux difficultés expérimentales.

Je remercie l'ensemble des membres de l'institut François Magendie qui ont participés de près ou de loin à la réalisation de ces travaux de thèse.

Bien sûr, comme tout étudiant en thèse, j'ai aussi eu une vie en dehors du laboratoire. Merci à tous les amis du master neurosciences, tous les amis bordelais, néo-bordelais ou ex-bordelais, pour tous ces moments mémorables ou plus difficiles passés ensemble qui ont fortement contribué à l'accomplissement de ma thèse. En espérant passer encore de bon moment avec vous, Briçou, Ade, Malo, Julie, Julien, Sarah, Wilou, l'Ours, Didine, Hélène, Cédric, Mathias, Mr Marich, Lolo et tous ceux que j'oublie.

Ces remerciements seraient incomplets si je n'en adressais pas à l'ensemble des membres de ma famille, et mes parents en particulier, pour m'avoir poussé et donné les moyens de réussir, et de m'avoir toujours encouragé dans tous mes projets. Merci également à mon frère, Jérémie, et sa famille de m'avoir toujours soutenue et d'avoir répondu présent à chaque moment important de ma thèse. Je tiens à vous dédier ce travail qui, je l'espère vous rendra fiers.

RÉSUMÉ

A l'heure actuelle, une des principales questions des neurosciences comportementales est de comprendre les bases neurales des apprentissages et de comprendre comment des modifications au sein de circuits neuronaux spécifiques contrôlent les changements comportementaux liés à une expérience particulière. De nombreuses études ont récemment mis en évidence le rôle important des circuits neuronaux dans les phénomènes d'apprentissages associatifs, et notamment dans la régulation des comportements de peur. Cependant, leurs caractéristiques anatomiques et fonctionnelles restent encore largement inconnues. L'une des principales fonctions des circuits neuronaux est leur capacité à adapter le comportement en fonction de la nature des informations internes ou environnementales disponibles. Malgré de nombreux progrès réalisés sur la compréhension des substrats et mécanismes neuronaux sous-tendant le conditionnement de peur au sein de structures telles que l'amygdale (AMG), le cortex préfrontal dorso-médian (dmPFC) et la substance grise periaqueducale (PAG), les mécanismes neuronaux gouvernant les interactions inter-structure ainsi que le contrôle local de ces différents circuits neuronaux restent encore largement inconnus. Dans ce contexte, ce travail de thèse a eu pour objectifs principaux, d'évaluer la contribution des voies de projections dmPFC-BLA et dmPFC-vIPAG dans la régulation des comportements de peur, et, d'identifier les mécanismes neuronaux sous-jacents contrôlant l'expression de la peur. Afin de répondre à ces questions, nous avons utilisé conjointement des enregistrements électrophysiologiques unitaires et de potentiels de champs couplés à des approches optogénétiques au cours de l'expression de la peur conditionnée. Nous avons pu mettre en évidence un nouveau mécanisme neuronal basé sur une oscillation cérébrale à 4 Hz entre le dmPFC et le BLA impliqué dans la synchronisation neuronale des neurones de ces deux structures nécessaire à l'expression de la peur. Nous avons aussi démontré que le dmPFC via ses projections sur le vIPAG contrôle directement l'expression de la peur. Ensemble, nos données contribuent à une meilleure compréhension des circuits neuronaux ainsi que des mécanismes du comportement de peur qui dans le futur pourront aider à une amélioration thérapeutique des troubles anxieux.

Mots clés : Electrophysiologie unitaire in vivo, comportement auditif de peur, optogénétique, oscillation cérébrale.

ABSTRACT

A central endeavour of modern neuroscience is to understand the neural basis of learning and how the selection of dedicated circuits modulates experience-dependent changes in behaviour. Decades of research allowed a global understanding of the computations occurring in hard-wired networks during associative learning, in particular fear behaviour. However, brain functions are not only derived from hard-wired circuits, but also depend on modulation of circuit function. It is therefore realistic to consider that brain areas contain multiple potential circuits which selection is based on environmental context and internal state. Whereas the role of entire brain areas such as the amygdala (AMG), the dorsal medial prefrontal cortex (dmPFC) or the periaqueductal grey matter (PAG) in fear behaviour is reasonably well understood at the molecular and synaptic levels, there is a big gap in our knowledge of how fear behaviour is controlled at the level of defined circuits within these brain areas. More particularly, whereas the dmPFC densely projects to both the basolateral amygdala (BLA) and PAG, the contributions of these two projection pathways during fear behaviour are largely unknown. Beside the involvement of these neuronal pathways in the transmission of fear related-information, the neuronal mechanisms involved in the encoding of fear behaviour within these pathways are also virtually unknown. In this context, the present thesis work had two main objectives. First, evaluate the contribution of the dmPFC-BLA and dmPFC-vIPAG pathways in the regulation of fear behaviour, and second, identify the neuronal mechanisms controlling fear expression in these circuits. To achieve these goals, we used a combination of single unit and local field potential recordings coupled to optogenetic approaches in behaving animals submitted to a discriminative fear conditioning paradigm. Our results first, identified a novel neuronal mechanism of fear expression based on the development of 4 Hz oscillations within dmPFC-BLA circuits that determine the dynamics of freezing behaviour and allows the long-range synchronization of firing activities to drive fear behaviour. Secondly, our results identified the precise circuitry at the level of the dmPFC and vIPAG that causally regulate fear behaviour. Together these data provide important insights into the neuronal circuits and mechanisms of fear behaviour. Ultimately these findings will eventually lead to a refinement of actual therapeutic strategies for pathological conditions such as anxiety disorders.

Keywords : In vivo single unit recording, auditory fear conditioning behaviour, optogenetic, cerebral oscillation.

RÉSUMÉ DE LA THESE

L'identification des mécanismes neuronaux permettant le contrôle des comportements représente un des challenges les plus importants de la recherche en neurosciences. L'une des principales fonctions du cerveau est sa capacité à adapter le comportement en fonction de la nature des informations internes ou environnementales disponibles. Cette fonction est en partie soutenue par des processus d'apprentissage et de mémoire. Alors que les mécanismes cellulaires et moléculaires soutenant ces processus sont désormais relativement bien décrits, l'implication des circuits neuronaux et des éléments cellulaires contrôlant l'activité neuronale au cours de l'apprentissage et de la mémoire restent largement inconnus.

Au cours de ces dernières années, un des modèles comportementaux les plus utilisés afin d'élucider les bases neurales de ces apprentissages a été une forme particulière du conditionnement Pavlovien, le conditionnement auditif de peur. Ce paradigme consiste à associer de façon répétitive un son (le stimulus conditionnel, SC) à un choc électrique périphérique léger (le stimulus inconditionnel, SI). A la suite du conditionnement, la réexposition des animaux au SC présenté de manière isolé induit un ensemble de modifications comportementales et neurovégétatives (réponses conditionnées), et en particulier une réaction d'arrêt comportemental (réponse émotionnelle conditionnée d'immobilisation ou « freezing ») aisément quantifiable. A la suite du conditionnement auditif de peur, la présentation répétée du SC en l'absence du SI induit une diminution progressive des réponses conditionnées de peur, un phénomène appelé extinction de la peur (Myers and Davis, 2007). L'extinction résulterait de la mise en place d'un nouvel apprentissage au cours duquel les animaux apprennent que le SC n'est plus renforcé, ce qui inhiberait l'apprentissage initial du conditionnement de peur sans l'effacer (Konorski, 1967). L'apprentissage de l'extinction peut conduire à la formation d'une mémoire d'extinction à court et long-terme dont le rappel dépend du contexte dans lequel la procédure d'extinction a eu lieu (Bouton et al., 2006). A la suite de l'extinction, les réponses conditionnées de peur peuvent réapparaître avec le simple passage du temps (« spontaneous recovery ») (Brooks and Bouton, 1993, Quirk, 2002), un changement de contexte («renewal ») (Bouton et al., 2006), ou une réexposition au SI («reinstatement») (Rescorla and Heth, 1975). Au cours de ces dernières années, un nombre important d'études ont amélioré notre compréhension des circuits neuronaux impliqués dans le comportement de peur. Ces travaux ont notamment mis en lumière

l'implication d'un circuit tripartite composé de l'amygdale (AMG), du cortex préfrontal médial (mPFC) et de la substance grise periaqueducule (PAG).

L'AMG, structure du lobe temporal médian, joue un rôle critique dans l'acquisition, l'expression et l'extinction des mémoires associatives de peur (Davis, 1992, LeDoux, 2000, Maren, 2001, Pape and Pare, 2010). L'AMG comprend plusieurs noyaux anatomiquement et fonctionnellement distincts dont les noyaux latéral (LA), basal (BA) (l'ensemble formant le complexe basolatérale de l'amygdale (BLA)) et central (CEA). Au cours du conditionnement de peur, le LA et le CEA sont considérés comme étant les sites privilégiés où se mettent en place les phénomènes de plasticité neuronale qui sous-tendent l'acquisition du conditionnement (Rogan et al., 1997, Rodrigues et al., 2004, Wilensky et al., 2006, Ciochi et al., 2010). A la suite de l'acquisition de la peur, de nombreuses données indiquent que les processus d'apprentissage de l'extinction impliquent le BLA et que les réponses de peur conditionnées sont contrôlées par les circuits du CEA (Veening et al., 1984, Holstege, 1992, Sotres-Bayon et al., 2007, Herry et al., 2008).

Bien que la plupart des recherches se soient focalisées sur le rôle joué par les circuits neuronaux de l'AMG dans le comportement de peur, certaines études ont également mis en évidence le rôle essentiel du mPFC dans la régulation des mémoires de peur (Quirk and Mueller, 2008, Herry et al., 2010, Sotres-Bayon and Quirk, 2010). Le mPFC situé dans le lobe frontal, est composé, du cortex antérieur cingulaire (ACC), de l'aire prelimbic (PL) et de l'aire infralimbic (IL). Il a été montré que le mPFC est impliqué dans les phases de consolidation de l'apprentissage de l'extinction et d'expression des mémoires de peur et d'extinction (Sotres-Bayon and Quirk, 2010, Courtin et al., 2013, Dejean et al., 2015). En dépit de ces nombreux progrès, les caractéristiques anatomiques et fonctionnelles du mPFC qui sous-tendent les comportements de peur restent largement inconnus. D'un point de vue anatomique, le dmPFC projette sur de nombreuses structures clés impliquées dans la régulation des comportements de peur, en particulier le BLA, mais également le PAG (Floyd et al., 2000, Gabbott et al., 2005). Cette dernière, situé au niveau du mésencéphale et composé de différentes colonnes fonctionnelles, en particulier les colonnes dorso-latérales et latérales du PAG (dlPAG et lPAG) impliquées dans les réponses de fuite comportementales mais aussi les colonnes ventro-latérales du PAG (vlPAG) impliquées dans la genèse du freezing. Bien que, le mPFC projette sur l'AMG et le vlPAG, le rôle fonctionnel de ces deux voies de projections pendant les comportements de peur reste encore

largement inexploré. Dans ce contexte, mon travail de thèse a consisté à identifier l'implication fonctionnelle des voies de projection dmPFC-BLA et dmPFC-vIPAG au cours de l'expression des réponses conditionnées de peur, mais aussi d'identifier les mécanismes neuronaux sous-jacents au sein de ces circuits permettant l'expression des réponses de peur. Afin de répondre à ces questions, nous avons utilisé conjointement des enregistrements électrophysiologiques unitaires et de potentiels de champs couplés à des approches optogénétiques au cours de l'expression de la peur conditionnée chez l'animal vigile.

Résultats

1^{er} partie : Rôle de l'oscillation corticale à 4 Hz et de la synchronisation des circuits du mPFC et AMG au cours de l'expression des réponses conditionnées de peur.

Dans la première partie de ma thèse, nous avons démontré pour la première fois que la réponse d'immobilisation comportementale post-conditionnement, plus communément appelé freezing, était étroitement associée à un état particulier interne de l'animal se manifestant sous la forme d'une oscillation cérébrale au rythme 4 Hz au sein des circuits du mPFC et de l'AMG. De plus, nous avons démontré que cet état neuronal pouvait prédire avec précision le début et la fin du freezing. En utilisant des enregistrements unitaires effectués simultanément dans l'AMG et le dmPFC (cortex préfrontal dorso-médial) chez l'animal vigile exprimant des réponses conditionnées de peur, nous avons démontré que cette oscillation particulière permettait une synchronisation à longue distance des circuits amygdaliens et préfrontaux. De plus, des analyses de cohérence entre l'oscillation à 4 Hz enregistrée au niveau de l'AMG et du mPFC, ont révélé que l'oscillation au niveau du mPFC précédait celle de l'AMG démontrant la directionnalité de ce mécanisme. Enfin, en utilisant des approches optogénétiques nous avons démontré que l'induction artificielle d'une oscillation à 4 Hz dans le dmPFC était suffisante pour induire du freezing, mais aussi, aboutissait à la formation d'une mémoire de peur à long terme.

Dans leur ensemble, ces résultats ont mis en évidence l'existence d'une signature physiologique de la mémoire de peur au sein des circuits du mPFC et AMG. De plus ils suggèrent que le blocage de l'oscillation 4 Hz dans ces circuits pourrait être une cible thérapeutique potentielle des troubles anxieux.

2^{ème} partie : Rôle fonctionnel des neurones du dmPFC projetant sur le vlPAG

Au cours de la deuxième partie de ce travail doctoral, nous avons identifié le profil de décharge des neurones du dmPFC projetant sur le vlPAG au cours de l'expression de la peur conditionnée. Pour cela, nous avons réalisé des enregistrements électrophysiologiques unitaires au niveau du dmPFC couplés à des identifications par stimulations électriques ou par stimulations optogénétiques des neurones du dmPFC projetant sur le vlPAG chez des animaux soumis à une procédure de conditionnement auditif de peur. Nous avons pu mettre en évidence que 24 heures à la suite du conditionnement, les neurones du dmPFC projetant sur le vlPAG présentaient une augmentation de leurs activités au cours de l'expression des réponses conditionnées de peur. Nous avons par la suite manipulé optogénétiquement l'activité des neurones du dmPFC projetant sur le vlPAG afin d'établir un lien de causalité entre les modifications d'activité de ces neurones et l'expression de la peur conditionnée. Nous avons démontré que le blocage de l'activation évoquée par le freezing des neurones du dmPFC projetant sur le vlPAG au cours de l'expression de la peur conditionnée par une inhibition optique était suffisant pour diminuer partiellement l'expression des réponses conditionnées de peur. Finalement, grâce à des approches novatrices de marquage par virus rabique trans-synaptique, nous avons démontré que les neurones du dmPFC projetant sur le vlPAG étaient localement régulés par deux types d'INs, les neurones exprimant la parvalbumine et la somatostatine. De plus l'enregistrement unitaires de ces deux sous populations, montrent que ces neurones présentent une diminution de leur activité au cours du freezing, un patron de décharge inverse à celui observé pour les neurones du dmPFC projetant sur le vlPAG. L'ensemble ces données démontre l'implication d'un microcircuit désinhibiteur au niveau du mPFC au cours des réponses de peur, même si le rôle causal de ce microcircuit dans l'expression des réponses conditionnées de peur nécessitera des expériences complémentaires.

Nos données suggèrent que le dmPFC via ses projections sur le vlPAG contrôle directement l'expression de la peur conditionnée. Cependant, l'inhibition partielle des réponses conditionnées de peur suite à la manipulation optogénétique suggère également le recrutement simultané d'autres circuits pour l'expression des réponses conditionnées de peur.

3^{ème} partie : Rôle de la substance grise periaqueducale au cours de l'expression des réponses conditionnées de peur.

Finally, in collaboration with the group of Dr. Andreas Lüthi, in Basel, Switzerland, we have shown in the periaqueductal gray (PAG) the existence of a microcircuit disinhibitory under the control of the central AMG allowing the direct regulation of motor centers involved in the execution of freezing. In fact, we have shown that the GABAergic projection neurons of the central AMG project onto the GABAergic neurons in the vPAG inducing a disinhibition of the glutamatergic neurons projecting to the ventral horn of the spinal cord. My contribution in this work was to determine what were the electrophysiological and functional characteristics of the neurons in the vPAG during the expression of fear-conditioned responses. For this, we performed single-unit electrophysiological recordings in mice subjected to a reminder of the fear-conditioned 24 hours after conditioning. These recordings allowed us to demonstrate the existence of two neuronal populations functionally distinct showing opposite modulations of their activity during freezing.

Conclusion

During my doctoral work, we were able to show that the projections dmPFC-BLA and dmPFC-vPAG could control independently the freezing behavior even though the manipulation of these pathways by optogenetics induced moderate modifications of the freezing behavior suggesting a possible cooperation within these circuits for the expression of fear-conditioned responses. In addition, we have elucidated a neuronal mechanism at the level of the mPFC allowing the acquisition and expression of the memory of fear-conditioned, but also the neuronal synchronization of two distant structures which are the AMG and the mPFC. Further studies will be necessary in order to understand how these circuits interact at the level of the vPAG, even though preliminary data in the laboratory suggest that the neurons of the dmPFC projecting onto the vPAG would preferentially contact the glutamatergic neurons of the vPAG (**Figure 1**). In addition, it would be interesting to understand which subpopulations of neurons in the mPFC are synchronized by the 4 Hz oscillation.

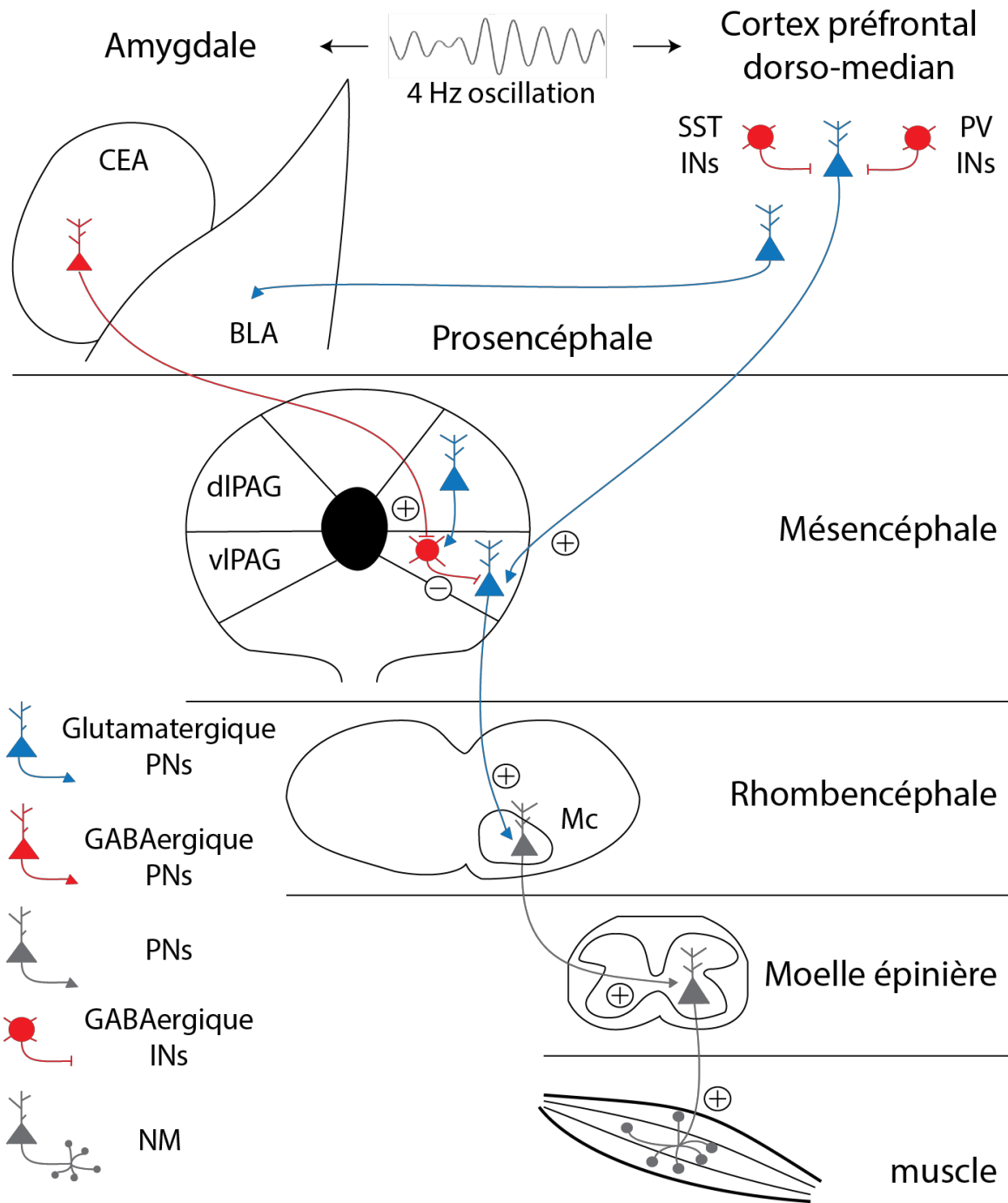


Figure 1: Schéma récapitulatif de l'interaction existant entre l'amygdale (AMG), le cortex préfrontal dorso-médian (dmPFC) et la substance grise periaqueducule (PAG). CEA : amygdale centrale, BLA : amygdale basolatérale, PV : parvalbumine, SST, somatostatine, dlPAG : dorso-latérale PAG, vlPAG : ventro-latéral PAG, NM : Moto-neurones.

TABLE OF CONTENTS

INTRODUCTION.....	1
I/ AMYGDALA IN CONDITIONED FEAR BEHAVIOUR	3
A/ GROSS ANATOMY OF THE RODENT AMYGDALA.....	4
a/ <i>Neuronal elements of the rodent amygdala</i>	4
b/ <i>Extrinsic connectivity of the amygdala</i>	5
B/ FUNCTIONAL ROLE OF THE AMYGDALA IN FEAR BEHAVIOUR.....	8
a/ <i>Role of the amygdala in the acquisition of auditory fear conditioning</i>	8
b/ <i>Role of the amygdala in fear expression and extinction learning</i>	12
II/ ROLE OF MEDIAL PREFRONTAL CORTEX CIRCUITS IN FEAR BEHAVIOUR	14
A/ GROSS ANATOMY OF THE MPFC.....	14
a/ <i>Neuronal elements</i>	14
b/ <i>Connectivity with other structures</i>	18
B/ ROLE OF THE MPFC IN CONDITIONED FEAR BEHAVIOUR.....	19
a/ <i>Involvement of the mPFC in fear behaviour</i>	19
i/ Lesional studies.....	19
ii/ Pharmacological studies.....	20
iii/ Immediate early gene expression studies	21
b/ <i>Modulation of fear behaviour in mPFC circuits</i>	22
c/ <i>Neuronal encoding of fear behaviour in the mPFC</i>	24
C/ NEURONAL MECHANISMS OF FEAR BEHAVIOUR IN PREFRONTAL-AMYGDALA CIRCUITS.....	25
III/ THE PERIAQUEDUCTAL GRAY MATTER: AN INTERFACE BETWEEN CORTICAL AND MOTOR FUNCTION	28
A/ GROSS ANATOMY OF THE PERIAQUEDUCTAL GREY MATTER	29
a/ <i>Neuronal elements</i>	29
b/ <i>Inputs and outputs of the PAG</i>	30
i/ Ascending pathway	30
ii/ Descending pathway	31
B/ FUNCTIONAL ROLE OF THE PAG IN FEAR BEHAVIOUR	32
a/ <i>Involvement of the PAG in fear behaviour:</i>	33
i/ Lesional and pharmacological studies:.....	33
ii/ Immunohistochemical studies:	34
iii/ Electrophysiological studies.....	35
iv/ PAG mechanisms for the encoding of fear and extinction memories.....	36
AIM OF THE THESIS:.....	38

MATERIAL AND METHOD:	39
I/ ANIMAL	39
II/ BEHAVIOURAL PARADIGM AND PROTOCOL:	39
A/ BEHAVIOURAL PARADIGM USED DURING SINGLE UNIT RECORDINGS:	39
B/ OPTOGENETIC MANIPULATIONS:	41
C/ PHARMACOLOGICAL EXPERIMENTS:	41
III/ SURGERY AND RECORDING	42
IV/ SINGLE UNIT ANALYSIS	43
V/ FIELD POTENTIAL ANALYSIS	46
VI/ PHASE LOCKING	49
VII/ VIRUS INJECTIONS AND OPTOGENETICS	50
VIII/ ANATOMICAL ANALYSIS	52
IX/ EXTRACELLULAR STIMULATION	53
X/ STATISTICAL ANALYSIS	54
RESULTS:	56
I/ 4 HZ OSCILLATIONS SYNCHRONIZED PREFRONTAL-AMYGDALA CIRCUITS DURING FEAR BEHAVIOUR.	56
II/ PREFRONTAL-MIDBRAIN CIRCUITS CONTROL FEAR EXPRESSION	61
III/ PERIAQUEDUCTAL GRAY MATTER CIRCUITS INVOLVED IN DEFENSIVE BEHAVIOUR. ..	69
GENERAL DISCUSSION:	71
PUBLICATIONS AND COMMUNICATIONS:	76
REFERENCES:	77

LIST OF ABBREVIATIONS:

ACC	Anterior cingulate cortex
AB	Accessory basal nucleus
AHN	Anterior hypothalamic nucleus
AMG	Amygdala
BA	Basal amygdala
BLA	Basolateral amygdala
BNST	Basal nucleus of the stria terminalis
CB	Calbindin
CCK	Cholecystokinin
CEA	Central amygdala
CEl	Lateral central amygdala
CEm	Medial central amygdala
CS	Conditioned stimulus
CR	Calretinin
dHPC	Dorsal hippocampus
DMH	Dorsomedial hypothalamus
dPAG	Dorsal periaqueductal grey
dmPFC	Dorsomedial prefrontal cortex (including ACC and PL)
dIPAG	Dorso-lateral periaqueductal grey
FC	Fear conditioning
GABA	Gamma aminobutyric acid
HB	Habituation
HPC	Hippocampus
IEG	Immediate early genes
IL	Infralimbic cortex
IN	Interneuron
ITC	Intercalated cells
LA	Lateral amygdala
LFP	Local field potential
IPAG	Lateral periaqueductal grey

LTP	Long term potentiation
mPFC	Medial prefrontal cortex
MD	Mediodorsal nucleus of the thalamus
NMDA	<i>N</i> -methyl-D-aspartate
MOR	Mu-opioid receptor
NPY	Neuropeptide Y
NR	Nucleus reuniens
MS	Medial septum
PAG	Periaqueductal grey matter
PFC	Prefrontal cortex
PN	Projection neuron
PMD	Premammillary dorsal nucleus
PL	Prelimbic cortex
PrCm	Medial precentral cortex
PV	Parvalbumin
PVT	Paraventricular nucleus
SST	Somatostatin
US	Unconditioned stimulus
vHPC	Ventral hippocampus
VIP	Vasoactive intestinal peptide
VMH	Ventromedial hypothalamic nucleus
vmPFC	Ventromedial prefrontal cortex
vlPAG	Ventro-lateral periaqueductal grey

INTRODUCTION

Our understanding of emotions in regulating behaviour is hampered by the abstract nature of emotion itself. It is well accepted that emotions regulate many cognitive processes and help to adapt our behaviour to many complicated daylife situations. This is achieved in part by modulating individual's perception of environmental cues and his abilities to express it. Emotions represent an important source of information acting as evaluation mechanisms on performance, filtering relevant data from noisy sources and providing a global management over other cognitive capabilities and processes. Earlier work by Ekman and colleagues defined 6 major emotions based on human facial expression, which are: fear, surprise, disgust, joy, sadness and anger (Ekman et al., 1969). Although these emotions can be easily observed and studied in humans, the understanding of the neuronal structures and circuits participating to emotion processing requires invasive approaches and the development of animal models. Despite the fact that animal studies on emotions are strongly limited by the animal's inability to tell us how they "feel", much of our understanding of the emotional brain comes from animal studies on fear behaviour in which we can directly measure behavioural outputs associated with fear states such as avoidance or immobilization response. Importantly, behavioural responses associated with fear or anxiety have been observed in many animal species, from insect to mammals, and this strongly suggest that the neuronal structures and functions related to fear processing are conserved across species. Fear behaviour is, in part, mediated by learning and memory processes that are supported by specific cellular and molecular mechanisms within dedicated neuronal circuits. One challenging question in modern behavioural neuroscience is to understand how modifications of neuronal activity in dedicated neuronal circuits give rise to appropriate behaviour associated with simple experiences. In the laboratory, one of the most used model to evaluate fear learning-dependent plasticity mechanisms is the auditory Pavlovian conditioning paradigm. In this rapid and robust emotional learning paradigm, an animal learns to associate a previously neutral tone (the conditioned stimulus, or CS, such as a sound) with a coincident aversive stimulus (the unconditioned stimulus, or US), which is typically a mild footstock. Following this training session, the presentation of the CS alone elicits a broad range of conditioned behavioural responses including an innate immobilization reaction called freezing, the most widely used behavioural variable to quantify fear memory. This form of associative learning can lead to long-

lasting fear memories (Davis, 1992, LeDoux, 2000, Gale et al., 2004), but repeated presentation of the CS alone also induces a temporary decrease of conditioned fear responses, a process known as fear extinction (Myers and Davis, 2007, Herry et al., 2010). It is thought that extinction is a new learning promoting the development of an inhibitory association between the CS and the US that can compete with the original fear memory rather than erasing it (Konorski, 1967). This new learning is context-dependent, and fear responses can still be expressed if the CS is presented in a different context from the one in which extinction was acquired (renewal) (Bouton et al., 2006). Moreover, fear extinction is generally not permanent, as the original CS-evoked fear behaviour can spontaneously recover over time (spontaneous recovery) (Brooks and Bouton, 1993, Quirk, 2002), or can be recovered by exposing animals to simple US presentations (reinstatement) (Rescorla and Heth, 1975). Perhaps the most fascinating aspect of this field of research is the growing refinement of our knowledge of the circuitry underlying fear behaviour. Nowadays, the canonical model of neuronal fear circuits can be viewed as a tripartite circuit including the amygdala (AMG), the prefrontal cortex (PFC) and the periaqueductal grey matter (PAG), which is highly conserved between rodents and humans (**Figure 2**).

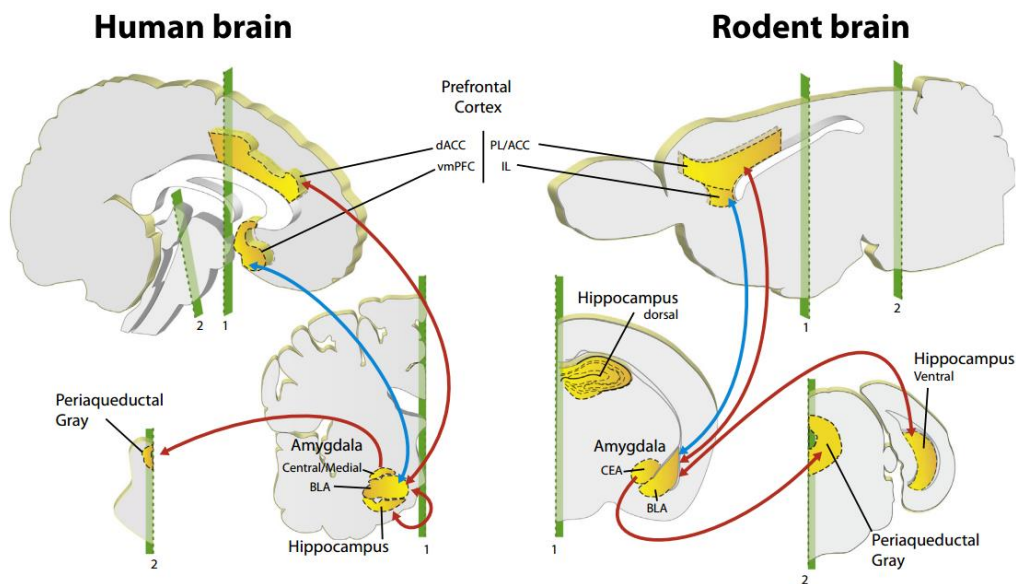


Figure 2: Schematic representation of the tripartite circuit involved in fear behaviour in humans and rodents. The first key neuronal structure is the amygdala (AMG) (composed of the basolateral amygdala (BLA) and the central amygdala (CEA)); the second is the medial prefrontal cortex (mPFC) (composed in human of the dorsal anterior cingulate cortex (dACC) and ventromedial prefrontal cortex (vmPFC) and in rodent of the anterior cingulate cortex (ACC), the prelimbic cortex (PL) and the infralimbic cortex (IL)). Finally, the last neuronal structure is the periaqueductal grey matter (PAG) located in the brainstem. Red line represents schematic connectivity during expression of fear behaviour whereas blue line represents the one involved during fear inhibition (Adapted from C. Dejean et al., 2015).

Over the past decades, it has become clear, mainly due to lesional and inactivation studies that these three structures largely contribute to the acquisition and expression of conditioned fear behaviour. More recently, the development of new challenging techniques such as optogenetic approaches coupled or not to single unit recordings allowed to investigate at the cellular level the contribution of dedicated neuronal populations and mechanisms encoding fear behaviour. In the following sections, I will review the gross anatomy and function of this tripartite network during fear behaviour and provide an updated model of the neuronal circuits and mechanisms controlling fear behaviour. Finally, based on this updated model I will introduce the main questions and hypothesis we addressed during this thesis.

I/ Amygdala in conditioned fear behaviour

In the past decades, numerous studies have attempted to define the neuronal substrates, and the cellular and molecular mechanisms mediating the acquisition, expression and extinction of conditioned fear responses. It emerged from clinical, anatomical and behavioural studies that the AMG is the major component responsible for the formation, expression and extinction of associative fear memory (LeDoux, 2000, Maren, 2001, Herry et al., 2010, Pape and Pare, 2010, Johansen et al., 2011). The AMG is an almond-shaped structure located in the medial temporal lobe and well-conserved across evolution, although species differences do exist (McDonald, 1998). The earliest demonstration of the involvement of the AMG in emotional behaviour can be traced back from a report by Brown and Schafer in 1888 in which they perform a bilateral ablation of the temporal lobe in a rhesus monkey. This lesion was associated with a deficit in understanding the significance of sensory inputs and also a loss of defensive behaviour. Furthermore, clinical studies from patients with bilateral AMG calcification (Urbach-Wiethe syndrome) revealed deficiencies in emotional and social behaviour, and more interestingly, a deficit in facial recognition of fear related events (Adolphs et al., 1994). Because studies presented in this thesis have been performed in rodents and since the structure of the AMG is highly conserved in mammals, the following section will describe the anatomy of the rodent AMG. For additional comparative data between the rodent and human AMG, we invite the reader to refer to recent reviews on this topic (Pitkanen and Kempainen, 2002, Dejean et al., 2015).

A/ Gross anatomy of the rodent amygdala

a/ Neuronal elements of the rodent amygdala

Based on embryological, morphological, neurochemical and physiological features, the AMG can be subdivided into two main sub-areas, one with a cortical developmental origin and the other with a striatal developmental origin. The “cortical-like AMG” is composed of several major nuclei including the lateral (LA), basal (BA), and the accessory basal (AB) nucleus. Together the LA and the BA form the basolateral amygdala (BLA) complex. The “striatal-like AMG” is composed of the central amygdala (CEA), which is located medially to the BLA. The CEA can be divided into two main sub-nuclei, namely the lateral CEA (CEl) and the medial CEA (CEm). It is important to note that at the interface between the BLA and the CEA there is a small group of inhibitory neurons called the intercalated cells (ITC). These neurons are part of the internal capsular region of the AMG and play an important role in the regulation of BLA inputs to the CEA. Furthermore, a structure of the extended AMG named the basal nucleus of the stria terminalis (BNST) shares similar embryologic developmental origin, cell morphology, neurotransmitter and efferent connections as compared to the CEA (Koikegami, 1963, McDonald, 1982a, Swanson and Petrovich, 1998, Sah et al., 2003, Crestani et al., 2013, Duvarci and Pare, 2014).

In order to explore the contribution of the AMG in processing fear behaviour, it is critical to identify the neuronal elements that composed this structure. The BLA is composed of approximately 80% of spiny, glutamatergic projection neurons (PNs) and 20% of aspiny, Gamma aminobutyric acid (GABA) interneurons (INs), randomly organized (McDonald, 1982b, 1985, Sah et al., 2003). PNs have a pyramidal shape with thick apical dendritic arborization and several thinner basal dendrites. The PNs send long axonal projections and collaterals to target extra-amygdaloid structures (Pare and Gaudreau, 1996). Conversely, INs are a more heterogeneous population with smaller somata and heterogeneous arborization. They are defined based on neuroanatomical and immunohistochemical properties. Morphologically INs can display distinct somatic, local dendritic and axonal innervation (basket cells, chandelier cells with bipolar, bitufted multipolar arborization) (Carlsen, 1988, Pare and Smith, 1993, Capogna, 2014). Several subtypes of INs can be defined at the neurochemical level, based on the expression of various calcium-binding proteins like parvalbumin (PV), calretinin (CR) and calbindin (CB). Also, the expression of some neuropeptides such as somatostatin (SST), vasoactive intestinal

peptide (VIP), cholecystinin (CCK), and neuropeptide Y (NPY) has been used to define INs (Kemppainen and Pitkanen, 2000, McDonald and Mascagni, 2001, Capogna, 2014). Numerous studies explored the role of two main classes of INs, namely PV and SST INs because of their differential innervations on PNs. These studies suggested that PV INs control the generation of action potential by contacting somata, proximal dendrites and the axon initial segment (Muller et al., 2006, Spanpanato et al., 2016), whereas SST INs control input integration and plasticity-related phenomenon by contacting preferentially distal dendrites and spines of BLA PNs (Muller et al., 2007). Moreover, it is widely accepted that a detailed dissection of INs functions will be useful to understand cellular functions of PNs, such as synaptic plasticity or oscillation generation/transmission in AMG (Herry and Johansen, 2014, Grundemann and Luthi, 2015, Tovote et al., 2015).

The CEA is mainly composed of medium spiny inhibitory neurons releasing GABA (Sah et al., 2003). CEm neurons have large somata, dendrites that branch sparingly and exhibit a low to moderate density of dendritic spines. In contrast, most CEI neurons have a smaller somata, multiple primary dendrites that branch profusely and exhibit a high density of spines, similar to the main type of cells found in the striatum (Hall, 1972). Immunohistochemical studies have demonstrated the presence of a wide variety of peptides (enkephalin, neurotensin, corticotropin, oxytocin and vasopressin releasing hormone) and receptors expression in the CEA (Roberts et al., 1982, Veinante et al., 1997, Huber et al., 2005). CEA neurons axons exhibit several local collaterals before leaving the nucleus. It is important to notice that long-range projections from the CEA are predominantly GABAergic compared to the BLA projections, which are mainly glutamatergic (Davis et al., 1994, McDonald et al., 2012). Finally the ITC cells form a group of GABAergic neurons comprising two types of cells, which are the medium and large spiny neurons. Because of their localization at the interface between the BLA and the CEA, ITC neurons allow the generation of a disynaptic inhibitory current in the CEA after activation of the BLA (Millhouse, 1986).

b/ Extrinsic connectivity of the amygdala

Tracing experiments revealed that the BLA receives polymodal sensory information from cortical areas and the thalamus. Two main pathways conveying sensory information to the BLA related to fear behaviour have been described in the literature: a direct subcortical pathway originating from the thalamus (in particular from the medial geniculate nucleus and the posterior

intralaminar nucleus) which reach the BLA through the internal capsule, and an indirect thalamo-cortical pathway (providing olfactory, somatosensory, auditory, visual and olfactory informations) which contact the BLA via the external capsule (Luskin and Price, 1983, LeDoux and Farb, 1991, Amaral and Insausti, 1992, Shi and Davis, 2001, Maren and Quirk, 2004). In addition, the BLA is bidirectionally connected with other brain areas allowing different kind of information to be processed. On the one hand, contextual information is conveyed to the BLA from a reciprocal rhinal and hippocampal connection (Canteras and Swanson, 1992b, McDonald, 1998, Pitkanen et al., 2000, McDonald and Zaric, 2015). On the other hand, bidirectional connectivity between the BLA and the PFC has been identified. More precisely, the LA is massively connected with the infralimbic cortex (IL) whereas the BA is mostly connected with the anterior cingulate cortex (ACC) and the prelimbic cortex (PL) (Krettek and Price, 1977, McDonald, 1991, Shinonaga et al., 1994, Hoover and Vertes, 2007). This specific connectivity suggests that the BLA is a good candidate to mediate CS-US associations during fear conditioning and that it can be modulated by external structures like the hippocampus (HPC) and PFC.

Recent work has demonstrated that CEA can work independently or in synergy with the BLA (Ehrlich et al., 2009). In fact, sensory information reaches the CEA by reciprocal connections with specific thalamic nuclei, which are the paraventricular, posterior intralaminar and subparafascicular nuclei (LeDoux et al., 1990, Turner and Herkenham, 1991, Alheid, 2003). In addition, the CEI received direct inputs from a major nociceptive pathway originating from the spinal cord and the trigeminal sensory nuclei (Neugebauer et al., 2004, Sarhan et al., 2005). On the efferent side, the CEA send projections to the parabrachial nucleus and the dorsal vagal complex to drive autonomic responses (Hopkins and Holstege, 1978, Veening et al., 1984). Furthermore the CEA project to many hypothalamus nuclei (Petrovich et al., 2001) directly or indirectly through the BNST (Davis and Whalen, 2001). Additionally, projections from the CEm to the ventrolateral and lateral part of the PAG have been well described in the regulation of fear responses (Rizvi et al., 1991). Finally, a recent study identified a functional connection between a particular class of SST-expressing INs in the CEI and the PAG (Penzo et al., 2014).

Compared to other structures, the AMG is heavily intrinsically connected. Within the BLA, glutamatergic projections prevalently run dorsoventrally, from LA to BA (Smith and Pare, 1994). Projection from the LA can reach the CEm and CEI indirectly via glutamatergic inputs

originating from the BA (Savander et al., 1996). In addition, LA neurons can also contact ITC or CEI GABAergic neurons which project to the CEm (Pitkanen et al., 1995, Savander et al., 1995).

Slice physiology experiments and extracellular recordings during auditory fear behaviour have complemented this model by identifying a local disinhibitory circuit within the CEA. These studies demonstrated that two particular classes of CEI neurons are either activated or inhibited during presentation of the CS⁺. The neurons have been named “CEI on neurons” (or alternatively PKC-delta⁻ neuron) and “CEI off neurons” (or PKC-delta⁺ neurons), respectively. “CEI on neurons” directly inhibit “CEI off neurons” that in turn disinhibit CEm neurons projecting to the PAG (Ciocchi et al., 2010, Haubensak et al., 2010). Anatomical and functional experiments also revealed that projections from CEm to CEI are weak or do not exist (Jolkkonen and Pitkanen, 1998, Ciocchi et al., 2010). Finally, the CEI is also heavily connected with the BNST (Huber et al., 2005) (**Figure 3**).

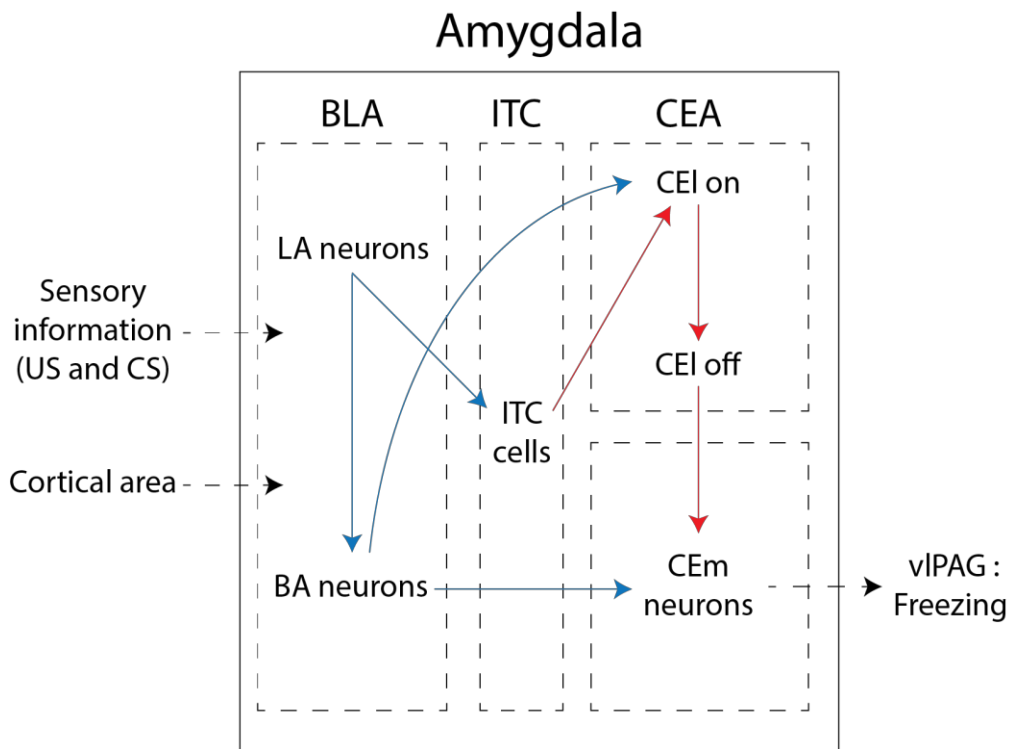


Figure 3: General organization of AMG circuitry. Scheme of the basic organization and overall flow of information's within the amygdaloid complex. During fear conditioning, sensory information about the CS and the US reaches the AMG through thalamo-LA and cortico-LA pathways. LA sends local projection to the BA or ITC. CEm neurons receive direct projection from BA neurons or indirect projection from a di-synaptic circuit within the CEI. In turn CEm neurons project to brainstem- and hypothalamus to mediate neuroendocrine, autonomic and motor responses associated with fear behaviour. Furthermore, AMG activity can also be regulated by higher cortical area like the PFC. Blue plain arrows represent glutamatergic neurons while red plain arrows GABAergic neurons. Dashed arrows represent external inputs and outputs.

B/ Functional role of the amygdala in fear behaviour

a/ **Role of the amygdala in the acquisition of auditory fear conditioning**

There is now strong evidence that the AMG, most particularly the BLA, is a locus for the formation and storage of CS-US associations during Pavlovian fear conditioning. Several studies using permanent and reversible inactivation of the AMG or neurophysiological recordings of AMG spiking activity demonstrated its importance in processing fear learning. More precisely, selective permanent lesions or reversible inactivation of the BLA reduced cued and contextual fear conditioning when made before training (Fanselow and Kim, 1994, Maren et al., 1996, Cousens and Otto, 1998). Mechanistically, fear acquisition within the AMG is thought to rely on activity-dependent associative plasticity. Quirk and colleagues were among the first to demonstrate that auditory fear conditioning induces short-latency plasticity elicited by acoustic CSs in LA neurons (Quirk et al., 1995, Quirk et al., 1997). In addition to this enhancing CS-elicited spike firing in the AMG, it was found that BLA neurons exhibit discriminative spike plasticity by specifically responding to the CS⁺ (CS paired with the US) as compared to the CS⁻ (Pare and Collins, 2000, Herry et al., 2008). One fundamental question raised in the field was to understand whether this form of plasticity was generated locally or in afferent brain areas such as the auditory thalamus or auditory cortex. In fact, inactivation of the BLA has been shown to be necessary for the development of neuronal plasticity in both the auditory thalamus (medial geniculate nucleus) and auditory cortex during auditory fear conditioning (Maren et al., 2001). This demonstrates that changes in CS-evoked spike firing in the LA does not reflect plasticity in upstream brain areas, but are mediated by neuronal plasticity processes within the LA.

Plasticity at sensory inputs from thalamus and cortex to the BLA, and particularly the LA, has been a major focus of work on the neural mechanisms of acquisition and expression of conditioned fear. Many studies support the notion that the LA is an essential site in which early, *N*-methyl-D-aspartate (NMDA) receptor-dependent changes in neuronal activity are required for the acquisition of conditioned fear (Miserendino et al., 1990, Quirk et al., 1995, Gewirtz et al., 1997, Quirk et al., 1997, Pare and Collins, 2000, Goosens and Maren, 2001, Rodrigues et al., 2001). This has led to the idea that NMDA receptor-dependent long-term potentiation (LTP) at sensory afferents to the LA projection neurons underlies this process (LeDoux, 2000, Maren and Quirk, 2004). In line with this concept, blocking and occlusion experiments have consistently supported the notion that LTP, potentiation of sensory evoked activity, and acquisition of

conditioned fear share the same mechanisms in the LA (Rogan and LeDoux, 1995, McKernan and Shinnick-Gallagher, 1997, Rogan et al., 1997, Tsvetkov et al., 2002, Rumpel et al., 2005). While substantial evidence supports the notion that thalamo-LA synapses change rapidly during fear acquisition (Quirk et al., 1997), this is less well understood in the cortico-LA pathway. Still, this represents one of the strongest established links between synaptic plasticity (i.e., LTP) and learning behaviour. Inhibitory gating of plasticity on LA glutamatergic synapses made by cortical afferents, contact spines in close proximity to those contacted by thalamic afferents, yet these spines are morphologically and functionally different (Humeau et al., 2005). Although the mechanisms underlying LTP induction and expression in thalamic and cortical sensory inputs are distinct, a common feature is that LTP is gated by the activity of local inhibitory circuits. At thalamo-LA synapses, LTP is predominantly induced and expressed post-synaptically. Induction requires postsynaptic depolarization to allow for activation of NMDA receptors, R-type and L-type voltage-dependent Ca^{2+} channels (Weisskopf et al., 1999, Bauer et al., 2002, Humeau et al., 2005, Rumpel et al., 2005, Humeau and Luthi, 2007), and this makes thalamo-LA LTP particularly sensitive to the level and temporal properties of postsynaptic GABA_A and GABA_B receptor-mediated inhibition (**Figure 4**). Indeed, like in other cortical structures, *in vitro* LTP induction at thalamo-LA synapses is facilitated by the addition of GABA_A and GABA_B receptor blockers (Bissiere et al., 2003, Shaban et al., 2006, Shin et al., 2006, Tully et al., 2007). LA projection neurons receive substantial GABAergic feedforward inhibition, which tightly controls their activity (Lang and Pare, 1997, Szinyei et al., 2000). This inhibitory constraint can be overcome or enhanced by neuromodulators. While dopamine, noradrenaline, or opioids suppress feedforward inhibition, and thereby gate LTP induction post-synaptically (Bissiere et al., 2003, Shaban et al., 2006, Tully et al., 2007), other modulators, including gastrin-related peptide and serotonin, enhance inhibition, thus possibly constraining LTP induction (Stutzmann and LeDoux, 1999, Shumyatsky et al., 2002). The cellular mechanisms of this control are diverse and, in the case of dopaminergic input two levels of control are possible. On one hand it control the modulation of inhibitory synapses onto projection neurons and local INs. On the other hand directly promotes the control of INs excitability leading to increased spontaneous inhibitory network activity but decreased stimulus-evoked inhibition (Bissiere et al., 2003, Loretan et al., 2004, Kroner et al., 2005). Neuromodulation of inhibitory activity and gating of LTP in this pathway are attractive candidate mechanisms in line with the requirement for neuromodulatory

input for fear conditioning *in vivo* at the physiological and behavioural level (Rosenkranz and Grace, 2002). In contrast, at cortico-LA synapses, LTP is mediated by different mechanisms. Induction requires coincident pre- and postsynaptic activity or concomitant activation of thalamo- and cortico-LA afferents (Huang and Kandel, 1998, Humeau et al., 2003, Humeau et al., 2005). Induction converges on a presynaptic expression that requires cAMP/PKA signaling and the presynaptic active zone protein RIM1a (Huang and Kandel, 1998, Tsvetkov et al., 2002, Fourcaudot et al., 2008). Although presynaptic LTP is insensitive to postsynaptic inhibition, it remains under the control of feedforward inhibitory pathways. GABA released from local feedforward INs activates presynaptic GABA_B receptors, which negatively control glutamate release from sensory afferents (Szinyei et al., 2000). Abolishing GABA_B receptor-mediated presynaptic inhibition at cortico-LA synapses unmasks a nonassociative, NMDA receptor-independent form of presynaptic LTP (Shaban et al., 2006). The presynaptic GABA_B receptors on glutamatergic inputs onto projection neurons, but not onto local INs (Shaban et al., 2006, Pan et al., 2009), are activated by volume transmission. Therefore, excitation/inhibition balance and induction of NMDA receptor-independent presynaptic LTP may be controlled by changes in inhibitory transmission associated with distinct patterns of neuromodulation and network activity (Pare and Collins, 2000, Pelletier and Pare, 2004). In addition, changes in inhibition associated with altered GABA release (Mahanty and Sah, 1998, Szinyei et al., 2000, Bauer et al., 2002) may result in a shift of the induction-threshold for associative LTP at cortico-LA synapses. At the behavioural level, genetic loss of presynaptic GABA_B hetero-receptors leads to generalized fear responses (Shaban et al., 2006). Consistent with this, a similar generalization phenotype is observed when the activity dependent GABA-synthesizing enzyme GAD65 is knocked out (Bergado-Acosta et al., 2008). Together, this suggests that GABAergic control of presynaptic LTP and GABA release at cortico-LA synapses likely determine stimulus specificity and generalization of fear responses.

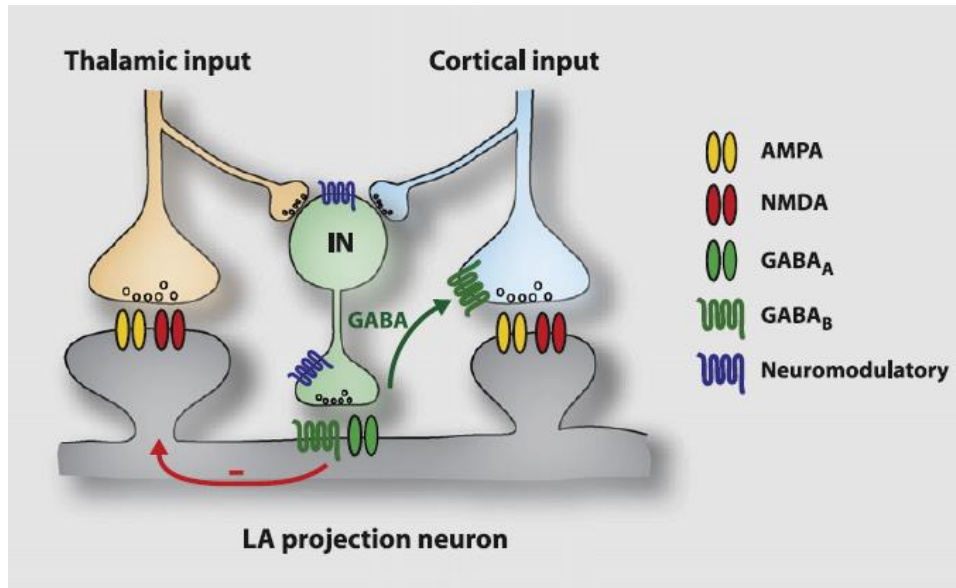


Figure 4: Inhibitory Gating of LTP in the LA. Projection neurons in the LA (gray) receive converging thalamic and cortical sensory afferents. LTP at thalamic and cortical afferents is tightly controlled by GABA released from feedforward interneurons (green). At thalamic afferents, this control is predominantly postsynaptic via GABA_A receptors. At cortical afferents, this control is presynaptic via GABA_B receptors. Interneurons are targets of neuromodulators that modify their output activity. This process gates the induction of glutamatergic LTP by transiently altering the level of pre- and postsynaptic inhibitory drive. (Adapted from I. Ehrlich et al., *Neuron* 2009).

While most studies focused on the role of the BLA in the acquisition of fear conditioning, some data also suggested that the CEA is critically involved in the formation of conditioned fear memories. Indeed, neurotoxic lesions of the CEA attenuate the acquisition of fear conditioning (Campeau and Davis, 1995b). In addition, reversible inactivation (with muscimol or NMDA receptor antagonist) of CEI induced a decrease in fear acquisition (Wilensky et al., 2006, Ciocchi et al., 2010). Electrophysiological studies have complemented this model by demonstrating that fear conditioning induce synaptic potentiation of BA neurons projecting to CEI (Watabe et al., 2013). Other data also demonstrated that fear conditioning induced robust plasticity of excitatory synapses onto inhibitory SST neurons in the CEI (Li et al., 2013). Furthermore, it has also been demonstrated that CEA neurons displays differential changes in CS⁺ and CS⁻-evoked activity in a discriminative fear conditioning paradigm (Pascoe and Kapp, 1985). Finally, a recent publication showed that changes of neuronal activity of a defined subpopulation of neurons expressing PKC-delta within the CEA (PKC-delta⁺ neurons) can orchestrate complex behaviour changes such as modification of anxiety and generalization levels via extrasynaptic inhibition

mediated by GABA_A receptor (Botta et al., 2015). Together this data demonstrate a complementary role of CEA neuronal activity and synaptic plasticity in mediating fear learning.

b/ Role of the amygdala in fear expression and extinction learning

Recent data highlighted the role of CEA and BLA circuits in mediating fear expression. Lesional studies demonstrated that precise lesion of the BA reduce fear expression (Anglada-Figueroa and Quirk, 2005, Amano et al., 2011). Additionally, electrophysiological studies demonstrated that BA neurons increase their firing rate in response to CS presentations associated with fear and that different neurons also present a sustained activity during freezing expression (Amano et al., 2011). Recently, the combination of retrograde labelling and electrophysiological techniques helped to complement the neuronal circuitry of fear behaviour by showing that BA neurons projecting to the PL were active during fear expression while the ones projecting to the IL displayed cell type specific plasticity related to extinction behaviour (Senn et al., 2014). As described above, the LA and BA neurons project directly or indirectly to the CEA, which is thought to be the output structure driving fear responses (Pitkanen et al., 1997, Duvarci and Pare, 2014). The use of new technology such as optogenetic manipulations or large scale recordings have refined the working model of CEA and BLA circuits in fear behaviour, showing for instance that within the CEI, a disinhibitory microcircuit can drive fear responses by activating CEM neurons projecting to the ventrolateral periaqueductal grey (vlPAG). In particular, electrophysiological data have demonstrated the presence of two classes of GABAergic cells within the CEI, the “CEI on neurons” (PKC- δ^- neurons), which are activated by CS inputs and in turn inhibit “CEI off neurons” (PKC- δ^+ neurons). This inhibition of “CEI off neurons” leads to a disinhibition of CEM neurons projecting to the vlPAG (Cicchi et al., 2010, Haubensak et al., 2010). In addition, a second pathway, which participates in fear expression, was identified and it involves a direct projections from the CEI SST neurons to the vlPAG or/and paraventricular nucleus (PVT) (Penzo et al., 2014, Do-Monte et al., 2015).

Over the past decade, there was also considerable interest in elucidating the neuronal circuits underlying fear extinction. A set of lesional studies examined the contribution of the BLA in fear extinction. However, because post-training BLA lesion was associated with a suppression of fear behaviour it was difficult to disentangle the contribution of the BLA to fear extinction and/or fear suppression (Campeau and Davis, 1995a, Cousens and Otto, 1998, Anglada-Figueroa

and Quirk, 2005, Amano et al., 2011). The use of reversible inactivation using the GABA_A receptor agonist muscimol allowed to investigate further this question and it was reported that, inactivation restricted to the BA completely blocks acquisition of extinction (Akirav et al., 2006, Herry et al., 2008, Hart et al., 2009). An important advanced for the understanding of the role of BLA in the acquisition of fear extinction was conducted with pharmacological studies using either micro-infusion of protein synthesis inhibitor, antagonist of NMDA receptor or mitogen-activated protein kinase inhibitors. These studies demonstrated that glutamatergic plasticity at the level of the BLA was necessary for fear memory extinction (Lu et al., 2001, Lin et al., 2003, Herry et al., 2006, Sotres-Bayon et al., 2007). Furthermore local infusion of muscimol in BLA potentiated fear extinction when made after extinction training (Myers and Davis, 2002, Akirav et al., 2006). Altogether, these studies demonstrated that the acquisition of extinction can be directly regulated at the level of the BLA.

Studies using *in vivo* extracellular electrophysiology allowed a rapid growing of our knowledge related to the contribution of specific neuronal elements in fear extinction. These studies established that in the BLA two types of cell populations showing opposite firing patterns during extinction learning. The first population of BLA neurons (fear neurons, 15% of BLA neurons) was selective of high fear states and displayed a reduced firing activity during extinction learning. In contrast, the second population (extinction neurons, 15% of BLA neurons) was selective of low fear states and displayed an increase firing activity during extinction learning (Herry et al., 2008). Furthermore it was shown that these two neuronal populations show a specific connectivity pattern with the medial prefrontal cortex (mPFC) and the ventral hippocampus (vHPC). Whereas fear neurons received inputs from the vHPC and project to the mPFC, extinction neurons were exclusively connected with the mPFC (Herry et al., 2008, Senn et al., 2014). Additionally, another study established the existence in the LA of two populations encoding differentially extinction, the first group, the ‘extinction susceptible’ neurons decrease their activity during extinction, while the second population, the ‘extinction resistant’ maintain their activity all along the extinction session. Furthermore they demonstrate that only the “susceptible extinction” displayed larger and more rapid potentiation after reconditioning providing a neural correlate of savings after extinction (An et al., 2012). Finally, two recent studies demonstrated that in the BLA some neurons decrease their specificity to CS responses after multiple conditioning, leading to fear generalization (Ghosh and Chattarji, 2015, Resnik and

Paz, 2015). Together these data demonstrate that subpopulation of BLA neurons encodes differentially fear and extinction learning, and that their activity can be regulated by hippocampal and cortical inputs for some of them.

While it is becoming clear that BLA is involved in the acquisition, expression and extinction of conditioned fear memory, it is highly probable that BLA activity is finely regulated by other connected structures such as the mPFC. In the following section we will review the involvement of the mPFC in auditory fear conditioning and its importance in the acquisition, expression and extinction of conditioned fear behaviour.

II/ Role of medial prefrontal cortex circuits in fear behaviour

Although most of the research on fear behaviour concentrated on the role played by AMG neuronal circuits, some reports highlighted the critical role played by the cortex in the regulation of AMG-dependent fear memories (Weinberger, 2004, Quirk and Mueller, 2008, Herry et al., 2010, Sotres-Bayon and Quirk, 2010). The mPFC is involved in the regulation of a broad range of brain functions related to attention, executive control or working memory. The capacity of the mPFC to sustain such complex functions is in part due to its numerous connections with a wide range of brain structures. One of the most investigated function of the mPFC is its role in the regulation of emotional behaviour. It is well known that dysfunction of the mPFC is related to psychiatric conditions such as post-traumatic stress disorder (Shin and Liberzon, 2010, Pitman et al., 2012). Because of the potential clinical implications of these findings, numerous animal studies have been conducted over the past decades in order to understand mPFC anatomy and to elucidate the precise role of the mPFC in modulating fear behaviour.

A/ Gross anatomy of the mPFC

a/ **Neuronal elements**

Over the past years there has been animated discussion about mPFC homology between animal species, in part due to cytoarchitectonic and hodological differences among species. Nowadays, it is commonly accepted that the rodent mPFC can be divided into four distinct areas which are, descending from the most dorsal region, the medial precentral cortex (PrCm), the ACC (dorsal and ventral part), the PL and the IL (Krettek and Price, 1977, Van Eden and

Uylings, 1985, Ray and Price, 1992, Van De Werd et al., 2010, Matyas et al., 2014). The mPFC can be functionally separated into the PrCm and ACC areas, which regulate various motor behaviour, whereas PL and IL are implicated in emotional, mnemonic, and cognitive processes (Heidbreder and Groenewegen, 2003). PL and IL can be separated using cytoarchitectural criterion such as the wideness of layer II, which is a characteristic of the IL subregion (Van Eden and Uylings, 1985, Ray and Price, 1992). More recently, it was suggested that the proportion of PV-expressing interneurons (PV⁺) in the dorsomedial PFC (dmPFC, including ACC and PL) could provide a mean to separate the PL from the IL in which PV⁺ are virtually absent (Matyas et al., 2014). Furthermore, based on their differing target structures, the PL has been involved in emotional regulation and cognitive processes whereas the IL functions were linked to the regulation of visceral and autonomic functions (Vertes, 2006).

To understand the cortical PFC functions that drive fear behaviour we have to appreciate the structural frame of the cortex, which contains complex elements with some stereotypies. The cortex has a paralleled laminar organization and based on cytoarchitectonic criterions it is possible to define six layers numbered in order from the most superficial to the deepest. The layer 1, so called 'molecular layer', is a thin layer located at the surface, below the pia, and is characterized by a low number of neurons, by the presence of axons organized parallel to the surface and by dendrites coming from deeper layers. Underneath are located the layers 2 and 3, representing the external granular layer and the external pyramidal layer, respectively. In most cortices there is not a clear anatomical segregation between this two layers since, both are composed of densely concentrated neurons with small sized cell body and vertically orientated PNs. Below is the layer 4, labelled the internal granular layer, is lacking in the rodent mPFC. This layer is characterized by high concentration of small size cell body. The layer 5 or the internal pyramidal layer is mostly composed of sparse and large PNs vertically oriented. The last layers called polymorph layers contain various neuronal type without specific organization. These six layers have distinct extrinsic connectivity. In particular, layers 2/3 support the cortico-cortical connections, layers 1 and 4 receive thalamic inputs and layers 5 and 6 are respectively the main sources of thalamic and subthalamic projections (**Figure 5A**) (Nieuwenhuys, 1994, Harris and Shepherd, 2015).

Across these layers, the cortex is composed of two main classes of neurons: the glutamatergic PNs and the GABAergic INs that represent respectively 80% and 20% of the

cortical neurons. PNs used glutamate as a neurotransmitter and are located in all six cortical layers, except layer 1. PNs are spiny neurons and their dendritic arbors typically display two different subregions. One containing short basal dendrites emerging from the base of the soma and apical dendrites arising from the top of the soma, running perpendicularly to the pia matter, terminating in a dendritic tuft in layer 1 (DeFelipe and Farinas, 1992, Spruston, 2008). The PNs have variable profile depending on their layers location and can project locally or externally to other cortical or subcortical areas. PNs are largely seen as the neural biological substrate that transmits information between structures. As opposed to PNs, the vast majority of INs (Lee et al., 2014) do not leave the cortex and are restricted to a local environment (Gonchar et al., 1995, Letinic et al., 2002). Cortical inhibitory INs are highly diverse and comprised many types defined on different criteria (morphological, electrophysiological and immunohistochemically criteria). However, none of these criterions alone can reliably classify cortical inhibitory INs (**Figure 5B**). Morphologically cortical INs can display distinct somatic, dendritic and axonal innervation (basket cells, martinotti cells, chandelier cells with bipolar, double bouquet, bitufted, neurogliaform arborization) (Markram et al., 2004). INs can also be defined based on their electrophysiological property (fast spiking, non adaptative non fast spiking, adaptating, irregular spiking, intrinsic burst firing and accelerating spiking cells) (Ascoli et al., 2008). Finally, INs can be characterized at the neurochemical level in which several categories of molecules have been recognized to provide the distinction of interneuronal subtypes (PV, CR, CB, SST, VIP, CCK, NYP). Because of their morphological, electrophysiological and molecular diversity, INs are believed to differentially sculpt cortical activity. Thus, it is widely accepted that a detailed understanding of INs functions is a prerequisite to understand the functional organization of cortical neuronal circuits (Hubel and Wiesel, 1962, Adesnik and Scanziani, 2010) (**Figure 5**).

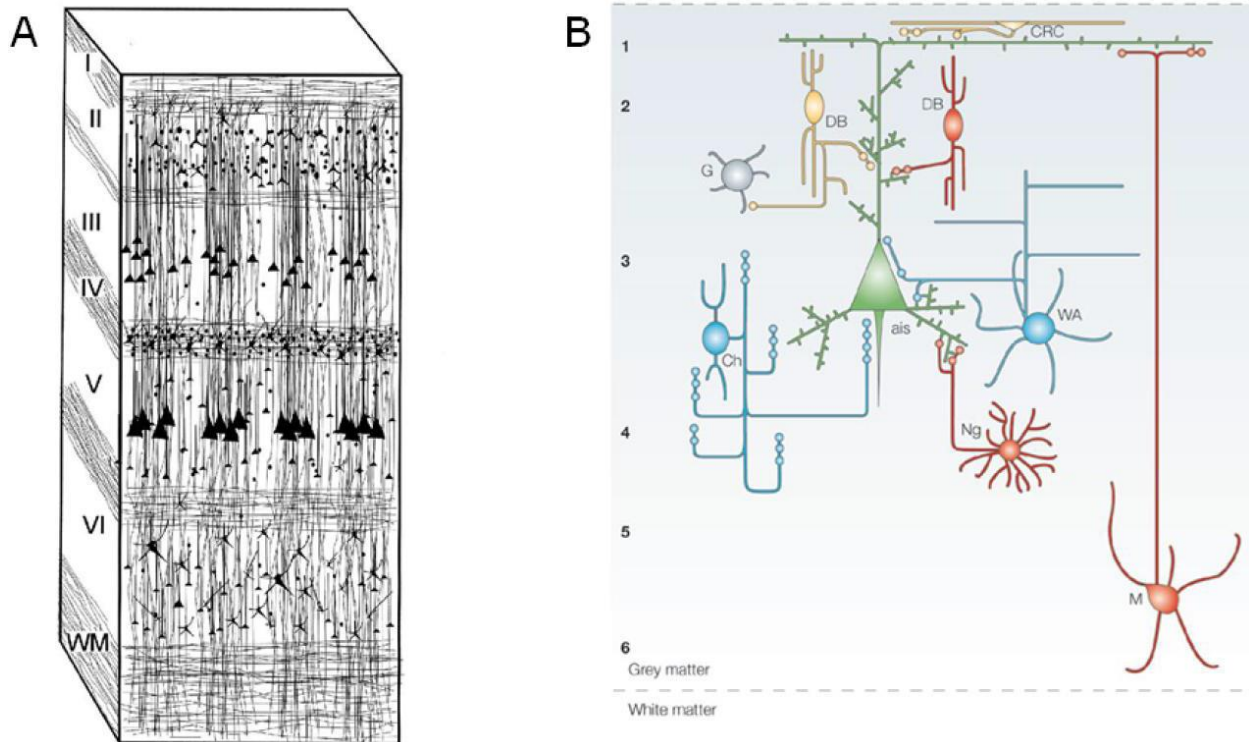


Figure 5: Schematic representation of cortical layers and neuronal population **A.** Cytoarchitecture of the different cortical layers. I to VI: Cortical layers; WM: White matter. Pyramidal neurons (PNs) are located in all layers except layer I, which is exclusively composed of interneurons (INs). INs can cross layers to regulate PNs activity. **B.** Organization of the mPFC microcircuits. PN cell (green) are modulated by different type of morphologically distinct neurons. Ch : chandelier cell, WA : Basket cells ; M : Martinotti cells ; NG : Neuroglial cells ; DB : Double bouquet cells ; CRC : Cajal-Retzius cells. Color code represents the different type of cells defined by immunohistochemistry: Parvalbumin cell (blue), Calbindin cells (red) and Calretinin cell (yellow) (adapted from Lewis et al., 2005).

The link between the global connectivity and the task-relevant responses of neurons has started to be complemented by microcircuit dissection, thanks to optogenetic tools allowing a precise identification and control of subpopulations of neurons (Deisseroth, 2015). The hypothesized functions of inhibition in cortical networks are diverse and range from maintenance of homeostasis, gain control and tuning sensitivity of individual neurons to pacing synchrony in large populations of neurons and mediating neuronal assembly formation (Isaacson and Scanziani, 2011). There is growing evidence that these multiple functions rely on genetically defined subtypes of INs. For example, a long-standing debate is whether inhibition has a divisive or subtractive effect on cell selectivity, which is a question that has recently been opened up by optogenetic manipulations suggesting that the two main populations of cortical INs have different functional role. PV INs mainly control the gain of sensory responses through division of responses whereas SST-expressing INs, dendrite targeting interneurons sharpen selectivity

through subtractions from excitatory responses (Wilson et al., 2012). Although this particular result is still under debate, it exemplifies the new perspective on inhibitory function that is highly diverse and relies on precise microcircuits of INs-PNs but also INs-INs interaction. In terms of INs-PNs interactions, large-scale extracellular recordings in the PFC have shown that PV INs exert brief and uniform inhibition on their targets while SST INs have longer and more variable inhibitory effects (Kvitsiani et al., 2013). These kinds of information are essential to understand circuits since feedforward and feedback inhibition can have a profoundly different impact on network dynamics (Pouille et al., 2009). Another function sustained by GABAergic INs is the generation/transmission of oscillation. Because of the convergence of excitatory inputs from multiple PNs onto single INs and the divergence of INs outputs, INs are perfectly positioned to synchronise networks activity (Allen and Monyer, 2015). In fact, *in vitro* experiments demonstrated that the rhythmic stimulation at theta frequency of a single GABAergic IN was sufficient to synchronize PNs activity (Cobb et al., 1995).

b/ Connectivity with other structures

Concerning hodological features, tracing experiments have reported that the mediodorsal nucleus of the thalamus (MD) is bidirectionally connected with the mPFC. More precisely, the medial segments of the MD preferentially contact the IL and PL, whereas its lateral segments more often contact the AC and PrCm (Groenewegen, 1988, Uylings and van Eden, 1990). These projections are mostly ipsilateral and terminate in layers I/III of the mPFC (Kuroda et al., 1993). The mPFC also receives massive inputs emanating from the BLA that terminate in the ventral ACC, PL, and IL. The mPFC projects back to both the BLA and the CeA (McDonald et al., 1996). However, the IL and PL display differences in the nuclei they preferentially contact. The IL is highly connected with lateral capsular, where ITC cells are located, and the LA. In contrast the ACC and PL project mostly to the BA (Krettek and Price, 1977, McDonald, 1991, Shinonaga et al., 1994, Hoover and Vertes, 2007). Additionally, the mPFC shares reciprocal connectivity with the ventral tegmental area (Thierry et al., 1973), the basal ganglia (Groenewegen et al., 1997), and the dorsal and lateral regions of the PAG (Gabbott et al., 2005).

The mPFC also projects to other cortical areas such as the paralimbic cortex, which send reciprocal projections back to the ventral ACC, PL and IL, and the somatosensory and motor cortices that primarily contact the PrCm and the dorsal ACC. The mPFC receives ipsilateral

inputs from the vHPC (CA1 region and subiculum) that terminate in all layers of the PL, with sparse inputs from the dorsal hippocampus (dHPC) (Jay and Witter, 1991, Cenquizca and Swanson, 2007, Hoover and Vertes, 2007). Interestingly, whereas a recent paper indicated direct projections from the ACC to the dorsal hippocampus (HPC) (Rajasethupathy et al., 2015), the mPFC can also regulate HPC via indirect projections to the nucleus reuniens of the thalamus (NR), which serves as a major source of thalamic input to the HPC (Vertes et al., 2007, Varela et al., 2014). The mPFC can also indirectly influence the HPC via projections to the entorhinal cortex, the MD, or the AMG (Vertes, 2006). Finally, the mPFC also contains important internal connections, with the PL projecting to the ventral ACC and the IL region projecting preferentially to the PrCm and dorsal ACC (Sesack et al., 1989, Hoover and Vertes, 2007).

B/ Role of the mPFC in conditioned fear behaviour

a/ **Involvement of the mPFC in fear behaviour**

i/ Lesional studies

In rodent, lesioning data evaluating the role of the mPFC in fear behaviour lead to divergent results due to the uncontrolled extent of the lesions, the different behavioural paradigm used and the time at which the lesions were performed. The main results from these studies are summarized in the following section. Pre- and post-training lesions of the dmPFC, including ACC and dorsal PL, enhanced fear conditioning (Morgan and LeDoux, 1995, Vouimba et al., 2000, Bissiere et al., 2008) and blocked fear extinction (Morgan and LeDoux, 1995). Additionally, pre-training electrolytic or pharmacological lesions of ventromedial prefrontal cortex (vmPFC), including the ventral PL and IL, had no effect on fear conditioning but selectively blocked fear extinction (Morgan et al., 1993, Morrow et al., 1999b, Lacroix et al., 2000, Fernandez Espejo, 2003). Post-training lesions of the vmPFC comprehending the ventral PL and IL produced somewhat inconsistent results. Some studies reported blockade of fear expression or extinction (Fryszak and Neafsey, 1991, Morrow et al., 1999b), whereas another did not (Morgan et al., 2003). Later on, several groups extended these findings by showing that pre-training vmPFC lesions blocked the consolidation but not the original formation of fear extinction memories (Quirk et al., 2000, Lebron et al., 2004, Tian et al., 2011). Although these data suggest that distinct mPFC subregions might play a differential role in fear behaviour, it is worth noting that a number of studies did not find any effect of mPFC lesions on fear

conditioning or extinction behaviour (Rosen et al., 1992, Gewirtz et al., 1997, Farinelli et al., 2006, Garcia et al., 2006). To summarize, all these lesion studies point out a clear role of the mPFC in fear behaviour, although the specific role of different subregions is still controversial and required more subtle technical approaches to be solved.

ii/ Pharmacological studies

In an attempt to further characterize the role of mPFC in fear behaviour, many studies used pharmacological agents to temporarily inactivate the mPFC during behavioural tasks. The use of local, reversible, pharmacological inactivation also yielded contrasting results as inactivation of both ventral PL and IL impaired between session extinction, prevented discrimination of a non-conditioned tone, increased, decreased, or did not change fear expression during a post-extinction retrieval test (Resstel et al., 2006, Sierra-Mercado et al., 2006, Lee and Choi, 2012, Morawska and Fendt, 2012). However, restricted pre-training or post-training inactivation of ACC, PL or IL provided more consistent results. Indeed, pre-training inactivation of the ACC with lidocaine, the Na⁺ channel blocker tetrodotoxin or muscimol blocked fear acquisition (Sacchetti et al., 2002, Tang et al., 2005, Bissiere et al., 2008). Furthermore targeted pre-training activation of the ACC using mGluR agonist (trans-(±)-1-amino-(1S, 3R)-cyclopentanedicarboxylic acid) or GABA_A receptor antagonist (bicuculline) revealed an enhancement of fear behaviour, suggesting an involvement of the ACC in the acquisition of fear behaviour (Tang et al., 2005, Bissiere et al., 2008). Concerning injections restricted in PL, it has been demonstrated that muscimol injection prior to extinction training impairs fear expression. However, this manipulation has no long-term effect on extinction recall, suggesting that PL inactivation does not interfere with the acquisition of extinction but rather with expression of fear behaviour (Corcoran and Quirk, 2007, Laurent and Westbrook, 2009, Sierra-Mercado et al., 2011, Stevenson, 2011). In contrast, when inactivation was restricted to the IL, the same manipulations has no effect on fear expression but impaired within session extinction. Nonetheless, one study reported a facilitating effect on extinction (Akirav et al., 2006). Interestingly, post-training activation of IL using the GABA_A receptor antagonist picrotoxin facilitates between session extinction of fear, further supporting a role of IL in consolidation of fear extinction (Thompson et al., 2010, Chang and Maren, 2011).

In summary, these studies indicated that massive lesions or inactivation of overlapping mPFC regions lead to inconsistent results whereas more delimited manipulations of ACC, PL and

IL have produced consistent and specific effects. In particular, these data strongly suggest that (i) ACC plays a key role in the acquisition of fear behaviour, (ii) PL in fear expression and (iii) IL is involved in the consolidation of fear extinction behaviour.

iii/ Immediate early gene expression studies

The understanding of the role of the different mPFC subregions has advanced due to the detection of immediate early genes (IEG) such as the c-fos protein following fear memory formation and expression. This approach assumes that the formation and expression of fear memories depends on specific signaling cascade that induces IEG transcription and de novo protein synthesis to stabilize fear memories. For example, following specific defensive fear behaviour, detection of IEG in the brain is thought to indicate where and when neurons were activated during the task. Smith and colleagues demonstrate that in rats the re-exposure to a CS previously paired with footstock induce an increase of c-fos expression in ACC (Smith et al., 1992). However, subsequent studies have shown that both PL and IL exhibit increase in IEG expression after fear conditioning (Morrow et al., 1999b, Herry and Mons, 2004) even if in the dmPFC this increase was less clear (Barrett et al., 2003, Santini et al., 2004, Plendl and Wotjak, 2010). Interestingly, an antisense oligonucleotide against c-fos mRNA, injected simultaneously into both PL and IL prior conditioning, attenuated fear responses during an extinction session (Morrow et al., 1999a) suggesting the involvement of c-fos in PL and/or IL for consolidation or expression of fear behaviour. It is worth noting that this effect was observed with simultaneous manipulations to PL and IL implying that there is some level of functional overlap between these two regions. Additionally, the lack of extinction assessed during retrieval was correlated with no change (as revealed with the quantification of the IEG zif268) or reduce (c-fos) expression within PL and IL (Herry and Mons, 2004), whereas successful consolidation of extinction memory assessed during retrieval was correlated with increased IEG in IL (Knapska and Maren, 2009). Moreover, IEG expression assessed during renewal of fear behaviour demonstrated an increase in the PL area suggesting the involvement of PL in modulating fear expression in a specific context dependent manner (Knapska and Maren, 2009). Finally, fear behaviour has recently gained insight from functional anatomical analyses combining both IEG and anatomical tracing approaches. The first innovative approach used transgenic rats expressing a PSD-95 Venus fusion protein under the control of a c-Fos promoter that was targeted to dendrites using the PSD-95 and

3'-UTR of *Arc* mRNA. Since PSD-95 is a major component of postsynaptic densities, and *Arc* UTRs contain dendrite-localizing sequences, Venus rats allow for fluorescent tagging of the dendrites and synapses of activated neurons following c-fos induction. In conjunction with anterograde tracer injections in distinct neuronal regions, this anatomical technique allows for the examination of discrete inputs onto the cell bodies and dendrites of IEG-activated neurons. Interestingly, a recent study using these approaches demonstrated that during the retrieval of extinction memory, the dominant inputs to c-fos activated neurons in the LA were from the IL, whereas recovery of fear memory was associated with c-fos active neurons receiving inputs from the PL and the vHPC (Knapska et al., 2012). All together, these data strongly support a differential regulation of fear behaviour within the PFC, with dorsal regions involved in the expression of fear behaviour and ventral region mediating consolidation of fear extinction.

b/ Modulation of fear behaviour in mPFC circuits

Previous results suggested that fear behaviour is differentially modulated by neuronal circuits involving IL and PL subregions. PL has been suggested to modulate fear expression via activation of BLA neurons projecting to CEM neurons. In line with this suggestion, it has been demonstrated that sustained spike firing in the PL during aversive CSs correlates with fear expression but not fear extinction (Burgos-Robles et al., 2009, Sierra-Mercado et al., 2011). Furthermore, a recent electrophysiological study demonstrated that disinhibition of PNs projecting to BLA, a phenomenon mediated by PV INs, is necessary and sufficient to drive fear expression (Courtin et al., 2014). Moreover, a recent tracing study shows that fear renewal increases c-fos expression in PL and vHPC neurons projecting to the BA and that a disconnection of these pathways induced a decrease of freezing responses (Orsini et al., 2011). Complementary to the previous experiment, the electrophysiological characterization of inputs/output on BA neurons responding during fear expression revealed that BA neurons preferentially activated during context-dependent fear renewal receive strong hippocampal inputs, compared to BA neurons preferentially activated during extinction learning (Herry et al., 2008). These studies suggest that BA neurons can be differentially regulated by a direct hippocampus or indirect hippocampus-mPFC pathway (Vertes, 2006). Finally, mPFC projections to the PAG, which is a neuronal structure involved in the genesis of freezing responses and conditioned fear behaviour (Vianna et al., 2001, Gabbott et al., 2005), may be directly involved in the control of fear expression. To our knowledge, the boundary conditions during which this direct mPFC-PAG

pathway might be involved to regulate fear responses are still unclear and will require further work.

In contrast to PL, it is thought that IL projections to the AMG inhibit fear behaviour. Several data suggest that electrical stimulation of the IL inhibits the output activity of the CEM, which is necessary to drive fear expression (Veening et al., 1984, Cassell and Wright, 1986, Quirk et al., 2003). Accumulating evidence support a model of inhibitory circuits from the IL to CEM that involved a relay via GABAergic ITC cells (Pare et al., 2004), although this view has been recently challenged (Adhikari et al., 2015). Nevertheless, recent research demonstrates that ITC cells are necessary for the expression of extinction memory. In fact, selective ablation of the ITC cells after extinction training induced a recovery of conditioned fear responses (Likhtik et al., 2008). IEG study coupled with pharmacological disinhibition by local infusion of GABA_A receptor antagonist picrotoxin demonstrated an increase of c-fos immunoreactive ITC cells suggesting that ITC activity could be driven by inputs from the IL (Berretta et al., 2005). Furthermore, an electrophysiological study on anesthetized rats using juxtacellular recordings demonstrated that ITC cells are responsive to IL stimulation (Amir et al., 2011). Even if the involvement of the IL-ITC pathway in processing fear extinction has become clear over the past years, a recent study demonstrated that extinction neurons within the amygdala share strong connection with the mPFC (Herry et al., 2008) indicating a role of the mPFC in the regulation of extinction processes via a relay in the BA (Figure 6).

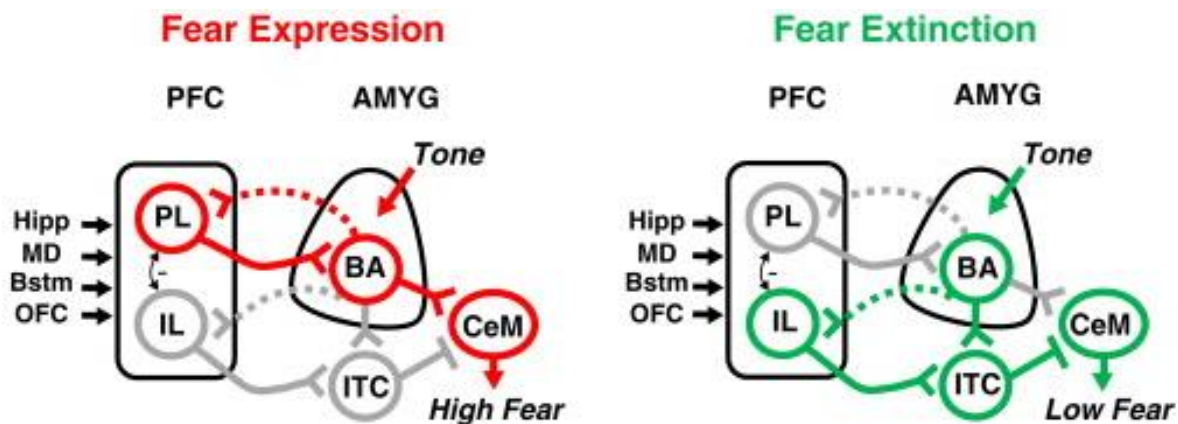


Figure 6: Prefrontal control of fear expression and extinction. During fear expression (left) and extinction (right) of auditory fear conditioning, tone responses from the amygdala (AMG) get integrated by the PL or IL. Fear expression involves PL projections back to basal amygdala (BA), whereas fear extinction involves IL projections to amygdala-intercalated cells (ITC). In turn, BA excites neurons in CEM to produce fear responses, while ITCs inhibit these amygdala output neurons thereby inhibiting fear responses. Thus, the same conditioned stimulus (e.g. a tone) signals either high fear (red) or low fear (green) states in the appropriate circumstances (Adapted from Sotres-Bayon & Quirk, 2010).

c/ Neuronal encoding of fear behaviour in the mPFC

Although the dmPFC is thought to be mainly involved in fear expression based on lesion, inactivation and immunohistochemical evidence stated above, a number of recent studies have suggested that the dmPFC itself might be involved in the acquisition and consolidation of fear memories. Accumulative evidence, demonstrated that inactivation and pharmacological manipulation of the dmPFC block cued and contextual fear acquisition (Sacchetti et al., 2002, Laviolette et al., 2005, Tang et al., 2005, Floresco and Tse, 2007, Bissiere et al., 2008, Einarsson and Nader, 2012). Moreover, electrical stimulation of the PL enhanced fear expression at the time of the manipulation. This effect was long lasting and still present after long lasting recovery (Vidal-Gonzalez et al., 2006). While some studies, have used pharmacological agents to evaluate the involvement of mPFC in encoding fear behaviour, the most promising results came from the use of single unit recordings in behaving mice submitted to fear conditioning and extinction. It has been shown that PL neurons correlated with fear behaviour rather than extinction memory. In particular, it has been shown that ~15% PL neurons acquired CS⁺-evoked responses with fear conditioning and that ~25% of PL neurons displayed sustained conditioned tone-evoked responses during fear behaviour (Burgos-Robles et al., 2009). Together these studies showed that dmPFC neurons acquired specific properties after conditioning reflecting its involvement in fear acquisition and expression.

Concerning the involvement of IL in the encoding of fear extinction, a number of studies revealed that plasticity blockade within the vmPFC does not impair the formation of extinction memories, but selectively blocks consolidation of extinction. For instance, blockade of NMDA receptors in the vmPFC impaired post-extinction retrieval (Sotres-Bayon et al., 2009). Furthermore electrophysiological studies demonstrate that IL, but not PL, neurons selectively increased their firing rate to extinguished CSs (Milad and Quirk, 2002), although this has been recently challenged (Fitzgerald et al., 2014). Additionally, bursting activity of IL neurons during extinction learning predicts subsequent consolidation of extinction and IL stimulation during extinction learning enhanced extinction retrieval (Milad and Quirk, 2002, Milad et al., 2004, Vidal-Gonzalez et al., 2006, Burgos-Robles et al., 2007). A similar result was obtained when high frequency stimulation of the IL was applied before extinction training (Maroun et al., 2012) whereas low frequency stimulation of the same structure impaired consolidation of extinction

(Shehadi and Maroun, 2013). Finally, *in vitro* experiments performed on mPFC slices from previously conditioned or extinguished animals revealed that fear conditioning is associated with a decrease of the IL neurons intrinsic excitability and bursting activity whereas extinction behaviour is associated with an increase of these properties (Santini et al., 2008). Together these results suggest that extinction behaviour is associated with changes in the firing activity of IL pyramidal neurons.

The data mentioned above have been very useful in identifying the neuronal structures for fear encoding behaviour. However they do not provide an understanding of the precise mechanisms regulating the encoding of fear behaviour. In the near future it will be necessary to identify the cellular constituents and the precise connectivity of PL/IL neuronal circuits controlling fear behaviour and to monitor the changes in neuronal activity and coding strategies that occur in such circuits during the entire learning episode.

C/ Neuronal mechanisms of fear behaviour in prefrontal-amygdala circuits

As mentioned earlier, mPFC neuronal elements likely play a pivotal role in fear behaviour. However, the fear related processes and the neuronal mechanisms involved are still largely unknown. Most of the progress in the understanding of the cortical encoding of fear behaviour comes from studies reporting correlations between firing rates and behavioural outcomes (Quirk et al., 1997, Milad and Quirk, 2002, Burgos-Robles et al., 2009). This coding scheme is referred to as “rate coding” and can account for many aspects of neuronal coding in the brain. It implies that precise firing patterns of neurons are less important than their average firing rates, and that encoding results from changes in these average firing rates. However, in addition, neurons with different and specific firing sequences may cooperate and collectively provide information, which is referred to as “temporal coding” (Buzsaki and Chrobak, 1995, Nicolelis et al., 1995, MacLeod et al., 1998, Singer, 1999). In temporal coding, the precise timing of firing is important, while the average firing rates can remain the same following learning. Furthermore, this temporal organization of the firing sequences of different neurons leads to their transient and simultaneous activation in order to form a neuronal assembly. One obvious advantage of temporal coding is the plasticity it can support. Thus, neurons might rapidly shift between multiple networks according to sensory and internal inputs, a mechanism that strongly

enhances coding power. Importantly, temporal coding allows for the synchronization of spiking activity within and among neuronal circuits for the accurate transmission of information during behavioural responses. Indeed, synchronized inputs have a stronger impact on targeted neurons than unsynchronized ones (Singer, 1999, Salinas and Sejnowski, 2001, Varela et al., 2001, Buzsaki and Draguhn, 2004, Sakata et al., 2005, Womelsdorf and Fries, 2007). A necessary condition of temporal coding is a tight control of firing sequences. Brain oscillations are thought to be instrumental in temporal coding through binding cell assemblies, organizing individual firing into meaningful collective activity, and coordinating remote areas. A prominent property of cortical circuits is their capacity to sustain rhythmic activity, also referred as cortical oscillations. Cortical oscillations can be studied *in vivo* with local field potential (LFP) recordings that reflect current (i.e. ion) flow through plasma membranes, including synaptic currents, voltage-dependent membrane oscillations, and calcium spikes. Indeed, LFPs are thought to reflect the global ongoing activity in neuronal populations surrounding the recording electrode and are characterized by three principle properties: amplitude, frequency and phase (Buzsaki et al., 2012). LFP recordings provide a powerful tool to explore cortical activity at the level of population dynamics within and between brain regions. Cortical oscillations have been observed in different species, in multiple behavioural tasks, either related to the behavioural state or evoked by external stimuli (Siapas et al., 2005, Sirota et al., 2008, Peyrache et al., 2009, Benchenane et al., 2010). Coordinated oscillations could for instance increase synaptic strength, through coincident pre and post-synaptic activation and simultaneous convergence of multiple inputs (Markram et al., 1997, Buzsaki and Draguhn, 2004, Fell and Axmacher, 2011). In the past decade, many studies have shown that fear behaviour depends on the interaction between the mPFC and remote structures like the AMG. For instance, in the mPFC, following fear conditioning, coherent theta (3-12 Hz) oscillations between the mPFC and BLA during paradoxical sleep are positively correlated with fear memory consolidation (Popa et al., 2010). Directional analysis indicated that the BLA led this coordinated activity, in agreement with the potentiation observed in the BLA-mPFC pathway (Popa et al., 2010, Vouimba and Maroun, 2011). Similar analysis performed during extinction learning revealed decreased correlations between mPFC and hippocampal or BLA theta oscillations (Lesting et al., 2011). Interestingly, genetic knockout of the serotonin transporter led to both impaired extinction memory and persistent theta correlation between LA and IL during and after extinction (Narayanan et al.,

2011). Moreover, theta synchronization between the vHPC and the mPFC was recently shown to be enhanced during anxious behaviour (Adhikari et al., 2010, 2011). More recently, in an elegant study using a partial reinforcement learning task that confers resistance to extinction in monkey, Livneh & Paz (2012) observed that the synchronized firing of mPFC and amygdala neurons was correlated with resistance of fear extinction (Livneh and Paz, 2012), possibly by a potentiation of the mPFC-BLA pathway (Vouimba and Maroun, 2011). Interestingly, a recent study demonstrated that safety signaling was associated with theta synchronization (4-12Hz) between the mPFC and BLA (Likhtik et al., 2014). Indeed, in animals trained to discriminate an aversive (CS^+) from a safety (CS^-) CS, mPFC and BA LFPs synchronize in the theta frequency range (4-12 Hz). In contrast, animals displaying generalized fear behaviour to the CS^- did not exhibit increased LFP synchrony. Noteworthy, directionality analyses suggested that mPFC LFP oscillations precede BA oscillations during discriminative fear behaviour. Whereas these data did not address directly if mPFC and BLA neuronal oscillations were necessary for the formation of neuronal assemblies, they indicated the importance of oscillations within mPFC and BLA neuronal circuits for the selection of appropriate behavioural outputs. Finally, recent data using single unit recordings and optogenetic approaches, demonstrate that following fear conditioning, two mechanisms dependent on PV INs were necessary to drive fear responses: (i) a disinhibitory mechanism that increased the excitability of PL and ACC PNs projecting to BLA and (ii) a resetting of slow local oscillations in the theta range (8–12 Hz) that synchronizes prefrontal PNs to drive fear expression. These results were the first to demonstrate the dual role played by PV INs to coordinate and enhance the efficiency of prefrontal PNs to drive fear expression (Courtin et al., 2014). Together these findings suggest that neuronal synchrony between mPFC and BLA is a necessary mechanism to drive emotional behaviour. To date, however, it is unclear why this mPFC-BLA loop is necessary for fear expression/inhibition and whether or not different mPFC inputs to the BLA are involved. Additional studies will be required to dissect the principles that govern the encoding of fear behaviour in cortical areas (**Figure 7**).

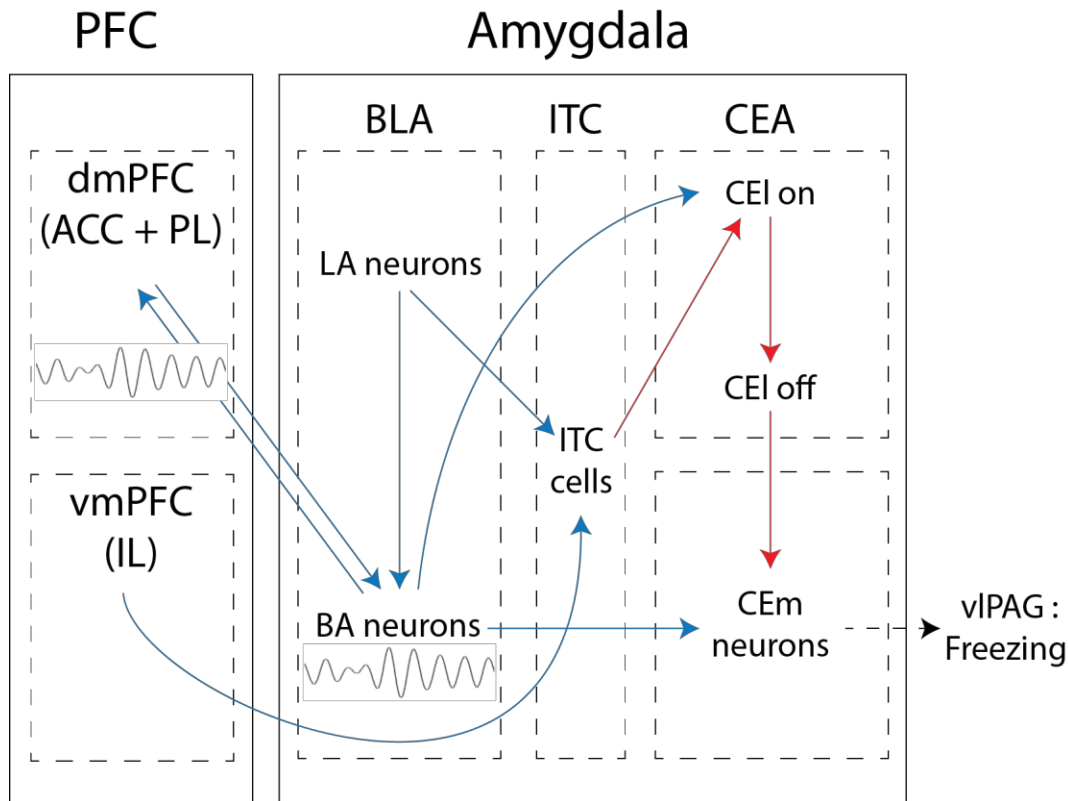


Figure 7: General organization of AMG and PFC circuitries. Scheme of the basic organization and overall flow of information's within the amygdaloid complex and PFC area. dmPFC neurons (ACC and PL) share reciprocal connections with BA neurons to drive fear responses while vmPFC neurons (IL cortex) share connection with ITC cells to reduce fear responses. Furthermore, neuronal synchrony between mPFC and BLA represented by oscillations is a necessary mechanism to drive emotional behaviour. Blue arrow represent glutamatergic neurons while red arrows GABAergic neurons. Dashed arrows represent external outputs.

III/ The periaqueductal gray matter: an interface between cortical and motor function

Responding adequately to events that threaten an animal's survival requires close interaction between sensory, autonomic and somatic/motor systems in order to generate appropriate integrated behavioural responses. In fact, several studies identified the PAG as the main midbrain output structure that drives autonomic and motor fear responses. For instance it has been demonstrated that the PAG is involved in a broad range of fear responses including analgesia (Reynolds, 1969, Besson and Chaouch, 1987), vocalizations (Jurgens and Pratt, 1979), cardiovascular control (Carrive and Bandler, 1991) and defensive reactions (Carrive, 1993, Lovick, 1993, Vianna et al., 2001, Vianna and Brandao, 2003). Due to the various inputs to the PAG from structures involved in fear behaviour (Floyd et al., 2000, Vianna and Brandao, 2003,

Vertes, 2004) and outputs to motor centers that can drive these behaviours (Vianna and Brandao, 2003), the PAG is considered as a hub for the integration and generation of fear responses, including motor responses (active (e.g. avoidance) and passive (e.g. freezing) fear reactions) along with autonomic fear responses (changes in arterial blood pressure, heart rate) and analgesia (Fardin et al., 1984a, b, Morgan et al., 1989, Behbehani, 1995, Butler and Finn, 2009, Heinricher et al., 2009). In this section, we will first review the gross anatomy of PAG and in a second step the studies, which emphasized a functional role of PAG circuits in motor conditioned fear responses.

A/ Gross anatomy of the periaqueductal grey matter

a/ Neuronal elements

The PAG is a structure of the tegmentum surrounding the cerebral aqueduct, which is well conserved across species. Despite the lack of clear cytoarchitectural and hodological criteria to delineate different PAG regions, based on functional data the PAG can be delineated in four distinct longitudinal columns from the dorsal to the ventral part which are: the dorsa-medial PAG (dPAG), the dorso-lateral PAG (dlPAG), the lateral PAG (lPAG) and the ventro-lateral PAG (vlPAG) (Beitz, 1985, Bandler and Keay, 1996). Beitz and colleagues were the first to describe the cellular organization within the PAG. They reported that PAG cells are randomly concentrically organized within the PAG with increase cell density around the aqueduct (Beitz and Shepard, 1985). Comparative studies of the PAG cellular morphology in rats, cats and monkeys revealed that this structure is composed of five different cell types with somata ranging from 10 μm to 45 μm . These studies described the presence of (i) fusiform neurons with one or several dendrites, (ii) multipolar neurons with a very large dendritic arborization, (iii) stellate cells, (iv) pyramidal cells with very diffuse dendritic arborization and (v) ependymal cells at the border of the cerebral aqueduct (Hamilton, 1973, Mantyh, 1982b, Beitz and Shepard, 1985). Although the PAG contains these five morphological different neuronal populations, there is to date no clear relation between cell morphology and neurotransmitter release. In fact, PAG neurons can released several neurotransmitters and neuromodulators such as acetylcholine, histamine, GABA, glutamate, serotonin (5-HT) and dopamine, but also various neuropeptides like enkephalin, substance P and neurotensin (Schmitt et al., 1986).

Since there is a vast literature on the involvement of PAG in processing pain function, I will summarize the key neuronal elements involved. Opioid and cannabinoid systems have been postulated to regulate pain related function at the cellular level. In the PAG it has been found that morphine acts through mu-opioid receptors (MOR), which are localized throughout the PAG. Furthermore, a recent study demonstrated that MOR and CB1 receptors co-localized in the PAG (Wilson-Poe et al., 2012) and can block pain responses by promoting analgesia (Basbaum and Fields, 1984). Additionally, recent set of studies demonstrate that MOR receptors are not only involved in the regulation of pain processing but also in signaling prediction error (McNally and Westbrook, 2006) (see section on PAG mechanisms for the encoding of fear and extinction memories below). Finally, a recent study demonstrated that dopaminergic neurons located at the border between the vPAG and the dorsal raphe mediate opiate anti-nociception potentially via an activation of downstream structure involved in analgesia (Meyer et al., 2009, Li et al., 2016).

b/ Inputs and outputs of the PAG

i/ Ascending pathway

Tracing experiments revealed that the PAG is highly interconnected with the hypothalamus nuclei, more specifically the anterior hypothalamic nucleus (AHN), the dorsomedial hypothalamus (DMH), the ventromedial hypothalamic nucleus (VMH) and the dorsal premammillary nucleus (PMD). These interconnections are consistent with the involvement of both structures in fear autonomic responses (Canteras and Swanson, 1992a, Canteras et al., 1994). More precisely, it has been described that the rostral dIPAG densely project to AHN and DMH, whereas other PAG regions project sparsely to hypothalamic nuclei. The PAG also receives differential inputs arising from hypothalamus nuclei. The AHN contacts strongly all PAG subdivisions, whereas VMH and PMD inputs contact massively only the posterior part of dIPAG.

The BLA and PAG also share connections through the CEA. These connections are direct and preferentially contact the vPAG (Rizvi et al., 1991, Herry et al., 2010). Recently a new study revealed a direct projection from CEI SST neurons to vPAG that are able to drive fear responses (Penzo et al., 2014). Finally, PAG shared reciprocal connections with different thalamic nuclei such as the medial and intralaminar nuclei (Kroust and Loewy, 2000), which have been involved in nociceptive transmission to higher cortical structures. Furthermore, all PAG subdivisions

project also to the nucleus reuniens with a clear higher density of projections for the caudal IPAG. PAG is also connected to many cortical areas including the mPFC (Mantyh, 1982a, Floyd et al., 2000). In particular, PL and ACC send massive projection to the IPAG and vIPAG whereas projections from the vmPFC reach mostly the dIPAG and vIPAG. Because of the diversity of projection sites from the dmPFC to many structures involved in fear behaviour, it is possible that specific subpopulation of dmPFC PNs can regulate PAG activity. In accordance with this statement, it has been shown that PFC PNs projecting to PAG are located in the deep layer V of the cortex whereas PFC PNs projection to BLA are located in the superficial layers II/III (Ferreira et al., 2015, Harris and Shepherd, 2015). Additionally, these studies also demonstrate that only a very small fraction of these two prefrontal populations overlap, suggesting that these two pathways are likely to modulate fear responses independently.

ii/ Descending pathway

As describe above, PAG is involved in many defensive responses and is thought to be a relay between cortical area and motor center. Notably, the PAG receives inputs from sensory neurons of the spinal cord dorsal horn and from the trigeminal nucleus (Holstege et al., 1996). In fact, spinal inputs to the PAG terminate in restricted regions within the PAG with a strong region-specific distribution pattern. Spinothalamic fibers originated from the lumbar system terminated mostly in the caudal vIPAG, while inputs from the cervical system ended mainly in the IPAG (Menetrey et al., 1982, Swett and Woolf, 1985, Herbert and Saper, 1992, Keay and Bandler, 1992, Keay et al., 1997). Furthermore, the vIPAG receives a dense innervation arising from the visceral afferent-recipient portion of the nucleus tractus solitarius (Bandler and Tork, 1987, Chen et al., 1995). All these inputs arising in the PAG are necessary for the transmission of the US information and more globally for the transmission of nociceptive information's. In turn, vIPAG and IPAG neurons project to the ventromedial and ventrolateral medullary region of spinal cord (Carrive et al., 1987, Bowman et al., 2013). Interestingly, the IPAG and vIPAG that have opposite function target the same ventromedial and ventrolateral medullary regions suggesting that these projections are either selectively excitatory or inhibitory, or target distinct neuronal populations within each area and can drive motor function (Fields et al., 1991, Verberne and Guyenet, 1992). Then dIPAG neurons does not project directly to the medulla, but innervate densely the cuneiforms nucleus (CNF), which is connected with the spinal cord (Mitchell et al., 1988, Redgrave et al., 1988) (**Figure 8**).

Even if a clear anatomical dissection of the pathway from the PAG to the medulla has been done, it is still not clear how nociceptive and motor pathways from the PAG to the medulla are segregated. In the future, additional work is required to dissect these pathways and to understand their interaction during fear behaviour.

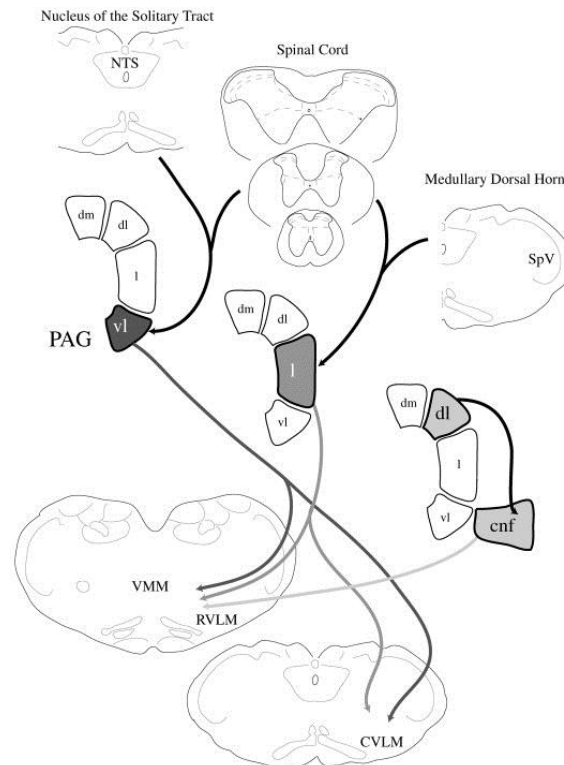


Figure 8: Schematic illustration of somatic and visceral afferents to different PAG neuronal columns (top half), and medullary projections arising from different PAG neuronal columns (bottom half). The vlPAG receives afferents from the spinal cord and the nucleus tractus solitarius (NTS), and projects to both the rostral and caudal ventromedial (VMM) and ventrolateral (VLM) medulla. The iPAG receives afferents from the spinal cord and the spinal trigeminal nucleus (SpV/medullary dorsal horn) and projects to both the rostral and caudal ventromedial and ventrolateral medulla. The dIPAG does not project directly to the medulla, but can influence the rostral ventromedial and ventrolateral medulla via a projection to the cuneiform nucleus (Adapted from Keay and Bandler 2001).

B/ Functional role of the PAG in fear behaviour

When facing a danger, mammals adapt their behavioural responses according to environmental contingencies, for instance adopting a motionless posture when the danger is far enough or an avoidance response when the threat is too close. The PAG is a good candidate for the selection of different fear behavioural strategies due to its connectivity with upstream structures involved in processing fear and downstream structures in regulating motor outputs. The

repertoire of fear responses can be conceptualized into passive or active coping strategies. Active coping strategies are evoked when the stressor is controllable or escapable and are behaviourally characterized by a confrontation to the danger, for instance fight responses to a predator or escape responses when animal is facing a danger. On the contrary, passive coping strategies are elicited when a stressor is inescapable and associated with immobilization and decrease responsiveness to the environment. It has been suggested that active and passive coping strategies are mediated by different neuronal pathways. In fact, active coping strategies are mediated by the hypothalamus projecting to the dlPAG/lPAG, whereas passive coping strategies are principally mediated by projections of the CEA to the vlPAG (Bandler and Shipley, 1994, Vianna et al., 2001). Although the neuronal circuits and mechanisms controlling active versus passive fear reactions will certainly become an important research topic in the coming years, in this introduction we will mainly concentrate on the role of the PAG in freezing-related behaviour. We invite the interested reader to reach recent research papers and review on this topic (Bandler et al., 1991, Depaulis et al., 1992, Behbehani, 1995, Bandler and Keay, 1996, Bernard and Bandler, 1998, Bandler et al., 2000, Vianna and Brandao, 2003).

a/ Involvement of the PAG in fear behaviour:

i/ Lesional and pharmacological studies:

The first evidence of the involvement of the PAG in mediating defensive behaviour was carried out by Bandler and colleagues who demonstrated that injection of excitatory amino acid (EAA) in the PAG induces rage-related responses (Bandler, 1982). In fact, injection of EAA in the dorsal intermediate PAG evoked vocalization and fight responses to an aggressor, whereas injections in the dorsal caudal PAG evoked flight responses (Carrive et al., 1987, Carrive et al., 1989). A study performed by the same group also demonstrated that when the EAA activation was made more ventrally in the caudal PAG it induced a decrease of both spontaneous locomotor activity and responsiveness to surrounding stimuli (Zhang et al., 1992). Several studies using microinjection of EEA, GABAergic antagonists or GABAergic agonists to manipulate PAG activity within different longitudinal columns obtained similar results. In particular, these studies revealed that the intermediate dlPAG/lPAG was involved in the fight process (defensive posture and rage) whereas the caudal dlPAG/lPAG was involved in the flight response. On the contrary,

the vIPAG has been involved in quiescence immobility (Sandner et al., 1979, Brandao et al., 1982, Hilton and Redfern, 1986, Carrive et al., 1989, Depaulis et al., 1992, 1994, Bandler and Keay, 1996). Furthermore, many pharmacological studies demonstrated that passive and active coping strategies are associated with specific autonomic changes, either an increase or decrease of autonomic and somatomotor activity after dlPAG/IPAG and vIPAG activation, respectively (Zhang et al., 1990, Bandler et al., 1991, Carrive and Bandler, 1991) (**Figure 9**).

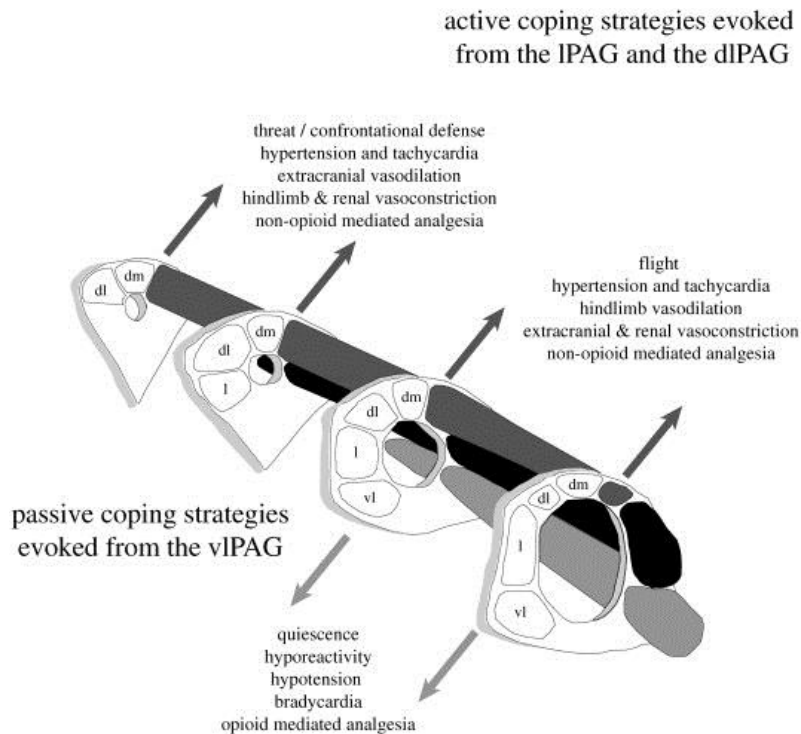


Figure 9: Schematic representation of the dorsomedial, dorsolateral, lateral and ventrolateral neuronal columns within (from left to right) the rostral PAG, the intermediate PAG and the caudal PAG. Evoked active and passive strategies, respectively, from the dl/IPAG (black color) and the vIPAG (grey color). Each of these strategies show specific somato-sensory evoked responses and differences in processes analgesia. (Adapted from Keay and Bandler 2001).

ii/ *Immunohistochemical studies:*

An early observation of IEG expression in the PAG following fear conditioned behaviour was reported by Beck and colleagues who demonstrated that after re-exposure to a context that had been previously associated with a footshock, there was an increase of c-fos expression in many structures involved in defensive fear behaviour, including the PAG (Beck and Fibiger, 1995). They demonstrated that this increase in c-fos expression could be abolished by pre-

treatment with anxiolytics (Beck and Fibiger, 1995). Similar studies replicated these findings but focusing on different sub-regions of the PAG. For instance, it was found that after contextual fear retrieval, there was a significant increase of IEG expression in the vIPAG compared to the dIPAG (Carrive et al., 1997, Izumi et al., 2006). Moreover, this specific activation of vIPAG neurons was dependent of the integrity of AMG outputs (Carrive et al., 2000, Rea et al., 2011). A numbers of studies also examined IEG expression after exposure to predator, a more naturalistic approach associated with innate fear behaviour. Rats exposed to a cat exhibited an increase of c-fos labelling relative to control in the intermediate dIPAG and the posterior vIPAG (Canteras and Goto, 1999, Comoli et al., 2003). A similar patterns of c-fos expression was also observed after electrical or chemical activation of the dIPAG but not the vIPAG, which was associated with freezing or escape behaviour (Sandkuhler and Herdegen, 1995). These data suggest a dual role of the PAG in the expression of defensive fear behaviour depending on the nature of the threat. In case of defensive responses elicited by natural predators, the dIPAG/IPAG was involved, whereas defensive responses induced by conditioned CS rely on the vIPAG.

Anatomically, the PAG receives dense inputs from different nuclei of the hypothalamus including the VMH and the PMD, which are involved in the expression of unconditioned defensive behaviour (Canteras and Swanson, 1992a, Canteras and Graeff, 2014). The first demonstration of the involvement of VMH nuclei came from studies combining anatomical tagging of VMH-PAG pathway and chemogenetic inactivation before the expression of different defensive behaviour. It was demonstrated that inactivation of VMH fibers projecting to the PAG using a hM4DI-DREADD based chemogenetic approach induced a selective decrease of unconditioned defensive responses to conditioned fear responses (Silva et al., 2013). Concerning the PMD, histochemical studies have indicated a key role of this structure in mediating defensive responses (Motta et al., 2009). For instance, inactivation of the PMD induced a decrease of defensive responses associated with an increase of c-fos expression in the dIPAG (Cezario et al., 2008).

iii/ Electrophysiological studies

As compared to standard approaches described above, there are only few studies, which investigated PAG functions using *in vivo* electrophysiological techniques. As described previously, the PAG receives massive inputs from the CEA and the first electrophysiological

evidence of a role of the CEA-PAG pathway in defensive behaviour came from antidromic/orthodromic stimulation experiments. Using electrical stimulations of the mesencephalic axon bundle which contains fibers from the CEA contacting the PAG (Pascoe and Kapp, 1985), Ciocchi et al, demonstrated that CEM neurons activated during CS-induced freezing behaviour project to the PAG (Ciocchi et al., 2010). More recently, using optogenetic approaches, a subclass of GABAergic interneurons in the CEI expressing somatostatin (SST INs), was shown to directly modulate fear behaviour through projection to the PAG (Li et al., 2013, Penzo et al., 2014). In these studies, the authors observed that the optogenetic inhibition of SST CEI neurons decreased fear expression whereas their activation drove unconditioned fear behaviour. Although, these studies identified key circuits within the CEA projecting to the PAG and involved in fear behaviour, it remains unclear how these two circuits cooperate and/or interact during fear expression and modulate PAG activity.

iv/ PAG mechanisms for the encoding of fear and extinction memories

It is well accepted that the formation of conditioned fear memories requires the co-occurrence of a CS and a US to mediate synaptic plasticity in the BLA. While it has been documented that aversive US information reach the BLA through the PIN (Shi and Davis, 1999), recent evidences also indicate a role of the PAG as a potential relay for aversive instructive signals to the amygdala. First, the PAG receives strong nociceptive inputs from the spinal and trigeminal dorsal horn (Holstege et al., 1996). Second, the association between an auditory CS with an electrical stimulation of the PAG in the absence of an aversive US is sufficient to induce fear learning, and this is dependent on the activity of BLA neurons (Di Scala et al., 1987, Kim et al., 2013). Last, inactivation of the PAG reduced shock-evoked responding in BLA neurons and the acquisition of fear learning (Johansen et al., 2010). Together these data clearly suggest a role of the PAG in encoding fear memories although the underlying neuronal mechanisms are unknown. Interestingly, prediction error coding has been observed in PAG neurons (Johansen et al., 2010), suggesting the existence of aversive US instructive signals generated in the PAG. Converging evidence also suggested the involvement of the vLPAG, more precisely the MOR receptors in driving prediction error signals during extinction learning (McNally and Westbrook, 2006). In fact, intra-vLPAG injection of the non-selective opioid receptor antagonist naloxone or the selective MOR antagonist (CTAP) impairs the acquisition of fear extinction (McNally et al.,

2004, McNally et al., 2005). In contrast, injection of an inhibitor of enkephalin-degradating enzymes (RB101) that induce an increase of the concentration of opioid molecules within the PAG, enhanced extinction acquisition (McNally, 2005). Based on these observation it has been postulated that the vlPAG, through MOR, is necessary to drive the acquisition of fear extinction (McNally and Westbrook, 2006). Altogether, the anatomical and functional data described above clearly indicate a key role of the PAG in the encoding and expression of conditioned fear behaviour. Moreover it is very likely that cortical and subcortical structures involved in conditioned fear behaviour such as the PFC and BLA directly modulate PAG activity to control fear responses. Furthermore, circuit-based models of anxiety disorders suggest that abnormal activity in the BLA and the PFC is associated with inappropriate regulation of fear responses. These findings might suggest that the coordination between the BLA, the PFC and the PAG is a prerequisite for driving adapted fear behaviour (**Figure 10**).

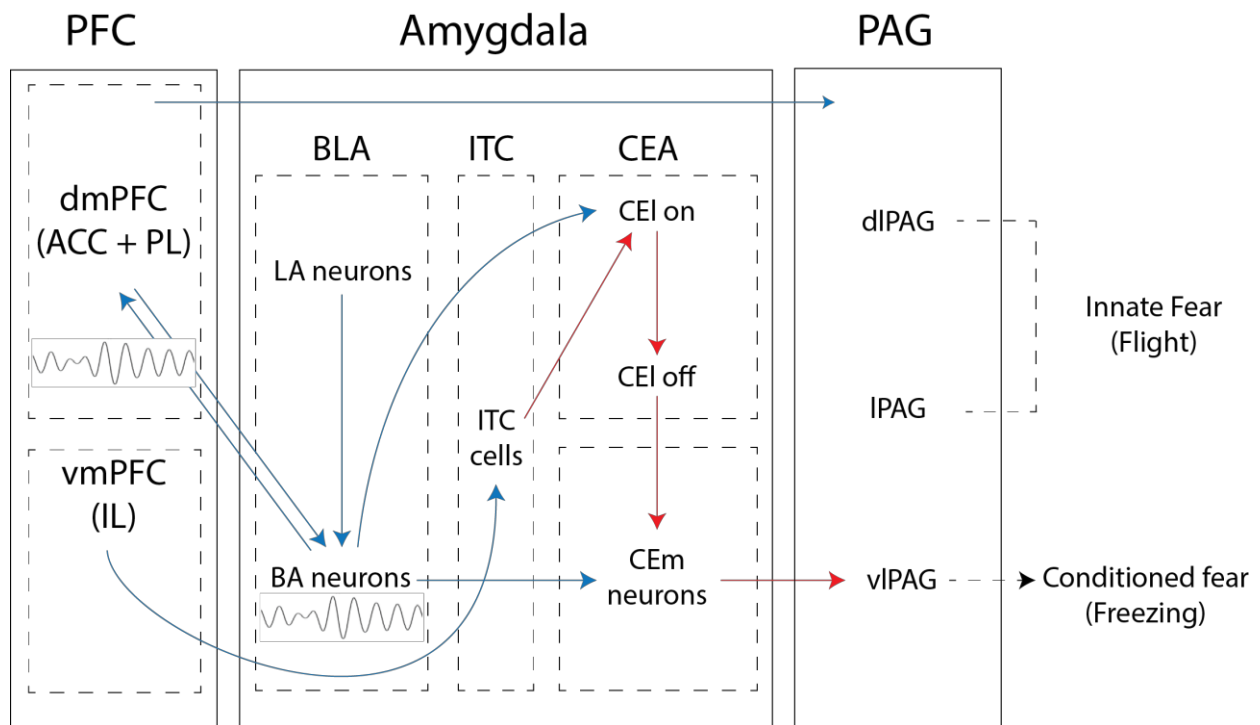


Figure 10: General organization of the tripartite circuit composed of the AMG, PFC and PAG. Scheme of the basic organization and overall flow of information's between the amygdaloid complex, PFC and PAG. Subdivisions of PAG are involved in the mediation of active coping strategy (dIPAG and IPAG) or in passive coping strategy (vlPAG). dmPFC neurons (ACC and PL) share connection with BA neurons and PAG where it can modulate fear responses. This scheme suggests that coordination between these 3 structures involved in fear response is a prerequisite to drive fear responses. Blue arrow represent glutamatergic neurons while red arrows GABAergic neurons. Dashed arrows represent external outputs.

Aim of the thesis:

Although the introductory sections above indicate that the role of the entire brain areas such as the AMG, mPFC and PAG in fear behaviour is reasonably well understood at the molecular and synaptic levels, there is a big gap in our knowledge of how fear behaviour is controlled at the level of defined circuits within these brain areas. More particularly, whereas the mPFC densely project to both the BLA and PAG, the contributions of these two projections pathway during fear behaviour are largely unknown. Beside the involvement of these neuronal pathways in the transmission of fear related-information, the neuronal mechanisms involved in the encoding of fear behaviour within these pathways are also virtually unknown. In this context, the present thesis work had two main objectives. First, evaluate the contribution of the mPFC-BLA and mPFC-vIPAG pathways in the regulation of fear behaviour, and second, identify the neuronal mechanisms controlling fear expression in these circuits. To achieve these goals, we used a combination of single unit and local field potential recordings coupled to optogenetic approaches in behaving animals submitted to a discriminative fear conditioning paradigm.

Material and method:

I/ Animal

Male C57BL6/J mice (3 months old, Janvier), PV-IRES-Cre mice (3 months old, Jackson Labs, B6;129P2-Pvalb^{tm1(cre)Arbr/J}) and SST-IRES-Cre mice (3 months old, Jackson Labs, SST^{tm2.1(cre)Zjh/J}) were individually housed for at least 7 days prior to all experiments, under a 12 h light/dark cycle, and provided with food and water *ad libitum*. Experiments were performed during the light phase. All procedures were performed in accordance with standard ethical guidelines (European Communities Directive 86/60-EEC) and were approved by the committee on Animal Health and Care of Institut National de la Santé et de la Recherche Médicale and French Ministry of Agriculture and Forestry (authorization A3312001).

II/ Behavioural paradigm and protocol:

A/ Behavioural paradigm used during single unit recordings:

* Discriminative cued fear conditioning

Habituation (HB) and fear conditioning (FC) took place in context A consisting of a square transparent plexiglas box (25cm side, 80 cm high) with a shock grid floor made of stainless steel rods placed inside a sound attenuating and temperature regulated cubicle. The walls of the cubicle were made of sound attenuating white foam. Inside the cubicle the floor and walls of the plexiglas square were cleaned with a 70 % ethanol solution before and after each session. Fear retrieval was performed in context B consisting of a cylinder transparent plexiglas (25 cm diameter, 40 cm high) with a grey plastic floor placed inside a sound attenuating and temperature regulated cubicle. The walls of the cubicle were made of sound attenuating black foam. The floor and walls of the plexiglas cylinder were cleaned with a 1 % acetic acid solution before and after each session. To score freezing behaviour independently of the experimenter, an automated infrared beam detection system located on the bottom of the experimental chambers was used (Coulbourn Instruments). Because the detection of our dependent variable (freezing) was independent of the experimenter, we did not use a blinding process for group allocation or behaviour scoring. The animals were considered to be freezing if no movement was detected for

at least 2 s. On day 1, mice were submitted to an HB session in context A, in which they received 4 presentations of the CS⁺ and CS⁻ (total CS duration: 30 s, consisting of 27, 50 ms pips repeated at 0.9 Hz, 2 ms rise and fall, pip frequency: respectively 7.5 kHz or white-noise, 80 dB sound pressure level). Discriminative FC was performed on the same day by pairing the CS⁺ with a US (1 s foot-shock, 0.6 mA, 5 CS⁺/US pairings; inter-trial intervals: 20-180 s). The onset of the US coincided with the offset of the CS⁺. The CS⁻ was presented after each CS⁺/US association but was never reinforced (5 CS⁻ presentations, inter-trial intervals: 20-180 s). The frequencies used for CS⁺ and CS⁻ were counterbalanced across animals. On day 2, conditioned mice were submitted to retrieval training in context B during which they received 4 and 12 presentations of the CS⁻ and CS⁺, respectively (**Figure 11**).

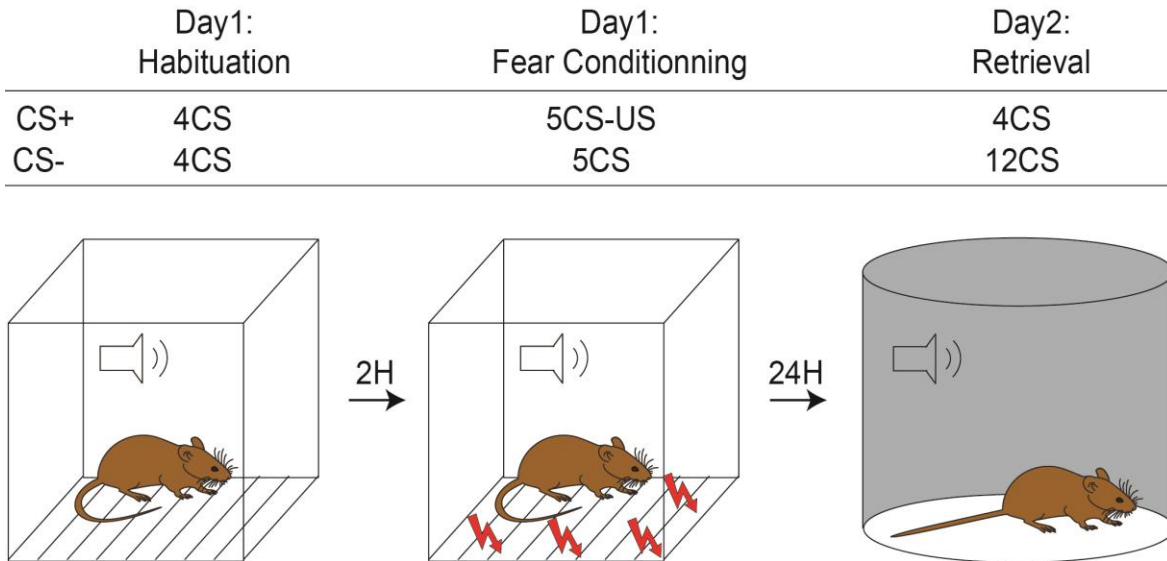


Figure 11: Discriminative auditory fear behaviour protocol used. Mice were submitted to an habituation session in context A where they receive 4 presentations of the CS⁻ and CS⁺ tones. 2h later mice were submitted to the fear conditioning session during which one of the tones (the CS⁺) was paired with a mild footshock while the second tone was not (the CS⁻). Fear retrieval was assessed 24 h later in a different context during which mice received 4 and 12 presentations of the CS⁻ and CS⁺ respectively.

***Contextual fear conditioning**

Contextual fear conditioning took place in contexts A and B as describe above. On day 1, C57BL6/J mice were subjected for 5 min to a HB session in context A. Contextual FC was performed 24 h later by pairing context B with a US. The next day, mice were subjected for 12 min to a testing session (retrieval session) in context B.

B/ Optogenetic manipulations:

For optogenetic experiments using channelrhodopsin, PV-IRES-Cre mice and GFP controls were exposed on day 1 to context A as described above. During the session, four blue-light 4-Hz rhythmic analog (2 or 10 mW, 30 s) stimulations were delivered in the dmPFC to activate PV-expressing INs. On days 2 and 3, mice were exposed to the same context as day 1 or to the neutral context B as described above, without any stimulation, respectively. To test for the frequency and structure specificity of the stimulation, other groups of naive PV-IRES-Cre mice were submitted to four blue-light rhythmic analog dmPFC stimulations at different frequencies (1, 8, 10 and 12 Hz, stochastic 4 Hz composed of 2–12 Hz frequency with an average at 4 Hz, 10 mW, 30 s) or to four blue-light rhythmic analog stimulations at 4 Hz of the motor cortex or the BLA. Randomization of group allocation (ChR2 versus GFP controls) was performed using an online randomization algorithm.

For optogenetic experiments using C57BL6/J mice infected with archeorhodopsin or GFP and targeting the dmPFC-vIPAG PNs, mice were exposed on day 1 to the context A as described above. During the stimulation session, 4 continuous yellow-light stimulations (10 mW, 30 s) were delivered in the dmPFC at the level of somata. On day 2, mice were exposed to the same context A and submitted to the HB and FC session as describe above. On day 3, a retrieval session were performed on the neutral context B and consisted of 4 presentations of the CS⁻ alone followed by 4 presentations of the CS⁺ alone, then 4 presentation of CS⁺ coupled to continuous yellow-light stimulations (4 time 30s light pulse at 10mW) and then 4 presentation of CS⁺ without any stimulation.

C/ Pharmacological experiments:

For pharmacological experiments, C57BL6/J mice were submitted to a FC paradigm consisting of CS⁺ and US pairings in context A as described above. On days 2, 3 and 4, conditioned mice were tested in context B, during which they received four presentations of the CS⁺ after muscimol bodipy control injections (day 2, test 1), 5 min after muscimol injections (day 3, Inac.) and 24 h after muscimol bodipy control injections (day 4, test 2). Six naive C57BL6/J mice were included in this experiment and the data collected in two distinct replicates.

III/ Surgery and recording

Mice were anesthetized with isoflurane (induction 3%, maintenance 1.5%) in O₂. Body temperature was maintained at 37 °C with a temperature controller system (FHC). Mice were secured in a stereotaxic koft frame. For dmPFC recordings mice were unilaterally implanted in the left dmPFC with a multi-wire electrode array or optrode (electrode plus optics fiber) aimed at the following coordinates (Franklin and Paxinos, 1997): 2 mm anterior to bregma; 0.37 mm lateral to the midline and 1 to 1.8 mm ventral to the cortical surface. Subsets of animals were additionally implanted in the left basolateral amygdala (BLA) with a multi-wire electrode array aimed at the following coordinates: 1.4 mm posterior to the bregma, 3.2 mm lateral to the midline and 4.3 mm ventral to the cortical surface. For vIPAG recordings, animals were implanted with a multi-wire electrode array aimed at the following coordinates (Franklin and Paxinos, 1997): -4.3 mm anterior to bregma; 0.55 mm lateral to the midline and 2.2 mm ventral to the cortical surface. The electrodes consisted of 16 individually insulated nichrome wires (13 µm inner diameter, impedance 30-100 KΩ; Kanthal) contained in a 26 gauge stainless steel guide cannula. The wires were attached to an 18 pin connector (Omnetics). For mice that received dmPFC and BLA multi-wire implants, two connectors were used. All implants were secured using Super-Bond cement (Sun Medical). After surgery mice were allowed to recover for 7 days and were habituated to handling. Analgesia was applied before, and 1 day after surgery (Metacam, Boehringer). Electrodes were connected to a headstage (Plexon) containing sixteen unity-gain operational amplifiers. The headstage was connected to a 16-channel preamplifier (gain 100 x, bandpass filter from 150 Hz to 9 kHz for unit activity and from 0.7 Hz to 170 Hz for field potentials, Plexon). Spiking activity was digitized at 40 kHz and bandpass filtered from 250 Hz to 8 kHz, and isolated by time-amplitude window discrimination and template matching using a Multichannel Acquisition Processor system (MAP Plexon system). At the end of the experiment, recording sites were marked with electrolytic lesions at the upper and downer electrode (electrolytic stimulation: 10 mA during 7s) before perfusion, and electrode tips locations were reconstructed with standard histological techniques. For electromyographic (EMG) recording experiments, Teflon-coated stainless steel electrodes (AM Systems) were sutured into the right and left nuchal muscles. Wires were connected to a multi-wire electrode array connector attached to the skull.

For pharmacological experiment, six mice were unilaterally implanted with stainless steel guide cannula (26 gauge; Plastics One) aimed at the medial septum (MS) at the following

coordinates (Franklin and Paxinos, 1997): 1 mm anterior to bregma; 0.7 mm lateral to midline and 3 to 3.3 mm ventral to the cortical surface with an angle of 10° in the coronal plane. Recording electrodes were also implanted in the dmPFC at the same coordinates described above and the dHPC at the following coordinates (Franklin and Paxinos, 1997): 2 mm anterior to bregma; 1.2 mm lateral to midline and 1.2 to 1.4 mm ventral to the cortical surface. The cannula and recording electrodes were secured using Super-Bond cement (Sun Medical). On the injection day, muscimol (Muscimol-Bodipy-TMR-X conjugate, Invitrogen; 0.8 mM in PBS 0.1 M) was infused at a rate of 0.2 μ L/min during 2 min (total volume of 0.4 μ L) 15 minutes before the behaviour. After the end of the experiment, muscimol was again infused with the same parameters to control for the drug diffusion within the medial septum. Brains were collected for histological analyses as described in the anatomical analysis section below.

IV/ Single unit analysis

Single-unit spike sorting was performed using Off-Line Spike Sorter (OFSS, Plexon) for all behavioural sessions. Principal component (PC) scores, peak to valley and normalized energy were calculated for unsorted waveforms and plotted in a 3D space; clusters containing similar valid waveforms were manually defined. A group of waveforms were considered to be generated from a single neuron if the waveforms formed a discrete, isolated, cluster in the 3D space, did not contain a refractory period less than 1 ms as assessed by using auto-correlogram analyses and if significantly separated from the noise cluster (**Figure 12**).

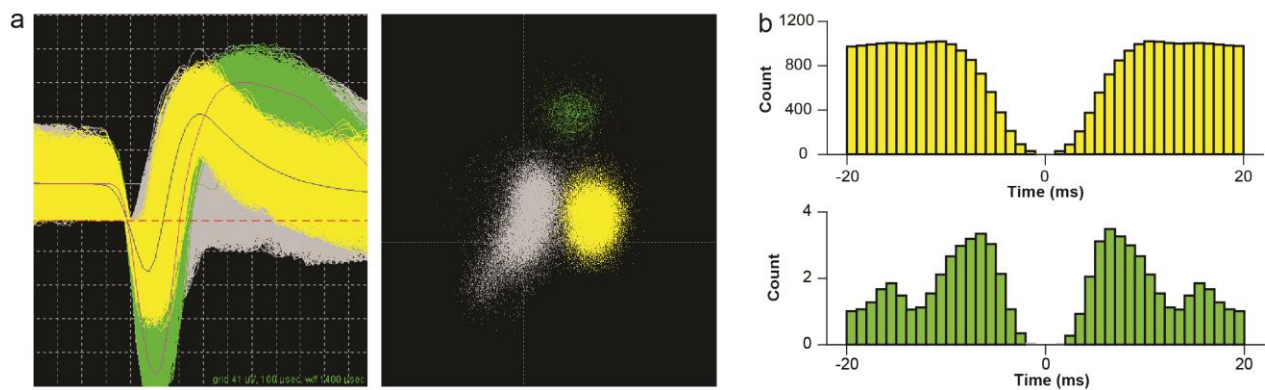


Figure 12: Separation of putative pyramidal neurons and putative interneurons. a, Left: superimposed waveforms recorded from 2 different units. Right: Spikes originating from individual units were sorted using 2D-principal component analysis. b, Corresponding auto-correlograms displaying clear refractory periods.

To avoid analysis of the same neuron recorded on different channels, we computed cross-correlation histograms. If a target neuron presented a peak of activity at a time that the reference neuron fired, only one of the two neurons was considered for further analysis. For neurons that were potentially recorded throughout different behavioural session or throughout anesthesia (see section “extracellular stimulation”) we compute a correlation coefficient between the waveforms and considered it as the same if the correlation coefficient is higher than 95%. However after FC, if the same neuron was sequentially recorded during different behavioural sessions, we considered only the first behavioural session in which it was recorded. To separate putative INs from putative PNs, we used an unsupervised clustering algorithm based on Ward’s method. In brief, the Euclidian distance was calculated between all neuron pairs on the basis of the three-dimensional space defined by each neuron’s average half-spike width (measured from trough to peak), the firing rate and the area under the hyperpolarization phase of the spike. An iterative agglomerative procedure was then used to combine neurons into groups based on the matrix of distances such that the total number of groups was reduced to give the smallest possible increase in within-group sum of squares deviation.

For the detection of interactions between units recorded in the dmPFC and BLA, the spike trains of each simultaneously recorded pair were binned (10 ms bin size), the cross-correlation of the binned histograms was calculated over multiple lags (maximum lag, ± 500 ms) and the peak cross-correlation coefficient for each pair was determined. For the detection of co-firing property for unit pairs, spike trains were binned as before and the co-firing index was calculated as the ratio of co-occurring (common) spikes to the total number of spikes for the two units. This provides a simple yet direct measure of the co-occurrence of unit spikes on multiple levels of temporal resolution. For the determination of the bin size and the robustness of the method, different bin sizes were tested; they all gave qualitatively similar results. Among those tested, 10 ms was selected because it allows the identification of potentially monosynaptic interactions. To evaluate whether neurons were oscillating at 4 Hz, we used Gabor functions, which are commonly used to fit autocorrelation (AC) histograms of nonstationary rhythmic biological time series such as neuronal spiking activity. Gabor functions are damped sine waves with two components: first, the sine wave frequency (f_0); second, a damping frequency (f_d) that modulates the amplitude of the sine wave. The Gabor functions served as a predicted AC (pAC) that was used to fit the actual AC of the frequencies of interest. We constructed a set of Gabor functions as

follows: $pAC_{f_0f_d} = \cos(2\pi * x * f_0) * \exp(C * x^2 * f_d)$ with f_0 and f_d both ranging from 1 to 25 Hz, hence creating 100×100 predicted ACs. The quality of the fit of each predicted AC was then assessed by its correlation (Spearman's ρ) with the actual AC of specific frequency bands (calculated for lags t of 0–500 ms), and this correlation score was plotted for each f_0, f_d pair. Points showing the highest correlation thus represent candidate f_0, f_d pairs capable of predicting oscillations.

Freezing-evoked activity of recorded neurons was calculated by comparing the firing rate during freezing episode with the one during non-freezing episodes, 2 s before stimulus onset or after stimulus offset (bin size: 100 ms) via a z -score transformation. Z -score values were calculated by subtracting the average baseline firing rate established over the 2 s during non-freezing episodes from individual raw values and by dividing the difference by the baseline standard deviation. A color representation of the peristimulus time histogram (PSTH) (heatmap) was used to reveal the increase activity with warm colors and decrease activity with cold colors. Furthermore, a rate histogram in time (0 to 740s) was computed (bin size 5s) to look at the change of activity in frequency induce by freezing episode (black bar) inside or outside CS presentation (pink and blue bar) during the retrieval session. In order to identify the main pattern of freezing-evoked activity among PNs, we used an unbiased receiving operator curve (ROC) analysis during the retrieval session. Only spiking activity from 0 to 740 s was considered to avoid neuronal activity associated within extinction session. To evaluate if dmPFC neurons were differently active during freezing and non-freezing periods the ROC analysis was performed to compare the two distributions of firing rates obtained by dividing the behavioral session into periods of 2s by estimating the discrimination power of an ideal observer. The ROC analysis presents the advantage over other evaluations of classifier accuracy of being insensitive to class distribution, that is the respective number of freezing and non-freezing bins in our case which can often be strongly skewed depending on the behavior of the animal. In our case, discriminating consists in placing a threshold (z) on spiking activity (r) below which the corresponding bin is classified as 'freezing' and above which it is classified as 'non-freezing'. The performance of this procedure can be fully determined by two parameters:

$$\alpha(z) = P(r > z | FR) , \text{ size or false alarm rate}$$

$$\beta(z) = P(r > z | NOFR), \text{ power or hit rate}$$

Plotting α and β for increasing values of z yields the ROC curve that moves from the point $\alpha=1$, $\beta=1$ when z is 0 because the ideal observer using this threshold will always classify non-freezing periods as non-freezing but all freezing periods also as non-freezing to $\alpha=0$, $\beta=0$ when z is infinite. Between these extremes the ROC curve describes the evolution of these two parameters depending on z . The area under the ROC curve (ROC value) represents the probability that an ideal observer can discriminate between a 2s period of freezing or no freezing based on the firing rate of the neuron at that time and therefore the firing rate of this neuron carries information about whether the animal is freezing or not if this value is significantly different from 0.5. This analysis allows defining population of neurons that present similar significant evoked-freezing activity (increase, decrease or no change).

CS-induced neural activity of recorded neurons was calculated by comparing the firing rate after stimulus onset with the firing rate recorded during the 500 ms before stimulus onset (bin size: 10 ms) using a z -score transformation. Z -score values were calculated by subtracting the average baseline firing rate established over the 500 ms preceding stimulus onset from individual raw values and by dividing the difference by the baseline standard deviation.

To identify the main firing patterns among vIPAG neurons, we used an unbiased principal component analysis (PCA) based on the neuronal activity evoked by freezing (z -score 2 before freezing onset and after, bin size 100ms, during retrieval session). This analysis allows to identify different patterns in a dataset, and express the data in such a way that it highlights their similarities and differences. Only the first PC was considered (PC1) because it explained most of the variance of our dataset. Freezing-activated and freezing inhibited vIPAG neurons were defined as correlated and inversely correlated with PC1 at the $P < 0.05$ significance level.

V/ Field potential analysis

Local field potentials were analyzed using custom-written Matlab programs. Raw LFP traces were filtered between 0.7 Hz and 400 Hz and downsampled to 1 kHz. All signals were filtered using zero-phase-distortion sixth-order Butterworth filters. For phase analyses, the signal was filtered in the desired frequency band (2–6 Hz for the 4-Hz oscillation) and the complex-valued analytic signal was calculated using the Hilbert transform as below: $\rho(t)e^{i\phi(t)}$. The vector length and the arctangent of the vector angle provide the estimation of the instantaneous

amplitude and instantaneous phase of the signal, respectively, at every time point. All analyses were performed during freezing episodes and, where indicated, during subsampled non-freezing epochs. A phase of 0° corresponds to the peak of prefrontal–amygdala oscillations. LFP power spectrum and LFP–LFP coherence estimations were, unless otherwise noted, performed using the multitaper method. Briefly, data were multiplied by a set of 2–5 orthogonal taper functions, Fourier transformed using a window size of 2 s and averaged to obtain a direct multitaper spectral estimate.

Signal to noise ratio (SNR) for 4-Hz power was calculated as the ratio of the mean power in the 2–6 Hz band to the mean power outside this band. Because one mouse did not show immobility behaviour during habituation, it was excluded from SNR analyses. For coherence analyses, a method based on imaginary coherence was employed. Imaginary coherence was calculated as $iCoh = \frac{Im(\sum_{bins} S_{xy})}{\sqrt{\sum_{bins}(S_{xx}) * \sum_{bins}(S_{yy})}}$ where S_{xy} is the cross-spectrum, S_{xx} and S_{yy} are the

auto-spectra and summation takes place over the spectrogram bins corresponding to the quantified state. By keeping the imaginary part of the normalized cross-spectrum, coherence value is weighted inversely proportionally to the time lag between the two signals. Consequently, it is sensitive only to time-lagged signals, whereas the effect of absolutely synchronous signals is eliminated. Given the very synchronous nature of the oscillation examined here and the small phase lag, imaginary coherence is expected to underestimate the strength of the interaction. However, we opted for this conservative variety of coherence analysis to avoid any influence of volume-conducted currents or artifacts that can artificially boost coherence values.

To investigate any potential causal interaction between the oscillations recorded in the two structures, spectrally resolved Granger causality was calculated for the unfiltered LFP signals. Granger causality is a statistical measure of the predictive power of one variable over another. Linear trends were removed from the LFP signals and signals were normalized before the analysis. For these analyses, the MVGC multivariate Granger causality toolbox was used to fit a higher order vector autoregressive model to the processes. Data were tested for stability in time and model order was determined using the Akaike information criterion. To identify directionality and quantify the lag between the two signals in terms of phase and amplitude, a point process was defined consisting of the peaks of the bandpass-filtered LFP signal for each of the two structures. The lag of the peak of the cross-correlation of these point processes identifies

the time lag of the oscillation in the two structures and the directionality of their potential interaction. To avoid any potential bias due to phase asymmetry, the same procedure was tested for the troughs, giving identical results. To investigate this relationship throughout the oscillation cycle, the phase of each analytical signal was extracted using the Hilbert transform and the distribution of the phase differences between the two structures was characterized for deviation from uniformity using circular statistics and Monte Carlo simulations. To evaluate the specific role of phase, amplitude and their interplay on the directionality and causality measures for the LFP data, a procedure was devised for the selective perturbation of phase and amplitude of the signals. Signals were converted in the spectral domain using a discrete Fourier transform and the phase (or amplitude) component of the signal was permuted, leaving the amplitude (or phase) intact. The modified signal was converted back to the time domain using the inverse Fourier transform. For the power co-modulation analysis, the power profile for each frequency bin in each structure was calculated and the correlation coefficient of every pair was calculated.

To compare the impact of CS⁺ during freezing on local theta and 4 Hz phase resetting, we used a multitaper analysis of LFP signals for frequencies ranging from 2 to 12 Hz and computed a stimulus-triggered spectrogram. For the CS⁺-triggered theta and 4 Hz phase overlays, signals were filtered in the corresponding range (theta, 8–12 Hz; 4 Hz, 2–6 Hz) and phases were extracted from the analytic signal as described above. To quantify phase stability across all CS⁺ pips during freezing episodes, we calculated the mean resultant length for all time–frequency pairs. To evaluate the predictive value of 4 Hz power for freezing behaviour, we used wavelet analysis, which in some instances allows a higher temporal resolution, to quantify the spectral content of the signal for frequencies between 2 and 12 Hz and computed freezing-triggered spectrograms. To evaluate the latency to freeze in response to the CS⁺, individual tone onsets and freezing period onsets for individual mice were binned (100 ms bin size), smoothed and averaged, and cross-correlation analysis was performed on these data taking freezing onset epochs as the reference event. In these conditions, negative lags indicate that conditioned stimuli precede freezing events. Statistical significance was evaluated using two different approaches and then combined. We first simulated 1,000 instances of a uniform distribution of freezing episodes and recomputed the cross-correlation analysis. We next shuffled 1,000 times the freezing ISIs of the actual freezing episodes to preserve the first-order statistics of freezing behaviour but perturb

its relation to CS⁺ and recomputed the cross-correlation analysis. The results of the two analyses were averaged to produce a more robust significance threshold.

For correlation analyses between freezing behaviour and 4 Hz oscillations, we first evaluated the percentage of time individual animals spent frozen during the entire recording session. For 4 Hz quantification, 4 Hz oscillation periods were evaluated as periods of significant 4 Hz SNR, as compared to baseline (a 2-min period before the first CS presentation). 4 Hz expressed as the percentage of total time corresponds to the ratio of the total duration of 4 Hz episodes to the recording session duration. For electromyographic recordings, unilateral EMG signals were band-pass filtered (100–1,000 Hz), rectified and integrated (convolution with 100-ms Gaussian kernel). The Δ EMG signal was calculated as the differential EMG recorded in the left and right nuchal muscle. The absolute value of Δ EMG was then Z-score transformed and averaged around freezing onsets (–500 ms to 500 ms) occurring during CS⁺ presentation, during both habituation and fear conditioning.

VI/ Phase locking

For phase modulation analysis, the variance-stabilized $\ln(Z)$ ($Z = R^2/n$, R being the resultant length and n the sample size) statistics for the Rayleigh test for uniformity against the von Mises distribution were calculated. To partially account for the sample size bias of the resultant length, only units with at least 100 spikes during freezing behaviour were taken into consideration. All results were corroborated using the pairwise phase consistency method, a bias-free estimate of neuronal synchronization based on the average pairwise circular distance $D = \frac{2}{N(N-1)} \sum_{i=1}^{N-1} \sum_{j=(i+1)}^N |\theta_i - \theta_j| \bmod \pi$, with θ_i and θ_j being the phases from two different spikes. This method is analytically equivalent to the squared phase-locking value. To calculate the statistics for each unit, bootstrap analyses and Monte Carlo simulations were performed. In the Monte Carlo simulations, the Y_{sim} value, indicating the expected value for a uniform prior distribution, was calculated for each sample size. Units for which the Y_{unit} exceeded the 95% percentile of the simulated Y_{sim} estimate were considered phase-locked. For the bootstrap statistics, in order to take into account the higher-order statistics of the spike trains, for each unit the inter-spike intervals were shuffled randomly and the potentially non-uniform prior distribution was calculated.

Phases for both dmPFC and BLA spikes were extracted using the dmPFC 4-Hz oscillation phase that exhibits the highest SNR and allows direct comparison of the phase-locking statistics. For the statistical evaluations, before the phase extraction, the prior distribution of phases of the 4 Hz oscillation was examined, and, as is the case for other neuronal slow oscillations, this prior distribution deviated from the uniform distribution. This bias can alter the phase-locking statistics and produce false positives. To account for this potential bias, the phases of the LFPs were transformed using the inverse of the empirical cumulative density function to return a signal with uniform prior distribution. Following this transformation, the spike phases were drawn from a uniform distribution, allowing the application of circular statistics for detecting deviations from uniformity. For normalized averaged phase density analyses, the circular histogram for each neuron was normalized to the maximum and the averaged circular histogram was computed.

VII/ Virus injections and optogenetics

For optical identification of PV-expressing INs or SST-expressing INs, conditional AAV encoding ChR2 (AAV-EF1a-DIO-hChR2(H134R)-EYFP, serotype 5, Vector Core, University of North Carolina) or ArchT (AAV-FLEX-ArchT-GFP, serotype 5, Vector Core, University of North Carolina) were bilaterally injected into the dmPFC of PV-IRES-Cre mice or SST-IRES-Cre mice from glass pipettes (WPI, 1B150F-4, tip diameter 10–20 μm) connected to a Picospritzer (Parker Hannifin Corporation; approximately 0.4 μL per hemisphere). Also, for optical identification of dmPFC-vIPAG PNs, conditional AAV encoding ArchT (AAV-FLEX-ArchT-GFP, serotype 5, Vector Core, University of North Carolina) were bilaterally injected into the dmPFC and a canine adenovirus type 2 that was kindly provided by Dr. E. Kremer (Cav-2, University of Montpellier, France) were injected at the level of vIPAG in C57BL6/J mice. Two weeks after the injection, mice were implanted bilaterally with optic fibers (diameter, 200 μm ; numerical aperture, 0.37; flat tip; Doric Lenses) at the same coordinates. All implants were secured using Super-Bond cement (Sun Medical). For experiments using optogenetic stimulation coupled to single-unit and LFP recordings, one of the two optic fibers was combined to the array of 16 or 32 individually insulated nichrome wires. Single-unit recordings during the manipulation of PV or SST INs were performed as described in the section “Optogenetic manipulation”.

Behavioural and recording experiments were performed 3–5 weeks after injection. The light (approximately 2 or 10 mW per implanted fiber) was bilaterally conducted from the laser (OptoDuet 473/593 nm, Ikecool) to the mouse via two fiber-optic patch cords (diameter, 200 μ m, Doric Lenses) connected to a rotary joint (1 \times 2 fiber-optic rotary joint, Doric Lenses) that allowed mice to freely move in the behavioural apparatus. For optical control of PV-expressing INs, conditional AAV encoding ChR2 (AAV-EF1a-DIO-hChR2(H134R)-EYFP, serotype 5, Vector Core, University of North Carolina) was bilaterally injected into the dmPFC or the BLA at the same coordinates as above or into the motor cortex of PV-IRES-Cre mice at the following coordinates (Franklin and Paxinos, 1997): 2.0 mm anterior to bregma, 1.5 mm lateral to midline and 1.3 mm ventral to the cortical surface. Control experiments were performed using an AAV containing the DNA construct for GFP alone (AAV-FLEX-GFP, serotype 5, Vector Core, University of North Carolina).

For optogenetic analog manipulation of PV INs during behaviour, we used a 30-s analog dmPFC stimulation delivered at 1, 4, 8, 10 or 12 Hz. As a control we also used a stochastic 4-Hz analog dmPFC stimulation generated by an oscillator with a randomly time-modulated frequency designed from a Gaussian distribution centered on 4 Hz. The power spectrum of the signal displayed a broad peak around 4 Hz, but the duration of each cycle varied randomly from 0.15 to 0.6 s, thereby destroying the regularity of the population activity. For motor cortex experiments, we used a 4 Hz analog stimulation. For BLA silencing experiments, a continuous pulse of blue light was applied during CS⁺ presentations 24 h after FC. For optogenetic manipulation of SST INs or dmPFC-vIPAG PNs during behaviour, we used respectively a 30-s dmPFC continuous blue-light stimulation at 10Hz (5 ms on/ 95 ms off, at 10mW) and a 30-s dmPFC continuous yellow-light stimulation during tone presentation (30s at 10mW). After behavioural and recording experiments, mice were perfused and histological analysis was performed.

To identify the presynaptic partners of dmPFC-vIPAG PNS within the dmPFC, we used a retrograde transsynaptic tracing approach based on the use of pseudotyped rabies viruses. Mice, we first injected with the retrograde virus Cav2-Cre (Vector core of the University of Montpellier, France) in the vIPAG. Then we injected in the dmPFC a cocktail of Cre-dependant AAVs allowing the expression of the rabies G protein (AAV/CA-FLEX-RG, serotype 5, Vector Core, University of North Carolina) and TVA receptor (AAV/EF1a-FLEX-TVA-mcherry, serotype 5, Vector Core, University of North Carolina). Three weeks later, we injected EnvA G-

deleted Rabies–EGFP (Vectore core of Salk institute for biological studies, University of California) into the dmPFC. Mice were killed 8 days thereafter, transcardially perfused with 4% paraformaldehyde in PB 0.1M, and brains were extracted and processed for histology as described below. To compare the relative inputs from PV and SST neurons onto dmPFC-vIPAG PNs, we counted the second order cells (GFP positive cell exclusively) within the dmPFC, and we quantified the percentage of GFP cells that colocalized with SST or PV (Far red positive cell) against the total number of cells count.

VIII/ Anatomical analysis

After completion of experiments, mice were euthanized with isoflurane and perfused through the left ventricle with 4% w/v paraformaldehyde (PFA) in 0.1 M PBS. Brains were dissected out and post-fixed for 4 h at 4°C in the same solution. For localization of recording and electrical stimulation sites (electrolytic lesions), 60µm-thick sections were cut, mounted on gelatin-coated microscope slides, and dried. Sections were stained with toluidine blue, dehydrated and mounted. Electrolytic lesions were identified with conventional transmission light microscopy. Only recordings with confirmed lesions in ACC, PL, BLA, dHPC and vIPAG areas were included in our analyses. For verification of muscimol (MUS) injections in medial septum (MS), viral injections and location of optic fiber in dmPFC and vIPAG, serial 80 µm-thick slices containing the MS, dmPFC and vIPAG (respectively) were imaged using an epifluorescence system (Leica DM 5000) fitted with a 10x dry objective. The location and the extent of the injections were visually controlled. All included MUS injections were targeted and limited to the MS. Similarly, only infections accurately targeting the dmPFC and vIPAG were considered for behavioural and electrophysiological analyses.

For the transsynaptic rabies experiments, mice were euthanized with isoflurane and were perfused with 10 ml of PBS (pH 7.4), and fixed with 75 ml of 4% PFA at 4°C (TAAB, pH 7.3; 25 ml at ~10 ml/min and 50 ml at ~6 ml/min). After short post-fixation, 60 micrometer-thick coronal sections were cut and kept in PB 0.1 until use. Immunostaining was performed to visualize PV, SST and to enhance fluorescence associated with viral mCherry expression. All reagents were diluted in PB 0.1 M containing triton X-100 0.3% v/v. Free-floating sections were blocked in 10 % normal goat serum (NGS, Vector laboratories) with 2.5% Bovin serum albumin (VWR) for 2 h

at room temperature. Then, sections were incubated at 4°C for 2 days with a solution of PV antibody made in guinea pig (Synaptic Systems 195-004) with 2% NGS (dilution 1/2000) or 3 days with a solution of SST antibody made in rabbit (Millipore AB5494, dilution 1/200). The day before the removal of the primary antibody solution, the sections were incubated with a solution of mCherry antibody conjugate to alexa fluor 594 (life technology M11240, dilution 1/500). Sections were washed and incubated at 4°C overnight in a solution containing Alexa 647-conjugated goat anti-guinea pig and Alexa 647-conjugated anti-rabbit antibody (Life technology respectively A21450 and A21244, dilution 1/500) with 2% NGS. After extensive washes, sections were mounted in Vectashield (Vector Laboratories). Confocal images stacks (3 µm steps, slice thickness 1 Airy unit) were acquired (Leica DMI6000 TCS SP8 X 40X oil immersion 1.3 NA objective) for each mouse, from different sections of dmPFC, close to the virus injection sites. Sequential acquisition was used to prevent cross-talk between GFP, mCherry and Alexa 647 signals (far red signal). Immunoreactivity of cell bodies for PV, SST and GFP was assessed independently for each stack.

IX/ Extracellular stimulation

At the end of the behavioural procedure, mice were anesthetized with urethane (1.4 g kg⁻¹) and concentric stimulating electrodes (FHC) were lowered in the BLA (1.4 mm posterior to bregma; 3.2 mm lateral to midline and 3.8 to 4.6 mm ventral to the cortical surface) and the PAG (4.35 mm posterior to bregma; 0.55 mm lateral to midline and 1.8 to 2.4 mm ventral to the cortical surface) (Franklin *et al.*, 1997). During the experiments, the stimulation electrodes were advanced in steps of 5 µm by a motorized micromanipulator (FHC) and dmPFC-evoked responses were recorded. Stimulation-induced and spontaneous spikes were sorted as described in the section “Surgery and recordings”. Stimulation-induced spike waveforms were quantitatively compared to the waveforms of units previously identified in the awake animal and recorded on the same wire using correlation analysis. This ensured that the same neurons were recorded across behaviour and under anesthesia. To be classified as antidromic, evoked-responses had to meet at least two out of three criteria: (1) stable latency (< 0.3 ms jitter), (2) collision with spontaneously occurring spikes, and (3) ability to follow high-frequency stimulation (250 Hz). At

the end of the experiments, stimulating sites were marked with electrolytic lesions before perfusion, and electrode locations were verified (see above).

X/ Statistical analysis

For each statistical analysis provided in the manuscript, the Kolmogorov–Smirnov normality test was first performed on the data to determine whether parametric or non-parametric tests were required. When multiple statistical tests were performed, Bonferroni corrections were applied. Two different approaches were used to calculate the sample size. For studies in which we had sufficient information on response variables, power analyses were carried out to determine the number of mice needed. For studies in which the behavioural effect of the manipulation could not be pre-specified, such as optogenetic experiments, we used a sequential stopping rule (SSR). In essence this method enables null-hypothesis tests to be used in sequential stages, by analysing the data at several experimental points using *t*-tests. Usually the experiment started by testing only a few animals and if the *P* value was below 0.05, the investigator declared the effect significant and stopped testing. If the *P* value was greater than 0.36, the investigator stopped the experiment and retained the null hypothesis. For sample-size estimation using power analyses, we used an on-line power analysis calculator (G*Power3). For each analysis, sample size was determined using a power > 0.9 and alpha error = 0.05. All tests were two-sided. Power analyses were computed for matched pairs. In our behavioural experiments, a critical parameter is freezing level, and the numerical endpoint typically ranges between 50 and 70% freezing for CS⁺ presentations immediately following auditory fear conditioning and between 10 and 30% freezing for CS⁻ presentations. A minimum biologically significant difference in the mean values between CS⁻ and CS⁺ conditions for cued FC or between habituation and test sessions for contextual FC, is 1.5-fold. If we assume a standard deviation of 1.5 for a mean value of 60% freezing for CS⁺ test session and 20% freezing for CS⁻ habituation (which are realistic numbers), then a minimal $n = 6$ is needed to reject the null hypothesis with 90% probability. Sample size determination using SSRs analyses were used for optogenetic experiments in which it was not possible to determine a priori the effect of the optical manipulation. We used *P* values of 0.05 and 0.36 for lower and upper criterion.

For behavioural statistical analysis between CS⁻ and CS⁺, and between habituation and retrieval, Repeated-Measures ANOVA ($P < 0.05$) was used. The same statistical analysis was used to compare the effect of light between the archeorhodopsin group and the GFP group. The post-hoc test Student-Newman-Keuls was used for further analyses.

To test the significance of the ROC value for each neuron, a bootstrap analysis was performed by shuffling 100 hundred times the identity (freezing or not freezing) of each time bin associated with a firing rate and thus constructing a distribution of ROC values representing the null hypothesis (no relation between firing and freezing behavior). The actual value could then be compared to the 95% confidence intervals of this distribution obtained by fitting a gaussian to evaluate significance.

Results:

The results section is divided in three main parts. The first part is devoted to the investigation of the contribution of the mPFC-BLA pathway to conditioned fear behaviour and the underlying neuronal mechanisms. This part of the result section has been published in Nature Neuroscience in 2016 (Karalis et al., 2016). The second part of the results section concerns the study of the role of the mPFC-vIPAG pathway in the control of conditioned fear responses and the manuscript is under finalization before submission to a high profile journal. The last part of the results section concerns a collaborative study during which we investigated the detailed neuronal circuits within the PAG contributing to fear expression. This work has been published in 2016 in Nature (Tovote et al., 2016).

I/ 4 Hz oscillations synchronized prefrontal-amygdala circuits during fear behaviour.

Our understanding of the role of prefrontal and amygdala regions in fear behaviour has considerably grown over the past decade, and it is relatively clear that the dmPFC-BLA pathway is actively recruited during the expression of freezing behaviour. For instance, synchronization of neuronal activity between spiking activity in these two structures has been observed during fear expression (Likhtik and Paz, 2015). However, to date, the mechanisms allowing the long-range neuronal synchronization of neuronal activity during fear behaviour between these two brain areas remain largely unknown. In the present study, we used a combination of single unit and local field potentials recordings along with optogenetic manipulations to demonstrate that during freezing behaviour, the emergence of slow oscillations in the dmPFC-BLA pathway coordinates dmPFC-BLA activities and is sufficient to induce fear behaviour. To our knowledge, these results identify for the first time the fine neuronal mechanisms allowing the long-range neuronal synchronization of mPFC-BLA networks to drive conditioned fear responses.

My main contribution to this work as a main first author was fourfold: it first consisted in evaluating the origin of 4 Hz oscillations and to test the effect of medial septum (MS) inactivation on dmPFC 4 Hz oscillations, a structure known to be involved in the genesis of hippocampal theta oscillations (Yoder and Pang, 2005). We combined reversible muscimol inactivation of the MS and single unit recordings in the dmPFC and dHPC in freely moving mice.

Animals were first conditioned and test the next days for fear retrieval with or without inactivation of the MS (**Figure 13a,b**). Targeted, reversible inactivation of the MS with muscimol impaired dmPFC theta but had no effect on dmPFC 4 Hz oscillations (**Figure 13c, d, e**). Furthermore, this manipulation had no effects on the percentage of dmPFC neurons phase-locked to 4-Hz oscillations but reduced the number of dmPFC neurons phase-locked to theta oscillations (**Figure 13f**). These data indicate that 4 Hz oscillations do not originate from the hippocampal region.

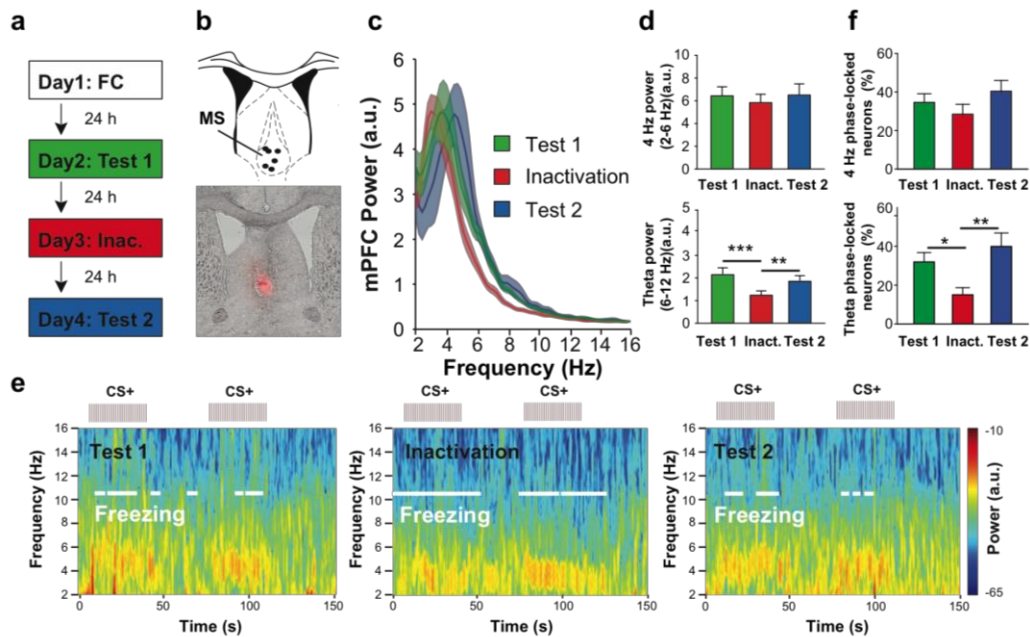


Figure 13: Reversible inactivation of the medial septum does not block dmPFC 4-Hz oscillations. **a,b.** Experimental strategy and location of injections sites in the medial septum (MS) and composite transmission light and epifluorescence micrograph showing the MS targeted injection of muscimol covalently bound to a fluorescent tag (bottom, dipyrromethene boron difluoride (BODIPY), red). **c.** Power spectra of dmPFC LFPs before (Day 2: Test 1), following (Day 3: Inact.) and after (Day 4: Test 2) MS inactivation ($n = 6$). **d.** Top, Quantification of dmPFC LFP 4 Hz power (2-6 Hz) before, during, and after MS inactivation. ($n = 6$ mice, One-way repeated measure ANOVA: $F(2,5) = 2.167$, $P = 0.165$). Bottom, Quantification of dmPFC LFP theta power (6-12 Hz) before, during, and after MS inactivation. MS inactivation significantly reduced dmPFC theta power ($n = 6$ mice, One way repeated measure ANOVA: $F(2,5) = 19.245$, $P < 0.001$, paired t-test Bonferroni corrected, Test 1 versus Inact.: $t(5) = 6.155$, $*** P < 0.001$; Inac. versus Test 2: $t(5) = 4.173$, $** P = 0.006$). **e.** Representative spectrograms of dmPFC LFPs before (Test 1), during (Inactivation) and after (Test 2) MS inactivation (red tick represents single CS+ pips). White lines on the spectrogram indicate immobility/freezing episodes. **f.** Percentage of dmPFC neurons phase-locked to 4 Hz (top), or theta (bottom) oscillations (6-12 Hz). (Test 1: $n = 80$ neurons; Inact.: $n = 100$ neurons; Test 2: $n = 120$ neurons. 4 Hz: One-way repeated measure ANOVA: $F(2,5) = 1.245$, $P = 0.329$; theta: One-way repeated measure ANOVA: $F(2,5) = 9.858$, $P = 0.004$, Bonferroni corrected t-tests; Test1 versus Inactivation: $t(5) = 2.956$, $P = 0.043$; Inactivation versus Test 2: $t(5) = 4.347$, $P = 0.004$). a.u.: arbitrary units. Shaded areas and error bars: mean \pm s.e.m. For the representative examples in (a, e), similar results were obtained for the 6 animals used in these experiments.

In a second step, we evaluated the causal link between the artificial analog induction of dmPFC 4 Hz oscillation and fear behaviour in freely moving animals. By using single unit recording coupled with optogenetic activation of dmPFC PV INs in behaving mice we showed that induction of an artificial analog 4 Hz oscillation in the dmPFC was sufficient to drive fear behaviour expression but also to induced fear memory when test the next day (**Figure 14a, b, c**). Furthermore, we also demonstrated that this effect was specific of the frequency used (4 Hz) (**Figure 14d**) and observed for different light intensity (**Figure 14e**). Finally, we also confirmed that dmPFC artificial induction of 4Hz oscillations induced an increase in the co-firing activity between the dmPFC and BLA neurons (**Figure 14**).

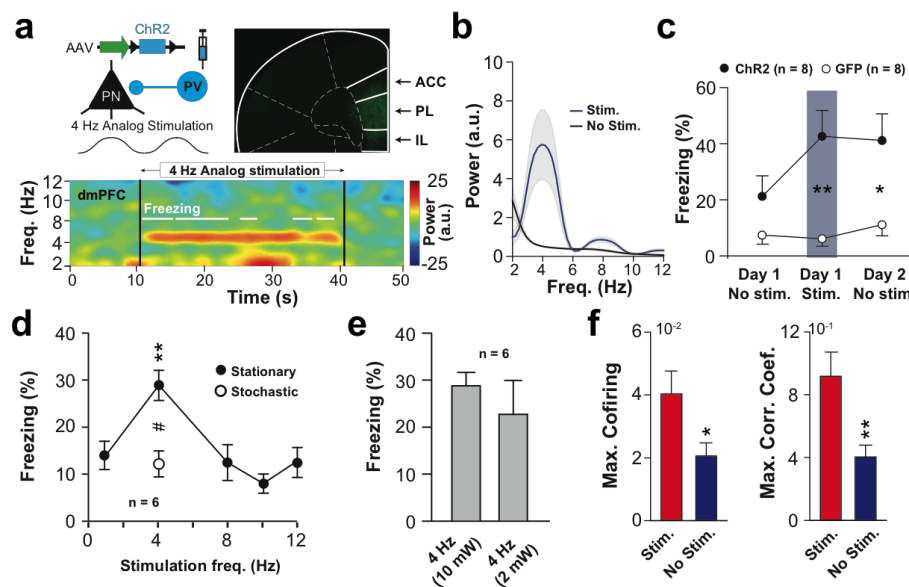


Figure 14: Optogenetic induction of dmPFC 4-Hz oscillations drives freezing. **a.** Top left, strategy used to activate parvalbumin-expressing (PV) interneurons. Top right, coronal dmPFC micrograph from a PV-IRES-Cre mouse expressing channelrhodopsin2 (ChR2). Solid and dashed lines represent the boundaries between the cingulate cortex (ACC), the prelimbic (PL) and infralimbic (IL) areas, and other cortical structures. Scale bar, 0.5 mm. Bottom, spectrogram during 4-Hz analog stimulation. **b.** Averaged normalized LFP power spectra of dmPFC LFPs during (Stim.) and outside (No stim.) stimulation ($n = 8$). **c.** Percentage of freezing for ChR2 ($n = 8$) or GFP ($n = 8$) mice before, during and after 4-Hz induction (two-way ANOVA repeated measures; group: $F(1,14) = 0.868$, $P = 0.367$, time $F(1,2) = 8.926$, $P = 0.001$, group \times time $F(1,28) = 6.925$, $P = 0.0036$); unpaired t -tests: day 1: Stim. $t(14) = 3.712$, $**P = 0.002$; day 2: No stim., $t(14) = 2.758$, $*P = 0.013$). **d.** Percentage of freezing for ChR2 mice ($n = 6$) during analog stimulation at 1, 4, 8, 10, 12 Hz (Stationary) or using a 4-Hz stochastic waveform (stochastic: one-way repeated measures ANOVA: $F(5,4) = 8.618$, $P < 0.001$; Bonferroni-corrected paired t -tests: 4 versus 1 Hz: $t(5) = 5.927$, $**P = 0.0019$; 4 versus 8 Hz: $t(5) = 4.712$, $**P = 0.0053$; 4 versus 10 Hz: $t(5) = 7.632$, $***P < 0.001$; 4 versus 12 Hz: $t(5) = 4.009$, $**P = 0.01$; paired t -test: 4-Hz stationary versus stochastic: $t(5) = 3.533$, $\#P < 0.016$). **e.** Percentage of freezing for ChR2 ($n = 6$) mice during dmPFC 4-Hz analog stimulation at 2 or 10 mW (paired t -test: $t(5) = 0.951$, $P = 0.385$). **f.** Maximum correlation and co-firing index for pairs of dmPFC and BLA neurons during and outside stimulation ($n = 31$ pairs, Mann-Whitney, $U = 326$ and 278 , $*P = 0.03$; $**P = 0.004$). a.u., arbitrary units. Power in log scale. Shaded area and error bars, mean \pm s.e.m. For box plots, the middle, bottom and top lines correspond to the median, bottom and top quartiles, and whiskers to lower and upper extremes minus bottom quartile and top quartile, respectively. For representative examples (**a**), similar images and traces were observed for the 16 (top, 8 ChR2 and 8 GFP mice) and 8 (bottom, 8 ChR2 mice) animals used in these experiments.

A third set of experiment performed in the framework of this project, was to demonstrate that not all the structures involved in fear behaviour expression present an increase in 4 Hz oscillations during freezing behaviour. By using single unit recording targeting both the IPAG and vIPAG, we demonstrated that freezing behaviour in this structure was not associated with 4 Hz oscillations (**Figure 15**). These data demonstrated that synchronization of co-firing activity in the 4 Hz oscillations depends at least from the dmPFC-BLA pathway.

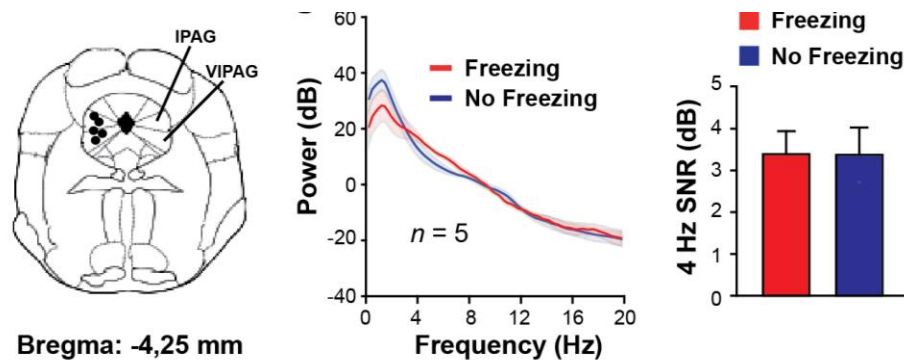


Figure 15: **Left** Location of recording sites in the lateral (IPAG) and ventrolateral periaqueductal grey (vIPAG) (n = 5 mice). **Middle.** Averaged power spectrum of PAG LFPs recorded during Retrieval for freezing and no freezing periods (n = 5 mice). **Right,** Averaged PAG 2-6 Hz power during Retrieval for freezing and no freezing periods (n = 5 mice, paired t-test, $t(4) = 0.098$, $P = 0.926$). Shaded areas and error bars: mean \pm s.e.m.

Finally, we conducted another set of experiments to demonstrate that the artificial induction of 4 Hz oscillation within the motor cortex or the BLA was not sufficient to drive fear expression behaviour and that the integrity of amygdala output neurons was a necessary condition for driving behavioural fear expression. For the first experiment we use combination of optogenetic tools combined with single unit recordings to activate PV INs within the motor cortex (M1) or the BLA and induced an artificial analog 4 Hz oscillation. We demonstrated that the induction of 4 Hz oscillations in the M1 or BLA was not sufficient to drive fear expression behaviour, which further demonstrated the specificity of our manipulation in the dmPFC (**Figure 16a, b**). For the second experiment we used a combination of optogenetic targeting PV INS of the BLA with single unit recordings in the BLA in freely moving mice. We demonstrated that the inactivation of BLA spiking activity decreased fear behaviour expression. (**Figure 16c,d,e**).

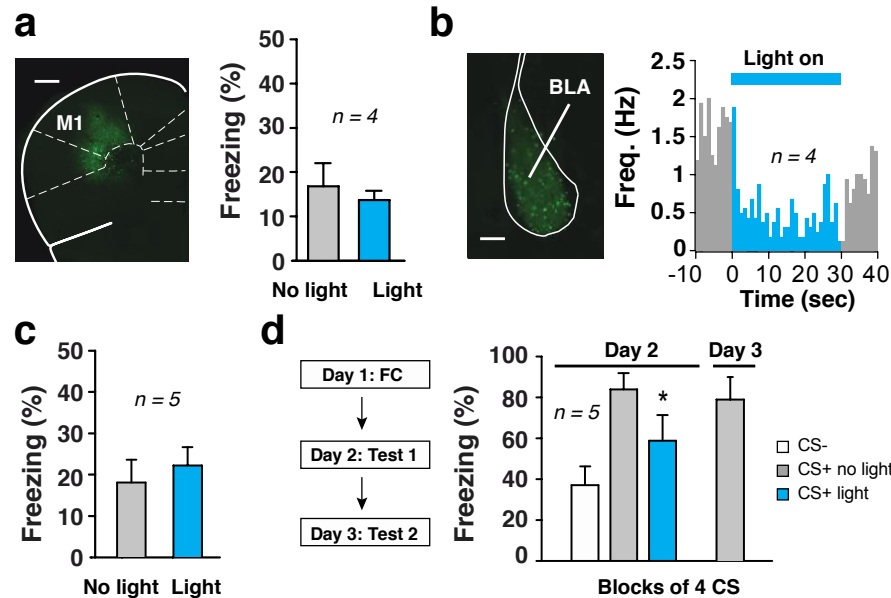


Figure 16: **a.** Left, representative micrograph of the motor cortex (M1) in a PV-Cre mouse infected with ChR2. Scale bar = 0.5 mm. Right, Percentage of freezing displayed by PV-Cre mice infected in the motor cortex with ChR2 during motor cortex 4 Hz analog stimulation ($n = 4$ mice; Paired t-test, $t(3) = 0.623$, $P = 0.578$). **b.** Left, representative micrograph of BLA in a PV-Cre mouse infected with ChR2. Scale bar = 0.4 mm. Right, Averaged peri-stimulus time histograms (PSTH) showing that light activation of BLA PV interneurons can suppress the activity of BLA putative principal neurons ($n = 4$ cells from 2 mice). **c.** Percentage of freezing displayed by PV-Cre mice infected in the BLA with ChR2 during baseline conditions ($n = 5$ mice; Paired t-test, $t(4) = -0.721$, $P = 0.511$). **d.** Left, behavioural protocol. Right, Percentage of freezing behaviour to CS- , and CS+ presentations during no-light or light exposure on Test 1 ($n = 5$ mice, Paired t-test, CS+ no light versus CS+ light, $t(4) = -4.265$, $P = 0.013$). Freezing levels to CS+ presentations during Test 2 normalized to CS+ evoked freezing levels during Test 1 ($n = 5$ mice, Paired t-test, CS+ Day 2 versus CS+ Day3, $t(4) = -1.080$, $P = 0.341$). Error bars: mean \pm s.e.m.

In summary, our data revealed a specific 4 Hz oscillatory mechanism allowing the expression of fear memories by long-range synchronization of neuronal activity between dmPFC and BLA neuronal circuits.

Publication: Karalis* N, Dejean* C, Chaudun* F, Khoder S, Rozeske RR, Wurtz H, Bagur S, Benchenane K, Sirota A, Courtin J and Herry C. (2016). 4 hz oscillations synchronize prefrontal-amygdala circuits during fear behaviour. *Nature Neuroscience*. 19, 605-612. **IF: 16.095.** * Shared authorship.

4-Hz oscillations synchronize prefrontal–amygdala circuits during fear behavior

Nikolaos Karalis^{1–3,6}, Cyril Dejean^{1,2,6}, Fabrice Chaudun^{1,2,6}, Suzana Khoder^{1,2}, Robert R Rozeske^{1,2}, H el ene Wurtz^{1,2}, Sophie Bagur⁴, Karim Benchenane⁴, Anton Sirota³, Julien Courtin^{1,2,5,7} & Cyril Herry^{1,2,7}

Fear expression relies on the coordinated activity of prefrontal and amygdala circuits, yet the mechanisms allowing long-range network synchronization during fear remain unknown. Using a combination of extracellular recordings, pharmacological and optogenetic manipulations, we found that freezing, a behavioral expression of fear, temporally coincided with the development of sustained, internally generated 4-Hz oscillations in prefrontal–amygdala circuits. 4-Hz oscillations predict freezing onset and offset and synchronize prefrontal–amygdala circuits. Optogenetic induction of prefrontal 4-Hz oscillations coordinates prefrontal–amygdala activity and elicits fear behavior. These results unravel a sustained oscillatory mechanism mediating prefrontal–amygdala coupling during fear behavior.

Long-range neuronal synchronization among groups of neurons is an effective mechanism that promotes the transmission of information between neural structures^{1–4}. This form of neuronal communication has been largely described in sensory and motor systems^{5–8} and more recently between neural structures involved in the processing of emotions such as fear-related information^{9–12}. Fear behavior is known to depend on the interaction between the dorsal medial prefrontal cortex (dmPFC) and the basolateral amygdala (BLA), and recent data indicate that local or distant synchronization of neuronal activity in this dmPFC–BLA network strongly correlates with fear behavior^{9–12}. In particular, synchronization of spiking activity between dmPFC and BLA has been associated with resistance to extinction learning, whereas fear discrimination has been associated with transient, sensory-driven dmPFC–BLA synchronization^{10,11}. However, the precise neuronal mechanisms mediating long-range network synchronization during fear behavior remain unknown. Furthermore, a causal role of neuronal synchrony among dmPFC and BLA circuits in driving fear behavior has not yet been demonstrated.

RESULTS

Internally generated freezing behavior

To address these questions, we performed single-unit and local field potential (LFP) recordings in the dmPFC and BLA of freely behaving mice subjected to auditory fear conditioning (Fig. 1a). Twenty-four hours after conditioning, re-exposure to the conditioned auditory stimulus (CS⁺) but not to the control auditory stimulus (CS⁻) induced conditioned freezing behavior, which we used as readout of fear memory acquired upon associative learning (Fig. 1b). Quantification of freezing episodes occurring during or between CS⁺ presentations

indicated that mice froze more often between CS⁺ presentations (Fig. 1c). Moreover, evaluation of freezing-period onset distribution during or between CS⁺ presentations indicated that a large fraction of freezing periods ($41.8 \pm 0.03\%$) were initiated outside of CS⁺ presentations (Fig. 1d). Finally, cross-correlation analysis performed between freezing and CS⁺ onset revealed that the freezing period onset was delayed by 1.5 s with respect to CS⁺ onset (Fig. 1e). These observations indicate, that in addition to freezing episodes driven by auditory inputs, internally generated mechanisms can initiate and maintain freezing episodes following CS⁺ presentations.

dmPFC and BLA 4-Hz oscillations predict freezing behavior

Analysis of dmPFC LFPs recorded throughout the behavioral sessions revealed a prominent and sustained 2–6 Hz oscillation with a peak frequency at 4 Hz (hereafter referred to as 4-Hz oscillations), which strongly correlated with episodes of freezing behavior following conditioning (Fig. 2a–d and Supplementary Fig. 1a,b). These oscillations were not present when animals were passively immobile during the habituation session (Fig. 2a and Fig. 3a–c). Moreover, the duration and power of 4-Hz oscillations in the dmPFC was strongly correlated with the length of freezing episodes (Fig. 3d).

To evaluate whether 4-Hz oscillations could predict freezing behavior, we first computed freezing-triggered spectrograms centered on the onset and offset of freezing episodes (Fig. 3e). Statistical analyses for the temporal progression of significant changes of 4-Hz power indicated that 4-Hz oscillations in the dmPFC emerged and terminated significantly earlier than freezing behavior. These results strongly suggest that 4-Hz oscillations are an accurate predictor of freezing onset and offset, rather than a consequence of freezing

¹INSERM, Neurocentre Magendie, U862, Bordeaux, France. ²Univ. Bordeaux, Neurocentre Magendie, U862, Bordeaux, France. ³Bernstein Center for Computational Neuroscience Munich, Munich Cluster of Systems Neurology (SyNergy), Faculty of Medicine, Ludwig-Maximilians Universit at M unchen, Planegg-Martinsried, Germany. ⁴Team Memory, Oscillations and Brain states (MOBs), Brain Plasticity Unit, CNRS UMR 8249, ESPCI ParisTech, Ecole Sup erieure de Physique et de Chimie Industrielles de la Ville de Paris, Paris, France. ⁵Friedrich Miescher Institute for Biomedical Research, Basel, Switzerland. ⁶These authors contributed equally to this work. ⁷These authors jointly directed this work. Correspondence should be addressed to C.H. (cyril.herry@inserm.fr) or N.K. (karalis@bio.lmu.de).

Received 23 October 2015; accepted 22 January 2016; published online 15 February 2016; doi:10.1038/nn.4251

Figure 1 Freezing behavior is triggered by internally generated mechanisms.

(a) Experimental protocol. Hab., habituation; FC, fear conditioning; Ret., retrieval; US, unconditioned stimulus. (b) Behavioral results.

During habituation, mice ($n = 13$) exhibited low freezing during the CS⁻ and CS⁺. After conditioning (day 2: retrieval), the CS⁺ (CS⁺ 1–12, grouped in blocks of four) induced higher freezing than CS⁻ (paired t -tests, CS⁻ versus each CS⁺ block: $t(12) = -11.929$;

$t(12) = -11.929$; $t(12) = -8.442$; all $***P < 0.001$). (c) Percentage of freezing exhibited during and between CS⁺ presentations (paired t -test, freezing inside versus between CS⁺: $t(12) = -2.480$, $*P = 0.029$).

(d) Distribution probability for freezing episode duration as a function of whether freezing was initiated inside or between CS⁺ presentations. Inset, percentage of freezing episodes initiated inside or between CS⁺ presentations ($n = 13$ mice, paired t -test, $t(12) = 2.762$, $*P = 0.016$).

(e) Cross-correlation analysis performed between freezing and CS⁺ onset ($n = 13$ mice, 100-ms bins). Red vertical dotted line represents freezing onset. Black horizontal dotted line represents significance level. Black arrow indicates the highest probability for CS⁺ onset at 1.5 s before freezing onset. Error bars, mean \pm s.e.m. For box plots, the middle, bottom and top lines correspond to the median, bottom quartile and top quartile, and whiskers to lower and upper extremes minus bottom quartile and top quartile, respectively.

behavior. This observation was further supported by analyses using supervised learning models, which allowed us to successfully predict freezing behavior on a trial-by-trial basis using the 4-Hz dmPFC signal-to-noise ratio (SNR) (Fig. 3f,g). 4-Hz oscillations developed during auditory fear conditioning (Supplementary Fig. 2) and dmPFC 4-Hz oscillations were also observed during freezing episodes in mice submitted to contextual fear conditioning, indicating that 4-Hz oscillations might correspond to a general physiological signature of freezing behavior (Supplementary Fig. 3). A similar but less

prominent phenomenon was observed in the BLA, although the coupling between 4-Hz oscillations and freezing behavior was stronger in the dmPFC, likely because of the different laminar anatomical organization of the two structures and putative localization of the source of the 4-Hz oscillation in the prefrontal circuits (Fig. 4 and Supplementary Figs. 1c,d and 4a–e).

To evaluate whether 4-Hz oscillations were the mere consequence of freezing-, motor- or respiratory-related behavior, we performed further recordings in the ventrolateral periaqueductal gray (vPAG),

Figure 2 Emergence of dmPFC 4-Hz oscillations during freezing behavior. (a) Top, representative dmPFC raw LFP traces recorded during retrieval. 4-Hz oscillatory activity is prominent during freezing behavior. Bottom, representative spectrograms of dmPFC LFPs during habituation and retrieval sessions during CS⁻ and CS⁺ presentations (blue lines, CS⁻ onset; red lines, CS⁺ onset; habituation, recording during CS⁻ 3 and 4; retrieval, recording during CS⁺ 1 and 2). White lines on the spectrogram indicate immobility or freezing episodes.

(b) Representative spectrogram of dmPFC LFPs at a finer time resolution before, during and after presentation of a CS⁺ during retrieval. Each red tick represents a single CS⁺ pip. White lines on the spectrogram indicate freezing episodes. a.u., arbitrary units. (c) Averaged power spectra of dmPFC LFPs recorded during retrieval for freezing and no-freezing periods ($n = 13$ mice). Inset, averaged dmPFC 2–6 Hz power during retrieval for freezing and no-freezing periods (paired t -test, freezing versus no freezing: $t(12) = -14.884$, $***P < 0.001$).

(d) Averaged SNR of 4-Hz oscillation (2–6 Hz) during habituation (Hab.) and retrieval (Ret.) ($n = 12$ mice, paired t -tests, habituation versus retrieval: dmPFC: $t(11) = -6.805$, $***P < 0.001$). Shaded areas, mean \pm s.e.m. For box plots, the middle, bottom and top lines correspond to the median, bottom quartile and top quartile, and whiskers to lower and upper extremes minus bottom quartile and top quartile, respectively. For representative examples (a,b), similar traces were observed for the 13 animals used in these experiments.

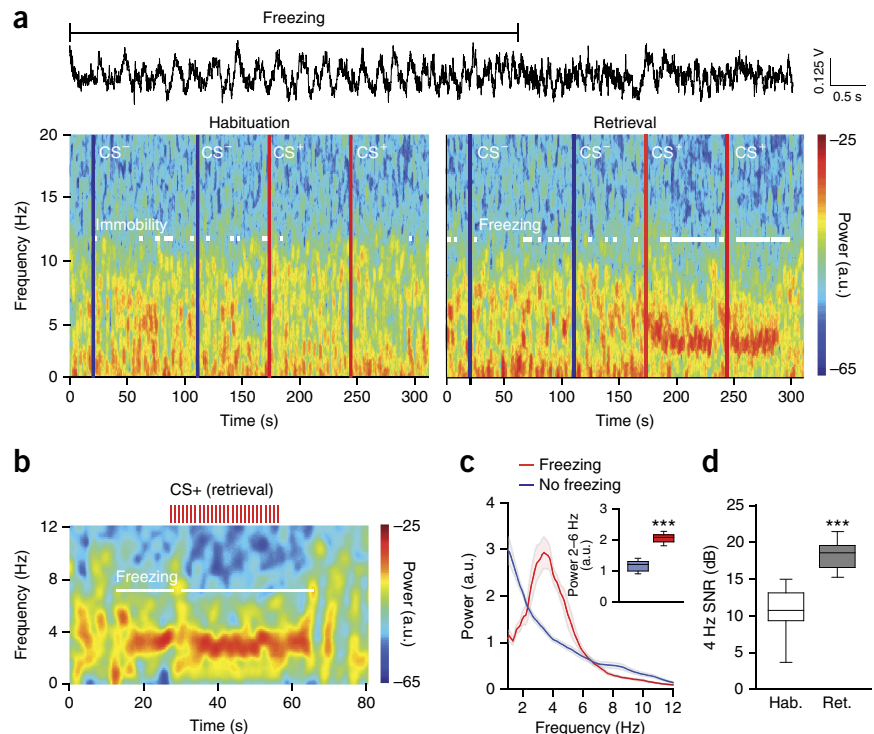
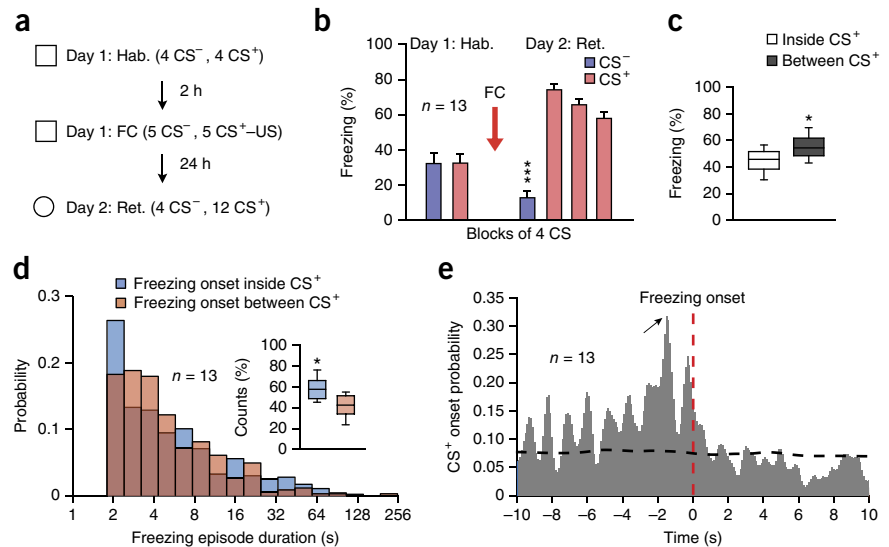
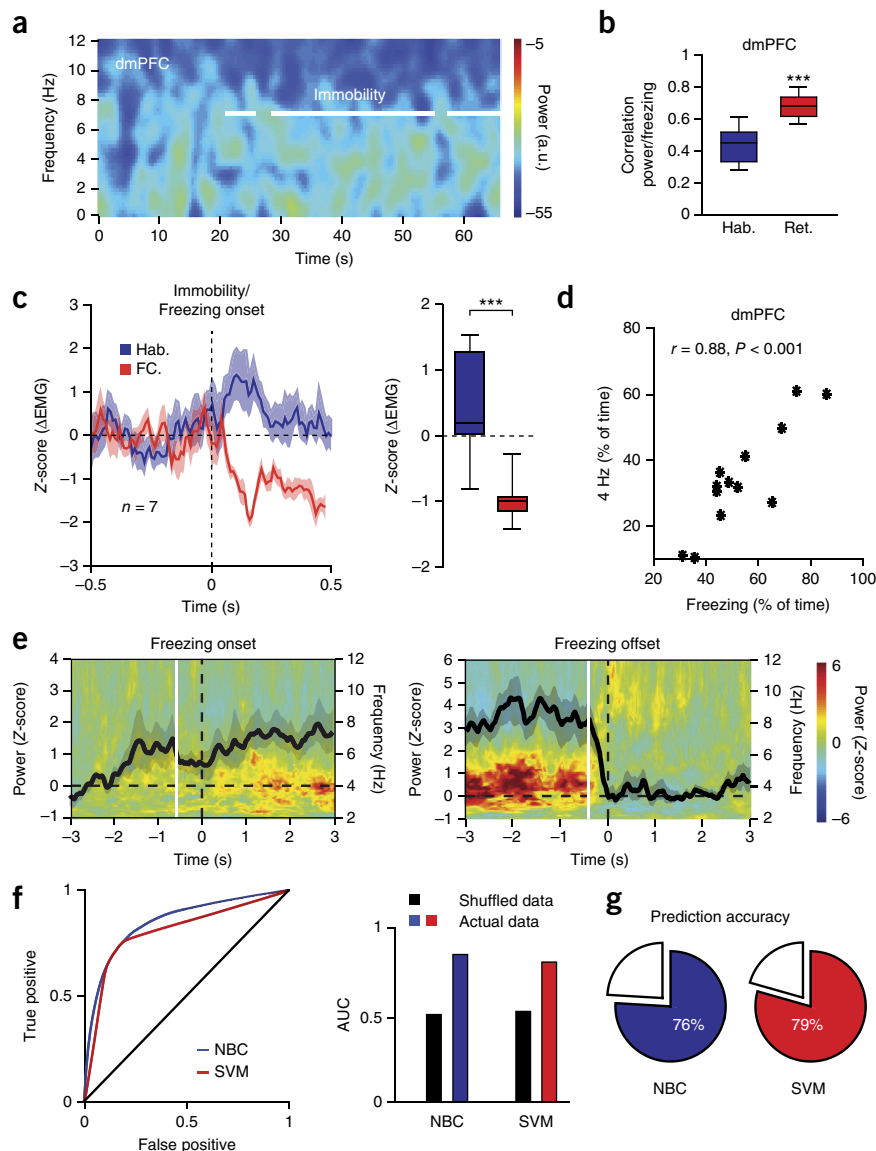


Figure 3 dmPFC 4 Hz oscillations predict freezing. **(a)** Spectrograms of dmPFC LFP during habituation. White lines indicate immobility. **(b)** Correlation between dmPFC 4-Hz power and freezing during habituation and retrieval ($n = 13$ mice, paired t -tests: $t(12) = 6.134$, $***P < 0.001$). **(c)** Left, mean Z-score for neck electromyography (EMG) during immobility or freezing ($n = 7$ mice) for CS⁺ presentations. Right, averaged EMG (0–500 ms after CS⁺, Mann-Whitney U test, habituation (Hab.) versus fear conditioning (FC): $U = 0$, $***P < 0.001$). **(d)** Correlation between freezing and dmPFC 4 Hz ($n = 13$ mice; Pearson's $r = 0.88$, $P < 0.001$). **(e)** Averaged freezing onset-triggered (left) and offset-triggered (right) Z-scored spectrograms of dmPFC LFPs ($n = 13$ mice; black lines, averaged Z-scored power envelope; white lines, first significant bin of 4-Hz power changes (increase, -0.53 ± 0.31 s; decrease, -0.39 ± 0.10 s; one-sample t -test: first significant bin versus hypothetical mean = 0, increase: $t(12) = 19.207$, $P < 0.001$; decrease: $t(12) = 16.615$, $P < 0.001$). **(f)** Left, receiver operating characteristics analysis performed on a naive Bayes classifier (NBC) and support vector machine (SVM) classifier trained on dmPFC 4-Hz SNR during freezing. Right, averaged area under the curve for both classifiers versus shuffled data. **(g)** Accuracy of both classifiers at predicting freezing; a.u., arbitrary units. Power in log scale. Shaded areas, mean \pm s.e.m. For box plots, the middle, bottom and top lines correspond to the median, bottom quartile and top quartile, and whiskers to lower and upper extremes minus bottom quartile and top quartile, respectively. For the representative example in **a**, similar traces were observed for the 13 animals used in these experiments.

a neuronal structure involved in the genesis of freezing behavior and the control of breathing during emotional load^{13–16}. Power spectrum analyses performed on vPAG recordings did not reveal significant 4-Hz oscillations during freezing episodes, which strongly suggests that 4-Hz oscillations do not reflect freezing-, motor- or respiratory-related activity (**Supplementary Fig. 4f,g**).

4-Hz oscillations are distinct from theta oscillations

To evaluate whether dmPFC 4-Hz oscillations could correspond to hippocampus-dependent low theta oscillations observed previously during conditioned stimulus presentations^{10,12,17,18}, we inactivated the medial septum, a neuronal structure known to be involved in the genesis of theta oscillations¹⁹. Targeted, reversible inactivation of the medial septum with muscimol, which is known to reduce theta power in the dorsal hippocampus¹⁹, impaired dmPFC theta but had no effect on dmPFC 4-Hz oscillations (**Supplementary Fig. 5a–e**). In addition, this manipulation had no effects on the percentage of dmPFC neurons phase-locked to 4-Hz oscillations but reduced the number of dmPFC neurons phase-locked to theta oscillations (**Supplementary Fig. 5f**). Furthermore, in contrast to transient dmPFC local theta oscillations, which displayed CS⁺-evoked phase resetting and were short-lasting (~ 300 ms)^{9,10}, the sustained dmPFC 4-Hz oscillations were not modulated by CS⁺ presentations, did not display CS⁺-evoked phase resetting (**Supplementary Fig. 6**) and could be maintained

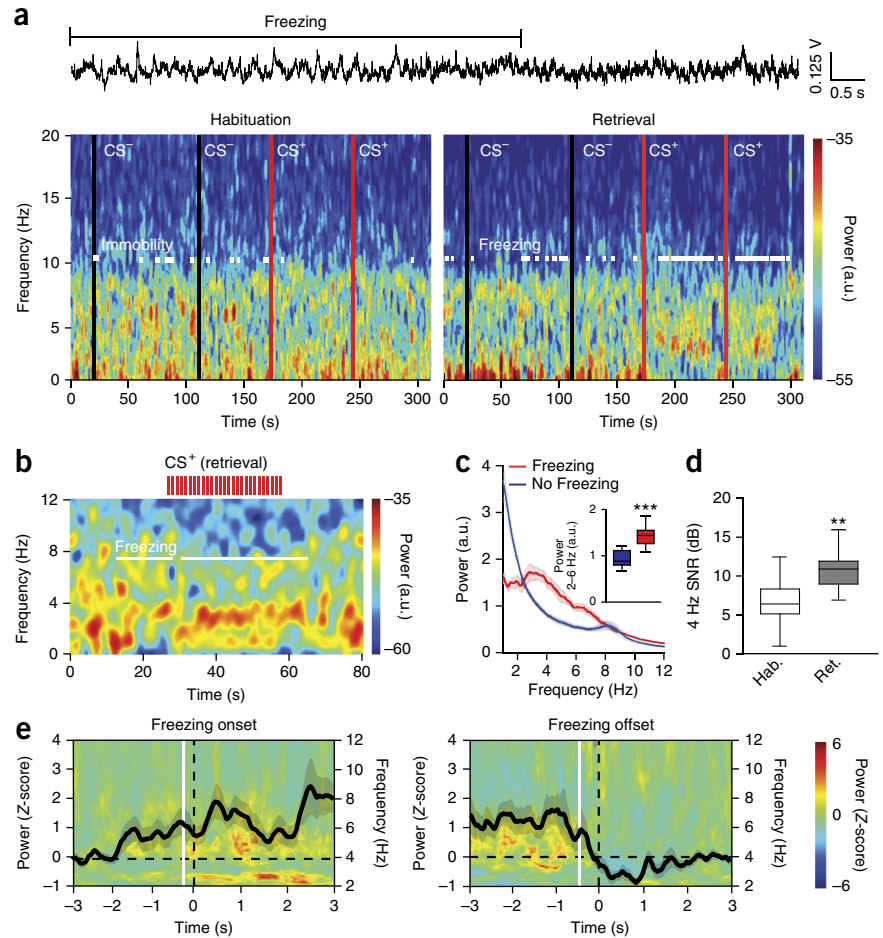


over long periods of freezing behavior even between CS⁺ presentations (**Figs. 2a,b, 3d** and **4a,b**), suggesting that the two phenomena are generated independently. Together these data indicate that the development of hippocampus-independent, internally generated 4-Hz oscillations in dmPFC–BLA circuits precede and therefore predict freezing behavior.

dmPFC 4-Hz oscillations drive BLA during freezing

Analyses of moment-to-moment covariations in oscillatory power and phase between structures revealed that during freezing episodes 4-Hz oscillations in the dmPFC and BLA were strongly synchronized (**Fig. 5a,b** and **Supplementary Fig. 7**). Consequently, coherence between dmPFC and BLA LFPs was significantly enhanced during freezing behavior (**Fig. 5c** and **Supplementary Fig. 7**). Moreover, a series of statistical directionality measures, in both the phase and the amplitude domains, revealed that dmPFC 4-Hz oscillations led BLA LFPs during freezing episodes but not during locomotor activity (**Fig. 5b–d** and **Supplementary Fig. 7**). Together, these data demonstrate that conditioned freezing behavior is associated with a preferential dmPFC-to-BLA phase coupling of 4-Hz LFP oscillations.

Figure 4 BLA 4-Hz oscillations emerge during freezing. **(a)** Top, representative BLA LFP traces recorded during retrieval. Bottom, spectrograms of BLA LFPs during habituation and retrieval during CS⁻ and CS⁺ (black lines, CS⁻ onset; red lines, CS⁺ onset). White lines indicate immobility or freezing. **(b)** Spectrogram of BLA LFPs before, during and after presentation of a CS⁺ during retrieval. Red ticks represent single CS⁺ pips. White lines indicate freezing. **(c)** Averaged power spectrum of BLA LFPs recorded during retrieval for freezing and no freezing ($n = 13$ mice). Inset, averaged BLA 2–6 Hz power during retrieval for freezing and no freezing (paired t -test, freezing versus no freezing: $t(12) = 6.077$, $***P < 0.001$). **(d)** Averaged 4-Hz SNR during habituation (Hab.) and retrieval (Ret.) ($n = 12$ mice, paired t -tests, habituation versus retrieval: BLA, $t(11) = 3.334$, $**P = 0.003$). **(e)** Averaged freezing onset-triggered (left) and offset-triggered (right) Z-scored spectrograms of BLA LFPs ($n = 13$ mice; black lines, averaged Z-scored power envelope; white lines, first significant bin of 4-Hz power changes (increase, -0.27 ± 0.20 s; decrease, -0.46 ± 0.22 s; one-sample t -test: first significant bin versus hypothetical mean = 0, increase: $t(12) = 10.976$, $P < 0.001$; decrease: $t(12) = 34.372$, $P < 0.001$); a.u., arbitrary units. Spectral power in log scale. Shaded areas, mean \pm s.e.m. For box plots, the middle, bottom and top lines correspond to the median, bottom and top quartile, and whiskers to lower and upper extremes minus bottom quartile and top quartile, respectively. For representative examples **(a,b)**, similar traces were observed for the 13 animals used in these experiments.



4-Hz oscillations organize dmPFC and BLA firing activity

To evaluate the consequences of synchronized 4-Hz oscillatory activity for individual dmPFC and BLA putative excitatory principal neurons ($n = 92$ and $n = 72$, respectively) and putative inhibitory interneurons ($n = 35$ and $n = 15$, respectively) (Supplementary Fig. 8), we measured the phase-locking to dmPFC 4-Hz oscillations and changes in firing frequency of dmPFC and BLA neurons during fear behavior. These analyses revealed that a large proportion of principal neurons and interneurons in both structures were significantly phase-locked to dmPFC 4-Hz oscillations during freezing episodes, among which the vast majority exhibited 4-Hz-related oscillatory activity (Fig. 6). Moreover, freezing episodes were associated with a global increase in the firing rate of principal neurons compared to the rate during no-freezing periods in both the dmPFC and the BLA (Supplementary Fig. 8). Correlation and co-firing analyses of pairwise spiking activity performed between neurons recorded in the dmPFC and neurons recorded in the BLA indicated that phase-locked pairs of principal neurons were more co-activated during freezing episodes as compared to both no-freezing periods and non-phase-locked neurons (Fig. 6c,h). Together, these data indicate that dmPFC and BLA principal neurons synchronize their firing activity to 4-Hz oscillations during freezing behavior.

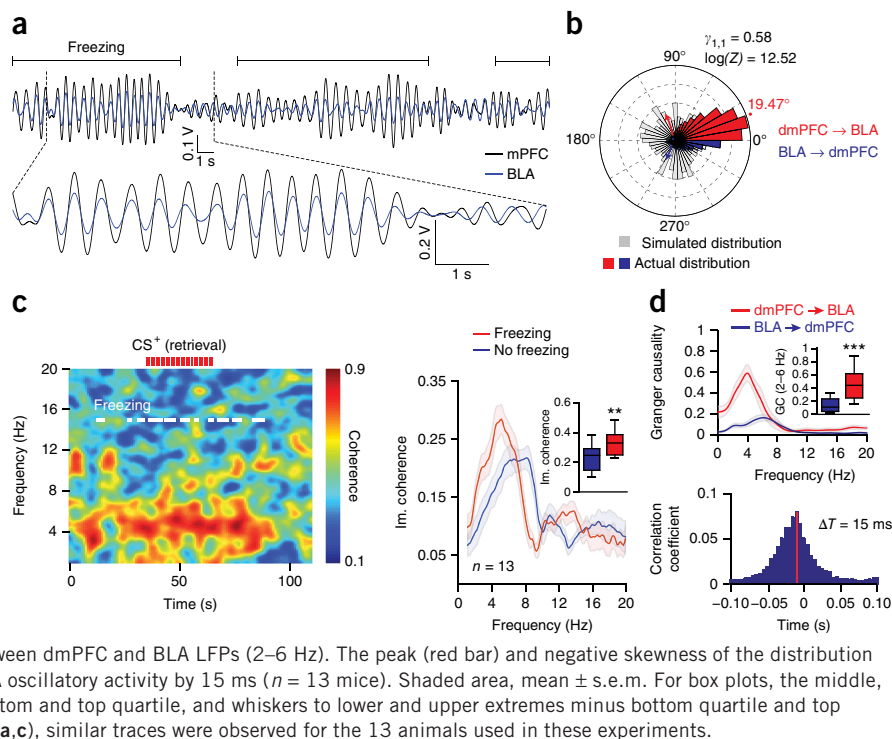
Optogenetic induction of dmPFC 4 Hz drives fear behavior

To further evaluate the causal role of 4-Hz oscillations in synchronizing dmPFC–BLA principal neurons firing activity during fear behavior, we artificially induced 4-Hz oscillations in the dmPFC

of naive animals by analog optogenetic modulation of dmPFC interneurons, which contribute to the emergence of dmPFC 4-Hz oscillations (Supplementary Fig. 9). In particular, we manipulated parvalbumin-expressing cells, which is an efficient approach for inducing rhythmic inhibition of cortical principal neurons at low frequencies^{20–22}. These genetically identified cells were predominantly phase-locked to 4-Hz oscillations and displayed 4-Hz oscillatory activity (Supplementary Fig. 9d–j). Rhythmically driving parvalbumin-expressing interneurons at 4 Hz resulted in prominent 2–6 Hz oscillations in the dmPFC and induced persistent fear behavior (Fig. 7a–c and Supplementary Fig. 10a,b). Freezing behavior was frequency and structure specific, as dmPFC rhythmic stimulation using a number of different control frequencies and BLA or motor cortex stimulation at 4 Hz were inefficient at inducing fear responses (Fig. 7d,e and Supplementary Fig. 10c,d). Furthermore, the artificial induction of dmPFC 4-Hz oscillations synchronized dmPFC and BLA spiking activity during freezing episodes (Fig. 7f and Supplementary Fig. 10g–i).

Given the emergence of 4-Hz oscillations during fear conditioning and retrieval of contextual fear memory (Supplementary Figs. 2 and 3), we retested the mice 24 h later in the context in which they received artificial induction of 4-Hz oscillations. In these conditions, mice exhibited more contextual fear behavior than GFP control animals (Fig. 7c and Supplementary Fig. 10a,b). Furthermore, mice exhibited low freezing levels when tested in a neutral context 24 h later, indicating that fear behavior was specific to the context where the optogenetic stimulation occurred (Supplementary Fig. 10b).

Figure 5 Synchronization of dmPFC and BLA 4-Hz oscillations during freezing. (a) Overlaid filtered (2–6 Hz) dmPFC and BLA LFP traces illustrating synchronized 4 Hz during freezing. (b) Circular distribution of the phase differences between dmPFC and BLA LFPs recorded for freezing during retrieval compared to a control bootstrap-simulated phase distribution ($n = 13$ mice). (c) Left, representative coherogram for dmPFC and BLA LFPs recorded during retrieval during CS⁺. Red ticks represent individual CS⁺ pips. White lines indicate freezing. Right, averaged dmPFC and BLA LFPs imaginary coherence (Im. coherence) for freezing and no freezing during retrieval (paired t -test, freezing versus no freezing: $t(12) = 3.933$, $**P = 0.002$). (d) Top, Granger causality (GC) analysis performed between dmPFC and BLA LFPs during freezing (retrieval, paired t -test, dmPFC \rightarrow BLA versus BLA \rightarrow dmPFC: $t(12) = -5.940$, $***P < 0.001$). Bottom, averaged cross-correlogram performed between dmPFC and BLA LFPs (2–6 Hz). The peak (red bar) and negative skewness of the distribution indicate that dmPFC 4-Hz oscillations lead the BLA oscillatory activity by 15 ms ($n = 13$ mice). Shaded area, mean \pm s.e.m. For box plots, the middle, bottom and top lines correspond to the median, bottom and top quartile, and whiskers to lower and upper extremes minus bottom quartile and top quartile, respectively. For representative examples (a,c), similar traces were observed for the 13 animals used in these experiments.



Together, these results indicate that freezing behavior upon artificial induction of dmPFC 4-Hz oscillations cannot be explained by motor impairments and further suggest that 4-Hz oscillations are causally involved in the synchronization of dmPFC–BLA spiking activity and the expression of aversive fear memories. Finally, post-training optogenetic silencing of BLA neurons during CS⁺ presentations reduced fear behavior, indicating that the BLA is necessary for the full expression of conditioned fear behavior (Supplementary Fig. 10e,f).

DISCUSSION

In this study, we demonstrated that expression of conditioned fear memories is associated with prominent synchronous 4-Hz oscillations in dmPFC–BLA circuits, which organize the spiking activity of local neuronal populations. Furthermore, both dmPFC and BLA 4-Hz oscillations develop specifically during fear conditioning and predict the onset and offset of freezing episodes. The length of freezing episodes was also strongly correlated with the duration and power of dmPFC 4-Hz oscillations, a phenomenon not observed in the BLA. This could be due to the different laminar anatomical organization of the two structures. Aligned pyramidal cells in the cortex form spatially coherent dipoles. The resulting summation of field potentials allows the detection of high-SNR oscillations in the extracellular space²³. The BLA, by contrast, is a nuclear structure with no clear anatomical organization (dipoles are distributed uniformly and not aligned). Consequently, the SNR of extracellularly recorded LFP oscillations is expected to be lower than in the dmPFC. Nonetheless, spike trains of a number of BLA neurons present both intrinsic 4-Hz oscillations and phase-locking to dmPFC 4 Hz, whether under physiological conditions or during light stimulation. Moreover, the presence of 4-Hz oscillations in LFP is indicative of the underlying synaptic activity; however, differences in the absolute power to SNR ratio between the two structures cannot be interpreted as a stronger involvement of the dmPFC. Again, because of the radically different neuronal organization between the two structures, synaptic

inputs are differentially filtered by the biophysical properties of the BLA neural tissue^{24,25}.

Our data indicate that internally generated freezing-related 4-Hz dmPFC oscillations constitute a specific oscillatory mechanism, distinct from the CS⁺-evoked dmPFC theta resetting observed previously^{9,10,12}. These previously published studies^{9,10} evaluated transient sensory-evoked theta oscillations in the dmPFC, which lasted around 300 ms and have been linked to sensory-driven processes during fear behavior or fear discrimination^{9,10}. In contrast, the 4-Hz oscillatory phenomenon correlated not only with long periods of freezing behavior observed during CS⁺ presentations, but also with spontaneously occurring freezing episodes. Functionally this implies that spontaneously occurring freezing periods are internally maintained or generated and not directly driven by sensory stimulations. To our knowledge, this is the first report of a sustained brain state (4-Hz oscillations) that predicts and temporally coincides with freezing episodes. The freezing responses observed between CS presentations are unlikely to have been triggered by the context for several reasons. First, mice were tested in a context distinct from the one used for the conditioning session. Second, freezing levels during CS⁻ presentations during retrieval were very low, indicating that the retrieval context was not aversive *per se* (Fig. 1b; 13.19% freezing on CS⁻ presentations). Our interpretation that freezing episodes occur between CS presentations relies on the induction of a fearful state after the initial CS-induced retrieval of the fear memory and thus the emergence of non-CS-related spontaneous freezing episodes.

Our data and analyses suggest that the 4-Hz oscillations represent a mechanism for the initiation and maintenance of freezing episodes, inside and outside of CS presentations. The data also confirm published observations that CS⁺ onset is associated with a transient resetting of the phase of theta oscillations^{9,10}, which is, however, specific for oscillations in the 8–12 Hz range and is associated with transient increases in theta power, but is not observed for the 4-Hz oscillations (Supplementary Fig. 6). Hence, these observations

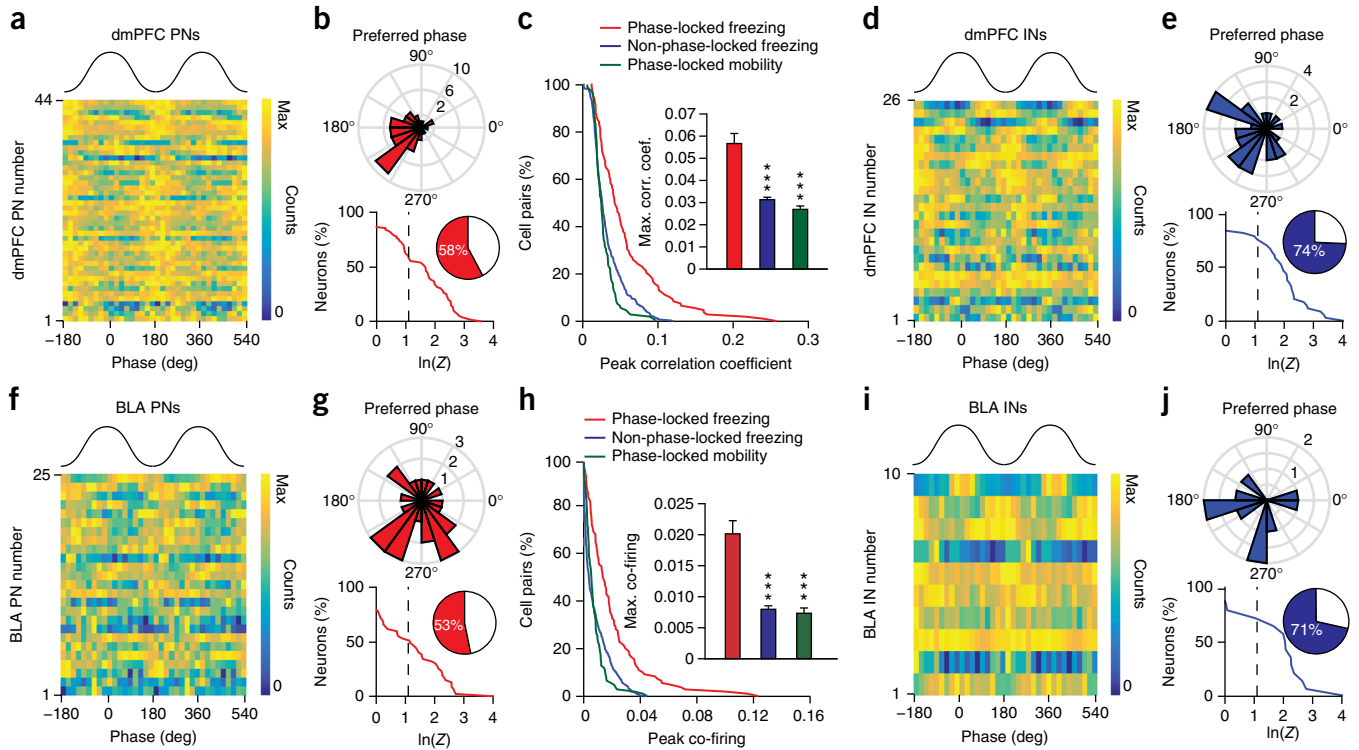


Figure 6 4-Hz oscillations synchronize dmPFC–BLA spiking activity. (**a,d,f,i**) Phase distribution relative to 4-Hz oscillations for dmPFC (**a,d**) and BLA (**f,i**) putative excitatory principal neurons (PN) (**a,f**) or putative inhibitory interneurons (IN) (**d,i**). (**b,g,e,j**) Circular distribution of the 4-Hz preferred phase for populations of dmPFC (**b,e**, top) and BLA (**g,j**, top) phase-locked PNs (**b,g**) and INs (**e,j**) during freezing (dmPFC: 44 PNs and 26 INs; BLA: 25 PNs and 10 INs) and cumulative distribution of log-transformed Rayleigh's test Z of dmPFC (**b,e**, bottom) and BLA (**g,j**, bottom) PNs (**b,g**) and INs (**e,j**). Inset, percentage of dmPFC and BLA neurons significantly phase-locked to 4-Hz oscillations. Dashed line, significant 4-Hz phase-locking threshold ($\ln(Z) = 1.097$, $*P < 0.05$, dmPFC: 44 of 92 PNs and 26 of 35 INs; BLA: 25 of 72 PNs and 10 of 15 INs). (**c,h**) Cumulative distribution of peak correlation coefficient (**c**) and co-firing index (**h**) for pairs of dmPFC and BLA phase-locked and non-phase-locked neurons during freezing and mobility. Insets, maximum correlation coefficient (**c**) and co-firing index (**h**) for all pairs of recorded dmPFC and BLA neurons (phase-locked pairs, $n = 180$; non-phase-locked pairs, $n = 911$; Mann-Whitney U test, top and bottom, phase-locked pairs during freezing versus mobility or non-phase-locked pairs: $U = 50,313, 7,893, 16,200, 9,413$, $**P < 0.001$, $***P < 0.001$). Error bars, mean \pm s.e.m.

indicate that sustained 4-Hz oscillations described in the present manuscript do not correspond to sensory-driven transient theta oscillations previously observed^{9,10}. Taken together, these results have important functional consequences, as they indicate the existence of distinct and independent dmPFC neuronal oscillations involved in the regulation of different aspects of fear behavior, such as stimulus-evoked attention processes related to the presentation of a salient CS, fear discrimination or the expression of freezing behavior. Notably, all of these findings were observed in mice, further studies are required to evaluate whether these oscillations also occurs in different species.

Our data also indicate that stationary dmPFC 4-Hz oscillations do not correspond to hippocampus-mediated dmPFC theta oscillations observed previously¹⁷, as muscimol inactivation of the medial septum blocked hippocampal theta recorded in the dmPFC without affecting prefrontal 4-Hz oscillations, nor the percentage of dmPFC neurons phase-locked to 4-Hz oscillations. Our observation of BLA 4-Hz oscillatory activity during freezing behavior is consistent with previous recordings of slow theta oscillations in the lateral amygdala during fear behavior, which correlate with dorsal hippocampal theta oscillations^{17,18}, although in these studies the temporal relation between CS⁺ onset, 4-Hz oscillatory activity and freezing onset and offset were not clearly established. A recent observation of power increase for 4–7.5 Hz oscillations in the cingulate cortex during a hippocampus-dependent trace fear-conditioning procedure is also partly consistent with our observation²⁶. Indeed, the authors observed

that in some conditioning trials, 4–7.5 Hz power increased during the interval separating the conditioned stimulus from the footshock. In that study, however, the neuronal interaction between the cingulate cortex and the BLA, the precise temporal relation between slow oscillation and freezing behavior, and the causal role of prefrontal 4-Hz oscillations were not established. These data nevertheless suggest that prefrontal 4-Hz oscillations might be a general mechanism of fear expression encompassing classical auditory and contextual fear conditioning.

A key finding of our study comes from the demonstration that, during freezing behavior, dmPFC 4-Hz oscillations entrain BLA oscillatory activity and synchronize spiking activity between dmPFC and BLA neurons. Recent publications have highlighted neuronal co-firing between prefrontal cortex and amygdala during resistance to extinction behavior¹¹, LFP coherence between dmPFC and BLA after CS⁺ onset during fear discrimination, and amygdala neurons phase-locked to dmPFC theta oscillations during fear discrimination¹⁰. To our knowledge, our data provide the first mechanistic demonstration of a 4-Hz-mediated long-range synchronization of spiking activity between dmPFC and BLA during freezing behavior. Moreover, our findings also indicate that dmPFC activity leads the BLA one during freezing behavior.

Accordingly, we found that the optogenetically mediated artificial induction of 4-Hz oscillations in dmPFC synchronizes dmPFC and BLA neuronal activity and increases freezing behavior in a persistent manner, which demonstrates that internally generated

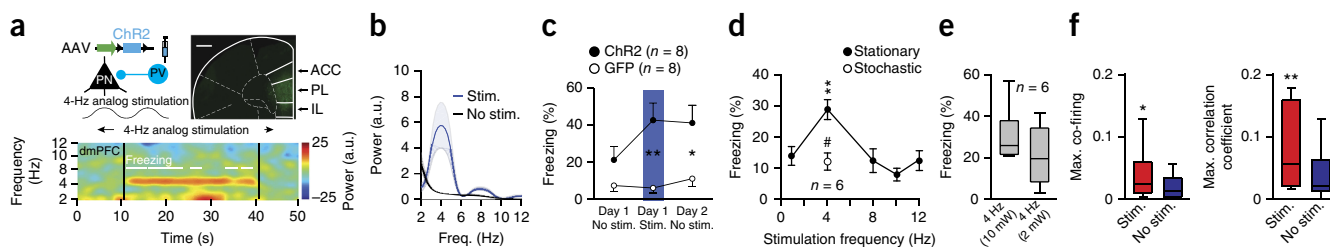


Figure 7 Optogenetic induction of dmPFC 4-Hz oscillations drives freezing. **(a)** Top left, strategy used to activate parvalbumin-expressing (PV) interneurons. Top right, coronal dmPFC micrograph from a PV-IRES-Cre mouse expressing channelrhodopsin2 (ChR2). Solid and dashed lines represent the boundaries between the cingulate cortex (ACC), the prelimbic (PL) and infralimbic (IL) areas, and other cortical structures. Scale bar, 0.5 mm. Bottom, spectrogram during 4-Hz analog stimulation. **(b)** Averaged normalized LFP power spectra of dmPFC LFPs during (Stim.) and outside (No stim.) stimulation ($n = 8$). **(c)** Percentage of freezing for ChR2 ($n = 8$) or GFP ($n = 8$) mice before, during and after 4-Hz induction (two-way ANOVA repeated measures; group: $F(1,14) = 0.868$, $P = 0.367$, time $F(1,2) = 8.926$, $P = 0.001$, group \times time $F(1,28) = 6.925$, $P = 0.0036$); unpaired t -tests: day 1: Stim. $t(14) = 3.712$, $**P = 0.002$; day 2: No stim., $t(14) = 2.758$, $*P = 0.013$). **(d)** Percentage of freezing for ChR2 mice ($n = 6$) during analog stimulation at 1, 4, 8, 10, 12 Hz (Stationary) or using a 4-Hz stochastic waveform (stationary: one-way repeated measures ANOVA: $F(5,4) = 8.618$, $P < 0.001$; Bonferroni-corrected paired t -tests: 4 versus 1 Hz: $t(5) = 5.927$, $**P = 0.0019$; 4 versus 8 Hz: $t(5) = 4.712$, $**P = 0.0053$; 4 versus 10 Hz: $t(5) = 7.632$, $***P < 0.001$; 4 versus 12 Hz: $t(5) = 4.009$, $**P = 0.01$; paired t -test: 4-Hz stationary versus stochastic: $t(5) = 3.533$, $\#P < 0.016$). **(e)** Percentage of freezing for ChR2 ($n = 6$) mice during dmPFC 4-Hz analog stimulation at 2 or 10 mW (paired t -test: $t(5) = 0.951$, $P = 0.385$). **(f)** Maximum correlation and co-firing index for pairs of dmPFC and BLA neurons during and outside stimulation ($n = 31$ pairs, Mann-Whitney, $U = 326$ and 278 , $*P = 0.03$; $**P = 0.004$). a.u., arbitrary units. Power in log scale. Shaded area and error bars, mean \pm s.e.m. For box plots, the middle, bottom and top lines correspond to the median, bottom and top quartiles, and whiskers to lower and upper extremes minus bottom quartile and top quartile, respectively. For representative examples **(a)**, similar images and traces were observed for the 16 (top, 8 ChR2 and 8 GFP mice) and 8 (bottom, 8 ChR2 mice) animals used in these experiments.

oscillations drive behavior. Neuronal synchronization between dmPFC and BLA has been classically evaluated using powerful correlational analyses^{10,11,18}, but never causally demonstrated. Our data indicate that the genesis of 4-Hz oscillations in the dmPFC is sufficient to synchronize neuronal activity between dmPFC and BLA and further drive the expression of freezing responses. Moreover, this effect was frequency and structure specific, as dmPFC manipulation at other frequencies or 4-Hz induction in the motor cortex and BLA did not induce any behavioral effects. However, our data indicate that when freezing behavior is induced following auditory fear conditioning, the BLA is necessary for its full expression. Together these data strongly suggest that dmPFC 4-Hz oscillations are instrumental for dmPFC–BLA synchronization of neuronal activities during fear behavior and that the synchronized firing activity of BLA neurons triggers fear responses (**Supplementary Fig. 11**).

The dmPFC 4-Hz analog optogenetic stimulation induced freezing behavior not only during the stimulation but also 24 h later in the context in which the mice were stimulated. This observation suggests that the artificial induction of dmPFC 4-Hz oscillations might be involved in the formation of associative fear memories. Another possibility could be that this artificial induction might lead to nonspecific anxiety behavior. However, it is unlikely that a sudden inactivation or rhythmic inhibition of prefrontal areas could lead to nonspecific anxiety behavior for at least two reasons. Optogenetic inactivation of the cingulate cortex during remote contextual memory retrieval results in a reduction of contextual fear behavior, an observation not consistent with a general increase in anxiety levels²⁷. Furthermore, in our optogenetic experiments (**Fig. 7**), dmPFC 4-Hz induction induced freezing in a context-specific manner, which is also an observation not consistent with a general increase in anxiety. Furthermore, while it is possible that induction of 4-Hz oscillations leads to the formation of associative fear memories, an alternative interpretation is that the contextual fear memory observed 24 h after optogenetic stimulation is a direct consequence of the association between contextual elements and the aversive state induced by 4-Hz oscillations. This interpretation is consistent with the notion that dmPFC–BLA 4-Hz oscillations are causally involved in the expression of freezing behavior.

Although our data indicate that dmPFC 4-Hz oscillations are causally involved in the neuronal synchronization of spiking activity between dmPFC and BLA during freezing behavior, it is conceivable that this mechanism could be involved in other emotional processes, such as avoidance, flight responses, sensory processes or cognitive tasks. For instance, recent reports have observed 4-Hz oscillations in the whisker barrel cortex during respiration²⁸ and in the rat dmPFC under working memory load during locomotor behavior²⁹. Another important question is the source of the 4-Hz oscillations. Although our data indicate that these oscillations do not originate from the hippocampus and are localized in dmPFC circuits, more work will be required to address this question and unequivocally identify the source of the 4-Hz oscillations. In summary, our data reveal a specific 4-Hz oscillatory mechanism allowing the expression of fear memories by long-range synchronization of neuronal activity between dmPFC and BLA neuronal circuits.

METHODS

Methods and any associated references are available in the [online version of the paper](#).

Note: Any Supplementary Information and Source Data files are available in the online version of the paper.

ACKNOWLEDGMENTS

We thank the members of the Herry laboratory for discussions and comments on the manuscript and K. Deisseroth (Stanford University) and E. Boyden (Massachusetts Institute of Technology) for generously sharing material. This work was supported by grants from the French National Research Agency (ANR-2010-BLAN-1442-01; ANR-10-EQPX-08 OPTOPATH; LABEX BRAIN ANR 10-LABX-43, LABEX TRAIL ANR 10-LABX-57), the European Research Council (ERC) under the European Union's Seventh Framework Program (FP7/2007-2013)/ERC grant agreement no. 281168, the Conseil Régional d'Aquitaine (C.H.), the Fondation pour la Recherche Médicale (FRM) (F.C.), the CNRS ATIP program (2014) and the city of Paris (Grant Emergence 2014), the French National Research Agency (ANR-10-LABX-54 MEMO LIFE; ANR-11-IDEX-0001-02 PSL) (K.B.), Munich Cluster for Systems Neurology (SyNergy, EXC 1010), Deutsche Forschungsgemeinschaft Priority Program 1665 and 1392 and Bundesministerium für Bildung und Forschung via grant no. 01GQ0440 (Bernstein Centre for Computational Neuroscience Munich) (A.S.) and a scholarship from the Erasmus Mundus program Neurasmus (N.K.).

AUTHOR CONTRIBUTIONS

S.B., K.B., F.C., J.C., C.D., N.K., S.K., R.R.R., A.S. and H.W. performed the experiments and analyzed the data. J.C., C.D., N.K. and C.H. designed the experiments. C.H. wrote the paper.

COMPETING FINANCIAL INTERESTS

The authors declare no competing financial interests.

Reprints and permissions information is available online at <http://www.nature.com/reprints/index.html>.

- Bosman, C.A. *et al.* Attentional stimulus selection through selective synchronization between monkey visual areas. *Neuron* **75**, 875–888 (2012).
- Siegel, M., Donner, T.H., Oostenveld, R., Fries, P. & Engel, A.K. Neuronal synchronization along the dorsal visual pathway reflects the focus of spatial attention. *Neuron* **60**, 709–719 (2008).
- Rodriguez, E. *et al.* Perception's shadow: long-distance synchronization of human brain activity. *Nature* **397**, 430–433 (1999).
- Hipp, J.F., Engel, A.K. & Siegel, M. Oscillatory synchronization in large-scale cortical networks predicts perception. *Neuron* **69**, 387–396 (2011).
- Friedrich, R.W., Habermann, C.J. & Laurent, G. Multiplexing using synchrony in the zebrafish olfactory bulb. *Nat. Neurosci.* **7**, 862–871 (2004).
- Riehle, A., Grün, S., Diesmann, M. & Aertsen, A. Spike synchronization and rate modulation differentially involved in motor cortical function. *Science* **278**, 1950–1953 (1997).
- Benchenane, K. *et al.* Coherent theta oscillations and reorganization of spike timing in the hippocampal–prefrontal network upon learning. *Neuron* **66**, 921–936 (2010).
- Gregoriou, G.G., Gotts, S.J., Zhou, H. & Desimone, R. High-frequency, long-range coupling between prefrontal and visual cortex during attention. *Science* **324**, 1207–1210 (2009).
- Courtin, J. *et al.* Prefrontal parvalbumin interneurons shape neuronal activity to drive fear expression. *Nature* **505**, 92–96 (2014).
- Likhtik, E., Stujenske, J.M., Topiwala, M.A., Harris, A.Z. & Gordon, J.A. Prefrontal entrainment of amygdala activity signals safety in learned fear and innate anxiety. *Nat. Neurosci.* **17**, 106–113 (2014).
- Livneh, U. & Paz, R. Amygdala-prefrontal synchronization underlies resistance to extinction of aversive memories. *Neuron* **75**, 133–142 (2012).
- Stujenske, J.M., Likhtik, E., Topiwala, M.A. & Gordon, J.A. Fear and safety engage competing patterns of theta-gamma coupling in the basolateral amygdala. *Neuron* **83**, 919–933 (2014).
- Gabbott, P.L., Warner, T.A., Jays, P.R., Salway, P. & Busby, S.J. Prefrontal cortex in the rat: projections to subcortical autonomic, motor, and limbic centers. *J. Comp. Neurol.* **492**, 145–177 (2005).
- Holstege, G. The periaqueductal gray controls brainstem emotional motor systems including respiration. *Prog. Brain Res.* **209**, 379–405 (2014).
- Subramanian, H.H., Balnave, R.J. & Holstege, G. The midbrain periaqueductal gray control of respiration. *J. Neurosci.* **28**, 12274–12283 (2008).
- Vianna, D.M., Landeira-Fernandez, J. & Brandão, M.L. Dorsolateral and ventral regions of the periaqueductal gray matter are involved in distinct types of fear. *Neurosci. Biobehav. Rev.* **25**, 711–719 (2001).
- Lesting, J. *et al.* Patterns of coupled theta activity in amygdala-hippocampal-prefrontal cortical circuits during fear extinction. *PLoS One* **6**, e21714 (2011).
- Seidenbecher, T., Laxmi, T.R., Stork, O. & Pape, H.C. Amygdalar and hippocampal theta rhythm synchronization during fear memory retrieval. *Science* **301**, 846–850 (2003).
- Yoder, R.M. & Pang, K.C. Involvement of GABAergic and cholinergic medial septal neurons in hippocampal theta rhythm. *Hippocampus* **15**, 381–392 (2005).
- Stark, E. *et al.* Inhibition-induced theta resonance in cortical circuits. *Neuron* **80**, 1263–1276 (2013).
- Siegle, J.H. & Wilson, M.A. Enhancement of encoding and retrieval functions through theta phase-specific manipulation of hippocampus. *eLife* **3**, e03061 (2014).
- Atallah, B.V., Bruns, W., Carandini, M. & Scanziani, M. Parvalbumin-expressing interneurons linearly transform cortical responses to visual stimuli. *Neuron* **73**, 159–170 (2012).
- Nunez, P.L. & Srinivasan, R. *Electric Fields of the Brain: The Neurophysics of EEG* 2nd edn. (Oxford Univ. Press, 2006).
- Magee, J.C. Dendritic integration of excitatory synaptic input. *Nat. Rev. Neurosci.* **1**, 181–190 (2000).
- Vaidya, S.P. & Johnston, D. Temporal synchrony and gamma-to-theta power conversion in the dendrites of CA1 pyramidal neurons. *Nat. Neurosci.* **16**, 1812–1820 (2013).
- Steenland, H.W., Li, X.Y. & Zhuo, M. Predicting aversive events and terminating fear in the mouse anterior cingulate cortex during trace fear conditioning. *J. Neurosci.* **32**, 1082–1095 (2012).
- Goshen, I. *et al.* Dynamics of retrieval strategies for remote memories. *Cell* **147**, 678–689 (2011).
- Ito, J. *et al.* Whisker barrel cortex delta oscillations and gamma power in the awake mouse are linked to respiration. *Nat. Commun.* **5**, 3572 (2014).
- Fujisawa, S. & Buzsáki, G. A 4 Hz oscillation adaptively synchronizes prefrontal, VTA, and hippocampal activities. *Neuron* **72**, 153–165 (2011).

ONLINE METHODS

Animals. Naive male C57BL6/J mice (3 months old, Janvier) and PV-IRES-Cre mice (3 months old, Jackson Laboratory, B6;129P2-*Pvalbtm1^{cre}Arbr/J*) were individually housed for at least 7 d before all experiments, under a 12-h light–dark cycle, and provided with food and water *ad libitum*. Experiments were performed during the light phase. All procedures were performed in accordance with standard ethical guidelines (European Communities Directive 86/60-EEC) and were approved by the committee on Animal Health and Care of Institut National de la Santé et de la Recherche Médicale and French Ministry of Agriculture and Forestry (authorization A3312001).

Behavior. Auditory fear conditioning and testing took place in two different contexts (context A and B). The conditioning and testing boxes were cleaned with 70% ethanol and 1% acetic acid before and after each session, respectively. To score freezing behavior independently of the experimenter, an automated infrared beam detection system located on the bottom of the experimental chambers was used (Coulbourn Instruments). Because the detection of our dependent variable (freezing) was independent of the experimenter, we did not use a blinding process for group allocation or behavior scoring. The animals were considered to be freezing if no movement was detected for 2 s. On day 1, C57BL6/J mice were subjected to a habituation session in context A, in which they received four presentations of the CS⁺ and of the CS⁻ (total CS duration, 30 s; consisting of 50-ms pips at 0.9 Hz repeated 27 times, 2 ms rise and fall, pip frequency, 7.5 kHz, or white-noise, 80 dB sound pressure level).

Discriminative fear conditioning was performed on the same day by pairing the CS⁺ with a US (1 s foot-shock, 0.6 mA, 5 CS⁺–US pairings, inter-trial intervals 20–180 s). The onset of the US coincided with the offset of the CS⁺. The CS⁻ was presented after each CS⁺–US association but was never reinforced (five CS⁻ presentations; inter-trial intervals, 20–180 s). The frequencies used for CS⁺ and CS⁻ were counterbalanced across animals and randomization of CS⁻ and CS⁺ allocation was performed using an online randomization algorithm (<http://www.randomization.com/>).

On day 2, conditioned mice were submitted to a testing session (retrieval session) in context B during which they received 4 and 12 presentations of the CS⁻ and CS⁺, respectively. Thirteen naive C57BL6/J mice recorded simultaneously in the dmPFC and BLA were included in this experiment and the data collected in two distinct replicates. Five additional naive C57BL6/J mice recorded in the vPAG were fear conditioned using the same protocol. Contextual fear conditioning took place in contexts A and B as describe above. On day 1, C57BL6/J mice were subjected for 5 min to a habituation session in context A. Contextual fear conditioning was performed 24 h later by pairing context B with a US. The next day, mice were subjected for 12 min to a testing session (retrieval) in context B. Six naive C57BL6/J mice were included in this experiment and the data collected in two distinct replicates. For neck muscle EMG recordings, C57BL6/J mice were exposed to 20 CS⁺ presentations in context B as describe above and auditory fear conditioning was performed on the same day by pairing the CS⁺ with a US. Seven naive C57BL6/J mice were included in this experiment and the data collected in two distinct replicates.

For optogenetic experiments using channelrhodopsin, PV-IRES-Cre mice and GPF controls were exposed on day 1 to context A as described above. During the session, four blue-light 4-Hz rhythmic analog (2 or 10 mW, 30 s) stimulations were delivered in the dmPFC to activate parvalbumin-expressing interneurons. On days 2 and 3, mice were exposed to the same context as day 1 or to the neutral context B as described above, without any stimulation, respectively. To test for the frequency and structure specificity of the stimulation, other groups of naive PV-IRES-Cre mice were submitted to four blue-light rhythmic analog dmPFC stimulations at different frequencies (1, 8, 10 and 12 Hz, stochastic 4 Hz composed of 2–12 Hz frequency with an average at 4 Hz, 10 mW, 30 s, $n = 6$ mice) or to four blue-light rhythmic analog stimulations at 4 Hz of the motor cortex ($n = 4$ mice) or the BLA ($n = 5$ mice). These five mice infected in the BLA were also submitted to auditory fear conditioning as described above and tested 24 and 48 h later to evaluate the effect of BLA silencing during fear behavior. Randomization of group allocation (Chr2 versus GFP controls) was performed using an online randomization algorithm (<http://www.randomization.com/>).

For pharmacological experiments, C57BL6/J mice were submitted to a fear conditioning paradigm consisting of CS⁺ and US pairings in context A as described above. On days 2, 3 and 4, conditioned mice were tested in context B,

during which they received four presentations of the CS⁺ before muscimol injections (day 2, test 1), 5 min after muscimol injections (day 3, Inac.) and 24 h after muscimol injections (day 4, test 2). Six naive C57BL6/J mice were included in this experiment and the data collected in two distinct replicates.

Surgery and recordings. Mice were anaesthetized with isoflurane (induction 3%, maintenance 1.5%) in O₂. Body temperature was maintained at 37 °C with a temperature controller system (FHC). Mice were secured in a stereotaxic frame and unilaterally implanted in the left dorsomedial prefrontal cortex (dmPFC) with a multi-wire electrode array aimed at the following coordinates: 2.0 mm anterior to the bregma, 0.3 mm lateral to the midline and 0.8 to 1.4 mm ventral to the cortical surface. They were implanted in the left basolateral amygdala (BLA) with a multi-wire electrode array aimed at the following coordinates: 1.7 mm posterior to the bregma, 3 mm lateral to the midline and 4 mm ventral to the cortical surface.

Another group of mice was implanted only in the ventrolateral periaqueductal gray at the following coordinates: –4.30 mm anterior to the bregma, 0.55 mm lateral to the midline and 2.20 mm ventral to the cortical surface. For contextual fear conditioning experiments, mice were implanted only in the dmPFC. For electromyographic (EMG) recording experiments, Teflon-coated stainless steel electrodes (AM Systems) were sutured into the right and left nuchal muscles. Wires were connected to a multi-wire electrode array connector attached to the skull.

For pharmacological experiments, animals were implanted in the dmPFC at the same coordinate as above and in dorsal hippocampus at the following coordinates: 2 mm posterior to bregma, 1.2 mm lateral to midline and 1.2 to 1.4 mm ventral to the cortical surface. The electrodes consisted of 16 individually insulated nichrome wires (13 μ m inner diameter, impedance 30–100 K Ω ; Kanthal) contained in a 26-gauge stainless steel guide cannula. The wires were attached to an 18-pin connector (Omnetics) and two connectors were used for each mouse. All implants were secured using Super-Bond cement (Sun Medical). After surgery, mice were allowed to recover for 7 d and were habituated to handling. Analgesia was applied before and 1 d after surgery (Metacam, Boehringer). Electrodes were connected to a headstage (Plexon) containing 16 unity-gain operational amplifiers. The headstage was connected to a 16-channel preamplifier (gain 100 \times , bandpass filter from 150 Hz to 9 kHz for unit activity; Plexon). Spiking activity was digitized at 40 kHz and bandpass filtered from 250 Hz to 8 kHz, and isolated by time-amplitude window discrimination and template matching using a Multichannel Acquisition Processor system (Plexon). At the conclusion of the experiment, recording sites were marked with electrolytic lesions before perfusion, and electrode tip locations were reconstructed with standard histological techniques.

Single-unit analyses. Single-unit spike sorting was performed using Off-Line Spike Sorter (OFSS, Plexon) for all behavioral sessions. Principal component scores were calculated for unsorted waveforms and plotted in a three-dimensional principal component space; clusters containing similar valid waveforms were manually defined. A group of waveforms were considered to be generated from a single neuron if the waveforms formed a discrete, isolated cluster in the principal component space and did not contain a refractory period less than 1 ms, as assessed using autocorrelogram analyses. To avoid analysis of the same neuron recorded on different channels, we computed cross-correlation histograms. If a target neuron presented a peak of activity at a time that the reference neuron fired, only one of the two neurons was considered for further analysis.

To separate putative inhibitory interneurons from putative excitatory principal neurons, we used an unsupervised clustering algorithm based on Ward's method. In brief, the Euclidian distance was calculated between all neuron pairs on the basis of the three-dimensional space defined by each neuron's average half-spike width (measured from trough to peak), the firing rate and the area under the hyperpolarization phase of the spike. An iterative agglomerative procedure was then used to combine neurons into groups based on the matrix of distances such that the total number of groups was reduced to give the smallest possible increase in within-group sum of squares deviation.

For the detection of interactions between units recorded in the dmPFC and BLA, the spike trains of each simultaneously recorded pair were binned (10 ms bin size), the cross-correlation of the binned histograms was calculated over multiple lags (maximum lag, ± 500 ms) and the peak cross-correlation coefficient for each pair was determined. For the detection of co-firing property for unit pairs,

spike trains were binned as before and the co-firing index was calculated as the ratio of co-occurring (common) spikes to the total number of spikes for the two units. This provides a simple yet direct measure of the co-occurrence of unit spikes on multiple levels of temporal resolution. For the determination of the bin size and the robustness of the method, different bin sizes were tested; they all gave qualitatively similar results. Among those tested, 10 ms was selected because it allows the identification of potentially monosynaptic interactions. To evaluate whether neurons were oscillating at 4 Hz, we used Gabor functions, which are commonly used to fit autocorrelation (AC) histograms of nonstationary rhythmic biological time series such as neuronal spiking activity^{30–32}. Gabor functions are damped sine waves with two components: first, the sine wave frequency (f_0); second, a damping frequency (f_d) that modulates the amplitude of the sine wave. The Gabor functions served as a predicted AC (pAC) that was used to fit the actual AC of the frequencies of interest. We constructed a set of Gabor functions as follows³²:

$$\text{pAC}_{\text{fofd}} = \cos(2\pi x f_0) \times \exp(-Cx^2 f_d)$$

with f_0 and f_d both ranging from 1 to 25 Hz, hence creating 100×100 predicted ACs. The quality of the fit of each predicted AC was then assessed by its correlation (Spearman's ρ) with the actual AC of specific frequency bands (calculated for lags t of 0–500 ms), and this correlation score was plotted for each f_0, f_d pair. Points showing the highest correlation thus represent candidate f_0, f_d pairs capable of predicting oscillations.

Local field potential and EMG analyses. Local field potentials were analyzed using custom-written Matlab programs. Raw LFP traces were filtered between 0.7 Hz and 400 Hz and downsampled to 1 kHz. All signals were filtered using zero-phase-distortion sixth-order Butterworth filters. For phase analyses, the signal was filtered in the desired frequency band (2–6 Hz for the 4-Hz oscillation) and the complex-valued analytic signal was calculated using the Hilbert transform as below.

$$\rho(t)e^{-i\phi(t)}$$

The vector length and the arctangent of the vector angle provide the estimation of the instantaneous amplitude and instantaneous phase of the signal, respectively, at every time point. All analyses were performed during freezing episodes and, where indicated, during subsampled non-freezing epochs. A phase of 0° corresponds to the peak of prefrontal–amygdala oscillations. LFP power spectrum and LFP–LFP coherence estimations were, unless otherwise noted, performed using the multitaper method³³. Briefly, data were multiplied by a set of 2–5 orthogonal taper functions (discrete prolate spheroidal sequences), Fourier transformed using a window size of 2 s and averaged to obtain a direct multitaper spectral estimate.

Signal to noise ratio (SNR) for 4-Hz power was calculated as the ratio of the mean power in the 2–6 Hz band to the mean power outside this band. Because one mouse did not show immobility behavior during habituation, it was excluded from SNR analyses. For coherence analyses, a method based on imaginary coherence was employed³⁴. Imaginary coherence was calculated as

$$\text{iCoh} = \frac{|\text{Im}(\sum_{\text{bins}} S_{xy})|}{\sqrt{\sum_{\text{bins}} S_{xx} \times \sum_{\text{bins}} S_{yy}}}$$

where S_{xy} is the cross-spectrum, S_{xx} and S_{yy} are the auto-spectra and summation takes place over the spectrogram bins corresponding to the quantified state. By keeping the imaginary part of the normalized cross-spectrum, coherence value is weighted inversely proportionally to the time lag between the two signals. Consequently, it is sensitive only to time-lagged signals, whereas the effect of absolutely synchronous signals is eliminated. Given the very synchronous nature of the oscillation examined here and the small phase lag, imaginary coherence is expected to underestimate the strength of the interaction. However, we opted for this conservative variety of coherence analysis to avoid any influence of volume-conducted currents or artifacts that can artificially boost coherence values.

To investigate any potential causal interaction between the oscillations recorded in the two structures, spectrally resolved Granger causality was

calculated for the unfiltered LFP signals. Granger causality is a statistical measure of the predictive power of one variable over another. Linear trends were removed from the LFP signals and signals were normalized before the analysis. For these analyses, the MVGC multivariate Granger causality toolbox³⁵ was used to fit a higher order vector autoregressive model to the processes. Data were tested for stability in time and model order was determined using the Akaike information criterion. To identify directionality and quantify the lag between the two signals in terms of phase and amplitude, a point process was defined consisting of the peaks of the bandpass-filtered LFP signal for each of the two structures. The lag of the peak of the cross-correlation of these point processes identifies the time lag of the oscillation in the two structures and the directionality of their potential interaction. To avoid any potential bias due to phase asymmetry, the same procedure was tested for the troughs, giving identical results. To investigate this relationship throughout the oscillation cycle, the phase of each analytical signal was extracted using the Hilbert transform and the distribution of the phase differences between the two structures was characterized for deviation from uniformity using circular statistics and Monte Carlo simulations. To evaluate the specific role of phase, amplitude and their interplay on the directionality and causality measures for the LFP data, a procedure was devised for the selective perturbation of phase and amplitude of the signals. Signals were converted in the spectral domain using a discrete Fourier transform and the phase (or amplitude) component of the signal was permuted, leaving the amplitude (or phase) intact. The modified signal was converted back to the time domain using the inverse Fourier transform. For the power comodulation analysis, the power profile for each frequency bin in each structure was calculated and the correlation coefficient of every pair was calculated³⁶.

To compare the impact of CS⁺ during freezing on local theta and 4-Hz phase resetting, we used a multitaper analysis of LFP signals for frequencies ranging from 2 to 12 Hz and computed a stimulus-triggered spectrogram. For the CS⁺-triggered theta and 4-Hz phase overlays, signals were filtered in the corresponding range (theta, 8–12 Hz; 4-Hz, 2–6 Hz) and phases were extracted from the analytic signal as described above. To quantify phase stability across all CS⁺ pips during freezing episodes, we calculated the mean resultant length for all time–frequency pairs. To evaluate the predictive value of 4-Hz power for freezing behavior, we used wavelet analysis, which in some instances allows a higher temporal resolution, to quantify the spectral content of the signal for frequencies between 2 and 12 Hz and computed freezing-triggered spectrograms. To evaluate the latency to freeze in response to the CS⁺, individual tone onsets and freezing period onsets for individual mice were binned (100 ms bin size), smoothed and averaged, and cross-correlation analysis was performed on these data taking freezing onset epochs as the reference event (Fig. 1e). In these conditions, negative lags indicate that conditioned stimuli precede freezing events. Statistical significance was evaluated using two different approaches and then combined. We first simulated 1,000 instances of a uniform distribution of freezing episodes and recomputed the cross-correlation analysis. We next shuffled 1,000 times the freezing ISIs of the actual freezing episodes to preserve the first-order statistics of freezing behavior but perturb its relation to CS⁺ and recomputed the cross-correlation analysis. The results of the two analyses were averaged to produce a more robust significance threshold. However, each individual result was not qualitatively and quantitatively different from the final average. One interesting characteristic of the cross-correlation is its oscillatory nature, which is due to the rhythmic repetition of CS⁺ (27 pips delivered at 1.1 Hz) and the tendency of elicited freezing to occur in response to these events (Fig. 1e).

For correlation analyses between freezing behavior and 4-Hz oscillations (Fig. 3d and Supplementary Fig. 2e), we first evaluated the percentage of time individual animals spent frozen during the entire recording session. For 4-Hz quantification, 4-Hz oscillation periods were evaluated as periods of significant 4-Hz SNR, as compared to baseline (a 2-min period before the first CS presentation). 4 Hz expressed as the percentage of total time corresponds to the ratio of the total duration of 4-Hz episodes to the recording session duration. For electromyographic recordings, unilateral EMG signals were band-pass filtered (100–1,000 Hz), rectified and integrated (convolution with 100-ms Gaussian kernel). The ΔEMG signal was calculated as the differential EMG recorded in the left and right nuchal muscle³⁷. The absolute value of ΔEMG was then Z-score transformed and averaged around freezing onsets (–500 ms to 500 ms) occurring during CS⁺ presentation, during both habituation and fear conditioning.

Phase-locking analyses. For phase modulation analysis, the variance-stabilized $\ln(Z)$ ($Z = R^2/n$, R being the resultant length and n the sample size) statistics for the Rayleigh test for uniformity against the von Mises distribution were calculated^{38,39}. To partially account for the sample size bias of the resultant length, only units with at least 100 spikes during freezing behavior were taken into consideration. All results were corroborated using the pairwise phase consistency method, a bias-free estimate of neuronal synchronization based on the average pairwise circular distance

$$D = \frac{2}{N(N-1)} \sum_{i=1}^{N-1} \sum_{j=(i+1)}^N |\theta_i - \theta_j| \bmod \pi$$

with θ_i and θ_j being the phases from two different spikes. This method is analytically equivalent to the squared phase-locking value⁴⁰. To calculate the statistics for each unit, bootstrap analyses and Monte Carlo simulations were performed. In the Monte Carlo simulations, the Y_{sim} value, indicating the expected value for a uniform prior distribution, was calculated for each sample size. Units for which the Y_{unit} exceeded the 95% percentile of the simulated Y_{sim} estimate were considered phase-locked. For the bootstrap statistics, in order to take into account the higher-order statistics of the spike trains, for each unit the inter-spike intervals were shuffled randomly and the potentially nonuniform prior distribution was calculated.

Phases for both dmPFC and BLA spikes were extracted using the dmPFC 4-Hz oscillation phase that exhibits the highest SNR and allows direct comparison of the phase-locking statistics. For the statistical evaluations, before the phase extraction, the prior distribution of phases of the 4-Hz oscillation was examined, and, as is the case for other neuronal slow oscillations, this prior distribution deviated from the uniform distribution. This bias can alter the phase-locking statistics and produce false positives^{38,39}. To account for this potential bias, the phases of the LFPs were transformed using the inverse of the empirical cumulative density function to return a signal with uniform prior distribution. Following this transformation, the spike phases were drawn from a uniform distribution, allowing the application of circular statistics for detecting deviations from uniformity. For normalized averaged phase density analyses, the circular histogram for each neuron was normalized to the maximum and the averaged circular histogram was computed.

Supervised learning algorithms. To establish the predictive value of dmPFC and BLA 4-Hz oscillations for the animal's behavioral state ("freezing" or "not freezing"), we used two distinct machine learning approaches. Specifically, we used the 4-Hz signal-to-noise ratio (SNR) of the two structures as features to train a naive Bayes classifier and a support vector machine (SVM). On the basis of the time-resolved spectral decomposition of the signals (spectrograms), we calculated the mean 4-Hz SNR across three consecutive time bins (with a bin size of 150 ms) and assigned a binary value based on the behavioral state of the animal during the corresponding time (450 ms: freezing = 1; mobility = 0). Each formed SNR–binary value pair constitutes a single data point used as an input to the classifier.

For this analysis, we considered the total duration of the recordings; that is, all time bins were used in this analysis. SVM projects data into a higher dimensional space and estimates a hyperplane that best separates the data points belonging to distinct classes⁴¹. Naive Bayes classifiers assume independence of the probability distributions of the features and classify the test data on the basis of the maximal posterior probability of class assignment⁴². The data set was randomly split into a training data set containing 70% of the data points, which was used to train the classifiers, and a test data set containing the remaining 30% of data points, that was used to test the accuracy of the algorithms. To estimate the stability of the algorithms and confidence intervals of the accuracy and receiver operating characteristics (ROC) curves of the classifiers, we implemented a Monte Carlo procedure whereby the data set was randomly split 1,000 times in mutually exclusive training and test data sets and the algorithms were trained and tested on the respective data sets. The accuracy, defined as

$$\text{accuracy} = \frac{\text{number of true positives} + \text{number of true negatives}}{\text{number of datapoints}}$$

and the area under the curve (AUC) of the ROC curve were used to characterize the performance of the classifiers and were compared with the same algorithms trained on shuffled data using the exact same Monte Carlo procedure.

Statistical analyses. For each statistical analysis provided in the manuscript, the Kolmogorov–Smirnov normality test was first performed on the data to determine whether parametric or non-parametric tests were required. When multiple statistical tests were performed, Bonferroni corrections were applied. Two different approaches were used to calculate the sample size. For studies in which we had sufficient information on response variables, power analyses were carried out to determine the number of mice needed. For studies in which the behavioral effect of the manipulation could not be prespecified, such as optogenetic experiments, we used a sequential stopping rule (SSR). In essence, this method enables null-hypothesis tests to be used in sequential stages by analyzing the data at several experimental points using t -tests. Usually the experiment started by testing only a few animals, and if the P value was below 0.05, the investigator declared the effect significant and stopped testing. If the P value was greater than 0.36, the investigator stopped the experiment and retained the null hypothesis.

For sample-size estimation using power analyses, we used a power analysis calculator (G*Power3). For each analysis, sample size was determined using a power >0.9 and α error = 0.05. All tests were two-sided. Power analyses were computed for matched pairs (cued and contextual fear conditioning protocol (Fig. 1 and Supplementary Fig. 4) and pharmacological experiments (Supplementary Fig. 5)). In our behavioral experiments, a critical parameter is freezing percentage, and the numerical endpoint typically ranged between 50% and 70% freezing for CS⁺ presentations immediately following auditory fear conditioning and between 10% and 30% freezing for CS⁻ presentations. A minimum biologically significant difference in the mean values between CS⁻ and CS⁺ conditions for cued fear conditioning (Fig. 1) or between habituation and test sessions for contextual fear conditioning (Supplementary Fig. 4) is 1.5-fold. If we assume a s.d. of 1.5 for a mean value of 60% freezing for CS⁺ test session and 20% freezing for CS⁻ habituation (which are realistic numbers), then a minimum $n = 6$ is needed to reject the null hypothesis with 90% probability. Sample size determination using SSR analyses was used for optogenetic experiments, in which it was not possible to determine a priori the effect of the optical manipulation. We used P values of 0.05 and 0.36 for the lower and upper criteria.

Muscimol inactivation. Mice were unilaterally implanted with a stainless steel guide cannula (26 gauge; Plastics One) aimed at the medial septum using an angle of 10° and recording electrodes were implanted in the dmPFC and the dorsal hippocampus as described in the section "Surgery and recordings". To target the medial septum, we used the following coordinates: 1 mm anterior to bregma; 0.7 mm lateral to midline and 3.0 to 3.3 mm ventral to the cortical surface with an angle of 10° in the coronal plane. The cannula was secured using Super-Bond cement (Sun Medical). On the injection day, muscimol (muscimol–bodipy–TMR-X conjugate, Invitrogen; 0.8 mM in PBS 0.1 M) was infused at a rate of 0.2 $\mu\text{L}/\text{min}$ over 2 min (total volume of 0.4 μL). On the injection day, muscimol was infused 15 min before the behavioral test. After the end of the experiment, muscimol was again infused with the same parameters to control for drug diffusion in the medial septum and mice were perfused. Brains were collected for histological analyses as described below.

Anatomical analysis. Mice were euthanized with isoflurane and perfused through the left ventricle with 4% w/v paraformaldehyde (PFA) in 0.1 M PBS. Brains were dissected out and postfixed for 24 h at 4 °C in the same solution. 60- μm -thick sections were cut, mounted on gelatin-coated microscope slides and dried. Sections were stained with toluidine blue, dehydrated and mounted. Electrolytic lesions were identified with conventional transmission light microscopy. Only recordings with confirmed lesions in cingulate or prelimbic areas of dmPFC and basolateral amygdala (BLA) were included in our analyses. For verification of muscimol injections in the medial septum and viral injections in dmPFC, BLA or motor cortex, serial 80- μm -thick slices were imaged using an epifluorescence system (Leica DM 5000) fitted with a 10 \times dry objective. The location and the extent of the injections or infections were visually controlled. All included muscimol injections were targeted and limited to the medial septum. Similarly, only infections accurately targeting the region of interest were considered for behavioral and electrophysiological analyses.

Virus injections and optogenetics. For optical identification of parvalbumin-expressing interneurons, conditional AAV encoding ChR2 (AAV-EF1a-DIO-hChR2(H134R)-EYFP, serotype 5, Vector Core, University of North Carolina)

or ArchT (AAV-FLEX-ArchT-GFP, serotype 5, Vector Core, University of North Carolina) were bilaterally injected into the dmPFC of PV-IRES-Cre mice ($n = 12$ mice) from glass pipettes (tip diameter 10–20 μm) connected to a Picospritzer (Parker Hannifin Corporation; approximately 0.4 μL per hemisphere) at the following coordinates: dmPFC: 2.0 mm anterior to bregma, 0.4 mm lateral to midline and 0.9 to 1.2 mm ventral to the cortical surface. One to 2 weeks after the injection, mice were implanted bilaterally with optic fibers (diameter, 200 μm ; numerical aperture, 0.37; flat tip; Doric Lenses) at the same coordinates. All implants were secured using Super-Bond cement (Sun Medical). For experiments using optogenetic stimulation coupled to single-unit and LFP recordings, one of the two optic fibers was combined to the array of 16 or 32 individually insulated nichrome wires. Single-unit recordings during the manipulation of PV interneurons were performed as described in the section “Surgery and recordings.”

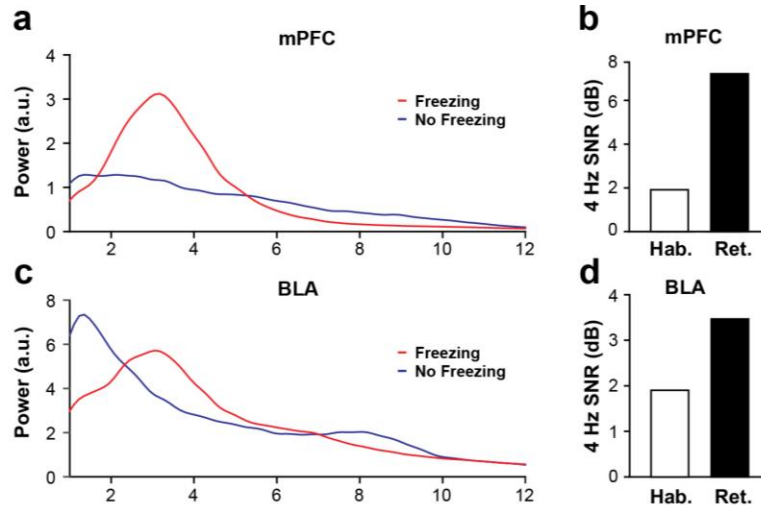
Behavioral and recording experiments were performed 3–5 weeks after injection. The light (approximately 2 or 10 mW per implanted fiber) was bilaterally conducted from the laser (OptoDuet 473/593 nm, Ikecool) to the mouse via two fiber-optic patch cords (diameter, 200 μm , Doric Lenses) connected to a rotary joint (1×2 fiber-optic rotary joint, Doric Lenses) that allowed mice to freely move in the behavioral apparatus. For optical control of parvalbumin-expressing interneurons, conditional AAV encoding ChR2 (AAV-EF1a-DIO-hChR2(H134R)-EYFP, serotype 5, Vector Core, University of North Carolina) was bilaterally injected into the dmPFC or the BLA at the same coordinates as above or into the motor cortex of PV-IRES-Cre mice at the following coordinates: 2.0 mm anterior to bregma, 1.5 mm lateral to midline and 1.3 mm ventral to the cortical surface. Control experiments were performed using an AAV containing the DNA construct for GFP alone (AAV-FLEX-GFP, Vector Core, University of North Carolina).

For optogenetic manipulation of PV interneurons during behavior, we used a 30-s analog dmPFC stimulation delivered at 1, 4, 8, 10 or 12 Hz. As a control we also used a stochastic 4-Hz analog dmPFC stimulation generated by an oscillator with a randomly time-modulated frequency drawn from a Gaussian distribution centered on 4 Hz. The power spectrum of the signal displayed a broad peak

around 4 Hz, but the duration of each cycle varied randomly from 0.15 to 0.6 s, thereby destroying the regularity of the population activity. For motor cortex experiments, we used a 4-Hz analog stimulation. For BLA silencing experiments, a continuous pulse of blue light was applied during CS⁺ presentations 24 h after fear conditioning. After behavioral and recording experiments, mice were perfused and histological analysis was performed.

A **Supplementary Methods Checklist** is available.

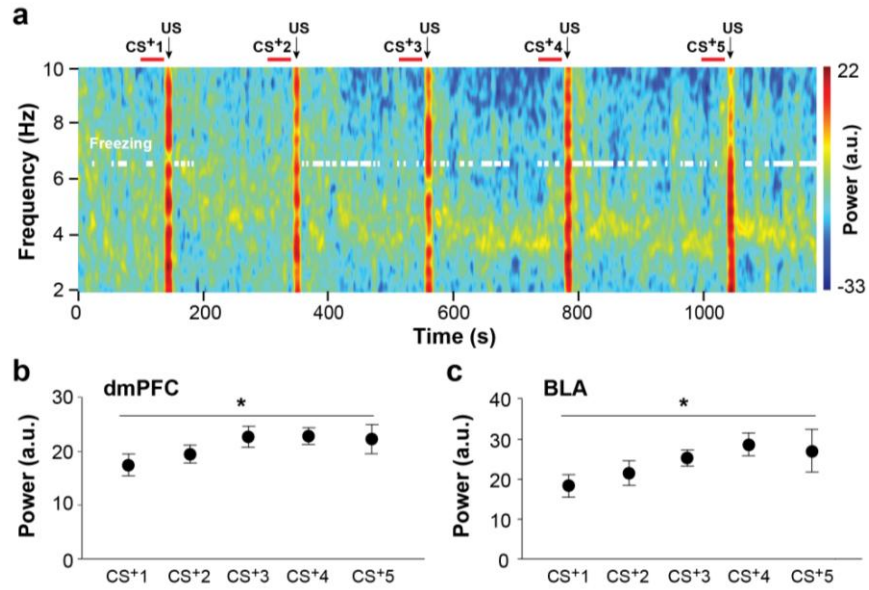
30. Engel, A.K., König, P., Gray, C.M. & Singer, W. Stimulus-dependent neuronal oscillations in cat visual cortex: inter-columnar interaction as determined by cross-correlation analysis. *Eur. J. Neurosci.* **2**, 588–606 (1990).
31. Gray, C.M., König, P., Engel, A.K. & Singer, W. Oscillatory responses in cat visual cortex exhibit inter-columnar synchronization which reflects global stimulus properties. *Nature* **338**, 334–337 (1989).
32. Young, M.P., Tanaka, K. & Yamane, S. On oscillating neuronal responses in the visual cortex of the monkey. *J. Neurophysiol.* **67**, 1464–1474 (1992).
33. Mitra, P.P. & Pesaran, B. Analysis of dynamic brain imaging data. *Biophys. J.* **76**, 691–708 (1999).
34. Nolte, G. *et al.* Identifying true brain interaction from EEG data using the imaginary part of coherency. *Clin. Neurophysiol.* **115**, 2292–2307 (2004).
35. Barnett, L. & Seth, A.K. The MVGC multivariate Granger causality toolbox: a new approach to Granger-causal inference. *J. Neurosci. Methods* **223**, 50–68 (2014).
36. Buzsáki, G. *et al.* Hippocampal network patterns of activity in the mouse. *Neuroscience* **116**, 201–211 (2003).
37. Steenland, H.W. & Zhuo, M. Neck electromyography is an effective measure of fear behavior. *J. Neurosci. Methods* **177**, 355–360 (2009).
38. Siapas, A.G., Lubenov, E.V. & Wilson, M.A. Prefrontal phase locking to hippocampal theta oscillations. *Neuron* **46**, 141–151 (2005).
39. Sirota, A. *et al.* Entrainment of neocortical neurons and gamma oscillations by the hippocampal theta rhythm. *Neuron* **60**, 683–697 (2008).
40. Vinck, M., van Wingerden, M., Womelsdorf, T., Fries, P. & Pennartz, C.M. The pairwise phase consistency: a bias-free measure of rhythmic neuronal synchronization. *Neuroimage* **51**, 112–122 (2010).
41. Cortes, C. & Vapnik, V. Support-vector networks. *Mach. Learn.* **20**, 273–297 (1995).
42. Bishop, C.M. *Pattern Recognition and Machine Learning* (eds. Jordan, M., Kleinberg J. & Schölkopf, B.) (Springer, 2006).



Supplementary Figure 1

Emergence of dmPFC and BLA 4-Hz oscillations during freezing behavior.

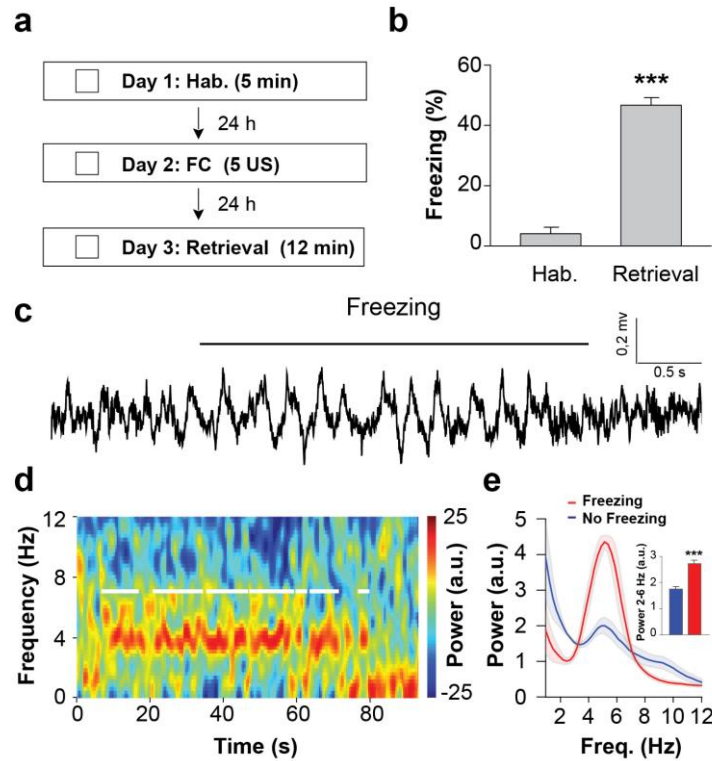
(a) Representative power spectrum of dmPFC LFPs recorded during Retrieval for freezing and no freezing periods. **(b)** Representative signal to noise ratio (SNR) of dmPFC 4 Hz oscillation (2-6 Hz) during Habituation (Hab.) and Retrieval (Ret.). **(c)** Representative power spectrum of BLA LFPs recorded during Retrieval for freezing and no freezing periods. **(d)** Representative signal to noise ratio (SNR) of BLA 4 Hz oscillation (2-6 Hz) during Habituation (Hab.) and Retrieval (Ret.). Similar results were obtained for the 13 animals used in these experiments.



Supplementary Figure 2

Development of dmPFC and BLA 4-Hz oscillations during fear conditioning.

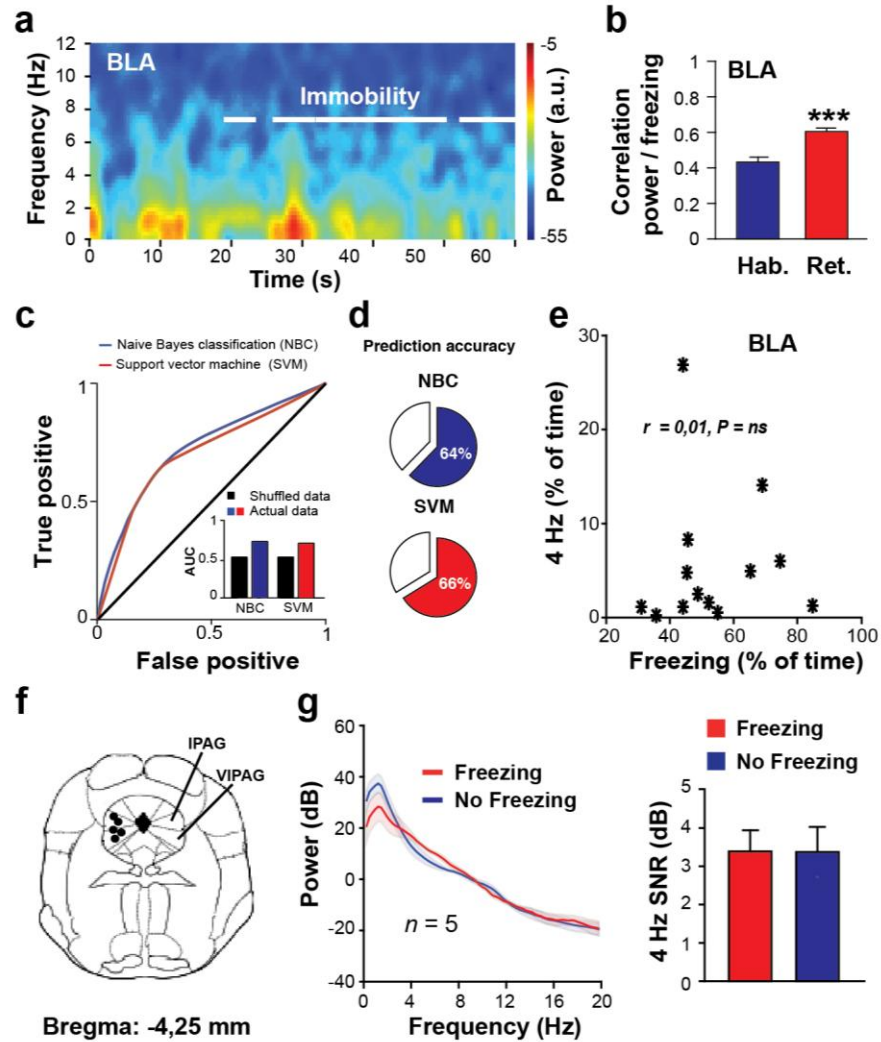
(a) Representative spectrogram of dmPFC LFPs recorded during auditory fear conditioning for successive CS⁺-US associations (top red lines: CS⁺ duration). White lines on the spectrogram indicate immobility/freezing episodes. **(b, c)** Averaged dmPFC **(b)** and BLA **(c)** power during CS⁺ presentations throughout the conditioning session ($n = 4$ mice, one way repeated measures ANOVA, dmPFC $F_{(3,4)} = 3.617$, $* P = 0.0372$; BLA: $F_{(3,4)} = 4.794$, $* P = 0.0153$). a.u.: arbitrary units. Spectral power in log scale. Error bars: mean \pm s.e.m. For the representative example in **(a)**, similar results were obtained for the 4 animals used in these experiments.



Supplementary Figure 3

Emergence of dmPFC 4-Hz oscillations during contextual fear behaviour.

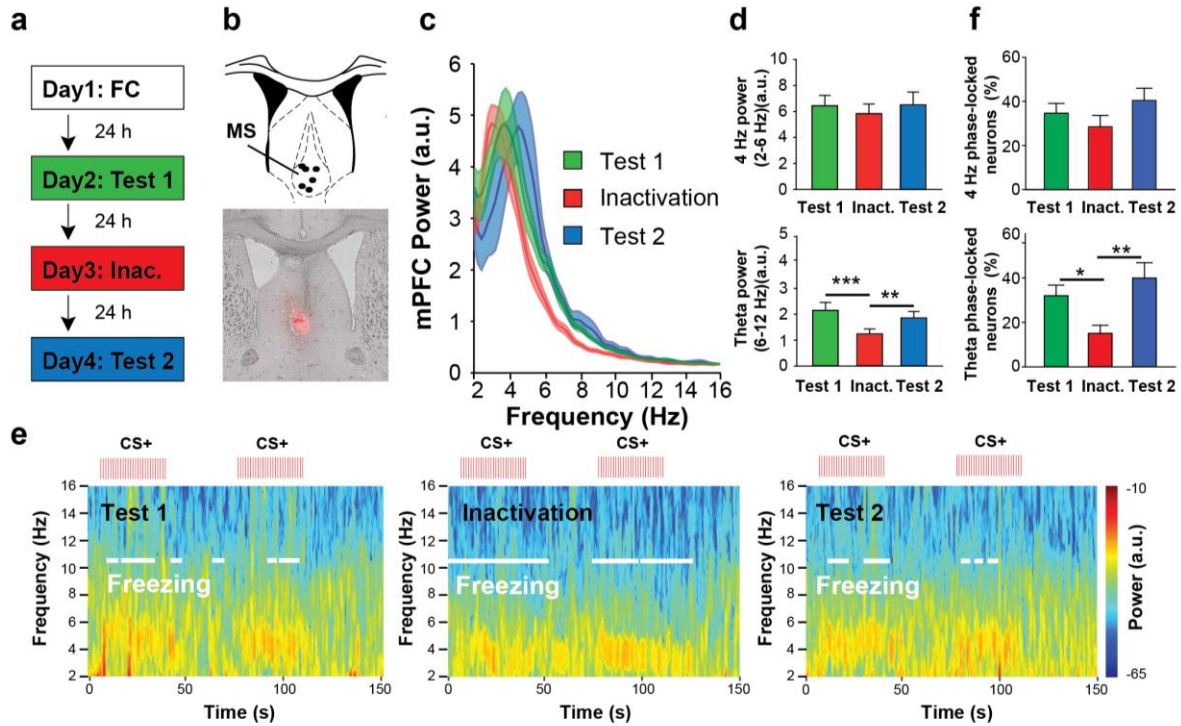
(a, b) Protocol and behavioural results. During Habituation (Hab.), mice ($n = 6$) exhibited low freezing whereas following contextual fear conditioning (Day 2: Retrieval), freezing values were significantly increased (Paired t -test, Hab. versus Retrieval: $t(5) = -11.639$, $*** P < 0.001$). **(c)** Representative dmPFC raw LFP traces recorded during the Retrieval session. 4 Hz oscillatory activity is visible during freezing behaviour. **(d)** Representative spectrogram of dmPFC LFPs at a fine time resolution during freezing episodes at Retrieval. White lines on the spectrogram indicate freezing episodes. **(e)** Averaged power spectrum of dmPFC LFPs recorded during Retrieval for freezing and no freezing periods ($n = 6$ mice). Inset: Averaged dmPFC 2-6 Hz power during Retrieval for freezing and no freezing periods (Paired t -test, Freezing versus No Freezing: $t(5) = -6.039$, $*** P < 0.001$). a.u.: arbitrary units. Spectral power in log scale. Shaded area and error bars: mean \pm s.e.m. For the representative examples **(c, d)**, similar results were obtained for the 6 animals used in these experiments.



Supplementary Figure 4

Relation of dmPFC and BLA 4-Hz oscillations with freezing, immobility and motor behavior.

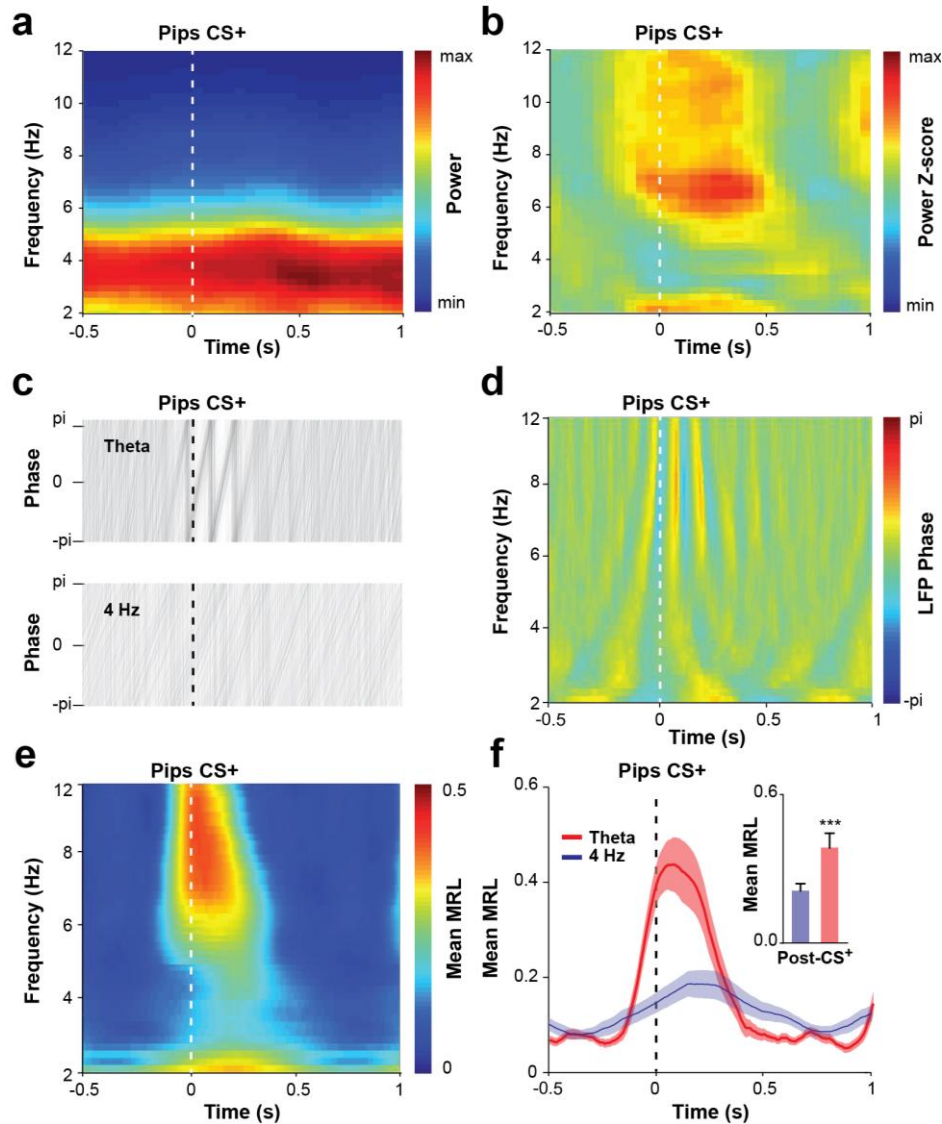
(a) Representative spectrograms of BLA LFPs recorded during Habituation. White lines on the spectrogram indicate immobility periods. (b) Correlation coefficient between the power envelope of the 4 Hz oscillations (2–6 Hz bandpass) recorded in the BLA and immobility/freezing behaviour during Habituation (Hab.) and Retrieval sessions ($n = 13$ mice, paired t -test, BLA: $t(12) = -4.871$, *** $P < 0.001$). (c) Receiver operating characteristics (ROC) analyses performed on Naive Bayes (NBC) and Support Vector Machine (SVM) classifiers trained on 4 Hz signal to noise ratio (SNR) of the BLA during freezing episodes (see Methods). Inset: averaged area under the curve for NBC and SVM classifiers compared to corresponding shuffled data. (d) Percentage of accuracy of the NBC and SVM classifiers to predict freezing behaviour based on BLA 4 Hz SNR (see Methods). (e) Correlation analysis performed between freezing and 4 Hz episodes for the BLA ($n = 13$ mice; BLA: Pearson's r coefficient = 0.01, $P = 0.974$). (f) Location of recording sites in the lateral (IPAG) and ventrolateral periaqueductal grey (vIPAG) ($n = 5$ mice). (g) **Left**, Averaged power spectrum of PAG LFPs recorded during Retrieval for freezing and no freezing periods ($n = 5$ mice). **Right**, Averaged PAG 2–6 Hz power during Retrieval for freezing and no freezing periods ($n = 5$ mice, paired t -test, $t(4) = 0.098$, $P = 0.926$). Shaded areas and error bars: mean \pm s.e.m. Spectral power in log scale. a.u.: arbitrary units. For the representative example in (a), similar results were obtained for the 13 animals used in these experiments.



Supplementary Figure 5

Reversible inactivation of the medial septum does not block dmPFC 4-Hz oscillations.

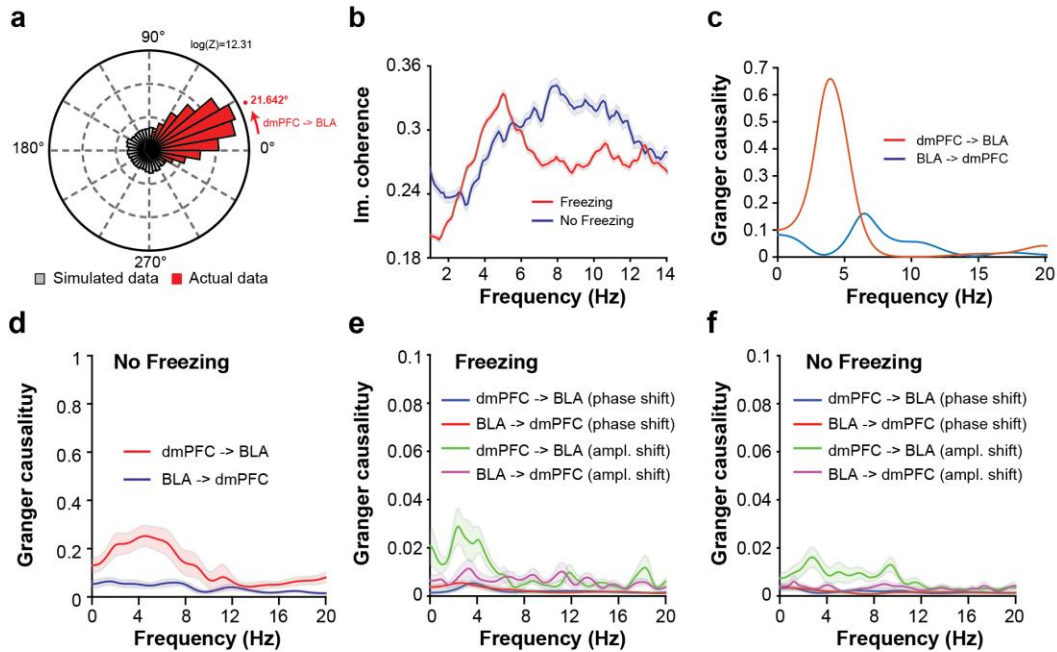
(a, b) Experimental strategy and location of injections sites in the medial septum (MS) and composite transmission light and epifluorescence micrograph showing the MS targeted injection of muscimol covalently bound to a fluorescent tag (bottom, dipyrromethene boron difluoride (BODIPY), red). (c) Power spectra of dmPFC LFPs before (Day 2: Test 1), following (Day 3: Inact.) and after (Day 4: Test 2) MS inactivation ($n = 6$). (d) **Top**, Quantification of dmPFC LFP 4 Hz power (2-6 Hz) before, during, and after MS inactivation. ($n = 6$ mice, One-way repeated measure ANOVA: $F_{(2,5)} = 2.167$, $P = 0.165$., **Bottom**, Quantification of dmPFC LFP theta power (6-12 Hz) before, during, and after MS inactivation. MS inactivation significantly reduced dmPFC theta power ($n = 6$ mice, One-way repeated measure ANOVA: $F_{(2,5)} = 19.245$, $P < 0.001$, paired t -test Bonferroni corrected, Test 1 versus Inact.: $t(5) = 6.155$, $*** P < 0.001$; Inac. versus Test 2: $t(5) = 4.173$, $** P = 0.006$). (e) Representative spectrograms of dmPFC LFPs before (Test 1), during (Inactivation) and after (Test 2) MS inactivation (red tick represents single CS⁺ pips). White lines on the spectrogram indicate immobility/freezing episodes. (f) Percentage of dmPFC neurons phase-locked to 4 Hz (**top**), or theta (**bottom**) oscillations (6-12 Hz). (Test 1: $n = 80$ neurons; Inact.: $n = 100$ neurons; Test 2: $n = 120$ neurons. 4 Hz: One-way repeated measure ANOVA: $F_{(2,5)} = 1.245$, $P = 0.329$; theta: One-way repeated measure ANOVA: $F_{(2,5)} = 9.858$, $P = 0.004$, Bonferroni corrected t -tests; Test1 versus Inactivation: $t(5) = 2.956$, $P = 0.043$; Inactivation versus Test 2: $t(5) = 4.347$, $P = 0.004$). a.u.: arbitrary units. Shaded areas and error bars: mean \pm s.e.m. For the representative examples in (a, e), similar results were obtained for the 6 animals used in these experiments.



Supplementary Figure 6

dmPFC local theta resetting and 4-Hz oscillations are independent phenomena.

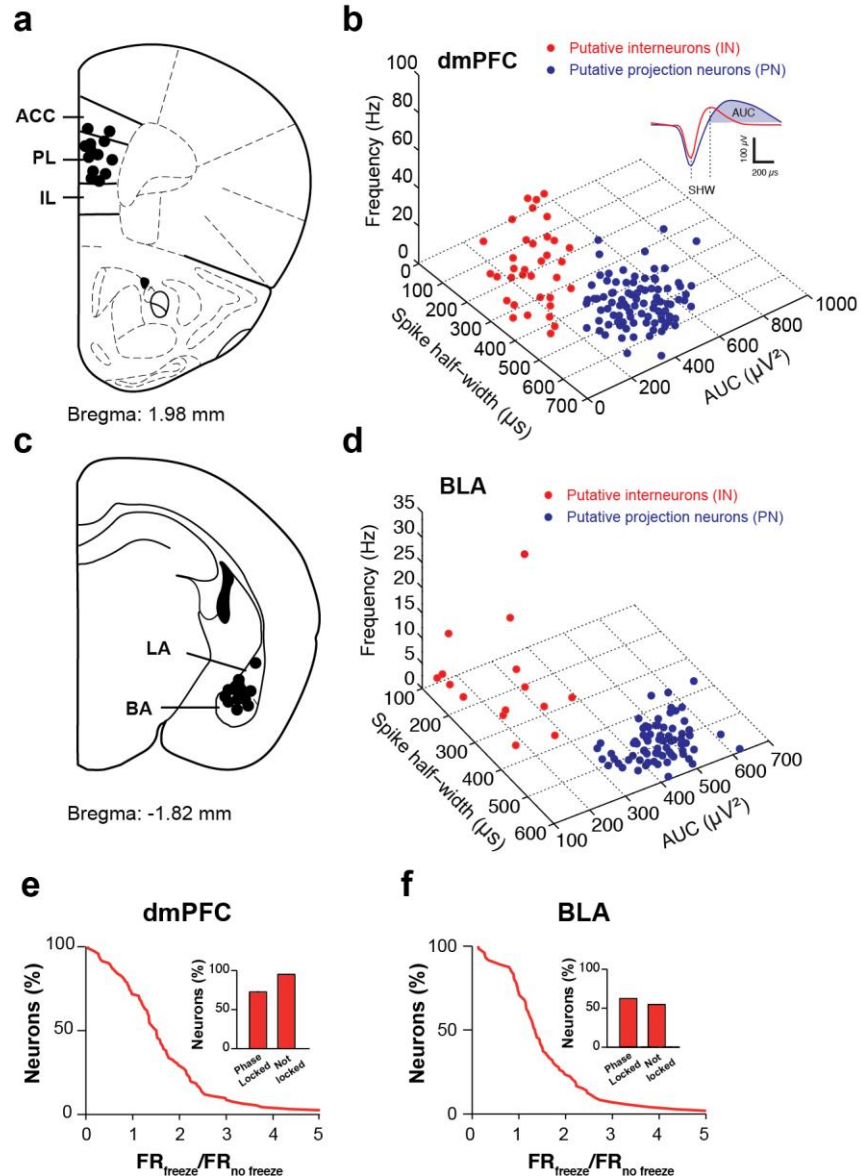
(a, b) Averaged raw (a) and Z-score normalized (b) LFP spectrogram in the 2-12 Hz frequency band around CS⁺ pip presentations during freezing episodes. CS⁺-associated theta was observed as a single burst occurring right after CS⁺ and spanning ~300 ms with frequency between 8 and 12 Hz (b). On the contrary 4 Hz oscillation was present throughout the triggered spectrogram, due to the co-occurring freezing behaviour and was not modulated by CS⁺ presentation (a). (c) Overlaid dmPFC local theta and 4 Hz phases of CS⁺-triggered LFP traces from a representative animal, illustrating theta but not 4 Hz phase resetting induced by CS⁺ pip presentations during freezing episodes. (d) LFP phase spectrogram in the 2-12 Hz frequency band around CS⁺ pip presentations from the same animal as in (c) revealing a sharp and stable versus a broad and unstable CS⁺-evoked phase for local theta and 4 Hz oscillations, respectively. (e) Color coded mean resultant length (MRL) of phases across animal for each time-frequency bin in the 2-12 Hz frequency band around CS⁺ pip presentations during freezing episodes ($n = 13$ mice). A low MRL value indicates an unstable phase (no modulation nor resetting of 4 Hz oscillations) whereas a high MRL value relates to a consistent phase (8-12 Hz theta burst and resetting). (f) Mean MRL for dmPFC 4 Hz (blue line) and 8-12 Hz theta (red line) revealing the changes in phase stability triggered by CS⁺ pip presentations during freezing episodes ($n = 13$ mice). Inset: Averaged MRL after (0 to 300 ms) CS⁺ pip onset ($n = 13$ mice, 12 CS⁺, paired t -test, 4 Hz versus Theta: $t(12) = 4.417$, *** $P < 0.001$). Shaded area and error bars: mean \pm s.e.m. Spectral power in log scale. For the representative examples in (c), similar results were obtained for the 13 animals used in these experiments.



Supplementary Figure 7

dmPFC and BLA directional analysis.

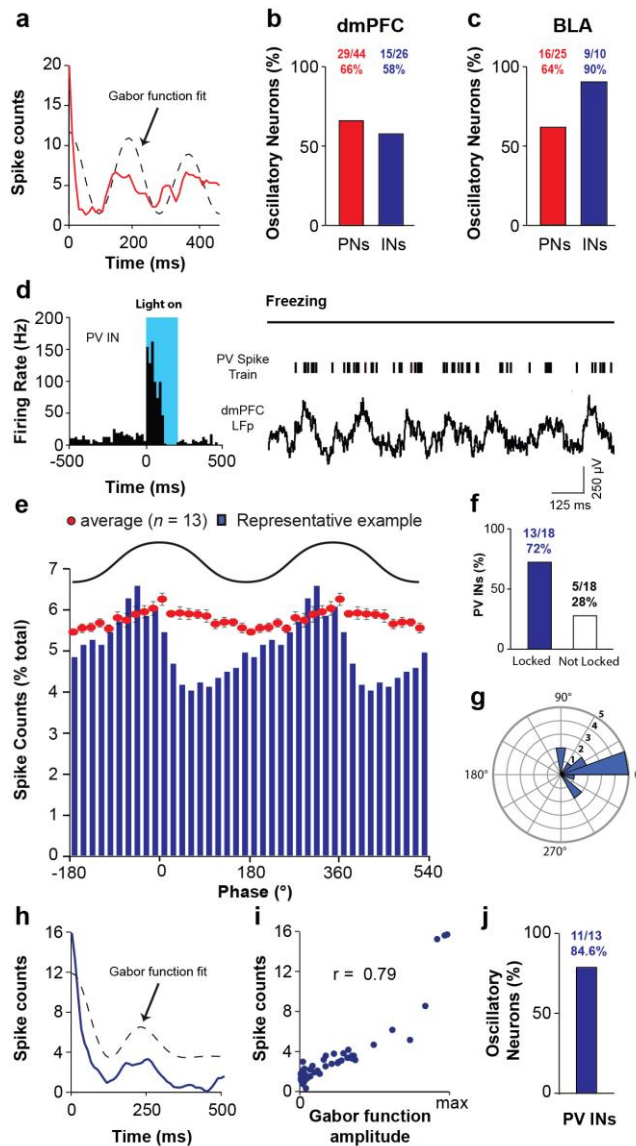
(a) Representative circular distribution of the phase differences between the filtered dmPFC and BLA LFP signals recorded for freezing episodes during Retrieval compared to a control bootstrap simulated phase distribution. **(b)** Representative dmPFC and BLA LFPs imaginary coherence (Im. coherence, see methods) for Freezing and No Freezing episodes recorded during Retrieval (shaded areas: mean \pm s.e.m.). **(c)** Representative Granger Causality (GC) analysis performed between dmPFC and BLA LFPs during freezing behaviour. **(d)** Granger Causality (GC) analyses performed between dmPFC and BLA LFPs during No Freezing periods at retrieval ($n = 13$ mice). No directional effect was observed in these conditions **(b, c)** GC analyses performed between dmPFC and BLA LFPs during Freezing **(b)** and No Freezing **(c)** periods at Retrieval and for which the phase or amplitude of 4 Hz LFPs was permuted (see Methods). The absence of directional effect in the freezing condition indicates that the direction of interaction between dmPFC and BLA is highly dependent on both 4 Hz phase and amplitude ($n = 13$ mice). For the representative examples in **(a, b, and c)**, similar results were obtained for the 13 **(a, b)** and 12 **(c)** animals used in these experiments.



Supplementary Figure 8

Separation between dmPFC and BLA putative principal neurons and putative interneurons.

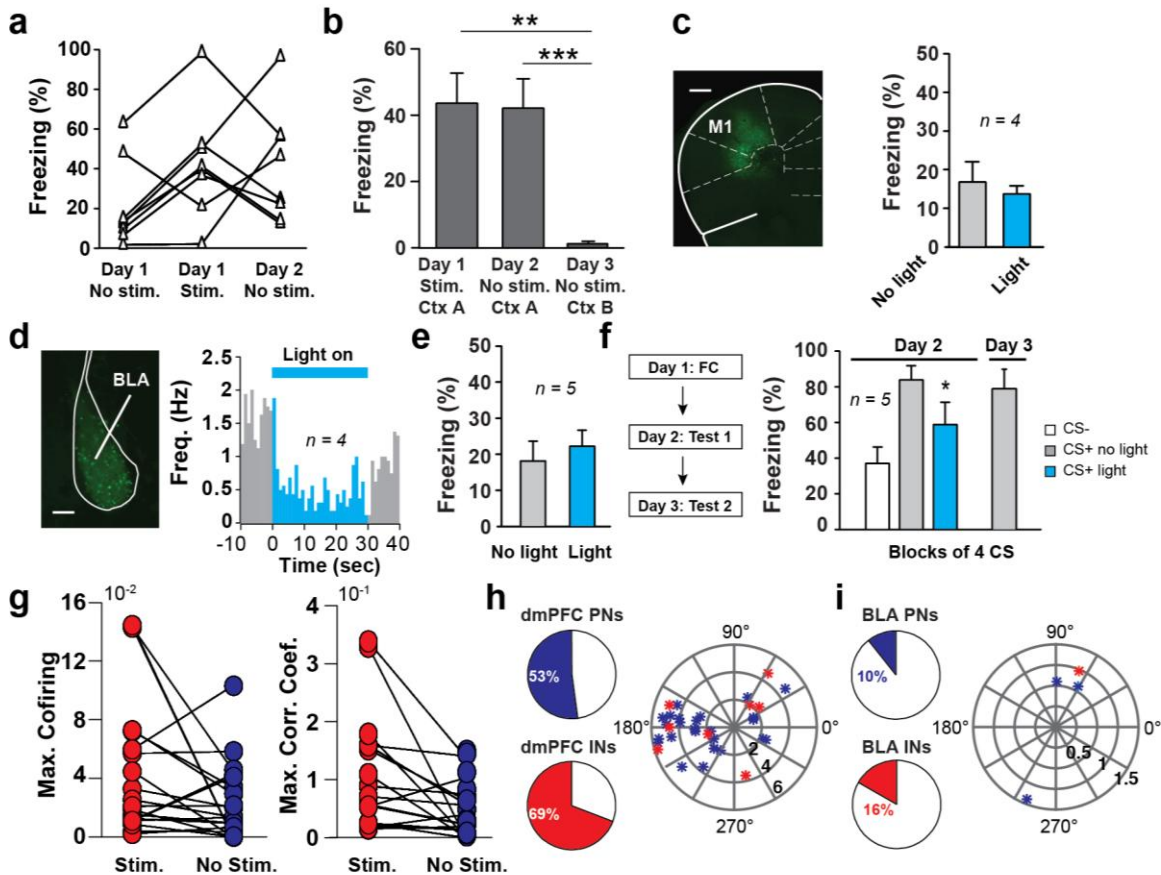
(a, b) Location of recording sites in the dmPFC **(a)** and BLA **(b)**. **(c)** Among dmPFC recorded neurons, 27.56 % were classified as putative inhibitory neurons (INs, red circle) and 72.44 % as putative projection neurons (PNs, blue circle) using an unbiased unsupervised cluster separation algorithm based on three extracellular electrophysiological properties: firing frequency, spike half width (SHW) and spike area under waveform (AUC) peak. Inset, average waveform of a representative PN and IN illustrating the methodology used to quantify SHW and AUC. **(d)** Among BLA recorded neurons, 17.24 % were classified as putative inhibitory neurons (INs, red circle) and 82.76 % as putative projection neurons (PNs, blue circle) using the same methodology as in **(c)**. **(e, f)** Cumulative distribution of firing rate ratio for freezing and no freezing periods of dmPFC **(e)** and BLA **(f)** putative PNs. Inset, percentage of phase-locked and non phase-locked dmPFC **(e)** and BLA **(f)** neurons to 4 Hz oscillations characterized by enhanced firing rate during fear behaviour ($n = 13$ mice, dmPFC: 46 cells; BLA: 21 cells).



Supplementary Figure 9

Oscillatory activity of dmPFC and BLA cells.

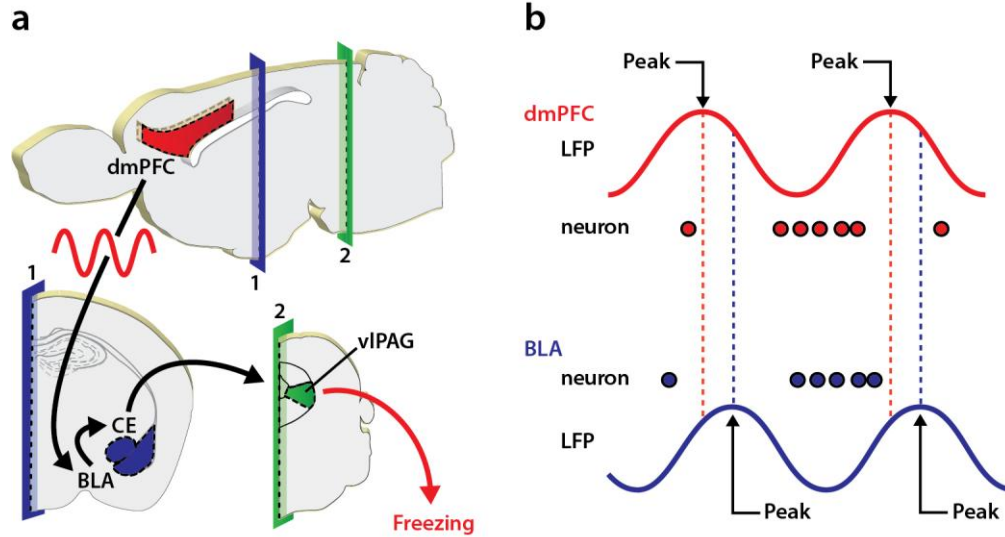
(a) Representative auto-correlogram from a dmPFC putative principal neuron on which a Gabor function was fitted to evaluate its oscillatory activity (see Method section). (b, c) Percentage of dmPFC (b) and BLA (c) putative excitatory principal neurons and inhibitory interneurons that were phase-locked to 4 Hz and displaying 4 Hz oscillatory activity. (d) **Left**, Representative post-stimulus time histogram (PSTH) during optogenetic stimulation of an identified dmPFC parvalbumin-expressing (PV) interneuron. Blue shaded area corresponds to the light stimulation period. **Right**, Representative spiking activity of an identified PV interneuron in relation to dmPFC LFPs recorded during freezing behaviour. (e) Representative (blue bars) and averaged (red dots) phase-histogram of optogenetically identified dmPFC PV interneurons ($n = 18$ PV cells collected in 13 mice). (f) Percentage of optogenetically identified dmPFC PV interneurons phase locked to dmPFC 4 Hz oscillations (13 out of 18 PV cells (72%)). (g) Circular distribution of the 4 Hz oscillation preferred phase for populations of optogenetically identified dmPFC PV interneurons phase-locked to 4 Hz during freezing behaviour. (h) Representative auto-correlogram from optogenetically identified dmPFC PV interneuron on which a Gabor function was fitted to evaluate its oscillatory activity (see Method section). (i) Corresponding representative correlation analysis performed between spike counts and Gabor function amplitude (Pearson's r coefficient = 0.79, $P < 0.001$). (j) Percentage of optogenetically identified dmPFC PV interneurons phase-locked to 4 Hz displaying 4 Hz oscillatory activity (11 out of 13 PV cells (84.6%)). For the representative traces in (a, d-e, and h-i), similar results were obtained for the animals used in these experiments (13 mice in a, and 13 mice in d-e and h-i).



Supplementary Figure 10

4-Hz analog stimulation-mediated freezing behavior.

(a) Percentage of freezing displayed by Chr2 mice in context A during (Day 1 Stim. Ctx A), or 24 hours after (Day 2 No Stim. Ctx A) 4 Hz optogenetic analog stimulation, or 48 hours later in a neutral context (Day 3 No Stim. Ctx B) ($n = 8$ mice, Mann-Whitney U test, Day 1 or Day 2 versus Day 3: $U = 2$ and 0 , $** P = 0.002$; $*** P < 0.001$). **(b) Left**, representative micrograph of the motor cortex (M1) in a PV-cre mouse infected with Chr2. Scale bar = 0.5 mm. **Right**, Percentage of freezing displayed by PV-Cre mice infected in the motor cortex with Chr2 during motor cortex 4 Hz analog stimulation ($n = 4$ mice; Paired t -test, $t(3) = 0.623$, $P = 0.578$). **(c) Left**, representative micrograph of BLA in a PV-cre mouse infected with Chr2. Scale bar = 0.4 mm. **Right**, Averaged peri-stimulus time histograms (PSTH) showing that light activation of BLA PV interneurons can suppress the activity of BLA putative principal neurons ($n = 4$ cells from 2 mice). **(d)** Percentage of freezing displayed by PV-Cre mice infected in the BLA with Chr2 during baseline conditions ($n = 5$ mice; Paired t -test, $t(4) = -0.721$, $P = 0.511$). **(e, f)** Percentage of dmPFC (**e, left**) and BLA (**f, left**) neurons significantly phase-locked to 4 Hz oscillations and circular distribution of the 4 Hz oscillation preferred phase for populations of dmPFC (**e, right**) and BLA (**f, right**) phase-locked putative excitatory principal neurons (PNs) and inhibitory interneurons (INs) during dmPFC 4 Hz analog optogenetic stimulation (dmPFC: 25 PNs, 9 INs; BLA: 3 PNs, 1 INs). **(g) Left**, behavioral protocol. **Right**, Percentage of freezing behaviour to CS⁻ and CS⁺ presentations during no-light or light exposure on Test 1 ($n = 5$ mice, Paired t -test, CS⁺ no light versus CS⁺ light, $t(4) = -4.265$, $P = 0.013$). Freezing levels to CS⁺ presentations during Test 2 normalized to CS⁺ evoked freezing levels during Test 1 ($n = 5$ mice, Paired t -test, CS⁺ Day 2 versus CS⁺ Day3, $t(4) = -1.080$, $P = 0.341$). Error bars: mean \pm s.e.m. For the representative micrographs in **(b and c)**, similar results were obtained for the animals used in these experiments (4 mice in **b**, and 5 mice in **c**). Data for panels **(a)** and **(g)** overlap with the data represented in **Figure 7c** and **7f**, respectively.



Supplementary Figure 11

Circuit and potential mechanism of 4-Hz-mediated freezing behavior.

(a) During freezing behaviour, the preferential dmPFC to BLA coupling at 4 Hz allows the expression of conditioned fear behaviour through the recruitment of BLA circuits contacting the central amygdala (CE) which project to ventrolateral periaqueductal grey (vIPAG). **(b)**, 4 Hz oscillations promote the cofiring of dmPFC and BLA neurons in the trough of the oscillation providing the conditions for fear expression.

II/ Prefrontal-midbrain circuits control fear expression

The canonical model of the neuronal circuits involved in fear postulates that the control of freezing behaviour following auditory fear conditioning is highly dependent on mPFC-BLA circuits. However, direct or indirect manipulations of this pathway during fear behaviour was often associated with partial effects on freezing suggesting that additional pathways could be involved in fear expression (Sierra-Mercado et al., 2011, Courtin et al., 2014, Do-Monte et al., 2015). Interestingly, the dmPFC densely project to the vIPAG, a structure involved in the genesis of freezing responses. However, to date, the functional role played by this mPFC-vIPAG pathway during freezing expression is virtually unknown.

To address this question, we performed single units recordings in mice submitted to auditory fear conditioning (**Fig. 18a**), a robust learning paradigm during which mice learned to associate a neutral stimulus (the conditioned stimulus, CS) with a coincident aversive footshock (the unconditioned stimulus, US). Twenty-four hours following conditioning, re-exposure to CS associated with the US (CS⁺), but not to the control non-conditioned CS (CS⁻) promoted freezing behaviour, which we used as a fear behavioural readout. As described previously (Karalis et al., 2016), freezing episodes were not only observed during CS⁺ presentations but occur spontaneously between CS presentations (Figure 1, Karalis et al., 2016). Among the 432 neurons recorded in the PFC we discriminated 350 putative PNs and 82 putative INs, using unsupervised clustering analysis, and validated the classification with crosscorrelogram analyses (**Fig. 17**).

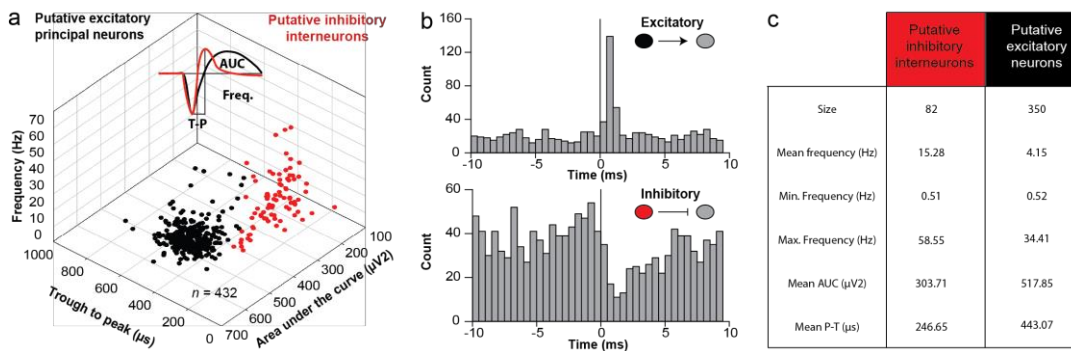


Figure 17: Separation of putative pyramidal neurons and putative interneurons. **a**, Among the population of dmPFC neurons recorded ($n = 432$), 81% were classified as putative pyramidal neurons (PNs, black circles, $n = 350$) and 19% as putative interneurons (INs, red circles, $n = 82$) using an unbiased unsupervised cluster separation algorithm based on three electrophysiological properties: firing frequency, trough to peak (T-P) and area under the curve (AUC). Insert, average waveform of a representative PN and IN illustrating the methodology used to quantify P-T and AUC. **b**, Top: representative cross-correlogram between a putative PN and a non-identified neuron. Bottom: representative cross-correlogram performed between a putative inhibitory IN and a non-identified neuron. Reference events correspond to the spikes of the pre-synaptic neuron (line at time 0, bins of 0.5 ms). **c**, Corresponding parameters for PNs and INs.

Among the 350 putative PNs recorded in the dmPFC, a fraction of them displayed significant increases or decreases of toning activity during freezing behaviour (**Fig. 18b-e**). To determine quantitatively which dmPFC PNs were selectively activated or inhibited during freezing behaviour we used a receiver operating characteristic (ROC) analysis. This analysis revealed that 13 % of dmPFC PNs were inhibited (hereafter referred as freezing-inhibited (FI) PNs, $n = 58$) whereas 10 % were activated during freezing behaviour (hereafter referred as freezing-activated (FA) PNs, $n = 45$, **Fig. 18e-b**).

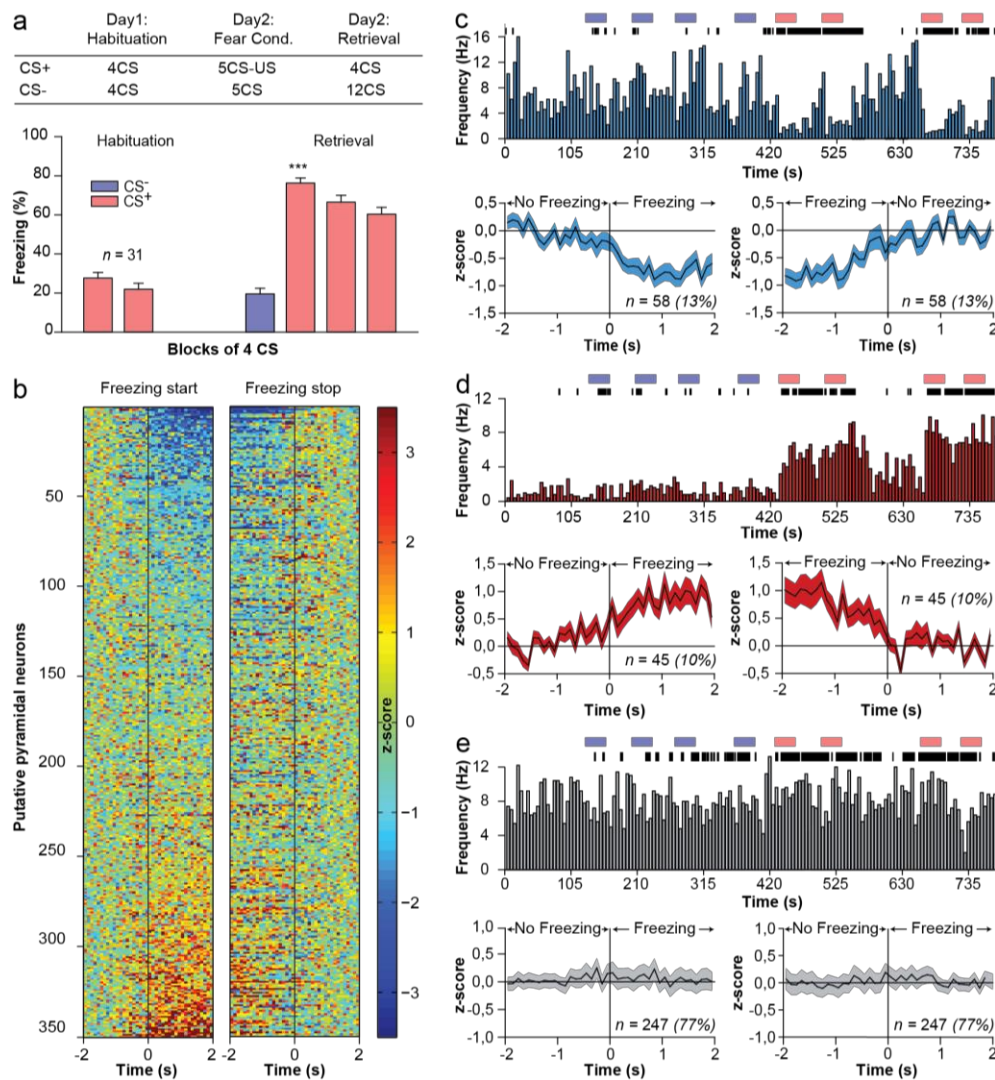


Figure 18: **a. Top:** Behavioural protocol. Mice were submitted to a discriminative fear conditioning protocol and tested 24 hrs later in a different context. **Bottom:** Percentage of freezing evoked by CS- and CS+ presentations during the retrieval session. One-way repeated measure ANOVA: $F(3,30) = 101,148$, $P = 0,001$, Student-Newman-Keuls; CS⁻ retrieval versus CS⁺ retrieval: $t(4) = 22,865$, $P = 0,001$. Error bars: mean \pm s.e.m. **b.** Average peri-stimulus time histogram (PSTH) of dmPFC PNs after freezing onset (Left) or freezing offset (Right). **c, d, e. Top:** Rate histograms of a representative dmPFC PN recorded during the retrieval session. Freezing episodes, CS- and CS+ presentations are represented in blue and red, respectively. **Bottom:** Average PSTH of Z-score activity during freezing onset (Left) and freezing offset (Right) for dmPFC PNs.

Interestingly, these variations were unchanged if we considered freezing episodes occurring inside or between CS presentations (**Fig. 19**) suggesting that sensory-driven or internally generated freezing episodes are encoded similarly by subpopulations of dmPFC neurons.

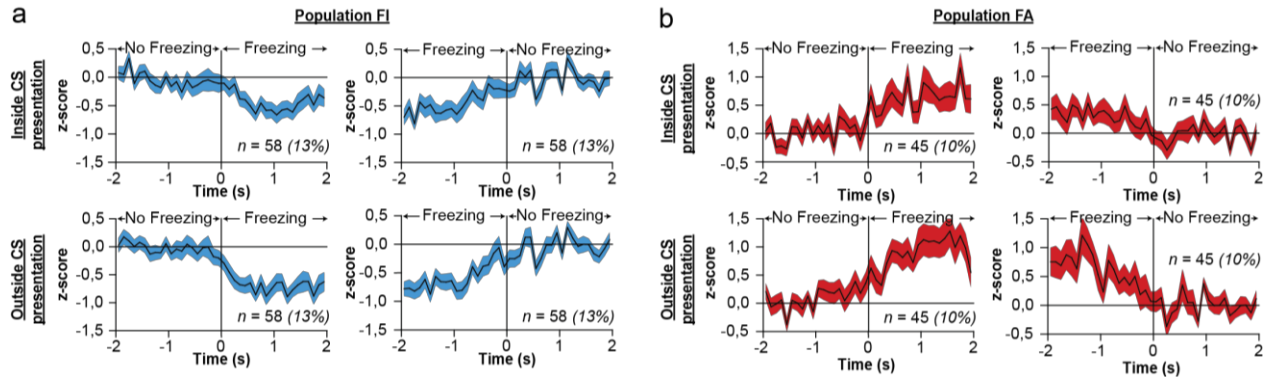


Figure 19: a,b. Average peri-stimulus time histogram (PSTH) of dmPFC PNs after freezing onset (**Left**) or freezing offset (**Right**) for the dmPFC freezing inhibited neurons (FI, blue color) and the dmPFC freezing activated neurons (FA, red color). **Top:** Average peri-stimulus time histogram restricted during period inside CS presentation. **Bottom:** Average peri-stimulus time histogram restricted during periods outside CS presentations.

Recent anatomical and functional data indicate that dmPFC neurons densely project to the basolateral amygdala (BLA), the ventrolateral periaqueductal grey (vlPAG), two structures involved in the regulation of conditioned fear behaviour ((Behbehani, 1995, Floyd et al., 2000, Keay and Bandler, 2001, Gabbott et al., 2005, Quirk and Mueller, 2008, Herry et al., 2010, Herry and Johansen, 2014). To identify the preferential connectivity of FI and FA dmPFC neurons we used two different approaches. The first strategy was based on the antidromic activation of dmPFC efferents using extracellular stimulation of the BLA or vlPAG in anaesthetized mice following completion of behaviour (Fig. 20a). This approach was complemented by a more selective strategy based on the optogenetic tagging of dmPFC PNs projecting to the BLA or vlPAG. To this end, mice were injected in the BLA or vlPAG with a retrogradely transported canine adenovirus type 2 expressing Cre-recombinase (CAV2-Cre) and then injected locally into the dmPFC with a conditional adeno-associated viral vector (AAV) encoding for archaeorhodopsin (ArchT) such that opsin expression was restricted to BLA or vlPAG dmPFC-projecting PNs (**Fig. 20 and Fig. 21b**). In these animals, optrodes for simultaneous single unit recordings and optogenetic manipulation were implanted in the dmPFC (**Fig. 20 and Fig. 21b**).

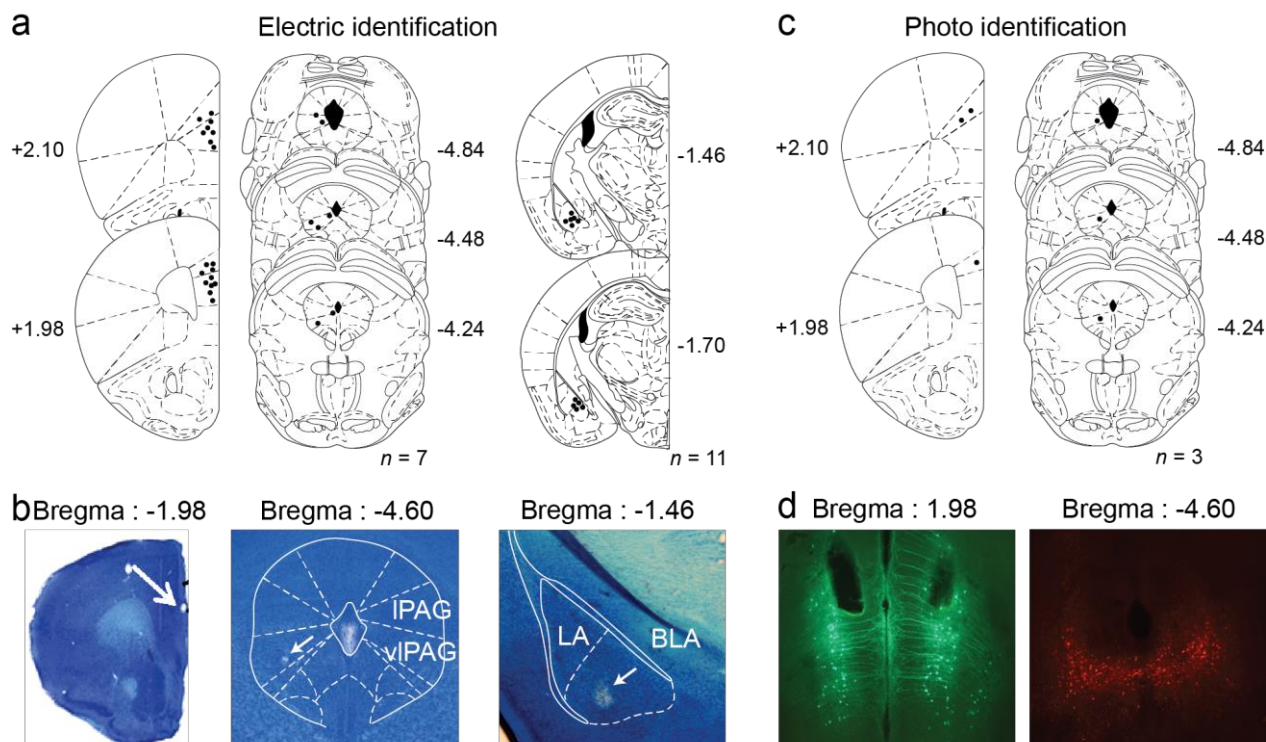


Figure 20: Location of recording sites in th PFC, injection sites in the vIPAG and electrical stimulation sites in both the BLA and vIPAG. **a. Left to right:** Placement of the recording electrode in the dmPFC and location of the stimulation site in the vIPAG or BLA. **b. Left to right:** Representative example of lesion in the dmPFC, vIPAG and BLA. **c. Left:** Location of the lesion in the dmPFC. **Right:** Location of the injection site in the vIPAG of the Cav-cre virus. **d. Left:** Representative example of infection and placement of the optrode in the dmPFC. **Right:** Location of the injection site in the vIPAG.

Using these strategies we were able to identify 16 dmPFC PNs projecting to the BLA and 20 projecting to the vIPAG (**Fig. 21**). Among the BLA dmPFC-projecting PNs, we observed a strong heterogeneity in the neuronal responses observed during freezing behaviour with the vast majority of neurons (10 neurons, 64%, **Fig. 21d**) being freezing non responsive neurons whereas only a small fraction was either inhibited (3 neurons, 18 %, **Fig. 21d**) or excited during freezing behaviour (3 neurons, 18 %, **Fig. 21d**). In striking contrast, the vast majority of vIPAG dmPFC-projecting PNs displayed an increased firing activity during freezing episodes consistent with the activity of FA dmPFC PNs (11, 55%, **Fig. 21d**), whereas only a small fraction of vIPAG dmPFC-projecting were non responsive neurons (6, 30%, **Fig. 21d**) or inhibited during freezing behaviour (3, 15%, **Fig. 21d**). Together, these data revealed that FA neurons preferentially project to the vIPAG whereas FI neurons connectivity was more heterogeneous.

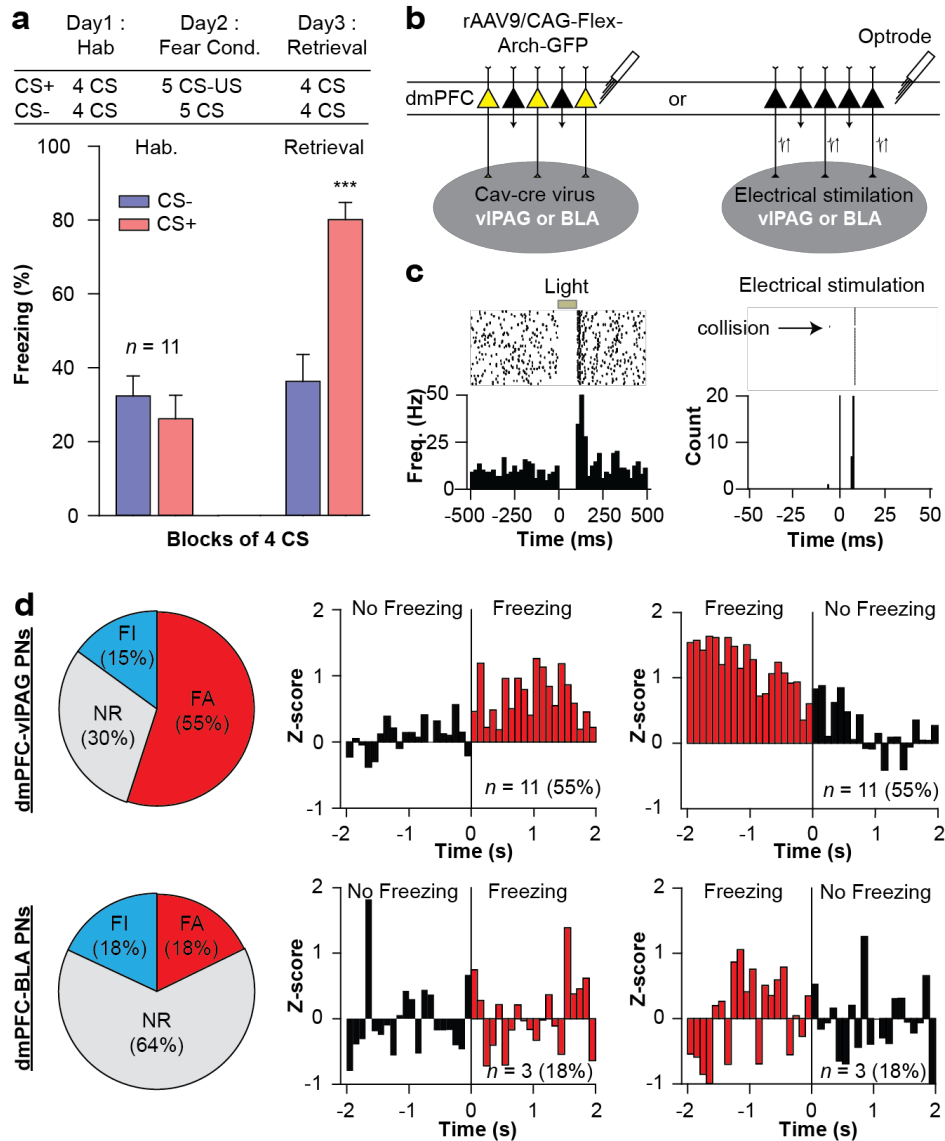


Figure 21: **a.** Top: Behavioural protocol. Mice were submitted to a discriminative conditioning protocol and tested 24 hrs later in a different context. Bottom: Percentage of freezing evoked by CS⁻ and CS⁺ presentations during the retrieval session. One-way repeated measure ANOVA: $F_{(3, 10)} = 32,126$, $P = 0,001$, Student-Newman-Keuls; CS⁻ retrieval versus CS⁺ retrieval: $t(2) = 10,094$, $P = 0,001$. Error bars: mean \pm s.e.m. **b.** Scheme of the strategy used to identified dmPFC-vIPAG PNs either with optogenetic phototaging (Left) or antidromic stimulations (Right). **c.** Left: PSTH and raster plot of a representative light-responsive dmPFC-vIPAG PNs. Right: PSTH and raster plot of an antidromic activated PNs showing a fixed latency and collision with spontaneously occurring spikes. **d** Averaged PSTH of Z-score activity during freezing onset (Left) and offset (Right) for dmPFC-vIPAG PNs (Top) and dmPFC-BLA PNs (Bottom) activated during freezing.

We recently reported that dmPFC PNs projecting to the BLA were preferentially modulated by local inhibitory inputs emanating from PV-expressing interneurons (PV INs) and that the CS-evoked inhibition of PV INs was associated with a disinhibition of BLA-dmPFC projecting neurons (Courtin et al., 2014). We thus evaluated if the same disinhibitory

mechanisms could explain the increased activity observed during freezing behaviour in vIPAG-dmPFC projecting neurons. To this end we first used an anatomical trans-synaptic rabies tracing strategy, which allowed us to label local monosynaptic inhibitory inputs to vIPAG-dmPFC projecting neurons (**Fig. 22a-c**). We then used conventional staining approaches targeting the two main classes of dmPFC INs, namely PV and SST INs and quantified the percentage of PV and SST INs directly contacting vIPAG-dmPFC projecting neurons (**Fig. 22a-c**). Our preliminary analyses revealed that vIPAG-dmPFC projecting neurons were directly contacted by both PV and SST dmPFC INs (**Fig. 22a-c**).

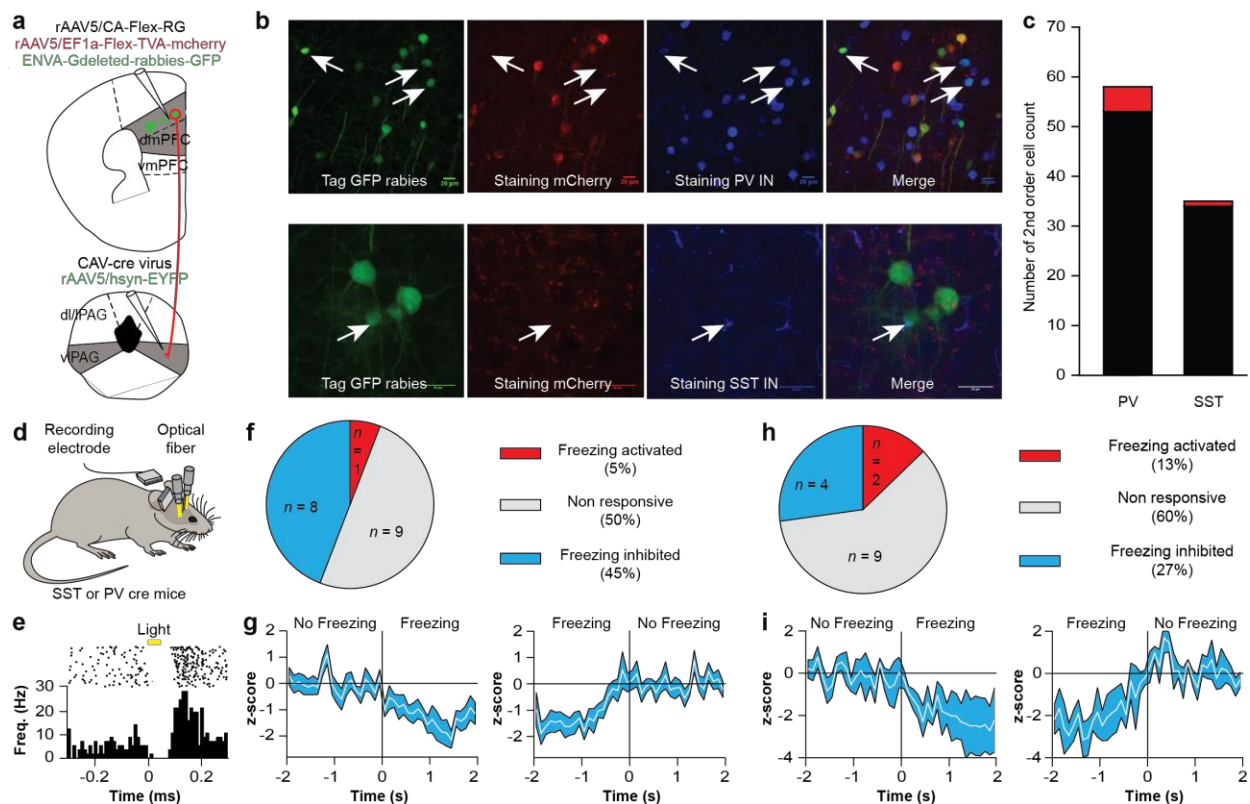


Figure 22: **a.** Transsynaptic rabies tracing strategy used to identify local inhibitory input onto dmPFC-vIPAG PNS. **b.** (Left to Right) Rabies-labelled cells within the dmPFC (green), starter cell labelled with mCherry (red), staining against parvalbumin (PV) or somatostatin (SST) (blue) and merged image showing starter cells, 2nd order cells and their molecular identity. **c.** Quantification of PV⁺ ($n = 5/54$) and SST⁺ 2nd order neurons ($n = 1/35$) (red bar). **d.** Scheme of the strategy used for recording and optical identification of dmPFC SST or PV INs. **e.** Representative example of a light inhibited SST IN. **f.** Number of optogenetically identified SST INs and their firing pattern during freezing. **g.** Averaged PSTH of Z-score activity for SST INs during freezing onset (**Left**) and offset (**Right**). **h.** Number of optogenetically identified PV INs and their firing pattern during freezing. **i.** Averaged PSTH of Z-score activity for PV INs during freezing onset (**Left**) and offset (**Right**).

Next, to identify the firing profile of PV and SST dmPFC INs that might contact vIPAG-dmPFC projecting neurons, we performed phototaging experiments combined with single unit recordings of PV and SST dmPFC INs. Using this strategy we were able to identify optogenetically 18 SST INs and 15 PV INs. Interestingly, applying a ROC analysis to the firing pattern of SST and PV INs during freezing behaviour revealed that among freezing-reactive neurons (SST: 50%; PV: 40%), the vast majority displayed a strong inhibition during freezing behaviour (SST: 89%; PV: 67%). This firing pattern, which is the opposite of the one observed in FA dmPFC PNs, suggest that the increase firing pattern of dmPFC FA neurons could results, at least in part, from a disinhibitory mechanism as recently observed in the cortex (Letzkus et al., 2011).

Finally, in order to causally demonstrate the role of the dmPFC-vIPAG projection pathway in the control of conditioned fear responses, we optogenetically manipulated dmPFC PNs projecting to the vIPAG during fear behaviour (**Figure 23**). To this purpose, C57BL6J mice were injected in the vIPAG with a retrograde CAV2-Cre virus and in the dmPFC with a Cre-dependent AAV expressing ArchT. Optic fibers were lowered in the dmPFC (**Figure 23a,b**). Before conditioning, the optogenetic inhibition of dmPFC-vIPAG projecting neurons did not induce any changes in freezing behaviour compared to GFP controls (**Figure 23c**). In contrast, the same manipulation applied during fear expression, significantly reduced conditioned fear behaviour in comparison to control animals (**Figure 23c**). Together these data indicate that the sustained activation of dmPFC-vIPAG projecting PNs is a necessary condition for the expression of freezing behaviour.

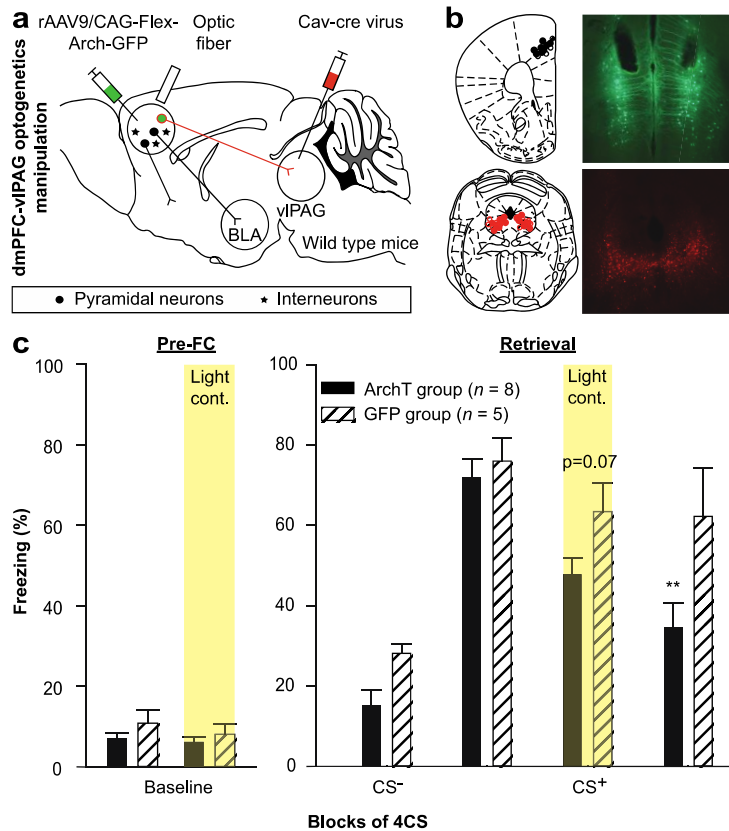


Figure 23: **a.** Viral strategy used to manipulate dmPFC neurons projecting to the vIPAG. Wildtype mice were injected with a CAV-Cre retrograde virus in the vIPAG and with a floxed AAV expressing ArchT or GFP in the dmPFC. **b. Top:** Virus injection sites within the dmPFC (prelimbic area (PL) and the anterior cingulate cortex (ACC)), and localization of optic fibers implanted above the dmPFC. **Bottom:** Viral injection sites within the vIPAG. **c.** Freezing levels evoked by CS⁻ and CS⁺ presentations. Continuous light inhibition of ArchT was performed during a pre-fear conditioning session and during presentation of the second block of CS⁺ during retrieval. Two-way repeated measure ANOVA: $F_{(1,3)} = 2,978$, $P = 0,046$, Student-Newman-Keuls; block 3 CS⁺ GFP versus ChR2: $t(2) = 2,606$, $P = 0,078$; block 4 CS⁺ GFP versus ChR2: $t(2) = 4,615$, $P = 0,004$). Error bars: mean \pm s.e.m.

In this study we evaluated the contribution of dmPFC-vIPAG projecting PNs to the regulation of conditioned fear responses. Our data identified a subpopulation of dmPFC putative excitatory neurons, which displayed enhanced firing activity during freezing episodes. Moreover, this subpopulation of dmPFC PNs preferentially project to the vIPAG and are locally modulated by both PV and SST-expressing dmPFC INs. Finally, the optogenetic manipulation of this neuronal population reduced conditioned fear responses. Interestingly, the optogenetic inhibition of dmPFC vIPAG projecting PNs only partially impaired freezing behaviour. This observation suggests that other brain areas are likely to be involved in fear expression and a strong candidate is the medial nucleus of the central amygdala, which is known to project to the vIPAG and can potentially control fear expression (Cicchi et al., 2011). The classical model of the neuronal

circuits of conditioned fear expression suggests that the prefrontal cortex control emotional behaviour through projection to the BLA. However, our data indicate that in addition to this circuit, a more direct dmPFC-vIPAG pathway can also control fear expression independently of the BLA. These findings raise some questions such as which are the boundaries conditions during which this direct dmPFC-vIPAG is involved in fear expression and whether or not both pathways cooperate to regulate fear behaviour. These questions will require additional investigations to be fully addressed.

Another interesting question is related to the inputs and outputs of this subpopulation of dmPFC PNs projecting to the vIPAG. Our data indicate that at the anatomical level, dmPFC-vIPAG projecting neurons are locally controlled by both PV and SST-expressing INs. However, the precise contribution of PV and SST INs to the regulation of dmPFC-vIPAG projecting PNs needs to be functionally addressed.

III/Periaqueductal gray matter circuits involved in defensive behaviour.

In a recent collaboration with the group of Dr. Andreas Lüthi, Basel, Switzerland, we investigated the neuronal circuits at the level of the PAG involved in the regulation of defensive responses. In particular we evaluated which neurons/circuits trigger fear-related freezing and how the freezing pathway interacts with pathways responsible for flight behaviour. Using novel neuroanatomical tracing methods in combination with electrophysiological approaches we identified glutamatergic neurons in the vIPAG that were activated during freezing episodes. We then demonstrated that this neuronal population projects to a medullary area involved in motor control. Furthermore using a transynaptic retrograde tracing strategy we identified a pathway originating from the CEA and targeting vIPAG GABAergic neurons. To our knowledge, this is the first demonstration of the existence of neuronal circuits underlying freezing execution from the CEA to neurons controlling muscle activation. In addition, we investigated whether and how freezing is influenced by neuronal circuits mediating flight reaction. We find evidence that the neuronal circuit triggering freezing behaviour interacts with the flight circuit at the anatomical and functional level. Our precise contribution to this paper consisted in evaluating the firing patterns of vIPAG neurons freezing behaviour in the vIPAG. To do so we used single unit recordings aiming at the vIPAG in mice (**Fig 24a, b**). Due to the low efficiency of recorded

neurons (maximum 6 neurons recorded using a bundle of 32 wires) and the difficulties to target specifically the vIPAG, a lot of mice were excluded from this data set (8 mice presented good location and neurons recorded, while 16 mice were excluded due to wrong location or no neurons recorded). After PCA analysis performed on the firing rate of vIPAG neurons during freezing onset, we identified 6/33 neurons that were activated during freezing episodes compare to non freezing episode and 11/33 neurons that decreased their activity during freezing behaviour (**Fig 24c**). This part of the project was performed during the first 6 months of my PhD and lead to a recent publication in Nature.

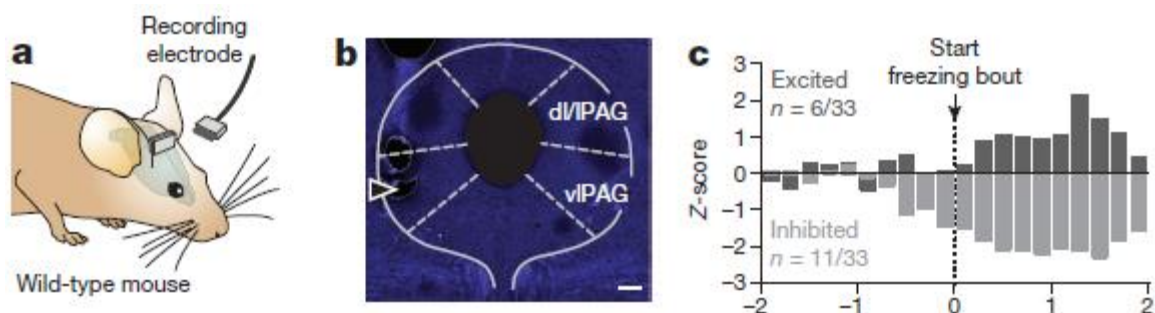


Figure 24: Identification of the main pattern of activity in the vIPAG during freezing episode **a.** Single-unit recordings in the vIPAG of freely moving wild-type mice. **b.** Example of a recording site (triangle; scale bar, 200 μ m). **c.** vIPAG neuronal populations showing increased or decreased activity during freezing ($n = 8$ mice; bin size, 10 ms).

Publications : Tovote P, Esposito MS, Botta P, Chaudun F, Fadok JP, Markovic M, Wolff SB, Ramakrishnan C, Fenno L, Deisseroth K, Herry C, Arber S and Luthi A. (2016) Midbrain circuits for defensive behaviour. *Nature*, 534:206-12. *IF: 41.456*.

Midbrain circuits for defensive behaviour

Philip Tovote^{1*}, Maria Soledad Esposito^{1,2*}, Paolo Botta^{1,†}, Fabrice Chaudun³, Jonathan P. Fadok¹, Milica Markovic¹, Steffen B. E. Wolff^{1,†}, Charu Ramakrishnan⁴, Lief Fenno⁴, Karl Deisseroth⁴, Cyril Herry³, Silvia Arber^{1,2} & Andreas Lüthi¹

Survival in threatening situations depends on the selection and rapid execution of an appropriate active or passive defensive response, yet the underlying brain circuitry is not understood. Here we use circuit-based optogenetic, *in vivo* and *in vitro* electrophysiological, and neuroanatomical tracing methods to define midbrain periaqueductal grey circuits for specific defensive behaviours. We identify an inhibitory pathway from the central nucleus of the amygdala to the ventrolateral periaqueductal grey that produces freezing by disinhibition of ventrolateral periaqueductal grey excitatory outputs to pre-motor targets in the magnocellular nucleus of the medulla. In addition, we provide evidence for anatomical and functional interaction of this freezing pathway with long-range and local circuits mediating flight. Our data define the neuronal circuitry underlying the execution of freezing, an evolutionarily conserved defensive behaviour, which is expressed by many species including fish, rodents and primates. In humans, dysregulation of this ‘survival circuit’ has been implicated in anxiety-related disorders.

Threatening situations, such as the presence of a predator or exposure to stimuli predicting imminent or perceived danger, evoke an evolutionarily conserved brain state, fear, which triggers defensive behaviours to avoid or reduce potential harm^{1–3}. A long-standing question in fear and anxiety research has been how brain circuits generate various forms of defensive behaviours, which have been used as a read-out for normal fear and maladaptive anxiety^{2,4–6}. In rodents, depending on threat imminence⁷ and contextual factors such as the existence of escape routes, defensive behaviours range from risk assessment⁸ and freezing^{9,10} to flight and defensive attack^{2,11}. These behaviours can be rapidly switched to adequately adapt to fluctuating threat levels or contextual challenges^{11,12}. On the basis of electrical stimulation, lesion and pharmacological studies, the midbrain periaqueductal grey region (PAG) has been proposed to present an essential part of the circuitry that elicits freezing and flight in response to threat^{12–22}. However, PAG circuit mechanisms underlying expression of defensive behaviours remain poorly understood. This includes a lack of knowledge about the functional roles of different PAG neuron types, their connectivity and regulation for expression of defensive behaviours. The PAG receives inputs from key forebrain regions involved in regulation of defensive behaviour, such as the central nucleus of the amygdala (CEA)^{23,24}, the hypothalamus^{25–27} and medial prefrontal cortex²⁸, but little is known about their specific PAG cellular targets. In addition, the functional roles of long-range inputs to PAG, neuronal subpopulations within PAG subregions and intra-PAG microcircuitry, as well as outputs from PAG, in the expression of active and passive defensive behaviours is poorly understood. Using optogenetic manipulations of specific cell types, single-unit recordings and rabies-mediated neuroanatomical tracings, we here define a pathway from the CEA to the ventrolateral PAG (vlPAG) that mediates freezing by disinhibition of vlPAG outputs to pre-motor targets in the magnocellular nucleus (Mc) of the medulla. Furthermore, we provide evidence for anatomical and functional interaction of this ‘freezing pathway’ with circuits mediating flight.

Freezing is mediated by glutamatergic vlPAG neurons

To determine cellular diversity in the vlPAG that could be associated with a distinct behavioural phenotype, we used an optogenetic

approach to specifically manipulate the activity of excitatory glutamatergic neurons, one of the main cell classes in the PAG. We targeted glutamatergic neurons expressing vesicular glutamate transporter 2 (vGluT2⁺) by local injection of adeno-associated viruses (AAV) delivering a construct that contained a Cre-dependent channel-rhodopsin-2 (ChR2) coupled to an mCherry tag into the vlPAG of *Vglut2-ires-Cre* mice (Fig. 1a, b and Extended Data Fig. 1a, b). Mice injected with AAVs containing a fluorescent tag only served as controls. We first optically manipulated cellular activity in naive mice under low-fear conditions (that is, at low freezing levels), during exposure to a novel context. Strikingly, light-activation of vGluT2⁺ neurons of the vlPAG reliably triggered strong freezing behaviour during the ‘light on’ period (Fig. 1c and Supplementary Video 1), which was reflected by a marked decrease in behavioural activity (Fig. 1d). To define the endogenous function of vlPAG glutamatergic neurons, we next used viral-vector-mediated, Cre-dependent expression of archaerhodopsin (Arch) to optically inhibit these neurons (Fig. 1b and Extended Data Fig. 1c). Under low-fear conditions in naive mice, we did not observe an effect on freezing or behavioural activity (Fig. 1e, f). To investigate the necessity of vlPAG glutamatergic neurons for conditioned freezing behaviour, we subjected mice to auditory fear conditioning, followed by next-day re-exposure to an aversively conditioned tone stimulus (CS) or to the context previously paired with mild electrical foot-shocks. We found that optical inhibition of vlPAG vGluT2⁺ neurons during the CS blocked tone-induced freezing (Fig. 1g and Supplementary Video 2). Similarly, freezing in the conditioning context was markedly reduced during optical inhibition of vlPAG vGluT2⁺ neurons (Fig. 1h). These results demonstrate a role of vlPAG glutamatergic neurons in mediating conditioned freezing responses.

To determine whether these neurons serve a more general role in mediating freezing, we next tested the necessity of these neurons for producing freezing to an innate threat. Mice exhibit strong fear responses when exposed to large moving objects, probably because these resemble visual features of a natural predator^{22,29}. We therefore exposed mice in an open-field arena to a remote controlled toy

¹Friedrich Miescher Institute for Biomedical Research, Maulbeerstrasse 66, 4058 Basel, Switzerland. ²Biozentrum, Department of Cell Biology, University of Basel, 4056 Basel, Switzerland.

³INSERM, Neurocentre Magendie, U862, 146 Rue Léo-Saignat, Bordeaux 33077, France. ⁴Stanford University, 318 Campus Drive West, Clark Center W080, Stanford, California 94305, USA.

[†]Present addresses: Champalimaud Centre for the Unknown, Avenida de Brasília, 1400-038 Lisbon, Portugal (P.B.); Center for Brain Science, Harvard University, Cambridge, Massachusetts 02138, USA (S.B.E.W.).

*These authors contributed equally to this work.

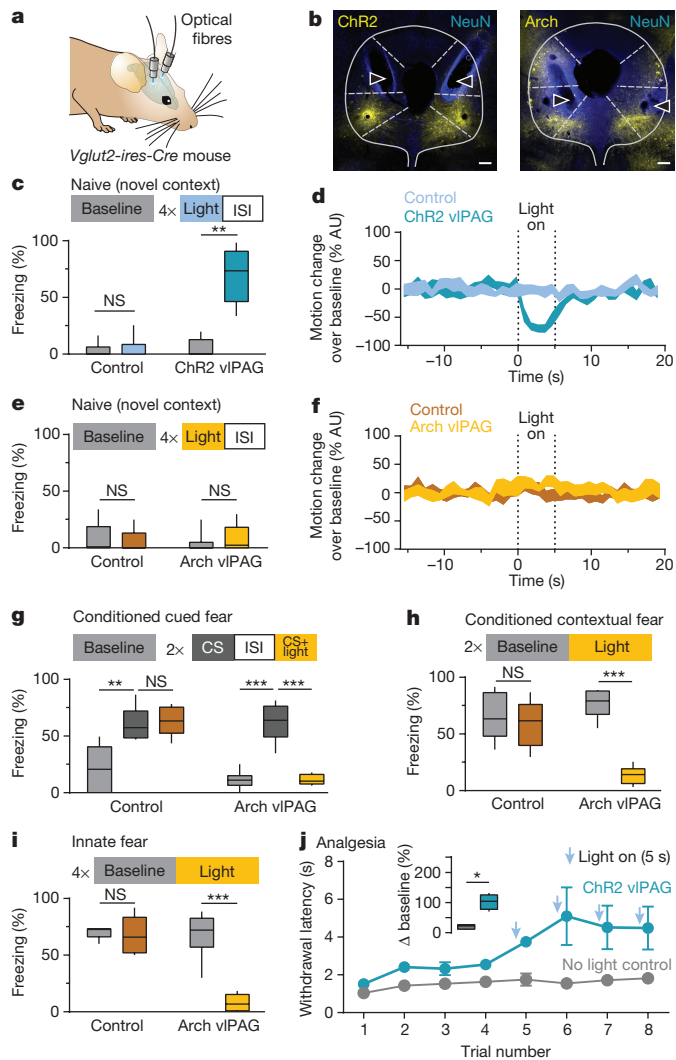


Figure 1 | Glutamatergic vPAG neurons drive defensive responses. **a**, Optogenetics in freely moving mice. **b**, Expression patterns of ChR2 (left) and Arch (right) within vGluT2⁺ vPAG neurons (triangles, fibre tracts; scale bars, 200 μm). **c, d**, Light activation of glutamatergic vPAG neurons triggered freezing behaviour ($n = 10$ ChR2, $n = 12$ control, two-tailed Wilcoxon signed-rank test). **e, f**, Inhibition of vPAG glutamatergic neurons had no effect on freezing or behavioural activity in naive mice ($n = 7$ Arch, $n = 12$ control, two-tailed Wilcoxon signed-rank test). **g–i**, Inhibition of vPAG glutamatergic neurons diminished CS-induced freezing ($n = 6$ per group, 1×3 analysis of variance (ANOVA), $F_{(2,10)} = 37.72$, $P < 0.001$, Tukey's post-hoc test), contextual freezing ($n = 6$ Arch, $n = 8$ control, paired two-tailed Student's t -test) and innate freezing responses ($n = 6$ Arch, $n = 5$ control, paired two-tailed Student's t -test). **j**, Light activation of vPAG glutamatergic neurons induced analgesia ($n = 6$ ChR2, $n = 10$ control, unpaired two-tailed Student's t -test). Box-whisker plots indicate median, interquartile range and 5th–95th percentiles of the distribution. Motion plots depict s.e.m. range. * $P < 0.05$; ** $P < 0.01$; *** $P < 0.001$.

snake (Extended Data Fig. 1d). We found that while mice exhibited strong freezing responses in the presence of the fear stimulus, this reaction was dramatically reduced by yellow-light-mediated inhibition of vPAG vGluT2⁺ neurons (Fig. 1i and Extended Data Fig. 1e). The reduction in freezing was attributable to optical inhibition and not to changes in threat imminence as measured by spatial distance between mouse and snake (Extended Data Fig. 1f, h). Taken together, these findings demonstrate that activation of vPAG glutamatergic neurons is necessary for both learned and innate freezing, and that it can generate freezing in the absence of threat.

Because the PAG is involved in processing ascending and descending pain information from the periphery^{30–32}, it is conceivable that the observed behavioural responses were related to enhanced light-evoked pain perception. However, when we tested nociception using a tail immersion test, we found that optical activation of vGluT2⁺ vPAG neurons had a marked analgesic effect (Fig. 1j). These experiments identify a cellular substrate in the vPAG for analgesia, an important part of the defensive response to threat.

A disinhibitory pathway from CEA to vPAG

To address the question of how vPAG vGluT2⁺ neurons are regulated, we first aimed to characterize inputs to the vPAG from the CEA, because of their suggested major roles in the expression of freezing^{5,12,33,34}. To identify the CEA neurons contacting vPAG, we injected retrogradely transported red fluorescent latex beads into the vPAG of a reporter mouse strain, in which GABAergic (γ -aminobutyric-acid-releasing) cells express enhanced green fluorescent protein (*Gad1-eGFP*; Fig. 2a). Retrogradely transported beads were found throughout the CEA (Fig. 2a). Quantification of overlap between beads and GFP⁺ neurons (Fig. 2b) showed that the CEA sends a GABAergic projection to vPAG, consistent with previous reports²⁴. Freezing is elicited through enhanced CEA output^{33,35}, but since these neurons are GABAergic, this would result in enhanced inhibition of their vPAG targets. However, our results from optogenetic manipulation of freezing behaviour suggest that freezing is associated with increased activity of vPAG glutamatergic neurons. Thus, the most parsimonious explanation consistent with these observations would involve a local vPAG disinhibitory circuit mechanism that could convert an inhibitory input from CEA into enhanced output of vPAG glutamatergic neurons.

To test this hypothesis, we traced monosynaptic connections of CEA cells onto either glutamatergic or GABAergic cells in the vPAG (Fig. 2c) using Cre-dependent, cell-type-specific infection with pseudotyped EnvA-G-deleted rabies virus (EnvA- Δ G-rabies)³⁶ in *Vglut2-ires-Cre* or *Gad2-ires-Cre* mouse lines. These experiments revealed that CEA projections preferentially target vPAG GABAergic cells (Fig. 2d, e). Complementary evidence for a disinhibitory CEA–vPAG circuit was provided by whole-cell patch-clamp recordings of vPAG GABAergic cells during optical activation of CEA terminals in acute brainstem slices containing PAG (Extended Data Fig. 2a). This experiment confirmed the existence of such inhibitory connections to vPAG GABAergic neurons (Extended Data Fig. 2b–f and Fig. 2f). We also probed the existence of functional connections between local GABAergic and glutamatergic cells in the vPAG. Glutamatergic cells were visualized by viral-vector-mediated, Cre-dependent expression of tdTomato in the vPAG of *Vglut2-ires-Cre* mice (Fig. 2g). Using a double-conditional viral approach³⁷, ChR2 was introduced into vPAG of non-vGluT2⁺ cells. We recorded from identified vGluT2⁺ neurons in acute brain slices during optical activation of local, non-vGluT2⁺ neurons (Fig. 2h). In 50% of all recorded vGluT2⁺ cells, we observed optically evoked inhibitory postsynaptic potentials (eIPSCs; average latency = 5.5 ms) (Fig. 2i) that were completely blocked by application of picrotoxin, a GABA_A receptor antagonist (Fig. 2i, j). Taken together, our data from slice recordings and tracing experiments suggest that freezing is caused by a disinhibitory process within vPAG that involves CEA-mediated inhibition of local GABAergic neurons resulting in enhanced activity of glutamatergic vPAG neurons (Fig. 2f).

Local vPAG GABAergic neurons control freezing

To investigate whether *in vivo* neuronal correlates of freezing in the vPAG would be consistent with a disinhibitory circuit mechanism, we next performed single-unit recordings within vPAG in freely moving mice (Fig. 3a). Mice with chronically implanted recording electrodes (Fig. 3b and Extended Data Fig. 3a) were fear conditioned and freezing responses were evoked during a fear retrieval session 24h

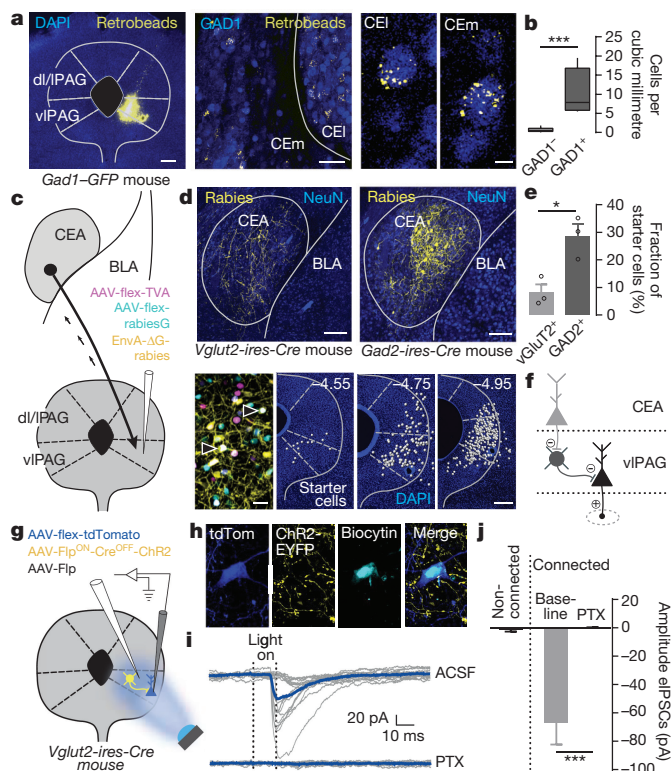


Figure 2 | A disinhibitory pathway from CEA to vIPAG. **a**, Fluorescent latex beads in vIPAG (left, scale bar, 200 μ m). Beads were found in medial (CEm) and lateral (CEl) CEA cells (middle, scale bar, 40 μ m; zoom-in shown in two right panels, scale bar, 5 μ m). **b**, Overlap between beads and GAD1⁺ or GAD1⁻ neurons ($n = 2$ mice, two-tailed Mann–Whitney test). **c**, Cell-type-specific monosynaptic rabies tracing strategy. **d**, Rabies-labelled cells within CEA of *Vglut2-Cre* or *Gad2-Cre* mice (top panels, scale bar, 100 μ m). Starter cells coexpressing TVA–GFP, rabiesG–V5 and EnvA– Δ G–mCherry–rabies (black triangles, bottom left panel, scale bar, 25 μ m). Example of starter cells (white dots, three bottom right panels; numbers indicate distance from bregma; scale bar, 200 μ m). **e**, Normalized number of rabies cells in CEA ($n = 3$ *Vglut2-Cre* mice, $n = 3$ *Gad2-Cre* mice, unpaired two-tailed Student’s *t*-test). **f**, Schematic model of a disinhibitory pathway from CEA to vIPAG. **g**, **h**, Expression of ChR2 in non-glutamatergic neurons and tdTomato in glutamatergic neurons for targeted whole-cell patch-clamp recordings (scale bar, 10 μ m). **i**, **j**, Light-evoked IPSCs (observed in 50% of all glutamatergic neurons tested) were blocked by PTX application ($n = 12$ cells from six slices of four mice, two-tailed 1×3 ANOVA, $F_{(2,15)} = 18.88$, $P < 0.0001$, Sidak’s post-hoc test). Box–whisker plots indicate median, interquartile range and 5th–95th percentiles of the distribution; bar plots indicate mean \pm s.e.m. * $P < 0.05$, *** $P < 0.001$.

later³⁸. Principal component analysis of single-unit activity in relation to freezing behaviour revealed that while one population of neurons (18%) was activated during freezing bouts, another population (33%) was inhibited (Fig. 3c). Consequently, we examined whether glutamatergic and GABAergic neurons could contribute to these differential activity patterns. To address this question, we performed recordings from optogenetically identified³⁹ GAD2⁺ and vGluT2⁺ neurons within vIPAG (Fig. 3d–f and Extended Data Fig. 3b). In agreement with a disinhibitory vIPAG freezing circuit, light-identified GAD2⁺ neurons ($n = 4$; Fig. 3g) exhibited a relatively high median baseline firing rate (8.3 Hz), and all showed lower firing rates during freezing compared with non-freezing periods (Fig. 3g, h). Recordings from identified vGluT2⁺ units ($n = 6$, median baseline firing rate = 3.0 Hz; Extended Data Fig. 3c–e) during freezing periods revealed a more heterogeneous picture, suggesting the existence of multiple subpopulations of glutamatergic neurons in vIPAG. Thus, the *in vivo* correlates

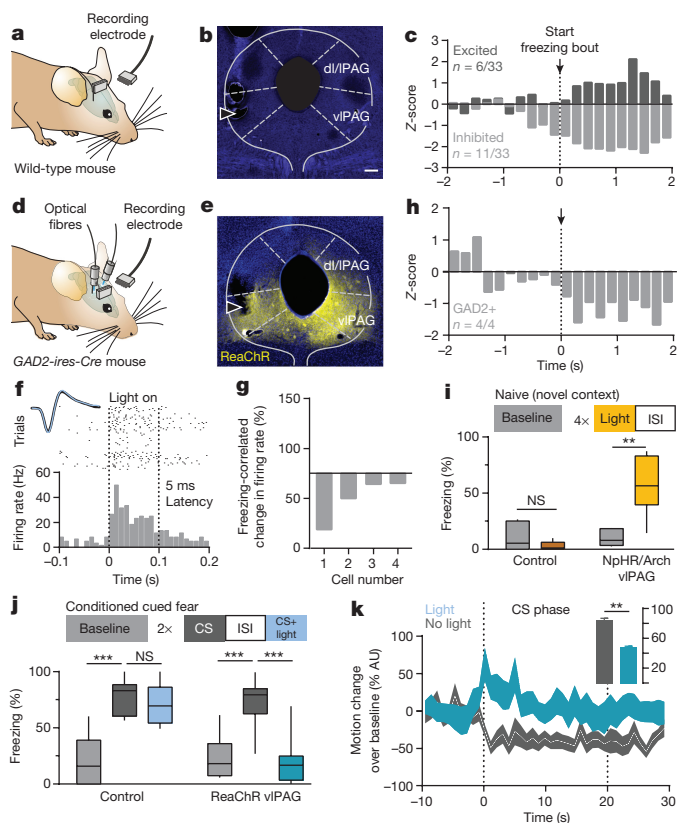


Figure 3 | GABAergic vIPAG neurons control freezing. **a**, Single-unit recordings in the vIPAG of freely moving wild-type mice. **b**, Example of a recording site (triangle; scale bar, 200 μ m). **c**, vIPAG neuronal populations showing increased or decreased activity during freezing ($n = 8$ mice; bin size, 10 ms). **d**, Optical identification of GAD2⁺ single units in the vIPAG. **e**, Example of ChR2 expression and recording site (triangle; scale bar, 200 μ m). **f**, Identified GAD2⁺ neuron activated by light with short latency (5 ms; bin size, 10 ms). Inset: mean spontaneous and light-evoked spike waveform. **g**, **h**, GAD2⁺ neurons exhibited reduced firing rates during freezing (four cells from three mice). **i**, Optical inhibition of GAD2⁺ neurons induced freezing in naive mice ($n = 6$ per group, two-tailed paired Student’s *t*-test). **j**, **k**, Optical activation of GAD2⁺ neurons impaired CS-evoked freezing ($n = 12$ per group, two-tailed Friedman test, $P < 0.0001$, Dunn’s multiple comparison test), and shifted CS-induced fear responses towards active behaviour ($n = 12$ per group, two-tailed paired Student’s *t*-test). Box–whisker plots indicate median, interquartile range, and 5th–95th percentiles of the distribution; bars indicate mean \pm s.e.m. Motion plots depict s.e.m. range. * $P < 0.05$, ** $P < 0.01$, *** $P < 0.001$.

of freezing are consistent with a disinhibitory circuit design leading to the activation of a subpopulation of glutamatergic vIPAG neurons during freezing.

An important prediction of this model is that manipulating the activity of GABAergic vIPAG neurons should affect freezing. In line with this interpretation, optogenetic inhibition of vIPAG GAD2⁺ neurons resulted in markedly enhanced freezing levels in naive animals (Fig. 3i and Extended Data Fig. 3f). Importantly, activation of GAD2⁺ neurons reduced freezing in response to a conditioned tone (Fig. 3j and Extended Data Fig. 3g). Moreover, this manipulation not only reduced CS-induced freezing but also resulted in transiently enhanced locomotor activity, resembling flight responses (Fig. 3k). Freezing was also reduced by optical activation of GAD2⁺ neurons during re-exposure to the conditioning context (Extended Data Fig. 3h), as well as in the presence of an unconditioned threatening stimulus (Extended Data Fig. 3i), while it had no effect on freezing in low-fear conditions (a novel context; Extended Data Fig. 3j). Taken together, these data are fully compatible with a circuit organization wherein inhibition of

local GABAergic vIPAG neurons leads to activation of glutamatergic neurons that is both necessary and sufficient to induce freezing behaviour.

vIPAG output to Mc drives freezing

We next sought to identify the output pathway mediating the freezing response. Analysis of axonal projections and synaptic boutons of vGluT2⁺ vIPAG neurons (Extended Data Fig. 4a) showed that medullary regions previously implicated in motor control, such as the Mc^{40,41}, were a major synaptic target. To determine whether vGluT2⁺ vIPAG neurons target pre-motor neurons in the Mc directly, we performed monosynaptic rabies tracing from forelimb motor neurons in adult *Chat-ires-Cre* mice (Fig. 4a). We visualized glutamatergic vIPAG terminals by unconditional viral expression of the presynaptic marker synaptophysin–GFP (Syn–GFP; Extended Data Fig. 4b) with synaptic co-localization of vGluT2 (Fig. 4b). Analysis of presynaptic inputs to forelimb pre-motor Mc neurons revealed that they were directly contacted by glutamatergic vIPAG neurons (Fig. 4c and Extended Data Fig. 4c–e).

We then asked whether vIPAG Mc-projecting glutamatergic neurons receive local inhibitory input. We first used a monosynaptic intersectional rabies tracing approach to specifically label presynaptic neurons in the vIPAG projecting onto glutamatergic neurons which target Mc (Extended Data Fig. 4f). We found that one-third of the local presynaptic neurons were GAD1⁺ (Extended Data Fig. 4g, h), and thus putative sources of GABAergic inhibition onto glutamatergic vIPAG output cells. Furthermore, we probed the existence of functional connections between local GABAergic and Mc-projecting glutamatergic vIPAG cells by combining the approach described in Fig. 2g with an injection of retrogradely transported latex beads into the Mc (Fig. 4d). All Mc-projecting vGluT2⁺ neurons recorded in whole-cell patch-clamp showed eIPSCs induced by light activation of vIPAG non-vGluT2⁺ cells, which were blocked by picrotoxin application (Fig. 4e). These findings provide evidence that excitatory vIPAG output to the Mc is under local GABAergic control and suggest that this pathway could be part of the disinhibitory circuit underlying freezing.

To establish functional relevance of this projection for the freezing response, we next used an intersectional optogenetic approach to specifically manipulate activity of the glutamatergic vIPAG-to-Mc projection. We injected into the Mc of *Vglut2-ires-Cre* mice retrogradely trafficked herpes simplex virus (HSV), which Cre-dependently expresses flipase (Flp)⁴². This allowed us to selectively introduce Chr2 into vIPAG glutamatergic neurons projecting to Mc (vIPAG-to-Mc) on the basis of their co-expression of both Cre and Flp using double conditional AAVs (Fig. 4f and Extended Data Fig. 4i–k). Optical activation of glutamatergic vIPAG-to-Mc neurons resulted in instantaneous and strong freezing behaviour as reflected by decreased behavioural activity (Fig. 4g, h, Extended Data Fig. 4l and Supplementary Video 3). Interestingly, and in contrast to the anti-nociceptive effect elicited upon projection-unspecific activation of vGluT2⁺ neurons in the vIPAG (Fig. 1j), no analgesia was observed after stimulation of the glutamatergic vIPAG-to-Mc neurons (Fig. 4i). Together, these findings demonstrate that vIPAG-to-Mc glutamatergic projection neurons are specifically involved in the expression of freezing behaviour and suggest that analgesia and freezing could be mediated by distinct subpopulations of vIPAG glutamatergic neurons.

Interactions between freezing and flight pathways

Our data show that activation of vIPAG vGluT2⁺ neurons induces freezing (Fig. 1). However, in mice with viral expression extending to dl/IPAG, we observed radically different, active defensive behavioural responses through optical activation of vGluT2⁺ neurons (Fig. 5a and Extended Data Fig. 5a). These consisted of strong light-induced locomotor activity (Fig. 5b), amounting to marked flight responses

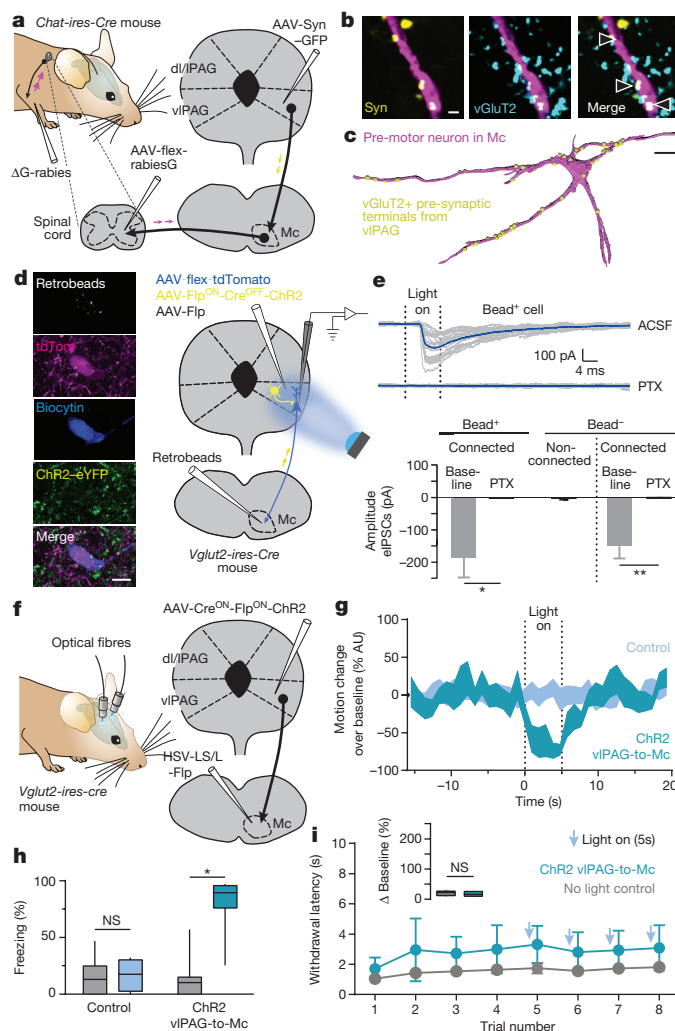


Figure 4 | Glutamatergic output to the Mc drives freezing. **a**, Strategy to assess vIPAG input onto Mc pre-motor neurons. **b**, vIPAG glutamatergic synapses contacting Mc pre-motor neurons were identified by co-staining of Syn–GFP and vGluT2 (triangles; scale bar, 2 μm). **c**, Three-dimensional reconstruction of a Mc pre-motor neuron contacted by vIPAG vGluT2⁺ synapses (yellow circles; scale bar, 10 μm). **d**, Intersectional approach to investigate connectivity of vIPAG GABAergic cells with Mc-projecting glutamatergic neurons. **e**, Light activation of non-glutamatergic fibres evoked IPSCs in all bead⁺ Mc-projecting glutamatergic neurons tested (nine out of nine cells, one example cell shown), and six out of nine glutamatergic, bead[−] neurons. All IPSCs were blocked by PTX application (four slices of four mice; bead⁺: two-tailed Wilcoxon signed-rank test; bead[−]: 1 × 3 ANOVA $F_{(2,10)} = 10.28$, $P < 0.01$, Sidak's post-hoc test). **f**, Strategy to express Chr2 selectively in glutamatergic vIPAG neurons projecting to Mc. **g**, **h**, Light activation of glutamatergic vIPAG neurons projecting to Mc in naive mice resulted in strong freezing ($n = 7$ Chr2, $n = 10$ control, two-tailed Wilcoxon signed-rank test). **i**, Light activation of the glutamatergic vIPAG-to-Mc projection had no effect on nociception ($n = 5$ Chr2, $n = 11$ control, unpaired two-tailed Student's t -test). Box-whisker plots indicate median, interquartile range and 5th–95th percentiles of the distribution; bar plots indicate mean ± s.e.m. Motion plots depict s.e.m. range. * $P < 0.05$; ** $P < 0.01$.

in some cases. Nonetheless, bouts of forward locomotor activity were often interrupted by short periods of freezing, which resulted, on average, in intermediate levels of freezing (Fig. 5c and Extended Data Fig. 5b). Broad activation of vGluT2⁺ neurons within PAG also resulted in strong analgesia (Fig. 5d). Given the observation of alternating active and passive defensive responses, this strongly suggests intricate interactions between flight and freezing circuits and raises

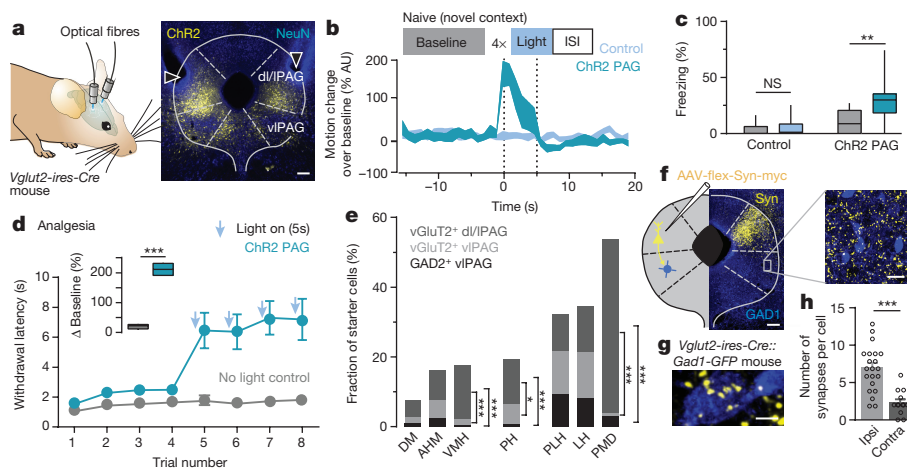


Figure 5 | Interactions between PAG freezing and flight pathways. **a**, Optogenetic manipulation of vGluT2⁺ neurons in dl/IPAG and vIPAG (triangles indicate fibre tracts; scale bar, 200 μ m). **b**, **c**, Light activation of PAG glutamatergic neurons in naive mice resulted in flight responses and intermediate freezing levels ($n = 12$ ChR2, $n = 12$ control, two-tailed Wilcoxon signed-rank test). **d**, Light activation of PAG glutamatergic neurons resulted in strong analgesia ($n = 9$ ChR2, $n = 10$ control, unpaired two-tailed Student's *t*-test). **e**, Hypothalamic presynaptic inputs onto vGluT2⁺ ($n = 3$ mice for each vIPAG and dl/IPAG) and GAD2⁺ ($n = 4$ mice) neurons within vIPAG or dl/IPAG (1×3 ANOVA, Tukey's post-hoc test for each analysed region). Quantification reveals differential input of hypothalamic subregions to vGluT2⁺ ($n = 3$ mice for each vIPAG and dl/IPAG) and GAD2⁺ ($n = 4$ mice) neurons within vIPAG or dl/IPAG. Ventromedial hypothalamic nucleus (VMH) (1×3 ANOVA, $F_{(2,7)} = 40.22$, $P < 0.0001$, Tukey's post-hoc test), posterior hypothalamic nucleus (PH) (1×3 ANOVA, $F_{(2,7)} = 21.01$, $P < 0.05$, Tukey's post-hoc test) and

premamillary nucleus (PMD) (1×3 ANOVA, $F_{(2,7)} = 287$, $P < 0.0001$, Tukey's post-hoc test) preferentially target dl/IPAG vGluT2⁺ neurons, whereas dorsomedial hypothalamic nucleus (DM) (1×3 ANOVA, $F_{(2,7)} = 4.082$, $P > 0.05$), anterior hypothalamus, medial part (AHM) (1×3 ANOVA, $F_{(2,7)} = 3.294$, $P > 0.05$), peduncular part of lateral hypothalamus (PLH) (1×3 ANOVA, $F_{(2,7)} = 0.153$, $P > 0.05$) and lateral hypothalamic area (LH) (1×3 ANOVA, $F_{(2,7)} = 0.948$, $P > 0.05$) showed no preference. **f**, Expression of Syn-myc in glutamatergic terminals of dl/IPAG projections to GABAergic neurons within vIPAG (left scale bar, 200 μ m; right scale bar, 20 μ m). **g**, High-resolution image of a GAD1⁺ vIPAG neuron with dl/IPAG input (scale bar, 5 μ m). **h**, Quantification of dl/IPAG vGluT2⁺ synapses onto vIPAG GAD1⁺ ($n = 21$ ipsilateral cells from four mice, $n = 13$ contralateral cells from two mice, unpaired two-tailed Student's *t*-test). Box-whisker plots indicate median, interquartile range and 5th–95th percentiles of the distribution; bar plots indicate mean \pm s.e.m.; motion plots depict s.e.m. * $P < 0.05$; *** $P < 0.001$.

the question of how such interactions are implemented within PAG circuitry.

We therefore examined whether distinct presynaptic inputs differentially connect onto specific PAG neuronal subpopulations (Extended Data Fig. 5c). Monosynaptic, cell-specific rabies tracing revealed high selectivity in the hypothalamic projections to defined PAG neuronal subpopulations (Fig. 5e and Extended Data Fig. 5d–f). It is conceivable that hypothalamic input to both dl/IPAG and vIPAG glutamatergic neurons promotes a range of defensive behaviours^{26,27}. In turn, activity of the disinhibitory pathway originating in the CEA might bias the behavioural response towards freezing instead of flight. We thus hypothesized that, because of their role in controlling freezing, GABAergic neurons of the vIPAG are poised to present a neuronal substrate for the interaction of freezing and flight pathways. Consequently, we asked whether glutamatergic, flight-promoting neurons of the dl/IPAG could negatively regulate vIPAG excitatory output via activation of vIPAG GABAergic neurons to inhibit the freezing response. In offspring of *Vglut2-ires-Cre* crossed with *Gad1-eGFP* mice, we performed minimal injections of diluted virus to Cre-dependently express Syn-Myc in vGluT2⁺ dl/IPAG neurons only (Fig. 5f). In line with our hypothesis, we found that dl/IPAG glutamatergic neurons form synaptic contacts with GABAergic vIPAG cells (Fig. 5g, h), whose optical activation can lead to flight responses (Fig. 3k). These results support the notion that vIPAG GABAergic neurons integrate multiple inhibitory and excitatory inputs from distinct upstream brain areas to regulate the selection of appropriate active or passive defensive behaviours.

Discussion

Our study defines an amygdala–midbrain–medullary circuit through which freezing behaviour, an evolutionarily conserved response to threat, is generated. Central to this process is a circuit mechanism

involving the disinhibition of vIPAG glutamatergic neurons projecting to pre-motor cells located in the Mc. Disinhibition of this vIPAG→Mc pathway is generated by a disinaptic GABAergic local micro-circuit receiving inhibitory input from CEA (Extended Data Fig. 6). It is important to note that the excitatory vIPAG to Mc pathway did not mediate concomitant analgesia, a hallmark of the general defensive response to threat. Consistent with this result, our single-unit data show that some glutamatergic neurons of the vIPAG are positively and others are negatively correlated with freezing behaviour. These findings suggest that different aspects of the defensive response, such as freezing, flight and analgesia, could be mediated by distinct glutamatergic output pathways from the PAG.

Our data suggest the existence of a dedicated vIPAG output mediating freezing. However, to ensure a rapid switch between passive and active coping with fluctuating threat levels, interactions between freezing and flight circuits are required. Active defensive behaviour including flight could be driven by different hypothalamic^{26,27} or prefrontal⁴³ inputs, directly or via disinhibition onto dl/IPAG glutamatergic neurons, which concomitantly might block freezing behaviour by activation of GABAergic neurons controlling excitatory vIPAG output to the medulla. This notion is supported by our finding of glutamatergic inputs from dl/IPAG onto GABAergic neurons of the vIPAG. While earlier models of PAG function have emphasized its columnar organization^{13,17,19,34,44,45}, or the existence of parallel input-output pathways mediating active or passive defensive behaviours^{3,12,46}, the model emerging from our study supports a key role for local PAG circuitry in the integration of extrinsic inputs to ensure rapid behavioural, autonomic and endocrine adaptations in the face of threat.

A growing body of evidence suggests that the interactions of distinct types of neuron within highly organized neuronal circuits are critical for any higher brain function^{47–49}, and that circuit dysregulation contributes to psychiatric conditions, among which fear

and anxiety-related disorders are the most prevalent^{4,5,50}. Our study shows that similar organizational principles and functional motifs exist even within evolutionarily old, mammalian 'survival circuits'³ dedicated to expression of defensive behaviours. A mechanistic functional understanding of these circuits will provide new insights into possible mechanisms underlying human psychiatric conditions associated with maladaptive coping behaviours under stressful conditions.

Online Content Methods, along with any additional Extended Data display items and Source Data, are available in the online version of the paper; references unique to these sections appear only in the online paper.

Received 10 September 2015; accepted 8 April 2016.

Published online 1 June 2016.

- Anderson, D. J. & Adolphs, R. A framework for studying emotions across species. *Cell* **157**, 187–200 (2014).
- Blanchard, D. C. & Blanchard, R. J. in *Handbook of Anxiety and Fear* Vol. 17 (eds Blanchard, R. J., Blanchard, D. C., Griebel, G. & Nutt, D.) Ch. 2.4, 63–79 (Academic, 2008).
- LeDoux, J. Rethinking the emotional brain. *Neuron* **73**, 653–676 (2012).
- Deisseroth, K. Circuit dynamics of adaptive and maladaptive behaviour. *Nature* **505**, 309–317 (2014).
- Tovote, P., Fadok, J. P. & Lüthi, A. Neuronal circuits for fear and anxiety. *Nature Rev. Neurosci.* **16**, 317–331 (2015).
- Rosen, J. B. & Schulkin, J. From normal fear to pathological anxiety. *Psychol. Rev.* **105**, 325–350 (1998).
- Perusini, J. N. & Fanselow, M. S. Neurobehavioral perspectives on the distinction between fear and anxiety. *Learn. Mem.* **22**, 417–425 (2015).
- Blanchard, D. C., Griebel, G., Pobbe, R. & Blanchard, R. J. Risk assessment as an evolved threat detection and analysis process. *Neurosci. Biobehav. Rev.* **35**, 991–998 (2011).
- Blanchard, R. J. & Blanchard, D. C. Crouching as an index of fear. *J. Comp. Physiol. Psychol.* **67**, 370–375 (1969).
- Fanselow, M. S. & Bolles, R. C. Naloxone and shock-elicited freezing in the rat. *J. Comp. Physiol. Psychol.* **93**, 736–744 (1979).
- Blanchard, D. C., Griebel, G. & Blanchard, R. J. Mouse defensive behaviors: pharmacological and behavioral assays for anxiety and panic. *Neurosci. Biobehav. Rev.* **25**, 205–218 (2001).
- Gross, C. T. & Canteras, N. S. The many paths to fear. *Nature Rev. Neurosci.* **13**, 651–658 (2012).
- Carrive, P. The periaqueductal gray and defensive behavior: functional representation and neuronal organization. *Behav. Brain Res.* **58**, 27–47 (1993).
- Leman, S., Dielenberg, R. A. & Carrive, P. Effect of dorsal periaqueductal gray lesion on cardiovascular and behavioural responses to contextual conditioned fear in rats. *Behav. Brain Res.* **143**, 169–176 (2003).
- Tomaz, C., Brandão, M., Bagri, A., Carrive, P. & Schmitt, P. Flight behavior induced by microinjection of GABA antagonists into periventricular structures in detelencephalated rats. *Pharmacol. Biochem. Behav.* **30**, 337–342 (1988).
- Walker, P. & Carrive, P. Role of ventrolateral periaqueductal gray neurons in the behavioral and cardiovascular responses to contextual conditioned fear and poststress recovery. *Neuroscience* **116**, 897–912 (2003).
- Zhang, S. P., Bandler, R. & Carrive, P. Flight and immobility evoked by excitatory amino acid microinjection within distinct parts of the subventral midbrain periaqueductal gray of the cat. *Brain Res.* **520**, 73–82 (1990).
- Morgan, M. M. & Clayton, C. C. Defensive behaviors evoked from the ventrolateral periaqueductal gray of the rat: comparison of opioid and GABA disinhibition. *Behav. Brain Res.* **164**, 61–66 (2005).
- Fanselow, M. S. in *The Midbrain Periaqueductal Gray Matter: Functional, Anatomical and Immunohistochemical Organization* (eds Depaulis, A. & Bandler, R.) 151–173 (Plenum, 1991).
- Bandler, R., Depaulis, A. & Vergnes, M. Identification of midbrain neurones mediating defensive behaviour in the rat by microinjections of excitatory amino acids. *Behav. Brain Res.* **15**, 107–119 (1985).
- Bandler, R. & Carrive, P. Integrated defence reaction elicited by excitatory amino acid microinjection in the midbrain periaqueductal grey region of the unrestrained cat. *Brain Res.* **439**, 95–106 (1988).
- Tovote, P. *et al.* Activation of central CRF receptor 1 by cortagine results in enhanced passive coping with a naturalistic threat in mice. *Psychoneuroendocrinology* **35**, 887–895 (2010).
- Rizvi, T. A., Ennis, M., Behbehani, M. M. & Shipley, M. T. Connections between the central nucleus of the amygdala and the midbrain periaqueductal gray: topography and reciprocity. *J. Comp. Neurol.* **303**, 121–131 (1991).
- Oka, T., Tsumori, T., Yokota, S. & Yasui, Y. Neuroanatomical and neurochemical organization of projections from the central amygdaloid nucleus to the nucleus reticulobulbus via the periaqueductal gray in the rat. *Neurosci. Res.* **62**, 286–298 (2008).
- Canteras, N. S., Simerly, R. B. & Swanson, L. W. Projections of the ventral premammillary nucleus. *J. Comp. Neurol.* **324**, 195–212 (1992).
- Silva, B. A. *et al.* Independent hypothalamic circuits for social and predator fear. *Nature Neurosci.* **16**, 1731–1733 (2013).
- Wang, L., Chen, I. Z. & Lin, D. Collateral pathways from the ventromedial hypothalamus mediate defensive behaviors. *Neuron* **85**, 1344–1358 (2015).
- An, X., Bandler, R., Ongür, D. & Price, J. L. Prefrontal cortical projections to longitudinal columns in the midbrain periaqueductal gray in macaque monkeys. *J. Comp. Neurol.* **401**, 455–479 (1998).
- Choi, J. S. & Kim, J. J. Amygdala regulates risk of predation in rats foraging in a dynamic fear environment. *Proc. Natl Acad. Sci. USA* **107**, 21773–21777 (2010).
- Behbehani, M. M. Functional characteristics of the midbrain periaqueductal gray. *Prog. Neurobiol.* **46**, 575–605 (1995).
- Depaulis, A., Morgan, M. M. & Liebeskind, J. C. GABAergic modulation of the analgesic effects of morphine microinjected in the ventral periaqueductal gray matter of the rat. *Brain Res.* **436**, 223–228 (1987).
- Vaughan, C. W., Ingram, S. L., Connor, M. A. & Christie, M. J. How opioids inhibit GABA-mediated neurotransmission. *Nature* **390**, 611–614 (1997).
- Ciocchi, S. *et al.* Encoding of conditioned fear in central amygdala inhibitory circuits. *Nature* **468**, 277–282 (2010).
- LeDoux, J. E. Emotion circuits in the brain. *Annu. Rev. Neurosci.* **23**, 155–184 (2000).
- Knobloch, H. S. *et al.* Evoked axonal oxytocin release in the central amygdala attenuates fear response. *Neuron* **73**, 553–566 (2012).
- Wall, N. R., Wickersham, I. R., Cetin, A., De La Parra, M. & Callaway, E. M. Monosynaptic circuit tracing *in vivo* through Cre-dependent targeting and complementation of modified rabies virus. *Proc. Natl Acad. Sci. USA* **107**, 21848–21853 (2010).
- Fenko, L. E. *et al.* Targeting cells with single vectors using multiple-feature Boolean logic. *Nature Methods* **11**, 763–772 (2014).
- Herry, C. *et al.* Switching on and off fear by distinct neuronal circuits. *Nature* **454**, 600–606 (2008).
- Lima, S. Q., Hromádka, T., Znamenskiy, P. & Zador, A. M. PINP: a new method of tagging neuronal populations for identification during *in vivo* electrophysiological recording. *PLoS ONE* **4**, e6099 (2009).
- Esposito, M. S., Capelli, P. & Arber, S. Brainstem nucleus MdV mediates skilled forelimb motor tasks. *Nature* **508**, 351–356 (2014).
- Orlovsky, G. N., Deliagina, T. G. & Grillner, S. in *Neuronal Control of Locomotion: From Mollusc to Man* Ch. 10 and 12 (Oxford Univ. Press, 1999).
- Stamatakis, A. M. *et al.* A unique population of ventral tegmental area neurons inhibits the lateral habenula to promote reward. *Neuron* **80**, 1039–1053 (2013).
- Halladay, L. R. & Blair, H. T. Distinct ensembles of medial prefrontal cortex neurons are activated by threatening stimuli that elicit excitation vs. inhibition of movement. *J. Neurophysiol.* **114**, 793–807 (2015).
- Keay, K. A. & Bandler, R. Parallel circuits mediating distinct emotional coping reactions to different types of stress. *Neurosci. Biobehav. Rev.* **25**, 669–678 (2001).
- Depaulis, A., Keay, K. A. & Bandler, R. Longitudinal neuronal organization of defensive reactions in the midbrain periaqueductal gray region of the rat. *Exp. Brain Res.* **90**, 307–318 (1992).
- Vianna, D. M., Landeira-Fernandez, J. & Brandão, M. L. Dorsolateral and ventral regions of the periaqueductal gray matter are involved in distinct types of fear. *Neurosci. Biobehav. Rev.* **25**, 711–719 (2001).
- Letzkus, J. J. *et al.* A disinhibitory microcircuit for associative fear learning in the auditory cortex. *Nature* **480**, 331–335 (2011).
- Wolff, S. B. *et al.* Amygdala interneuron subtypes control fear learning through disinhibition. *Nature* **509**, 453–458 (2014).
- Hangya, B., Pi, H. J., Kvitsiani, D., Ranade, S. P. & Kepecs, A. From circuit motifs to computations: mapping the behavioral repertoire of cortical interneurons. *Curr. Opin. Neurobiol.* **26**, 117–124 (2014).
- Lüthi, A. & Lüscher, C. Pathological circuit function underlying addiction and anxiety disorders. *Nature Neurosci.* **17**, 1635–1643 (2014).

Supplementary Information is available in the online version of the paper.

Acknowledgements We thank C. Müller, J. Lüdke, K. Bylund, J. Alonso, T. Lu, P. Argast and P. Buchmann for technical assistance, J. J. Letzkus for input on the manuscript, and all members of the Lüthi and Arber laboratories for discussions and other help with the project. We thank L. Gelman and S. Bourke for help with microscopy, and M. Stadler for statistical advice. We are grateful to G. Keller for providing viruses for optogenetics, Z. J. Huang for initially providing the *Gad2-ires-Cre* mouse line and L. Xiao and P. Scheiffele for the anti-rabiesG antibody. This work was supported by the Novartis Research Foundation, by the National Center of Competences in Research: 'SYNAPSY — The Synaptic Bases of Mental Diseases' (financed by the Swiss National Science Foundation) as well as by a Swiss National Science Foundation Core Grant, and a European Research Council Advanced Grant to A.L. Support for S.A. and M.S.E. was provided by a European Research Council Advanced Grant, the Swiss National Science Foundation and the Kanton Basel-Stadt. P.T. and J.P.F. were supported by NARSAD Young Investigator Grants by the Brain and Behavior Foundation. M.S.E. was also supported by a long-term post-doctoral fellowship of the Human Frontier Science Program and a Synapsis Foundation Grant. F.C. and C.H. were supported by grants from the European Research Council (ERC)

under the European Union's Seventh Framework Program (FP7/2007-2013)/ERC grant agreement number 281168 and the Fondation pour la Recherche Médicale.

Author Contributions P.T. conceived, designed, performed and analysed most of the experiments and wrote the manuscript. M.S.E. conceived, designed, performed and analysed neuroanatomical tracing experiments. P.B. performed and analysed *in vitro* slice recordings. F.C. and C.H. performed single-unit recordings in the PAG. S.B.E.W. established optogenetic methodology. J.P.F. performed experiments. M.M. designed and tested viruses

for optogenetics. C.R., L.F. and K.D. produced viruses for optogenetics. S.A. designed viruses for tracing and optogenetics. A.L. conceived the project and wrote the manuscript. All authors contributed to the experimental design and commented on the manuscript.

Author Information Reprints and permissions information is available at www.nature.com/reprints. The authors declare no competing financial interests. Readers are welcome to comment on the online version of the paper. Correspondence and requests for materials should be addressed to P.T. (philip.tovote@fmi.ch) or A.L. (andreas.luthi@fmi.ch).

METHODS

Animals. Experimental subjects were adult (2- to 5-month-old) male, wild-type (Charles River Laboratories) or mutant mice of the C57BL/6J strain. *Slc17a6^{tm2(cre)Loxl}* (*Vglut2-ires-Cre*) and *Chat^{tm2(cre)Loxl}* (*Chat-ires-Cre*) mice were obtained from Jackson Laboratories. Founders for a *Gad2^{tm2(cre)Zjh}* (*Gad2-ires-Cre*) and *Gad1-eGFP* mice colony were initially provided by Z. J. Huang. *Tau-lox-stop-lox-SynGFP-IRES-nlsLacZpa* mice came from an in-house colony⁴⁰. All mice were individually housed in a 12 h light/dark cycle and all experiments were performed during the light cycle. Food and water was available *ad libitum*. Sample sizes were estimated based on previous studies using similar experimental designs^{26,33,38,40,47}. All animal procedures were performed in accordance with institutional guidelines and were approved by the Veterinary Department of the Canton of Basel-Stadt.

Viral injections and optogenetics. Isoflurane (Attane, induction 3%, maintenance 1.5%; Provet) in oxygen-enriched air (Oxymat 3; Weinmann) was used to anaesthetize mice fixed in a stereotactic frame (Kopf Instruments 1900 series). Before opening of the scalp, local injections of ropivacain (Naropin; AstraZeneca) provided analgesia during surgery. After completion of surgery, intraperitoneal injections of meloxicam were administered to alleviate pain (60 µl of 0.5 mg ml⁻¹, Metacam; Boehringer). A feedback-controlled heating pad (FHC) ensured maintenance of core body temperature at 36 °C. A volume of 50–200 nl virus solution (depending on respective viral titre and observed expression strength) was pressure-injected intracranially using calibrated glass pipets (5 µl microcapillary tube; Sigma-Aldrich) connected to a picospritzer III (Parker). To avoid the subcranial midline blood sinus targeting the vIPAG, holes with a diameter of 0.3 mm were drilled bilaterally into the skull at ±1.7 mm (dl/IPAG; ±1.4 mm) from midline suture, and at the level of the lambda suture. The injection capillary was then slowly lowered using a hydraulic micropipet (Kopf Instruments model 2650) at a zenith angle of 26° to the target depth of 3 mm (dl/IPAG; ±2.6 mm) below brain surface. Coordinates for CEA injections were –1.1 mm caudal and ±2.7 mm mediolateral to bregma, at –4.2 mm perpendicularly below brain surface. The Mc of the medulla was targeted with bilateral perpendicular injections –6.4 mm caudal and ±0.95 mm mediolateral to bregma, with an injection depth of 5.6 mm. Cell-type-specific expression of optical actuators was achieved using the following, Cre-dependent AAV: rAAV(2/5)/EF1a-flex-hChR2(T159C)-mCherry (UNC Vector Core), rAAV(2/9)/CAG-flex-ReaChR-Citrine-YFP-WPRE (custom design, Vector Biolabs), rAAV(2/7) EF1a-flex-ChR2(H134R)-2A-NpHR-2A-Venus⁴⁷ and rAAV(2/5)CBA-flex-ARCH-GFP⁴⁸. For characterization of the functional connection between GABAergic and glutamatergic neurons in the vIPAG, we introduced ChR2 into vGluT2⁺, putative GABAergic neurons in the vIPAG using a double-conditional approach in *Vglut2-ires-Cre* mice. We co-injected two AAVs: one that delivered Flp recombinase in an unconditional manner and one that mediated expression of ChR2 only in the presence of Flp and in the absence of Cre (AAVdj/hSyn-Cre^{OFF}-Flp^{ON}-hChR2(H134R)-eYFP)³⁷. Visual targeting of vGluT2⁺ neurons was achieved by Cre-dependent expression of tdTomato (rAAV(2/9)-flex-tdTomato). For Cre- and Flp- dependent expression of ChR2 in the glutamatergic vIPAG-to-Mc projection, we combined an injection of a retrogradely trafficked HSV (HSV/hEF1a-LS1L-mCherry-IRES-flpo; R. Neve) into the Mc with another injection of AAV(dj)/hSyn-Cre^{ON}/Flp^{ON}-hChR2(H134R)-mCherry³⁷ into the vIPAG of *Vglut2-ires-Cre* mice. Control mice were injected with the following AAVs: AAV(2/5)EF1a-flex-tdTomato (provided by G. Keller), AAV(2/9)CAG-flex-eGFP-WPRE-bGH, AAV(2/9)CAG-flex-tdTomato-WPRE-bGH (both Penn Vector) and AAV(dj)/hSyn-Cre^{ON}/Flp^{ON}-mCherry³⁷.

For optical manipulation or electrophysiological recordings, mice were implanted with custom-built fibre connectors (fibre: 0.48 numerical aperture, 200 µm diameter; Thorlabs) 3–4 weeks after virus injections. The tip of the fibre was lowered at an angle of 26° to 250 µm above the injection site in the PAG. Implants were fixed to the skull with skull screws (P.A. Precision Components), cyanoacrylate glue (Ultra Gel; Henkel) and dental cement (Paladur; Heraeus). All fibre connectors were tested for effective light transduction before implantation. For optical stimulation of ChR2, laser light of 473 nm (CNI Laser) was applied, whereas laser light of 594 nm was used for optical stimulation of NpHR or Arch. Light intensity was adjusted with an optical power meter (Thorlabs) to reach 10–15 mW at the end of the implanted fibre stub.

Histology. After completion of experiments, mice were transcardially perfused with 4% paraformaldehyde in phosphate-buffered saline (PBS). Fixed brains were cryoprotected in 30% sucrose/PBS and cut on a cryostat in 80 µm coronal slices. Antibody stainings were performed on single-well floating tissue sections. Sections were incubated for 48 h in primary antibodies at 4 °C followed by one overnight incubation with secondary antibodies at 4 °C. Primary antibodies used in this study were as follows: chicken anti-GFP 1:1,000 (A10262, Molecular Probes), rabbit anti-RFP 1:5,000 (600-401-379, Rockland Immunochemicals), guinea pig anti-vGluT2 1:5,000 (AB5907, Chemicon), mouse anti-V5 1:1,000 (R960CUS, Invitrogen),

mouse anti-NeuN 1:1,000 (MAB377, Chemicon), mouse anti-Myc 1:100 (CRL-1729, ATCC), goat anti-Bgal 1:4,000 (AR2282, Biogenesis), mouse anti-channelrhodopsin-2 1:2 (clone 15E2, 651180, PROGEN Biotechnik), guinea pig anti-rabiesG 1:500 (provided by P. Scheiffele). Fluorophore-tagged secondary antibodies used were Alexa Fluor 488 donkey anti-chicken IgY 1:1,000 (703-545-155, Jackson), Cy3 donkey anti-rabbit IgG 1:1,000 (711-165-152, Jackson), Alexa Fluor 657 donkey anti-guinea pig IgG 1:1,000 (706-605-148, Jackson), Alexa Fluor 657 donkey anti-mouse IgG 1:1,000 (715-605-150, Jackson), Alexa Fluor 657 donkey anti-goat IgG 1:1,000 (705-605-147, Jackson) or Alexa Fluor 488 donkey anti-mouse IgG 1:1,000 (A21202, Molecular Probes). For counterstaining, sections were incubated for 10 min with 4',6-diamidin-2-phenylindol (DAPI, 1:10,000, Sigma). Stained brain sections were mounted on gelatin-coated slides and coverslipped with custom-made glycerol-based medium (Fluorostab). Slides were imaged using an automated slide scanner microscope (Zeiss AxioScan).

Placement of the optical fibres was assessed on the basis of the lesion the fibre tip inside the brain tissue. Mice with no or unilateral expression of the virus, or fibre tip placement outside of the PAG, were excluded from the analysis. To analyse virus expression in *Vglut2-ires-Cre* mice expressing ChR2(T159C), we outlined the area of somatic viral expression on the respective sections in a mouse brain atlas⁵¹ for each animal, and then overlaid the areas at 30% transparency (Adobe Illustrator) to visualize the average centre of expression in each behavioural group.

Behaviour. Mice of different litters but the same genotype were used in individual experiments. No criteria were used to allocate mice to experimental groups, and, for blinding, experimental subjects had unique letter/number identifiers that indicated genotype but no group assignment. All basic testing of light-induced behavioural effects was performed under low-fear conditions in a novel, circular Plexiglas cylinder with smooth white floor (diameter 27 cm) under dim-light conditions in a dark-walled sound-attenuated chamber. Acetic acid (1%) was used to clean the context and to provide a distinct olfactory stimulus. After 1 min of habituation, light was applied four times for 5 s, with an inter-stimulus interval of 55 s. Total duration of freezing during the four 'light on' periods was compared with time spent freezing in the period of equivalent length immediately before onset of the first light stimulus.

To investigate light-mediated effects on conditioned freezing, mice were subjected to auditory fear conditioning in a brightly illuminated square context (27 cm × 27 cm) with a metal grid floor. A train of 20 tone beeps (7.5 kHz, 75 dB sound pressure level, 500 ms duration, 500 ms inter-beep-interval) was used as the conditioned stimulus (CS) and an electrical foot-shock (0.6 mA dc, 1 s duration) was used as the unconditioned stimulus (US). The conditioning session lasted 440 s during which the mice were exposed to three back-to-back CS-US pairings in a pseudo-random fashion, with a baseline period of 180 s and a minimal inter-stimulus interval of 80 s. On the day after conditioning, mice were exposed to four CS-only presentations in a dimly illuminated context different from the conditioning context. While the conditioning context was cleaned with 70% ethanol, the retrieval context was wiped down with 1% acetic acid. The duration of the retrieval session was 540 s, with a baseline period of 180 s and a pseudo-random presentation of the CS with a minimal inter-stimulus interval of 120 s. To test for light-activation effects on CS-induced defensive behaviour, the second and fourth presentation of the CS was paired with 20 s of continuous laser light. Total duration of freezing during the two CS-alone periods (first and third) was compared with time spent freezing during the two CS periods (second and fourth) paired with 'light on', and with a baseline period of equal length (40 s) directly before onset of the first CS. Contextual fear was tested a day later by re-introducing the experimental subject into the original conditioning context for 5 min. To test for effects of light activation on contextual freezing laser illumination was turned on twice for 1 min, with a 1 min pre-baseline and a 1 min inter-stimulus interval. Total duration of freezing during the two 'light on' periods was compared with time spent freezing in the time period of equivalent length immediately before light onset.

For *in vivo* recordings of unidentified PAG single units, auditory fear conditioning and testing took place in two different contexts (contexts A and B). To measure movement, an automated infrared beam detection system located on the bottom of the experimental chambers was used (Coulbourn Instruments). The animals were considered to be freezing if no movement was detected for 2 s (ref. 38). On day 1, C57BL6/J mice were submitted to a habituation session in context A, in which they received four presentations of the CS⁺ and the CS⁻ (total CS duration, 30 s; consisting of 50-ms pips at 0.9 Hz repeated 27 times, 2 ms rise and fall, pip frequency, 7.5 kHz or white-noise, 80 dB sound pressure level). Discriminative fear conditioning was performed on the same day by pairing the CS⁺ with a US (1 s foot-shock, 0.6 mA, 5 CS⁺-US pairings, inter-trial intervals, 20–180 s). The onset of the US coincided with the offset of the CS⁺. The CS⁻ was presented after each CS⁺-US association but was never reinforced (five CS⁻ presentations; inter-trial intervals, 20–180 s). The frequencies used for CS⁺ and CS⁻ were counterbalanced

across animals. On day 2, conditioned mice were submitted to a testing session (retrieval session) in context B during which they received four presentations of the CS⁻ and CS⁺.

To test for effects on unconditioned freezing, mice were exposed to a remote-controlled toy snake in an open-field arena (50 cm × 50 cm). To control for baseline activity and laser effects, mice were pre-exposed to the open field alone for 10 min, with four laser illumination periods of 20 s (inter-stimulus interval 40 s) in the second half of this phase. After introduction of the snake, mice remained in the open field for another 5 min, during which the snake's movement was remotely controlled by the experimenter outside the chamber. To maintain high freezing levels, the snake was moved around the area, thereby covering varying distances to the mouse without establishing direct contact.

Locomotor activity was recorded by an infrared beam system (Coulbourn Instruments) or an overhead video tracking system (CinePlex Studio). Freezing was defined as immobility detected by lack of beam breaks for 2 s, as described before³⁸. Using the video tracking system, freezing was extracted with the freezing detector plug-in (CinePlex Editor). A 2 s criterion of the thresholded motion measure, based on a contour-tracking algorithm, was used to define freezing. Motion measure was automatically computed as the normalized frame-by-frame difference of the animal's body contour in pixels. Automatically detected freezing behaviour was cross-checked on the video recording to exclude false-positive freezing bouts, for example during grooming episodes, or include false negative freezing intervals, for example owing to motion artefacts caused by cable movement in front of the camera. Timestamps for freezing episodes and stimulation events (CS, US, laser) were imported into data analysis software (Neuroexplorer 5, Nex Technologies) and averaged over the respective time interval. Behavioural activity of the animal was assessed using the motion measure of the video tracking system. Motion was averaged over 1-s bins and normalized as the percentage change in relation to a baseline period. Baseline was the time directly before stimulus onset: that is, 16 s before 'light on' in experiments with naive mice, and 10 s before CS/CS⁺'light on' in cued fear-conditioning experiments. Combined contour tracking of the mouse and colour-tracking of the toy snake were used to extract *x-y* coordinates of the two subjects and calculate their distance.

Tail immersion test. To test for analgesic effects induced by optical stimulation of glutamatergic cells of the PAG, mice tail tips were immersed in hot water with a temperature of 50 °C. This was done eight times with an inter-trial interval of 40 s, and tail withdrawal latency was scored frame-by-frame (Windows Live Movie Maker) from the video recorded during the test session (Plexon Cineplex). On the last four trials, laser light was turned on for 5 s directly before the tail immersion. If the mouse did not withdraw its tail within 10 s of immersion, the trial was terminated. Tail withdrawal latencies of the first four non-manipulated trials were averaged as baseline and compared with average withdrawal latency during the last four light-stimulated trials.

Slice electrophysiology. Standard procedures were used to prepare 300 μm thick coronal slices from 12- to 14-week-old male *Vglut2-ires-Cre* or *Vglut2-ires-Cre::Gad1-eGFP* mice, which received intracranial virus injections 4 weeks before. The brain was dissected in ice-cold artificial cerebrospinal fluid, mounted on an agar block and sliced with a vibrating-blade microtome (HM 650 V, Carl Zeiss) at 4 °C. Slices were maintained for 45 min at 37 °C in an interface chamber containing artificial cerebrospinal fluid equilibrated with 95% O₂/5% CO₂ and containing the following (in mM): 124 NaCl, 2.7 KCl, 2 CaCl₂, 1.3 MgCl₂, 26 NaHCO₃, 0.4 NaH₂PO₄, 18 glucose, 4 ascorbate. Recordings were performed with artificial cerebrospinal fluid in a recording chamber at a temperature of 35 °C at a perfusion rate of 1–2 ml min⁻¹. PAG neurons were visually identified with infrared video microscopy using an upright microscope equipped with a ×40 objective (Olympus). Patch electrodes (3–5 MΩ) were pulled from borosilicate glass tubing. For voltage clamp experiments to record eIPSCs, patch electrodes were filled with a solution containing the following (in mM): 110 CsCl, 30 K-gluconate, 1.1 EGTA, 10 HEPES, 0.1 CaCl₂, 4 Mg-ATP, 0.3 Na-GTP (pH adjusted to 7.3 with CsOH, 280 mOsm) and 4 *N*-(2,6-dimethylphenylcarbamoylmethyl) triethylammonium bromide (QX-314; Tocris-Cookson).

Evoked IPSCs were elicited by 10 ms blue-light stimulation of either local vPAG axon terminals of non-glutamatergic neurons expressing ChR2 or ChR2⁺ CEA axons projecting to PAG. To exclude glutamatergic inputs, CNQX (6-cyano-7-nitroquinoxaline-2,3-dione, 10 μM; AMPA receptor antagonist) and (R)-CPP ((RS)-3-(2-carboxypiperazin-4-yl)-propyl-1-phosphonic acid, 10 μM; NMDA receptor antagonist) were added to the artificial cerebrospinal fluid. To confirm the eIPSCs GABAergic nature, picrotoxin (100 μM) was added at the end of the recordings. Successful connections were scored if the amplitude of eIPSCs was higher than 10 pA, with the latency within 10 ms for at least 60% of the trials (six out of ten trials). Whole-cell patch-clamp recordings were excluded if the access resistance exceeded 13 MΩ and changed more than 20% during the recordings.

Data were recorded with a MultiClamp 700B (Molecular Devices) amplifier, filtered at 0.2 kHz and digitized at 10 kHz. Data were acquired and analysed with Clampex 10.0, Clampfit 10.0 (Molecular Devices). All chemicals for the internal and external solutions were purchased from Fluka/Sigma. Glutamatergic blockers were purchased from Tocris Bioscience.

Anatomical tracing. To characterize CEA inputs to vPAG, we injected retrogradely transported fluorescent latex beads (Lumafuor) into the vPAG of *Gad1-eGFP* mice. Four days after injection, mice were killed, transcardially perfused with 4% paraformaldehyde in PBS, and brains were extracted and processed for histology as described above. On four coronal sections from each mouse, bead⁺ cells in the CEI and CEM were counted and normalized against total cells stained by NeuN.

To identify the presynaptic partners of specific neuronal subpopulations in the PAG, we used a monosynaptically restricted pseudotyped rabies virus³⁶. We performed a local injection in the vPAG or lPAG of AAVs conditionally delivering rabies glycoprotein (AAV(2/9)CAG-flex-rabiesG-2A-H2B-10xV5-tag, short: AAV-flex-rabiesG)⁴⁰ and TVA (AAV(2/9)CAG-flex-TVA-2A-H2B-eGFP, short: AAV-flex-TVA)⁴⁰ into either *Vglut2-ires-Cre* or *Gad2-ires-Cre* mice. Two weeks later, we injected EnvA-ΔG-mCherry-rabies³⁶ into the same location. Mice were killed 7 days thereafter, transcardially perfused with 4% paraformaldehyde in PBS, and brains were extracted and processed for histology as described above. Brain sections corresponding to the injection site were stained for GFP, red fluorescent protein (RFP) and V5, and counterstained with DAPI. Brain sections outside the injection site were stained for RFP and NeuN. To compare the relative input to the different PAG subpopulations, we quantified the number of starter cells within the PAG (mCherry, GFP and V5 triple-positive cells) in four sections around the injection site and we counted the number of mCherry⁺ cells within the entire CEA. Images were acquired with an Olympus confocal microscope (FV1000) with a motorized stage, using a ×20 objective, a 3 × 3 tiled scan with 15% overlap and a step size of 1.5 μm along the depth of the slice. Triple-positive cells in the PAG and mCherry⁺ cells in CEA were counted manually along every confocal plane using Imaris software (Bitplane). To quantify the hypothalamic input to PAG subpopulations, we analysed approximately half the volume of the hypothalamus by imaging every other section along the rostro-caudal axis with an automated slide scanning microscope (Zeiss AxioScan Z1) using a ×10 objective. mCherry⁺ neurons were counted manually on the image projection. We use the following nomenclature for the hypothalamic nuclei: dorsomedial hypothalamic nucleus (DM), anterior hypothalamus, medial part (AHM, including the entire anterior hypothalamic area, the latero-anterior hypothalamic nucleus and the paraventricular hypothalamic nucleus), ventromedial hypothalamic nucleus (VMH), posterior hypothalamic nucleus (PH), peduncular part of lateral hypothalamus (PLH, including the Mc of the lateral hypothalamus), lateral hypothalamic area (LH, including the parasubthalamic nucleus), premammillary nucleus (PMD). All quantifications were performed by an experimenter blind to the subject's genotype.

To study PAG projections to brainstem neurons directly connected to spinal motor neurons (pre-motor neurons), we combined an anterograde vPAG injection of an AAV expressing presynaptic fluorescent markers and monosynaptic rabies spreading from spinal motor neurons. To label pre-motor neurons, we injected a monosynaptic rabies virus into forelimb muscles that retrogradely infected the corresponding spinal motor neurons. To allow for spreading of the rabies virus in adult mice, we complemented cervical motor neurons with an AAV conditionally expressing rabies glycoprotein through an intra-spinal injection in *Chat-Cre* mice. First, we injected into the vPAG of *Chat-Cre* adult mice a custom-made AAV that unconditionally expressed GFP-tagged synaptophysin (Syn) in presynaptic terminals (AAV(2/9)/CAG-flex-SynGFP + AAV(2/9)/CMV-Cre)⁴⁰. In the same surgery session, we injected AAV(2/9)CAG-flex-rabiesG-2A-H2B-10xV5-tag⁴⁰ into the cervical part of the spinal cord. Two weeks thereafter, G-delated rabies virus coated with the CVS-glycoprotein was injected in triceps and biceps muscles. Eight days after rabies injection, mice were killed and brains were immunostained against GFP, RFP and vGluT2 and counterstained with DAPI. High-resolution three-dimensional images of eight complete pre-motor cells in the Mc were acquired on a custom-made dual motorized spinning-disk microscope (Life Imaging Services) using a ×63 objective, 8 × 8 tile scan and 0.2 μm step size. We quantified the number of GFP⁺ (vGluT2⁺) vPAG inputs to soma and dendritic tree of these cells manually in eight neurons from three mice. The Mc was defined as described before⁴⁰ and included lateral paragigantocellular, as well as ventral and alpha parts of the gigantocellular, reticular nucleus.

To assess local vPAG inputs specifically onto Mc-projecting glutamatergic neurons, we used an intersectional viral approach (Extended Data Fig. 4f–h). We injected a retrogradely transported HSV that Cre-dependently delivered rabies G-protein (HSV/hEF1α-LS1L-rabiesG; R. Neve) into the Mc of offspring from *Vglut2-ires-Cre* crossed with *Gad1-eGFP* mice. In the same surgery session, we

injected conditional AAV into the vPAG to virally express the TVA receptor in glutamatergic cells (rAAV(2/9)CAG-flex-TVA-2A-H2B-eGFP, custom designed, Vector Biolabs). Two weeks later, we injected EnvA- Δ G-mCherry-rabies into the Mc. Mice were killed 7 days later and brains processed as described above. We then used standard immunohistochemistry to stain for GFP, RFP and rabies G-protein. High-resolution confocal images ($\times 40$) of vPAG were taken from three coronal sections of the PAG (rostral, medial, caudal) and individual cells were manually counted using Imaris software (Bitplane). Triple-positive cells were identified as starter cells, whereas GFP and RFP double-positive cells represented local GAD1⁺ cells connected to glutamatergic Mc-projecting neurons.

We performed several controls to demonstrate the specificity of the monosynaptic rabies tracing technology. To check for the specificity of the AAV viruses delivering the TVA receptor (AAV-flex-TVA) and rabiesG protein (AAV-flex-rabiesG), we injected those viruses in the vPAG of offspring from *Vglut2-Cre* and *Tau-lox-stop-lox-SynGFP-IRES-nlsLacZpA* reporter mouse lines. After 2 weeks, animals were killed and the injection site was cut, immunostained and co-localization of GFP or V5 with b-Gal was analysed. In an additional experiment, *Vglut2-ires-Cre* animals were injected with AAV-flex-TVA followed by EnvA- Δ G-mCherry-rabies 2 weeks later. Furthermore, to test for the leakiness of the EnvA- Δ G-mCherry-rabies, we injected this virus in the vPAG of wild-type animals combined with latex beads. Animals were killed 1 week later and the entire PAG, amygdala and hypothalamus were cut and stained for mCherry and NeuN. Lastly, wild-type animals were injected with AAV-flex-TVA, AAV-flex-rabiesG and EnvA- Δ G-mCherry-rabies following the same protocol used for monosynaptic tracing experiments.

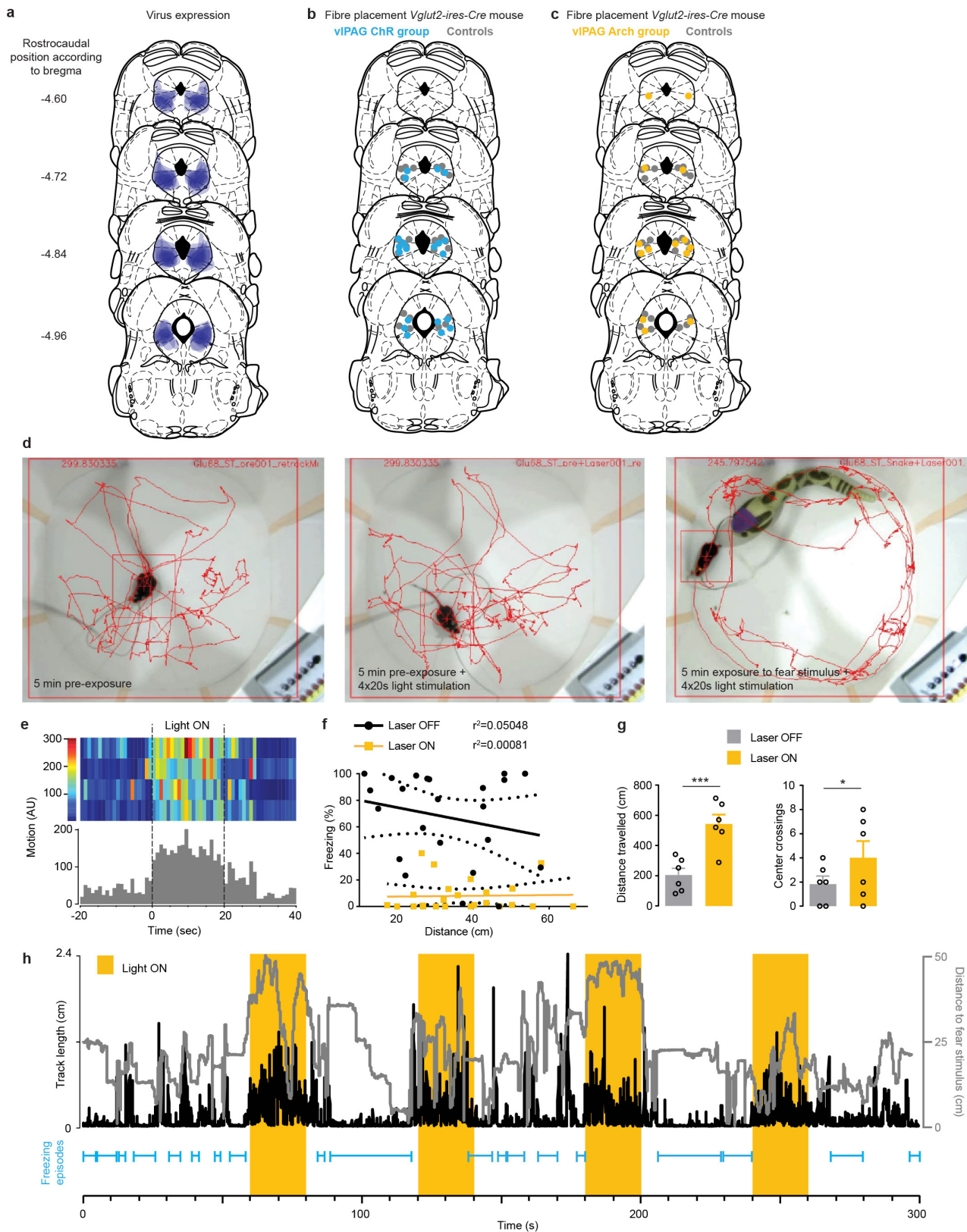
To characterize the connectivity from dIPAG to vPAG, we injected AAV(2/9)CAG-flex-Synaptophysin-Myc⁴⁰ into offspring of *Vglut2-ires-Cre* mice crossed with *Gad1-eGFP* mice ($n = 4$ mice) to visualize glutamatergic dIPAG contacts onto GFP⁺ GABAergic vPAG neurons. To quantify opposing synaptic contacts, we selected neurons with complete soma and acquired $\times 60$ confocal images at a step size of 0.2 μ m with a confocal microscope (Olympus FV1000). Quantification of synaptic inputs from ipsilateral ($n = 21$ cells from four mice) and contralateral ($n = 13$ cells from two mice) hemispheres was performed manually using Imaris software (Bitplane).

Single-unit recordings. Custom-built, chronically implanted 16-wire electrodes³⁸ were used to record electrical activity in the vPAG. Electrodes were connected to a headstage (Plexon) containing 16 unity-gain operational amplifiers. The headstage was connected to a 16-channel preamplifier (gain 100 \times bandpass filter from 150 Hz to 9 kHz for unit activity, Plexon). Spiking activity was digitized at 40 kHz, bandpass filtered from 250 Hz to 8 kHz, and isolated by time-amplitude window

discrimination and template matching using a Neural Data Acquisition System (Omniplex, Plexon). Single-unit spike sorting was performed using Off-Line Spike Sorter (OFSS, Plexon) for all behavioural sessions. Principal-component scores were calculated for unsorted waveforms and plotted in a three-dimensional principal-component space; clusters containing similar valid waveforms were manually defined. A group of waveforms were considered to be generated from a single neuron if the waveforms formed a discrete, isolated, cluster in the principal-component space and did not contain a refractory period less than 1 ms, as assessed using auto-correlogram analyses. To avoid analysis of the same neuron recorded on different channels, we computed cross-correlation histograms. If a target neuron presented a peak of activity at a time that the reference neuron fired, only one of the two neurons was considered for further analysis. Spike timestamps were analysed (Neuroexplorer 5, Nex Technologies) to calculate average firing rates and z-score transformations of cells depending on behavioural parameters: that is, within and outside freezing episodes. Optical identification of single units was performed as previously described⁴⁸. Briefly, laser light pulses of 100–300 ms duration were used to evoke spiking activity. Short latencies (GAD2⁺ cells: ≤ 15 ms; vGluT2⁺ cells: ≤ 10 ms) of reliable light-evoked spiking were considered to indicate direct light activation and, thus, allowed for identification of the cell type. To correlate single-unit activity with freezing behaviour, we calculated z-scores 2 s before and after onset of freezing during the entire recall session for recordings both of unidentified or of optically identified single units.

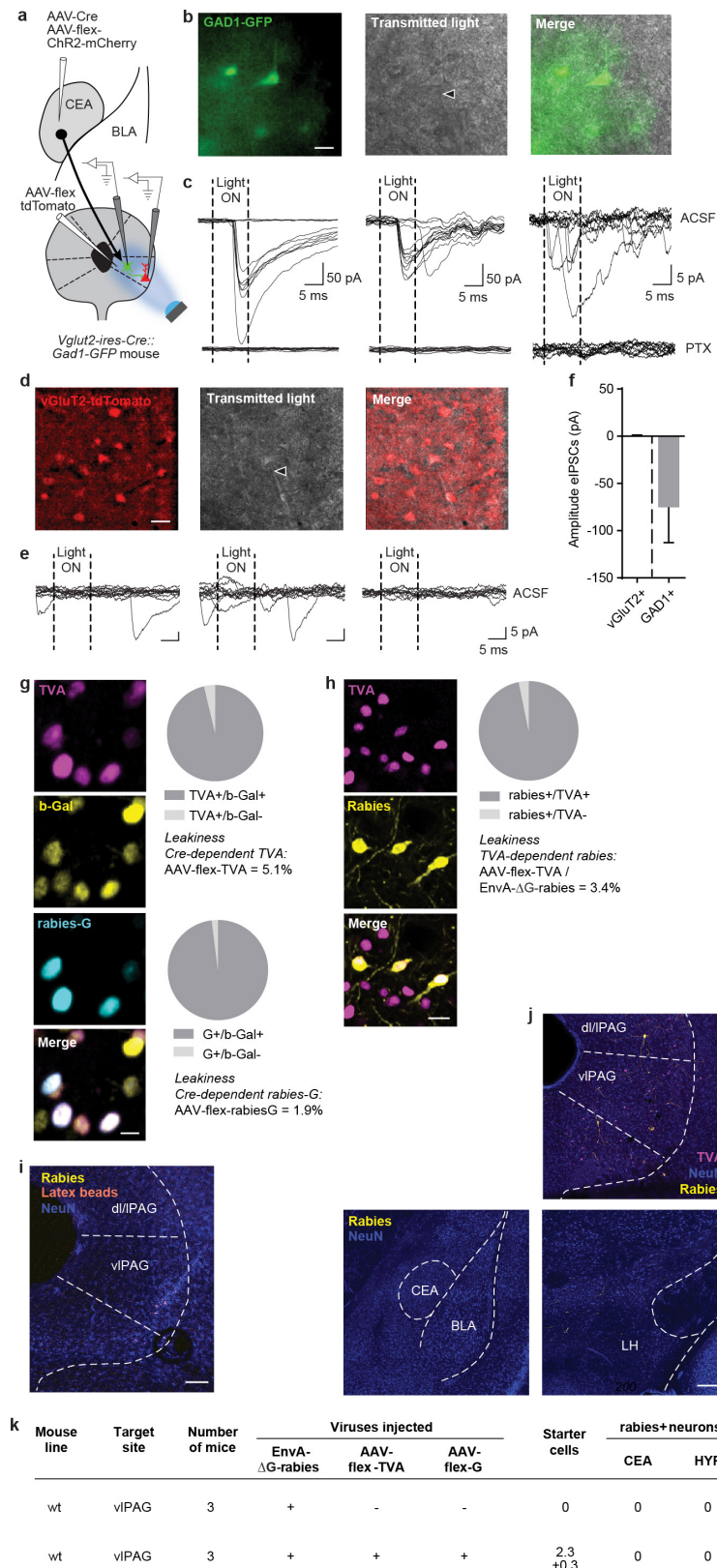
Statistics. The experiments were not randomized. No statistical methods were used to predetermine sample size. Data presented in box-whisker plots indicate medians, interquartile range and 5th–95th percentiles. Motion data are presented as s.e.m. range. All other data are presented as means \pm s.e.m. Statistical analyses were performed in Graphpad Prism 6.0a or using R. Normality was assessed using Shapiro-Wilk tests. Whenever the normality test failed, non-parametric Mann-Whitney or Wilcoxon signed-rank (for repeated measures) tests were used for pairwise comparisons. Within-subject group analysis of non-parametric data was performed using Friedmann's test with a post-hoc Dunn's multiple comparisons test. Between-subject group analysis of non-parametric data was done with Kruskal-Wallis statistics and a post-hoc Dunn's multiple comparisons test. Variance in normally distributed data sets was analysed with one-way ANOVA and Tukey's or Sidak's post-hoc tests. Significance levels are indicated as follows: * $P < 0.05$; ** $P < 0.01$; *** $P < 0.001$. See Supplementary Information for statistics table.

51. Franklin, K. B. J. & Paxinos, G. *Atlas of the Mouse Brain* 4th edn (Academic, 2001).



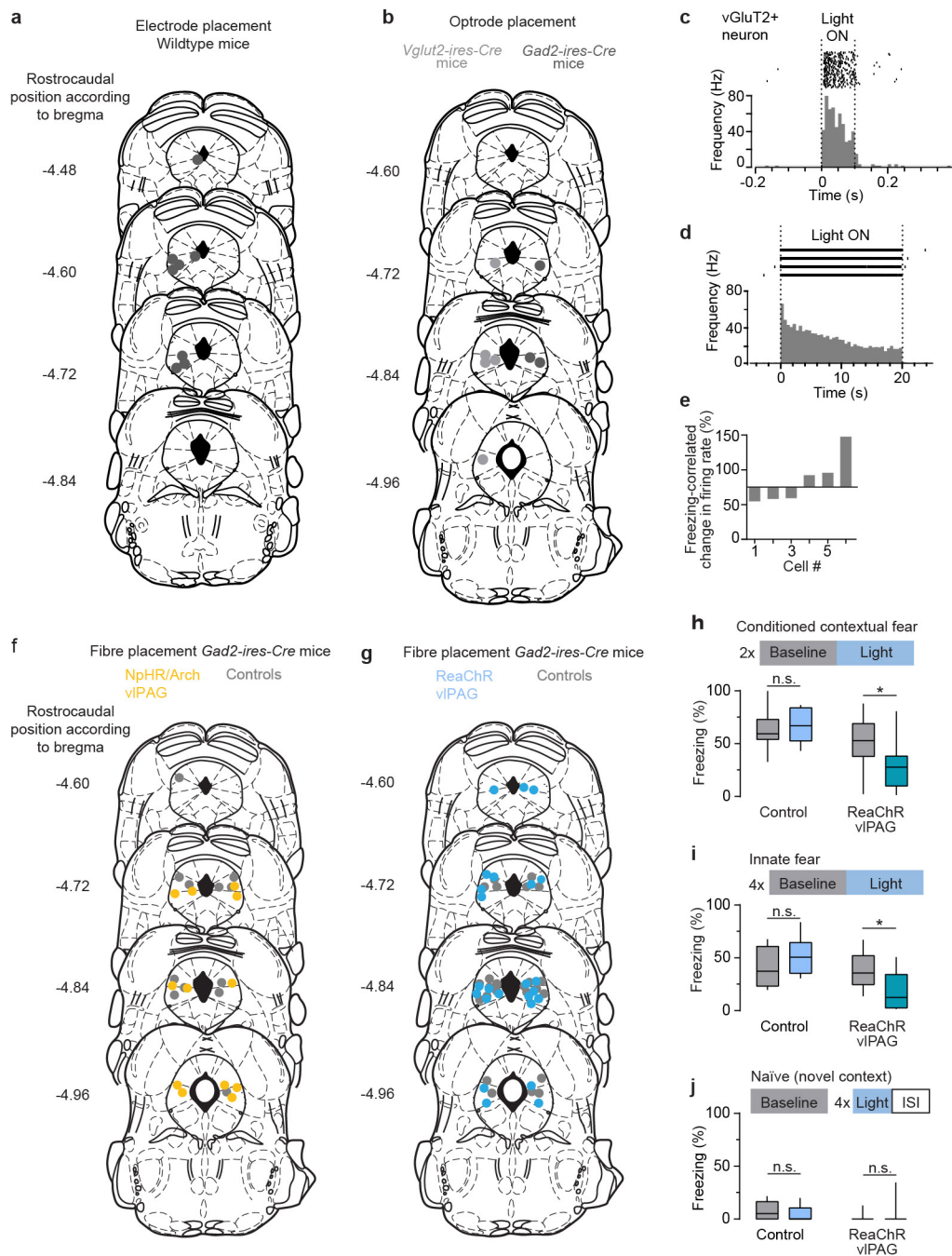
Extended Data Figure 1 | **a**, Expression of Chr2 throughout vIPAG in consecutive coronal brain sections⁵¹. **b**, **c**, Fibre placements in *Vglut2-ires-Cre* mice of experimental and control groups. **d**, Supplementary Video stills with superimposed representative movements tracks during the snake open-field test for unconditioned defensive responses. **e**, Colour-coded plot for a mouse's motion before, during and after light-mediated inhibition of vIPAG glutamatergic neurons expressing Arch during a snake open-field test session. **f**, Freezing responses plotted against mouse-snake distance during 'light on' and 'light off' periods showing no linear

correlation. **g**, Effects of light-mediated inhibition of vIPAG glutamatergic neurons on anxiety-like behaviour in the open field test with no snake present. Inhibition of vIPAG glutamatergic cells resulted in enhanced track length ($n = 6$ mice, paired two-tailed Student's t -test) and more frequent visits to the centre of the open field ($n = 6$ mice, paired two-tailed Student's t -test). **h**, Example of an entire snake open-field test session, with track length, freezing episodes and mouse-snake distance. Values are means \pm s.e.m.



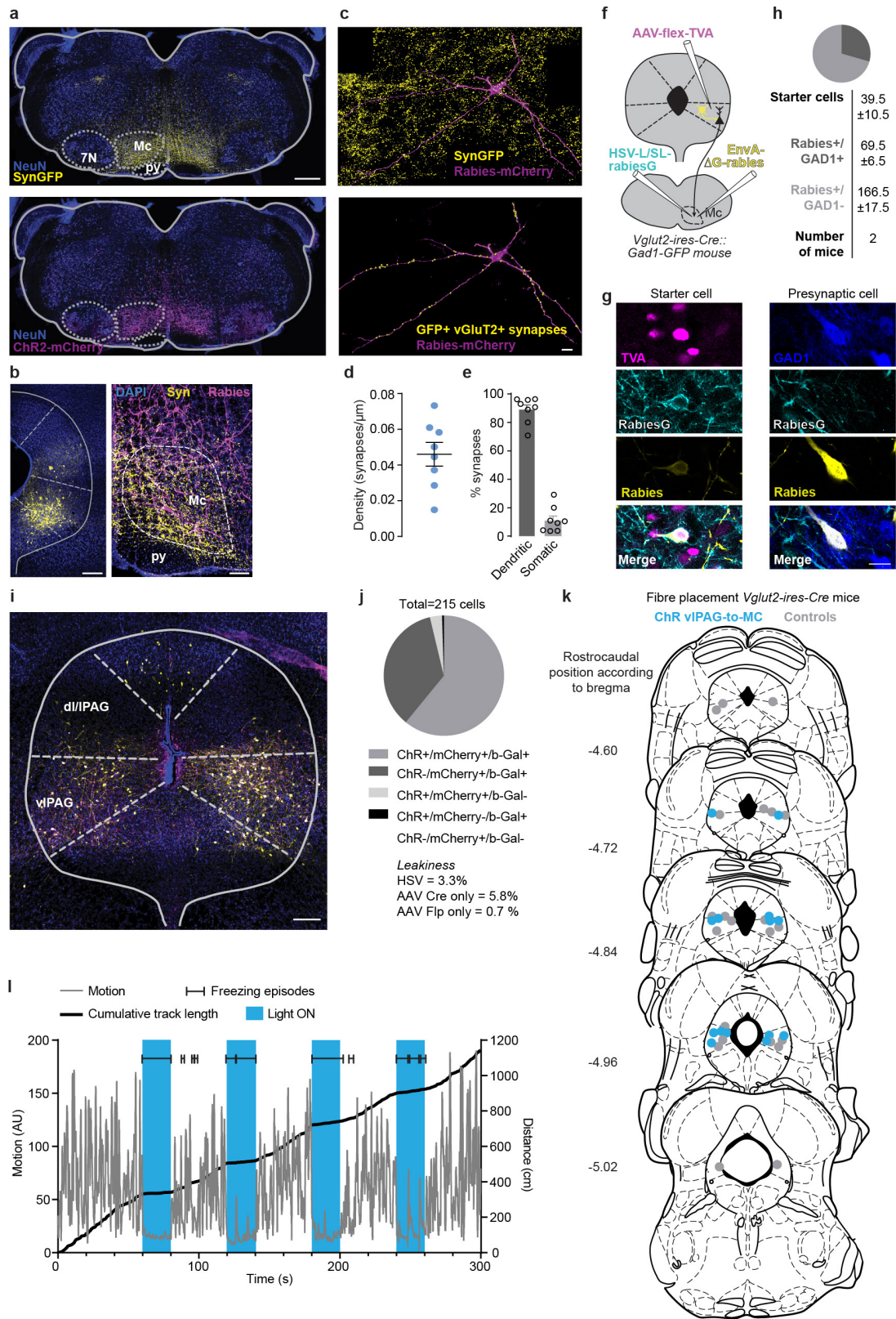
Extended Data Figure 2 | a, *In vitro* slice recordings of functional connectivity between CEA and GABAergic or glutamatergic neurons in vIPAG. **b**, Targeting of fluorescently labelled GAD1⁺ neurons for whole-cell patch clamp recordings (triangle indicates patch pipette, scale bar, 20 μm). **c**, Example traces of three GAD1⁺ cells (from three slices of three mice) showing eIPSCs upon light stimulation (10 ms duration) of afferents from the CEA (upper traces), and blockage of eIPSCs by PTX (lower traces). **d**, Targeting of fluorescently labelled vGluT2⁺ neurons for whole-cell patch clamp recordings (triangle indicates patch pipette; scale

bar, 20 μm). **e**, Example traces of three light non-responsive vGluT2⁺ neurons (from the same three slices as in **c**). **f**, Quantification of eIPSCs amplitudes. **g**, Analysis of specificity of AAV-mediated expression of TVA and rabiesG (scale bar, 10 μm). **h**, Analysis of specificity of TVA-dependent EnvA-ΔG-mCherry-rabies infection (scale bar, 20 μm). **i**, **k**, Lack of EnvA-ΔG-mCherry-rabies infection after injection into wild-type mice (scale bar, 100 μm). **j**, **k**, Leakiness analysis of the combined AAV and EnvA-ΔG-mCherry-rabies tracing system in wild-type mice (scale bar, 200 μm). Values are means ± s.e.m.



Extended Data Figure 3 | **a**, Electrode placements for the recordings of unidentified single units. **b**, Placements of optrodes for the recordings of identified neurons. **c**, Raster-frequency plot of an optically identified vIPAG vGluT2⁺ neuron. **d**, A glutamatergic neuron exhibiting marked optical activation during constant illumination for 20 s. **e**, Identified vGluT2⁺ neurons ($n = 6$) showed both increased and decreased activity during freezing. **f**, **g**, Fibre placements in *Gad2-ires-Cre* mice expressing inhibitory or excitatory optical actuators. **h**, **i**, Activation of vIPAG

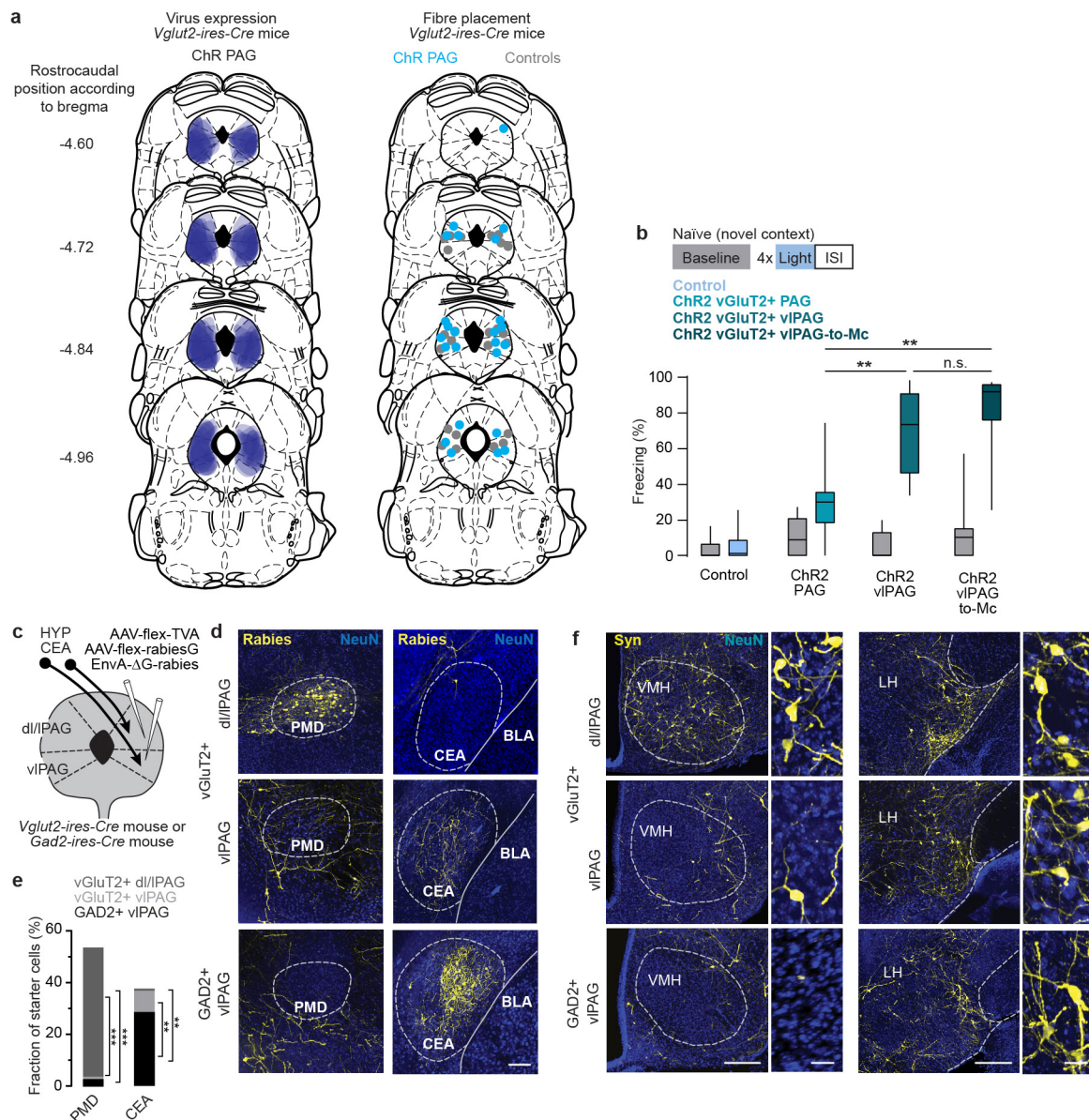
GAD2⁺ neurons resulted in reduced conditioned contextual freezing ($n = 12$ Chr2, $n = 7$ control, paired two-tailed Student's t -test) and lower innate freezing levels during the snake open-field test ($n = 10$ Chr2, $n = 8$ control, two-tailed Wilcoxon signed-rank test). **j**, Optical activation of vIPAG GAD2⁺ neurons had no effect on freezing in naive mice ($n = 8$ Chr2, $n = 8$ control, two-tailed Wilcoxon signed-rank test). Box-whisker plots indicate median, interquartile range, and 5th–95th percentiles of the distribution. * $P < 0.05$.



Extended Data Figure 4 | See next page for caption.

Extended Data Figure 4 | **a**, Projection pattern of glutamatergic vIPAG axonal inputs to the rostral medulla. Terminals of vGluT2⁺ vIPAG projection neurons were labelled by AAV-mediated expression of GFP fused to presynaptic marker synaptophysin (top; scale bar, 400 μ m), and Chr2-mCherry expression was visualized using immunohistochemistry (bottom). **b**, Concomitant AAV-mediated expression of Syn-GFP in vIPAG neurons (left panel, scale bar, 200 μ m) labelled presynaptic terminals within Mc (right panel, scale bar, 100 μ m). **c**, High-resolution image of a retrogradely traced Mc pre-motor neuron (rabies-mCherry) and SynGFP⁺ vIPAG inputs (top), and visualization of identified glutamatergic synaptic contacts (bottom; scale bar, 10 μ m). **d, e**, Density of vGluT2⁺ vIPAG synaptic inputs to pre-motor neurons in Mc ($n = 8$ cells from three mice), and quantification of their distribution between the dendritic or somatic compartment. **f**, Intersectional EnvA- Δ G-mCherry-rabies tracing approach to identify local GABAergic inputs to vIPAG-to-Mc-projecting glutamatergic cells. **g**, TVA-, rabiesG- and EnvA- Δ G-

mCherry-rabies triple-positive cells were identified as starter cells (left panels), while GAD1 and EnvA- Δ G-mCherry-rabies double positive cells indicated presynaptic GABAergic neurons (right panels; scale bar, 20 μ m). **h**, Quantification of GAD1⁺ or GAD1⁻ presynaptic cells ($n = 2$ mice; dark grey, rabies⁺/GAD1⁺; light grey, rabies⁺/GAD1⁻). **i**, Example picture of glutamatergic vIPAG neurons retrogradely traced from the Mc, expressing Chr2 in presence of Cre and Flp recombinase (scale bar, 200 μ m). **j**, Analysis of viral efficacy and leakiness. Overlaps of Chr2 delivered by AAV-Cre^{ON}Flp^{ON}-Chr2, HSV-delivered Cre-dependent Flp-mCherry and Cre-dependent β -Gal were quantified in *Vglut2::LacZ* reporter mice. **k**, Fibre placement in *Vglut2-ires-Cre* mice expressing Chr2 in glutamatergic vIPAG-to-Mc projection neurons. **l**, Example of an entire session of light activation of glutamatergic vIPAG-to-Mc projection neurons, with the mouse's motion, cumulative track length and light-induced freezing bouts. Values are means \pm s.e.m.



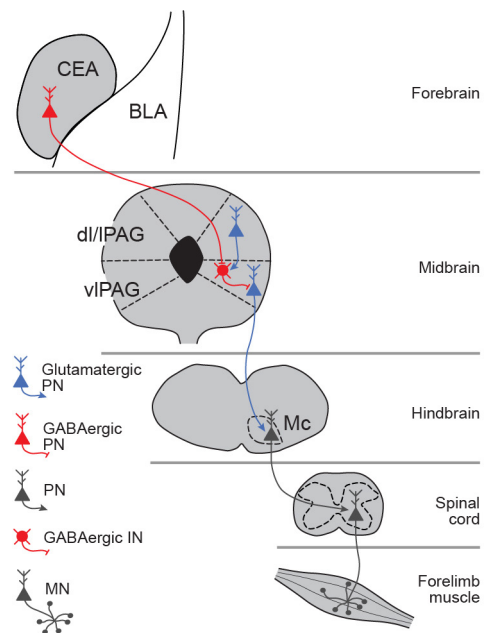
g

Target site	Target cell type	Number of mice	Number of starter cells	Number of presynaptic cells							
				CEA	DM	AHM	VMH	PH	PLH	LH	PMD
dl/IPAG	vGluT2+	3	509 ±154	5 ±3	30 ±14.6	53.33 ±28.7	86.67 ±35.3	71.33 ±30.7	60 ±26.9	77 ±33.1	251.7 ±77.4
vIPAG	vGluT2+	3	695 ±135	58 ±27	12.67 ±7.3	38 ±9.5	11.67 ±2.7	36.33 ±5.8	83 ±19.9	81.67 ±17.9	6.333 ±1.7
vIPAG	GAD2+	4	265 ±105	94.3* ±53.2	3.7 ±2.8	7 ±3.7	1.5 ±0.9	3.75 ±3.1	20.75 ±7.4	22.25 ±9.5	6.25 ±3.1

*one outlier (=271) was removed (Grubb's test, alpha = 0.01)

Extended Data Figure 5 | a, Expression of Chr2 throughout PAG in consecutive coronal brain sections (left), and fibre placements in *Vglut2-ires-Cre* mice of experimental and control groups (right). **b**, Light-evoked effect on freezing behaviour induced by activation of different glutamatergic subpopulations of PAG neurons in naive animals ($n = 12$ PAG, $n = 10$ vIPAG, $n = 7$ vIPAG-to-Mc, Kruskal–Wallis test, $P < 0.001$, Dunn's multiple comparison post-hoc test). **c**, EnvA-ΔG-mCherry-rabies-mediated, Cre-dependent monosynaptic retrograde tracing of inputs to GAD2+ and vGluT2+ neurons in the vIPAG and dl/IPAG. **d**, Rabies-mediated labelling of presynaptic neurons within PMD (left panels) and CEA (right panels) of *Gad2-ires-Cre* and *Vglut2-ires-Cre* mice (scale bar, 100 μm). **e**, Statistical analysis reveals differential input to vGluT2+ ($n = 3$

mice for each vIPAG and dl/IPAG) and GAD2+ ($n = 4$ mice) neurons within vIPAG or dl/IPAG. While CEA preferentially targets GAD2+ neurons of the vIPAG (1×3 ANOVA, $F_{(2,6)} = 21.67$, $P < 0.01$, Tukey's post-hoc test), vGluT2+ neurons of the dl/IPAG receive stronger inputs from PMD (1×3 ANOVA, $F_{(2,7)} = 287$, $P < 0.0001$, Tukey's post-hoc test). **f**, Cell-type-specific monosynaptic rabies tracing of VMH and LH inputs to vGluT2+ neurons in the dl/IPAG, vIPAG and vIPAG GAD2+ neurons (scale bars in overview, 200 μm; in zoom-in, 25 μm). **g**, Quantification of starter cells in the PAG and presynaptic cells in CEA and hypothalamic subregions. Boxes indicate median and 25th–75th percentiles of the distribution. ** $P < 0.01$; *** $P < 0.001$.



Extended Data Figure 6 | Schematic representation of the freezing pathway. PN, projection neuron; IN, interneuron; MN, motor neuron.

General discussion:

The identification of circuit elements and mechanisms controlling neuronal activity during learning and memory formation represent one of the most labored challenges in neuroscience research. More importantly, one of the main questions still unanswered is related to the mechanisms allowing the long-range synchronization between distant neuronal structures to produce consistent and adapted fear behavioural output and the precise underlying neuronal circuits. By combining single unit and local field potential recordings, pharmacological and optogenetic manipulations in behaving mice submitted to classical auditory fear conditioning, we addressed these questions and identified novel neuronal mechanisms and functional circuits involved in the expression of conditioned fear behaviour. First, we observed that the expression of conditioned fear memories is associated with synchronous 4 Hz oscillations in dmPFC-BLA circuits. This oscillation allowed the synchronization of dmPFC and BLA firing activities during expression of fear behaviour. Secondly, we discovered a novel functional pathway from the dmPFC to the vIPAG that regulates conditioned fear behaviour expression while bypassing BLA circuits. Finally, using state of the art transsynaptic rabies tracing, electrophysiology and optogenetics methodologies we unraveled functional pathways at the level of the midbrain driving innate and conditioned fear responses. Nevertheless, the work performed during the time course of this doctoral thesis also raises important unanswered questions we will discuss below.

During the time frame of this doctoral thesis, we first demonstrated the existence of an internally generated 4 Hz neuronal oscillation within the dmPFC and BLA circuits. This oscillation was sufficient to drive the synchronization of neuronal activity between PFC and BLA circuits during fear behaviour. We demonstrated that the emergence of 4 Hz oscillations determine the dynamics of conditioned fear responses as we could predict the initiation, length and termination of freezing episodes. Although our results suggest that 4 Hz oscillations synchronized dmPFC neurons projecting to the BLA, this was not formally demonstrated. Because the dmPFC is composed of heterogeneous PNs populations with different output patterns as a function of their localization in specific dmPFC layers, it will be important in the future to precisely identify which dmPFC PNs are phase locked to 4 Hz oscillations. For instance, dmPFC-BLA and dmPFC-vIPAG projecting PNs are located in superficial and deep layers, respectively (Ferreira et al., 2015, Harris and Shepherd, 2015) and could be differentially locked

to 4 Hz oscillations. Also, it is still not clear whether different fear responses such as freezing and avoidance behaviour would rely on similar synchronization mechanisms. It is conceivable, that the activation of dmPFC PNs differentially phase locked to 4 Hz oscillations or to different oscillatory band will result in the selection of different behavioural outputs, which would represent an efficient way of encoding opposite fear responses.

In this first study we also demonstrated that 4 Hz oscillations are distinct from the CS⁺-evoked theta resetting observed in previous studies (Livneh and Paz, 2012, Courtin et al., 2014, Likhtik et al., 2014). In fact, these studies demonstrated transient sensory-evoked theta oscillations (8-12Hz) in dmPFC that have been link to sensory-driven process during fear behaviour or discrimination. In comparison, we demonstrate that the 4 Hz oscillation was long lasting (dependent of the length of freezing behaviour) and observed during freezing periods initiated during or outside CS presentations. This implies that 4 Hz oscillations are internally generated and not driven by sensory stimulation. To our knowledge, this study was the first causal demonstration, that a sustained brain state is involved in the initiation and maintenance of freezing behaviour. Furthermore, we also demonstrated in this study that the stationary 4 Hz oscillation is not hippocampus dependent as revealed by medial septum inactivation experiments. However, it is still unclear what is the origin of this 4 Hz oscillation. Several data suggest that it could be generated in the olfactory bulb or the VTA (Fujisawa and Buzsaki, 2011, Ito et al., 2014), two hypotheses that remain to be formally demonstrated.

In addition to the involvement of 4Hz oscillation in the expression of fear responses we demonstrated that this oscillation appears during the conditioning session after few CS-US pairings. Moreover, the artificial induction of dmPFC 4 Hz oscillations induced long-lasting fear memories. This suggests that the artificial induction of dmPFC 4 Hz oscillations might be involved in the formation of associative fear memories. Another possibility could be that this artificial induction of 4 Hz oscillations leads to nonspecific anxiety behaviour. However, it is unlikely that a sudden inactivation or rhythmic inhibition of prefrontal areas could promote nonspecific anxiety behaviour for at least two reasons. Optogenetic inactivation of the cingulate cortex during remote contextual memory retrieval results in a reduction of contextual fear behaviour (Goshen et al., 2011), an observation not consistent with a general increase in anxiety levels. Furthermore, in our optogenetic experiments, dmPFC 4-Hz induction give rise to freezing in a context-specific manner, which is also inconsistent with a general increase in anxiety. It is

reasonable to think that the artificial induction of dmPFC 4 Hz oscillations promotes an aversive state in the context in which the stimulation was performed thereby promoting the formation of contextual associative fear memories. In this sense the artificial induction of 4 Hz oscillations will act as a US and lead to long-lasting contextual fear memories as observed in our study. Finally, all together, our data related to this first set of study strongly suggest that 4 Hz oscillations represent a physiological signature of freezing behaviour as it determines the temporal frame of freezing episodes. Importantly, although we demonstrated that 60 % of dmPFC PNs were phase locked to 4 Hz oscillations we did not identify in this study the precise firing patterns of these neurons nor their specific targets in the brain. We attempted to address these questions in the second project of this doctoral thesis.

In the second project of this thesis, we performed extensive recordings of dmPFC PNs during auditory fear conditioning and we separated putative PNs into three neuronal populations based on their firing patterns during freezing episodes following fear conditioning. The first subpopulation (10 % of the neurons recorded) showed an increase in neuronal activity during the entire length of freezing episodes, the second (13 % of the neurons recorded) exhibited an inhibition of activity during freezing behaviour whereas the third subpopulation (77% of neurons recorded) showed no evidence of activity variation during freezing episodes. The opposite firing pattern of the two first subpopulations of dmPFC PNs during freezing episodes is interesting as it may suggest that these two populations encode differentially freezing episodes. Alternatively, these two neuronal populations may correspond to neurons encoding two antagonist behavioural fear responses such as freezing and avoidance as recently suggested (Corcoran and Quirk, 2007, Martinez et al., 2013, Bravo-Rivera et al., 2015, Dejean et al., 2015, Tovote et al., 2015). Because in our behavioural paradigm the expected fear response is freezing behaviour, neurons encoding avoidance would be inhibited to allow the expression of freezing behaviour. Functionally, the strong inhibitory pattern observed in the second populations of neurons will result in less excitation at the level of projection region, which is somehow inconsistent with the fact that the initiation of the motor freezing response depends on the activation of neurons in both the CEM and PAG (Bandler and Carrive, 1988, Ciochi et al., 2010). Based on these elements, it is likely that the first, but not the second population of dmPFC PNs directly encode freezing behaviour. Furthermore, the mechanisms by which these two populations are activated or inhibited remain to

be identified and could involve long-range excitatory inputs, local inhibitory circuits or a disinhibitory mechanisms. In term of connectivity we demonstrated that dmPFC-vIPAG neurons that correspond to the activated population during freezing behaviour are contacted by SST and PV INs equivalently. Interestingly we demonstrated that the pattern of activity of a large proportion of the SST and PV INs during freezing episodes correspond to a sustained inhibition. This suggests a cooperative contribution of these two subtypes to disinhibit dmPFC-vIPAG neurons, although a direct sustained excitation of this neuronal pool is also possible. These results indicate that during freezing behaviour dmPFC-vIPAG PNs receive both a dendritic and perisomatic inhibition mediated by SST and PV INs. Such changes can affect dendritic spiking and therefore the parameters essential to neuronal integration such as excitability and plasticity (Gentet et al., 2012, Gidon and Segev, 2012, Roux and Buzsaki, 2015). Furthermore, preliminary optogenetics activation of SST INs during fear behaviour or optogenetics inhibition of dmPFC-vIPAG PNs induced a decrease of freezing behaviour demonstrating that the inhibition of SST INs or the activation of dmPFC-vIPAG projecting PNs is necessary to drive freezing behaviour. It is important to notice, that although the decrease of freezing induced during optogenetics experiment is significant, it is only partial, which suggested that other pathways are recruited during conditioned fear expression. In collaboration with the group of Andreas Lüthi, we demonstrated, in fact, that CEm neurons project to GABAergic cells in the vIPAG and induced a disinhibition of VGLUT2-expressing neurons projecting to the rostro-ventral medulla. Our preliminary data suggest that dmPFC-vIPAG projecting neurons preferentially contact VGLUT2-expressing neurons in the vIPAG, although we don't know if these VGLUT2-expressing neurons project to the rostro-ventral medulla. Thus an appealing hypothesis would be that the initiation of freezing behaviour in the vIPAG relies on the cooperation between a direct excitatory pathway emanating from the dmPFC and a disinhibitory pathway originating from the CEm that will result in a strong activation of VGLUT2-expressing neurons projecting to the rostro-ventral medulla (**Figure 25**).

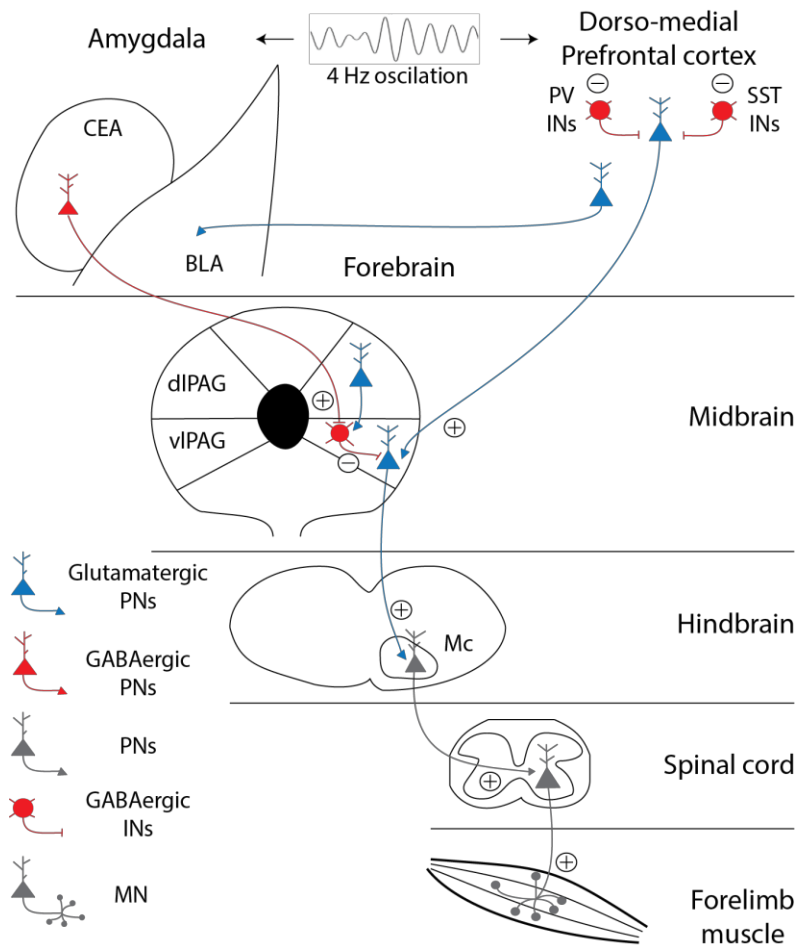


Figure 25: Schematic representation of the neuronal circuits involved in the expression of conditioned fear behaviour. An appealing hypothesis would be that the initiation of freezing behaviour in the vIPAG relies on the cooperation between a direct excitatory pathway emanating from the dmPFC and a disinhibitory pathway originating from the CEM. PNs, projection neurons; INs, interneurons; MN, motor neuron; CEA, centram amygdala; BLA, Basolateral amygdala; PV, parvalbumin; SST, somatostatin; dIPAG, dorsolateral periaqueductal gray; vIPAG, ventrolateral periaqueductal gray; Mc, Magnocellular nucleus.

We are currently evaluating this interesting hypothesis by using an intersectional optogenetic strategy in order to manipulate both pathways during fear behaviour. Furthermore, in the collaborative work with the group of Andreas Lüthi we demonstrated a direct interaction between the flight responses evoked after stimulation of glutamatergic neurons in the dIPAG with the freezing response evoked after stimulation of glutamatergic in the vIPAG. In the future, it would be very interesting to understand how these two regions are regulated by higher cortical areas, and integrate the different inputs to drive passive or active fear responses. A mechanistic functional understanding of these circuits will provide new insights into possible mechanisms underlying human psychiatric conditions associated with maladaptive coping behaviours under stressful conditions.

Publications and communications:

Publications

Courtin J, **Chaudun F**, Rozeske, RR, Karalis, N, Gonzalez-Campo C, Wurtz H, Abdi A, Baufreton J, Bienvenu TCM, and Herry C. (2014) Prefrontal parvalbumin interneurons shape neuronal activity to drive fear expression. *Nature*, 505, 92-96. **IF: 41.456.**

Rozeske RR, Valerio S, **Chaudun F**, Herry C. (2014) Prefrontal neuronal circuits of contextual fear conditioning. *Genes Brain Behav.* **IF: 3.661.**

Karalis N*, Dejean C*, **Chaudun F***, Khoder S, Rozeske RR, Wurtz H, Bagur S, Benchenane K, Sirota, Courtin J and Herry C. (2016) 4-Hz oscillations synchronize prefrontal-amygdala circuits during fear behavior. *Nature Neuroscience*, 19, 605-612. **IF: 16.095. * equal contribution**

Tovote P, Esposito MS, Botta P, **Chaudun F**, Fadok JP, Markovic M, Wolff SB, Ramakrishnan C, Fenno L, Deisseroth K, Herry C, Arber S and Luthi A. (2016) Midbrain circuits for defensive behaviour. *Nature*, 534:206-12. **IF: 41.456.**

Dejean C, Courtin J, Karalis N, **Chaudun F**, Wurtz H, Bienvenu TC and Herry C. Prefrontal neuronal assemblies temporally control fear behaviour (2016). *Nature*, doi 10.1038. **IF : 41.456.**

Posters

Chaudun, F., Courtin, J., Wurtz, H. and Herry, C. Distinct pathway-specific prefrontal projection neurons control fear expression. French Society for Neurosciences, Lyon, France, May 2013.

Chaudun, F., Courtin, J., Wurtz, H. and Herry, C. Distinct pathway-specific prefrontal projection neurons differentially control fear expression. Magendie center seminary, Bordeaux, France, October 2013.

Chaudun, F., Courtin, J., Dejean, C., Rozeske, R.R., Valerio, S., Wurtz, H. and Herry, C. Prefrontal-ventral periaqueductal gray pathway regulates fear behaviour. Fens meeting, Milan, Italia, June 2014.

Chaudun, F., Dejean, C., Bagur, S., Rozeske, R.R., Valerio, S., Wurtz, H., Courtin, J. and Herry, C. Prefrontal-ventral periaqueductal gray pathway regulates fear behaviour. Amygdala in Health & Disease, Gordon Research Conference, Easton MA, United states, July 2015. **Price poster award.**

Chaudun, F., Bagur, S., Dejean, C., Chadney O., Rozeske, R.R., Wurtz, H., Courtin, J. and Herry, C. Prefrontal-ventral periaqueductal gray pathway regulates fear behaviour. Fens meeting, Copenhagen, Denmark, July 2016.

References:

Adesnik H, Scanziani M (2010) Lateral competition for cortical space by layer-specific horizontal circuits. *Nature* 464:1155-1160.

Adhikari A, Lerner TN, Finkelstein J, Pak S, Jennings JH, Davidson TJ, Ferenczi E, Gunaydin LA, Mirzabekov JJ, Ye L, Kim SY, Lei A, Deisseroth K (2015) Basomedial amygdala mediates top-down control of anxiety and fear. *Nature* 527:179-185.

Adhikari A, Topiwala MA, Gordon JA (2010) Synchronized activity between the ventral hippocampus and the medial prefrontal cortex during anxiety. *Neuron* 65:257-269.

Adhikari A, Topiwala MA, Gordon JA (2011) Single units in the medial prefrontal cortex with anxiety-related firing patterns are preferentially influenced by ventral hippocampal activity. *Neuron* 71:898-910.

Adolphs R, Tranel D, Damasio H, Damasio A (1994) Impaired recognition of emotion in facial expressions following bilateral damage to the human amygdala. *Nature* 372:669-672.

Akirav I, Raizel H, Maroun M (2006) Enhancement of conditioned fear extinction by infusion of the GABA(A) agonist muscimol into the rat prefrontal cortex and amygdala. *The European journal of neuroscience* 23:758-764.

Alheid GF (2003) Extended amygdala and basal forebrain. *Annals of the New York Academy of Sciences* 985:185-205.

- Allen K, Monyer H (2015) Interneuron control of hippocampal oscillations. *Current opinion in neurobiology* 31:81-87.
- Amano T, Duvarci S, Popa D, Pare D (2011) The fear circuit revisited: contributions of the basal amygdala nuclei to conditioned fear. *The Journal of neuroscience : the official journal of the Society for Neuroscience* 31:15481-15489.
- Amaral DG, Insausti R (1992) Retrograde transport of D-[3H]-aspartate injected into the monkey amygdaloid complex. *Experimental brain research* 88:375-388.
- Amir A, Amano T, Pare D (2011) Physiological identification and infralimbic responsiveness of rat intercalated amygdala neurons. *Journal of neurophysiology* 105:3054-3066.
- An B, Hong I, Choi S (2012) Long-term neural correlates of reversible fear learning in the lateral amygdala. *The Journal of neuroscience : the official journal of the Society for Neuroscience* 32:16845-16856.
- Anglada-Figueroa D, Quirk GJ (2005) Lesions of the basal amygdala block expression of conditioned fear but not extinction. *The Journal of neuroscience : the official journal of the Society for Neuroscience* 25:9680-9685.
- Ascoli GA, Alonso-Nanclares L, Anderson SA, Barrionuevo G, Benavides-Piccione R, Burkhalter A, Buzsaki G, Cauli B, Defelipe J, Fairen A, Feldmeyer D, Fishell G, Fregnac Y, Freund TF, Gardner D, Gardner EP, Goldberg JH, Helmstaedter M, Hestrin S, Karube F, Kisvarday ZF, Lambolez B, Lewis DA, Marin O, Markram H, Munoz A, Packer A, Petersen CC, Rockland KS, Rossier J, Rudy B, Somogyi P, Staiger JF, Tamas G, Thomson AM, Toledo-Rodriguez M, Wang Y, West DC, Yuste R (2008) Petilla terminology: nomenclature of features of GABAergic interneurons of the cerebral cortex. *Nature reviews Neuroscience* 9:557-568.
- Bandler R (1982) Induction of 'rage' following microinjections of glutamate into midbrain but not hypothalamus of cats. *Neuroscience letters* 30:183-188.
- Bandler R, Carrive P (1988) Integrated defence reaction elicited by excitatory amino acid microinjection in the midbrain periaqueductal grey region of the unrestrained cat. *Brain research* 439:95-106.
- Bandler R, Carrive P, Zhang SP (1991) Integration of somatic and autonomic reactions within the midbrain periaqueductal grey: viscerotopic, somatotopic and functional organization. *Progress in brain research* 87:269-305.
- Bandler R, Keay KA (1996) Columnar organization in the midbrain periaqueductal gray and the integration of emotional expression. *Progress in brain research* 107:285-300.
- Bandler R, Keay KA, Floyd N, Price J (2000) Central circuits mediating patterned autonomic activity during active vs. passive emotional coping. *Brain research bulletin* 53:95-104.
- Bandler R, Shipley MT (1994) Columnar organization in the midbrain periaqueductal gray: modules for emotional expression? *Trends in neurosciences* 17:379-389.

- Bandler R, Tork I (1987) Midbrain periaqueductal grey region in the cat has afferent and efferent connections with solitary tract nuclei. *Neuroscience letters* 74:1-6.
- Barrett D, Shumake J, Jones D, Gonzalez-Lima F (2003) Metabolic mapping of mouse brain activity after extinction of a conditioned emotional response. *The Journal of neuroscience : the official journal of the Society for Neuroscience* 23:5740-5749.
- Basbaum AI, Fields HL (1984) Endogenous pain control systems: brainstem spinal pathways and endorphin circuitry. *Annual review of neuroscience* 7:309-338.
- Bauer EP, Schafe GE, LeDoux JE (2002) NMDA receptors and L-type voltage-gated calcium channels contribute to long-term potentiation and different components of fear memory formation in the lateral amygdala. *The Journal of neuroscience : the official journal of the Society for Neuroscience* 22:5239-5249.
- Beck CH, Fibiger HC (1995) Conditioned fear-induced changes in behavior and in the expression of the immediate early gene c-fos: with and without diazepam pretreatment. *The Journal of neuroscience : the official journal of the Society for Neuroscience* 15:709-720.
- Behbehani MM (1995) Functional characteristics of the midbrain periaqueductal gray. *Progress in neurobiology* 46:575-605.
- Beitz AJ (1985) The midbrain periaqueductal gray in the rat. I. Nuclear volume, cell number, density, orientation, and regional subdivisions. *The Journal of comparative neurology* 237:445-459.
- Beitz AJ, Shepard RD (1985) The midbrain periaqueductal gray in the rat. II. A Golgi analysis. *The Journal of comparative neurology* 237:460-475.
- Benchenane K, Peyrache A, Khamassi M, Tierney PL, Gioanni Y, Battaglia FP, Wiener SI (2010) Coherent theta oscillations and reorganization of spike timing in the hippocampal- prefrontal network upon learning. *Neuron* 66:921-936.
- Bergado-Acosta JR, Sangha S, Narayanan RT, Obata K, Pape HC, Stork O (2008) Critical role of the 65-kDa isoform of glutamic acid decarboxylase in consolidation and generalization of Pavlovian fear memory. *Learn Mem* 15:163-171.
- Bernard JF, Bandler R (1998) Parallel circuits for emotional coping behaviour: new pieces in the puzzle. *The Journal of comparative neurology* 401:429-436.
- Berretta S, Pantazopoulos H, Caldera M, Pantazopoulos P, Pare D (2005) Infralimbic cortex activation increases c-Fos expression in intercalated neurons of the amygdala. *Neuroscience* 132:943-953.
- Besson JM, Chaouch A (1987) Peripheral and spinal mechanisms of nociception. *Physiological reviews* 67:67-186.
- Bissiere S, Humeau Y, Luthi A (2003) Dopamine gates LTP induction in lateral amygdala by suppressing feedforward inhibition. *Nature neuroscience* 6:587-592.

- Bissiere S, Plachta N, Hoyer D, McAllister KH, Olpe HR, Grace AA, Cryan JF (2008) The rostral anterior cingulate cortex modulates the efficiency of amygdala-dependent fear learning. *Biological psychiatry* 63:821-831.
- Botta P, Demmou L, Kasugai Y, Markovic M, Xu C, Fadok JP, Lu T, Poe MM, Xu L, Cook JM, Rudolph U, Sah P, Ferraguti F, Luthi A (2015) Regulating anxiety with extrasynaptic inhibition. *Nature neuroscience* 18:1493-1500.
- Bouton ME, Garcia-Gutierrez A, Zilski J, Moody EW (2006) Extinction in multiple contexts does not necessarily make extinction less vulnerable to relapse. *Behaviour research and therapy* 44:983-994.
- Bowman BR, Kumar NN, Hassan SF, McMullan S, Goodchild AK (2013) Brain sources of inhibitory input to the rat rostral ventrolateral medulla. *The Journal of comparative neurology* 521:213-232.
- Brandao ML, de Aguiar JC, Graeff FG (1982) GABA mediation of the anti-aversive action of minor tranquilizers. *Pharmacology, biochemistry, and behavior* 16:397-402.
- Bravo-Rivera C, Roman-Ortiz C, Montesinos-Cartagena M, Quirk GJ (2015) Persistent active avoidance correlates with activity in prelimbic cortex and ventral striatum. *Frontiers in behavioral neuroscience* 9:184.
- Brooks DC, Bouton ME (1993) A retrieval cue for extinction attenuates spontaneous recovery. *Journal of experimental psychology Animal behavior processes* 19:77-89.
- Burgos-Robles A, Vidal-Gonzalez I, Quirk GJ (2009) Sustained conditioned responses in prelimbic prefrontal neurons are correlated with fear expression and extinction failure. *The Journal of neuroscience : the official journal of the Society for Neuroscience* 29:8474-8482.
- Burgos-Robles A, Vidal-Gonzalez I, Santini E, Quirk GJ (2007) Consolidation of fear extinction requires NMDA receptor-dependent bursting in the ventromedial prefrontal cortex. *Neuron* 53:871-880.
- Butler RK, Finn DP (2009) Stress-induced analgesia. *Progress in neurobiology* 88:184-202.
- Buzsaki G, Anastassiou CA, Koch C (2012) The origin of extracellular fields and currents--EEG, ECoG, LFP and spikes. *Nature reviews Neuroscience* 13:407-420.
- Buzsaki G, Chrobak JJ (1995) Temporal structure in spatially organized neuronal ensembles: a role for interneuronal networks. *Current opinion in neurobiology* 5:504-510.
- Buzsaki G, Draguhn A (2004) Neuronal oscillations in cortical networks. *Science* 304:1926-1929.
- Campeau S, Davis M (1995a) Involvement of subcortical and cortical afferents to the lateral nucleus of the amygdala in fear conditioning measured with fear-potentiated startle in rats trained concurrently with auditory and visual conditioned stimuli. *The Journal of neuroscience : the official journal of the Society for Neuroscience* 15:2312-2327.
- Campeau S, Davis M (1995b) Involvement of the central nucleus and basolateral complex of the amygdala in fear conditioning measured with fear-potentiated startle in rats trained

- concurrently with auditory and visual conditioned stimuli. *The Journal of neuroscience : the official journal of the Society for Neuroscience* 15:2301-2311.
- Canteras NS, Goto M (1999) Fos-like immunoreactivity in the periaqueductal gray of rats exposed to a natural predator. *Neuroreport* 10:413-418.
- Canteras NS, Graeff FG (2014) Executive and modulatory neural circuits of defensive reactions: implications for panic disorder. *Neuroscience and biobehavioral reviews* 46 Pt 3:352-364.
- Canteras NS, Simerly RB, Swanson LW (1994) Organization of projections from the ventromedial nucleus of the hypothalamus: a Phaseolus vulgaris-leucoagglutinin study in the rat. *The Journal of comparative neurology* 348:41-79.
- Canteras NS, Swanson LW (1992a) The dorsal premammillary nucleus: an unusual component of the mammillary body. *Proceedings of the National Academy of Sciences of the United States of America* 89:10089-10093.
- Canteras NS, Swanson LW (1992b) Projections of the ventral subiculum to the amygdala, septum, and hypothalamus: a PHAL anterograde tract-tracing study in the rat. *The Journal of comparative neurology* 324:180-194.
- Capogna M (2014) GABAergic cell type diversity in the basolateral amygdala. *Current opinion in neurobiology* 26:110-116.
- Carlsen J (1988) Immunocytochemical localization of glutamate decarboxylase in the rat basolateral amygdaloid nucleus, with special reference to GABAergic innervation of amygdalostriatal projection neurons. *The Journal of comparative neurology* 273:513-526.
- Carrive P (1993) The periaqueductal gray and defensive behavior: functional representation and neuronal organization. *Behavioural brain research* 58:27-47.
- Carrive P, Bandler R (1991) Viscerotopic organization of neurons subserving hypotensive reactions within the midbrain periaqueductal grey: a correlative functional and anatomical study. *Brain research* 541:206-215.
- Carrive P, Bandler R, Dampney RA (1989) Somatic and autonomic integration in the midbrain of the unanesthetized decerebrate cat: a distinctive pattern evoked by excitation of neurones in the subtentorial portion of the midbrain periaqueductal grey. *Brain research* 483:251-258.
- Carrive P, Dampney RA, Bandler R (1987) Excitation of neurones in a restricted portion of the midbrain periaqueductal grey elicits both behavioural and cardiovascular components of the defence reaction in the unanaesthetised decerebrate cat. *Neuroscience letters* 81:273-278.
- Carrive P, Lee J, Su A (2000) Lidocaine blockade of amygdala output in fear-conditioned rats reduces Fos expression in the ventrolateral periaqueductal gray. *Neuroscience* 95:1071-1080.
- Carrive P, Leung P, Harris J, Paxinos G (1997) Conditioned fear to context is associated with increased Fos expression in the caudal ventrolateral region of the midbrain periaqueductal gray. *Neuroscience* 78:165-177.

- Cassell MD, Wright DJ (1986) Topography of projections from the medial prefrontal cortex to the amygdala in the rat. *Brain research bulletin* 17:321-333.
- Cenquizca LA, Swanson LW (2007) Spatial organization of direct hippocampal field CA1 axonal projections to the rest of the cerebral cortex. *Brain research reviews* 56:1-26.
- Cezario AF, Ribeiro-Barbosa ER, Baldo MV, Canteras NS (2008) Hypothalamic sites responding to predator threats--the role of the dorsal preammillary nucleus in unconditioned and conditioned antipredatory defensive behavior. *The European journal of neuroscience* 28:1003-1015.
- Chang CH, Maren S (2011) Medial prefrontal cortex activation facilitates re-extinction of fear in rats. *Learn Mem* 18:221-225.
- Chen LW, Rao ZR, Shi JW (1995) Catecholaminergic neurons in the nucleus tractus solitarius which send their axons to the midbrain periaqueductal gray express Fos protein after noxious stimulation of the stomach: a triple labeling study in the rat. *Neuroscience letters* 189:179-181.
- Ciocchi S, Herry C, Grenier F, Wolff SB, Letzkus JJ, Vlachos I, Ehrlich I, Sprengel R, Deisseroth K, Stadler MB, Muller C, Luthi A (2010) Encoding of conditioned fear in central amygdala inhibitory circuits. *Nature* 468:277-282.
- Cobb SR, Buhl EH, Halasy K, Paulsen O, Somogyi P (1995) Synchronization of neuronal activity in hippocampus by individual GABAergic interneurons. *Nature* 378:75-78.
- Comoli E, Ribeiro-Barbosa ER, Canteras NS (2003) Predatory hunting and exposure to a live predator induce opposite patterns of Fos immunoreactivity in the PAG. *Behavioural brain research* 138:17-28.
- Corcoran KA, Quirk GJ (2007) Activity in prelimbic cortex is necessary for the expression of learned, but not innate, fears. *The Journal of neuroscience : the official journal of the Society for Neuroscience* 27:840-844.
- Courtin J, Bienvenu TC, Einarsson EO, Herry C (2013) Medial prefrontal cortex neuronal circuits in fear behavior. *Neuroscience* 240:219-242.
- Courtin J, Chaudun F, Rozeske RR, Karalis N, Gonzalez-Campo C, Wurtz H, Abdi A, Baufreton J, Bienvenu TC, Herry C (2014) Prefrontal parvalbumin interneurons shape neuronal activity to drive fear expression. *Nature* 505:92-96.
- Cousens G, Otto T (1998) Both pre- and posttraining excitotoxic lesions of the basolateral amygdala abolish the expression of olfactory and contextual fear conditioning. *Behavioral neuroscience* 112:1092-1103.
- Crestani CC, Alves FH, Gomes FV, Resstel LB, Correa FM, Herman JP (2013) Mechanisms in the bed nucleus of the stria terminalis involved in control of autonomic and neuroendocrine functions: a review. *Current neuropharmacology* 11:141-159.
- Davis M (1992) The role of the amygdala in fear and anxiety. *Annual review of neuroscience* 15:353-375.

- Davis M, Rainnie D, Cassell M (1994) Neurotransmission in the rat amygdala related to fear and anxiety. *Trends in neurosciences* 17:208-214.
- Davis M, Whalen PJ (2001) The amygdala: vigilance and emotion. *Molecular psychiatry* 6:13-34.
- DeFelipe J, Farinas I (1992) The pyramidal neuron of the cerebral cortex: morphological and chemical characteristics of the synaptic inputs. *Progress in neurobiology* 39:563-607.
- Deisseroth K (2015) Optogenetics: 10 years of microbial opsins in neuroscience. *Nature neuroscience* 18:1213-1225.
- Dejean C, Courtin J, Rozeske RR, Bonnet MC, Dousset V, Michelet T, Herry C (2015) Neuronal Circuits for Fear Expression and Recovery: Recent Advances and Potential Therapeutic Strategies. *Biological psychiatry* 78:298-306.
- Depaulis A, Keay KA, Bandler R (1992) Longitudinal neuronal organization of defensive reactions in the midbrain periaqueductal gray region of the rat. *Experimental brain research* 90:307-318.
- Depaulis A, Keay KA, Bandler R (1994) Quiescence and hyporeactivity evoked by activation of cell bodies in the ventrolateral midbrain periaqueductal gray of the rat. *Experimental brain research* 99:75-83.
- Di Scala G, Mana MJ, Jacobs WJ, Phillips AG (1987) Evidence of Pavlovian conditioned fear following electrical stimulation of the periaqueductal grey in the rat. *Physiology & behavior* 40:55-63.
- Do-Monte FH, Quinones-Laracuente K, Quirk GJ (2015) A temporal shift in the circuits mediating retrieval of fear memory. *Nature* 519:460-463.
- Duvarci S, Pare D (2014) Amygdala microcircuits controlling learned fear. *Neuron* 82:966-980.
- Ehrlich I, Humeau Y, Grenier F, Ciochi S, Herry C, Luthi A (2009) Amygdala inhibitory circuits and the control of fear memory. *Neuron* 62:757-771.
- Einarsson EO, Nader K (2012) Involvement of the anterior cingulate cortex in formation, consolidation, and reconsolidation of recent and remote contextual fear memory. *Learn Mem* 19:449-452.
- Ekman P, Sorenson ER, Friesen WV (1969) Pan-cultural elements in facial displays of emotion. *Science* 164:86-88.
- Fanselow MS, Kim JJ (1994) Acquisition of contextual Pavlovian fear conditioning is blocked by application of an NMDA receptor antagonist D,L-2-amino-5-phosphonovaleric acid to the basolateral amygdala. *Behavioral neuroscience* 108:210-212.
- Fardin V, Oliveras JL, Besson JM (1984a) A reinvestigation of the analgesic effects induced by stimulation of the periaqueductal gray matter in the rat. I. The production of behavioral side effects together with analgesia. *Brain research* 306:105-123.
- Fardin V, Oliveras JL, Besson JM (1984b) A reinvestigation of the analgesic effects induced by stimulation of the periaqueductal gray matter in the rat. II. Differential characteristics of the analgesia induced by ventral and dorsal PAG stimulation. *Brain research* 306:125-139.

- Farinelli M, Deschaux O, Hugues S, Thevenet A, Garcia R (2006) Hippocampal train stimulation modulates recall of fear extinction independently of prefrontal cortex synaptic plasticity and lesions. *Learn Mem* 13:329-334.
- Fell J, Axmacher N (2011) The role of phase synchronization in memory processes. *Nature reviews Neuroscience* 12:105-118.
- Fernandez Espejo E (2003) Prefrontocortical dopamine loss in rats delays long-term extinction of contextual conditioned fear, and reduces social interaction without affecting short-term social interaction memory. *Neuropsychopharmacology : official publication of the American College of Neuropsychopharmacology* 28:490-498.
- Ferreira AN, Yousuf H, Dalton S, Sheets PL (2015) Highly differentiated cellular and circuit properties of infralimbic pyramidal neurons projecting to the periaqueductal gray and amygdala. *Frontiers in cellular neuroscience* 9:161.
- Fields HL, Heinricher MM, Mason P (1991) Neurotransmitters in nociceptive modulatory circuits. *Annual review of neuroscience* 14:219-245.
- Fitzgerald PJ, Whittle N, Flynn SM, Graybeal C, Pinard CR, Gunduz-Cinar O, Kravitz AV, Singewald N, Holmes A (2014) Prefrontal single-unit firing associated with deficient extinction in mice. *Neurobiology of learning and memory* 113:69-81.
- Floresco SB, Tse MT (2007) Dopaminergic regulation of inhibitory and excitatory transmission in the basolateral amygdala-prefrontal cortical pathway. *The Journal of neuroscience : the official journal of the Society for Neuroscience* 27:2045-2057.
- Floyd NS, Price JL, Ferry AT, Keay KA, Bandler R (2000) Orbitomedial prefrontal cortical projections to distinct longitudinal columns of the periaqueductal gray in the rat. *The Journal of comparative neurology* 422:556-578.
- Fourcaudot E, Gambino F, Humeau Y, Casassus G, Shaban H, Poulain B, Luthi A (2008) cAMP/PKA signaling and RIM1alpha mediate presynaptic LTP in the lateral amygdala. *Proceedings of the National Academy of Sciences of the United States of America* 105:15130-15135.
- Franklin KBJ, Paxinos G (1997) *The mouse brain in stereotaxic coordinates*. San Diego: Academic Press.
- Fryszak RJ, Neafsey EJ (1991) The effect of medial frontal cortex lesions on respiration, "freezing," and ultrasonic vocalizations during conditioned emotional responses in rats. *Cereb Cortex* 1:418-425.
- Fujisawa S, Buzsaki G (2011) A 4 Hz oscillation adaptively synchronizes prefrontal, VTA, and hippocampal activities. *Neuron* 72:153-165.
- Gabbott PL, Warner TA, Jays PR, Salway P, Busby SJ (2005) Prefrontal cortex in the rat: projections to subcortical autonomic, motor, and limbic centers. *The Journal of comparative neurology* 492:145-177.

- Gale GD, Anagnostaras SG, Godsil BP, Mitchell S, Nozawa T, Sage JR, Wiltgen B, Fanselow MS (2004) Role of the basolateral amygdala in the storage of fear memories across the adult lifetime of rats. *The Journal of neuroscience : the official journal of the Society for Neuroscience* 24:3810-3815.
- Garcia R, Chang CH, Maren S (2006) Electrolytic lesions of the medial prefrontal cortex do not interfere with long-term memory of extinction of conditioned fear. *Learn Mem* 13:14-17.
- Gentet LJ, Kremer Y, Taniguchi H, Huang ZJ, Staiger JF, Petersen CC (2012) Unique functional properties of somatostatin-expressing GABAergic neurons in mouse barrel cortex. *Nature neuroscience* 15:607-612.
- Gewirtz JC, Falls WA, Davis M (1997) Normal conditioned inhibition and extinction of freezing and fear-potentiated startle following electrolytic lesions of medial prefrontal cortex in rats. *Behavioral neuroscience* 111:712-726.
- Ghosh S, Chattarji S (2015) Neuronal encoding of the switch from specific to generalized fear. *Nature neuroscience* 18:112-120.
- Gidon A, Segev I (2012) Principles governing the operation of synaptic inhibition in dendrites. *Neuron* 75:330-341.
- Gonchar YA, Johnson PB, Weinberg RJ (1995) GABA-immunopositive neurons in rat neocortex with contralateral projections to S-I. *Brain research* 697:27-34.
- Goosens KA, Maren S (2001) Contextual and auditory fear conditioning are mediated by the lateral, basal, and central amygdaloid nuclei in rats. *Learn Mem* 8:148-155.
- Goshen I, Brodsky M, Prakash R, Wallace J, Gradinaru V, Ramakrishnan C, Deisseroth K (2011) Dynamics of retrieval strategies for remote memories. *Cell* 147:678-689.
- Groenewegen HJ (1988) Organization of the afferent connections of the mediodorsal thalamic nucleus in the rat, related to the mediodorsal-prefrontal topography. *Neuroscience* 24:379-431.
- Groenewegen HJ, Wright CI, Uylings HB (1997) The anatomical relationships of the prefrontal cortex with limbic structures and the basal ganglia. *J Psychopharmacol* 11:99-106.
- Grundemann J, Luthi A (2015) Ensemble coding in amygdala circuits for associative learning. *Current opinion in neurobiology* 35:200-206.
- Hall E (1972) The amygdala of the cat: a Golgi study. *Z Zellforsch Mikrosk Anat* 134:439-458.
- Hamilton BL (1973) Cytoarchitectural subdivisions of the periaqueductal gray matter in the cat. *The Journal of comparative neurology* 149:1-27.
- Harris KD, Shepherd GM (2015) The neocortical circuit: themes and variations. *Nature neuroscience* 18:170-181.
- Hart G, Harris JA, Westbrook RF (2009) Systemic or intra-amygdala injection of a benzodiazepine (midazolam) impairs extinction but spares re-extinction of conditioned fear responses. *Learn Mem* 16:53-61.

- Haubensak W, Kunwar PS, Cai H, Ciochi S, Wall NR, Ponnusamy R, Biag J, Dong HW, Deisseroth K, Callaway EM, Fanselow MS, Luthi A, Anderson DJ (2010) Genetic dissection of an amygdala microcircuit that gates conditioned fear. *Nature* 468:270-276.
- Heidbreder CA, Groenewegen HJ (2003) The medial prefrontal cortex in the rat: evidence for a dorso-ventral distinction based upon functional and anatomical characteristics. *Neuroscience and biobehavioral reviews* 27:555-579.
- Heinricher MM, Tavares I, Leith JL, Lumb BM (2009) Descending control of nociception: Specificity, recruitment and plasticity. *Brain research reviews* 60:214-225.
- Herbert H, Saper CB (1992) Organization of medullary adrenergic and noradrenergic projections to the periaqueductal gray matter in the rat. *The Journal of comparative neurology* 315:34-52.
- Herry C, Ciochi S, Senn V, Demmou L, Muller C, Luthi A (2008) Switching on and off fear by distinct neuronal circuits. *Nature* 454:600-606.
- Herry C, Ferraguti F, Singewald N, Letzkus JJ, Ehrlich I, Luthi A (2010) Neuronal circuits of fear extinction. *The European journal of neuroscience* 31:599-612.
- Herry C, Johansen JP (2014) Encoding of fear learning and memory in distributed neuronal circuits. *Nature neuroscience* 17:1644-1654.
- Herry C, Mons N (2004) Resistance to extinction is associated with impaired immediate early gene induction in medial prefrontal cortex and amygdala. *The European journal of neuroscience* 20:781-790.
- Herry C, Trifilieff P, Micheau J, Luthi A, Mons N (2006) Extinction of auditory fear conditioning requires MAPK/ERK activation in the basolateral amygdala. *The European journal of neuroscience* 24:261-269.
- Hilton SM, Redfern WS (1986) A search for brain stem cell groups integrating the defence reaction in the rat. *The Journal of physiology* 378:213-228.
- Holstege G (1992) The emotional motor system. *European journal of morphology* 30:67-79.
- Holstege G, Bandler R, Saper CB (1996) The emotional motor system. *Progress in brain research* 107:3-6.
- Hoover WB, Vertes RP (2007) Anatomical analysis of afferent projections to the medial prefrontal cortex in the rat. *Brain structure & function* 212:149-179.
- Hopkins DA, Holstege G (1978) Amygdaloid projections to the mesencephalon, pons and medulla oblongata in the cat. *Experimental brain research* 32:529-547.
- Huang YY, Kandel ER (1998) Postsynaptic induction and PKA-dependent expression of LTP in the lateral amygdala. *Neuron* 21:169-178.
- Hubel DH, Wiesel TN (1962) Receptive fields, binocular interaction and functional architecture in the cat's visual cortex. *The Journal of physiology* 160:106-154.

- Huber D, Veinante P, Stoop R (2005) Vasopressin and oxytocin excite distinct neuronal populations in the central amygdala. *Science* 308:245-248.
- Humeau Y, Herry C, Kemp N, Shaban H, Fourcaudot E, Bissiere S, Luthi A (2005) Dendritic spine heterogeneity determines afferent-specific Hebbian plasticity in the amygdala. *Neuron* 45:119-131.
- Humeau Y, Luthi A (2007) Dendritic calcium spikes induce bi-directional synaptic plasticity in the lateral amygdala. *Neuropharmacology* 52:234-243.
- Humeau Y, Shaban H, Bissiere S, Luthi A (2003) Presynaptic induction of heterosynaptic associative plasticity in the mammalian brain. *Nature* 426:841-845.
- Isaacson JS, Scanziani M (2011) How inhibition shapes cortical activity. *Neuron* 72:231-243.
- Ito J, Roy S, Liu Y, Cao Y, Fletcher M, Lu L, Boughter JD, Grun S, Heck DH (2014) Whisker barrel cortex delta oscillations and gamma power in the awake mouse are linked to respiration. *Nature communications* 5:3572.
- Izumi T, Inoue T, Kitaichi Y, Nakagawa S, Koyama T (2006) Target brain sites of the anxiolytic effect of citalopram, a selective serotonin reuptake inhibitor. *European journal of pharmacology* 534:129-132.
- Jay TM, Witter MP (1991) Distribution of hippocampal CA1 and subicular efferents in the prefrontal cortex of the rat studied by means of anterograde transport of Phaseolus vulgaris-leucoagglutinin. *The Journal of comparative neurology* 313:574-586.
- Johansen JP, Cain CK, Ostroff LE, LeDoux JE (2011) Molecular mechanisms of fear learning and memory. *Cell* 147:509-524.
- Johansen JP, Tarpley JW, LeDoux JE, Blair HT (2010) Neural substrates for expectation-modulated fear learning in the amygdala and periaqueductal gray. *Nature neuroscience* 13:979-986.
- Jolkkonen E, Pitkanen A (1998) Intrinsic connections of the rat amygdaloid complex: projections originating in the central nucleus. *The Journal of comparative neurology* 395:53-72.
- Jurgens U, Pratt R (1979) Role of the periaqueductal grey in vocal expression of emotion. *Brain research* 167:367-378.
- Karalis N, Dejean C, Chaudun F, Khoder S, Rozeske RR, Wurtz H, Bagur S, Benchenane K, Sirota A, Courtin J, Herry C (2016) 4-Hz oscillations synchronize prefrontal-amygdala circuits during fear behavior. *Nature neuroscience* 19:605-612.
- Keay KA, Bandler R (1992) Anatomical evidence for segregated input from the upper cervical spinal cord to functionally distinct regions of the periaqueductal gray region of the cat. *Neuroscience letters* 139:143-148.
- Keay KA, Bandler R (2001) Parallel circuits mediating distinct emotional coping reactions to different types of stress. *Neuroscience and biobehavioral reviews* 25:669-678.

- Keay KA, Feil K, Gordon BD, Herbert H, Bandler R (1997) Spinal afferents to functionally distinct periaqueductal gray columns in the rat: an anterograde and retrograde tracing study. *The Journal of comparative neurology* 385:207-229.
- Kempainen S, Pitkanen A (2000) Distribution of parvalbumin, calretinin, and calbindin-D(28k) immunoreactivity in the rat amygdaloid complex and colocalization with gamma-aminobutyric acid. *The Journal of comparative neurology* 426:441-467.
- Kim EJ, Horovitz O, Pellman BA, Tan LM, Li Q, Richter-Levin G, Kim JJ (2013) Dorsal periaqueductal gray-amygdala pathway conveys both innate and learned fear responses in rats. *Proceedings of the National Academy of Sciences of the United States of America* 110:14795-14800.
- Knapska E, Macias M, Mikosz M, Nowak A, Owczarek D, Wawrzyniak M, Pieprzyk M, Cymerman IA, Werka T, Sheng M, Maren S, Jaworski J, Kaczmarek L (2012) Functional anatomy of neural circuits regulating fear and extinction. *Proceedings of the National Academy of Sciences of the United States of America* 109:17093-17098.
- Knapska E, Maren S (2009) Reciprocal patterns of c-Fos expression in the medial prefrontal cortex and amygdala after extinction and renewal of conditioned fear. *Learn Mem* 16:486-493.
- Koikegami H (1963) Amygdala and other related limbic structures; experimental studies on the anatomy and function. I. Anatomical researches with some neurophysiological observations. *Acta medica et biologica* 10:161-277.
- Konorski J (1967) Integrative activity of the brain; an interdisciplinary approach. Chicago,: University of Chicago Press.
- Krettek JE, Price JL (1977) The cortical projections of the mediodorsal nucleus and adjacent thalamic nuclei in the rat. *The Journal of comparative neurology* 171:157-191.
- Kroner S, Rosenkranz JA, Grace AA, Barrionuevo G (2005) Dopamine modulates excitability of basolateral amygdala neurons in vitro. *Journal of neurophysiology* 93:1598-1610.
- Krout KE, Loewy AD (2000) Periaqueductal gray matter projections to midline and intralaminar thalamic nuclei of the rat. *The Journal of comparative neurology* 424:111-141.
- Kuroda M, Murakami K, Oda S, Shinkai M, Kishi K (1993) Direct synaptic connections between thalamocortical axon terminals from the mediodorsal thalamic nucleus (MD) and corticothalamic neurons to MD in the prefrontal cortex. *Brain research* 612:339-344.
- Kvitsiani D, Ranade S, Hangya B, Taniguchi H, Huang JZ, Kepecs A (2013) Distinct behavioural and network correlates of two interneuron types in prefrontal cortex. *Nature* 498:363-366.
- Lacroix L, Spinelli S, Heidbreder CA, Feldon J (2000) Differential role of the medial and lateral prefrontal cortices in fear and anxiety. *Behavioral neuroscience* 114:1119-1130.
- Lang EJ, Pare D (1997) Similar inhibitory processes dominate the responses of cat lateral amygdaloid projection neurons to their various afferents. *Journal of neurophysiology* 77:341-352.

- Laurent V, Westbrook RF (2009) Inactivation of the infralimbic but not the prelimbic cortex impairs consolidation and retrieval of fear extinction. *Learn Mem* 16:520-529.
- Laviolette SR, Lipski WJ, Grace AA (2005) A subpopulation of neurons in the medial prefrontal cortex encodes emotional learning with burst and frequency codes through a dopamine D4 receptor-dependent basolateral amygdala input. *The Journal of neuroscience : the official journal of the Society for Neuroscience* 25:6066-6075.
- Lebron K, Milad MR, Quirk GJ (2004) Delayed recall of fear extinction in rats with lesions of ventral medial prefrontal cortex. *Learn Mem* 11:544-548.
- LeDoux JE (2000) Emotion circuits in the brain. *Annual review of neuroscience* 23:155-184.
- LeDoux JE, Farb C, Ruggiero DA (1990) Topographic organization of neurons in the acoustic thalamus that project to the amygdala. *The Journal of neuroscience : the official journal of the Society for Neuroscience* 10:1043-1054.
- LeDoux JE, Farb CR (1991) Neurons of the acoustic thalamus that project to the amygdala contain glutamate. *Neuroscience letters* 134:145-149.
- Lee AT, Vogt D, Rubenstein JL, Sohal VS (2014) A class of GABAergic neurons in the prefrontal cortex sends long-range projections to the nucleus accumbens and elicits acute avoidance behavior. *The Journal of neuroscience : the official journal of the Society for Neuroscience* 34:11519-11525.
- Lee YK, Choi JS (2012) Inactivation of the medial prefrontal cortex interferes with the expression but not the acquisition of differential fear conditioning in rats. *Experimental neurobiology* 21:23-29.
- Lesting J, Narayanan RT, Kluge C, Sangha S, Seidenbecher T, Pape HC (2011) Patterns of coupled theta activity in amygdala-hippocampal-prefrontal cortical circuits during fear extinction. *PLoS one* 6:e21714.
- Letinic K, Zoncu R, Rakic P (2002) Origin of GABAergic neurons in the human neocortex. *Nature* 417:645-649.
- Letzkus JJ, Wolff SB, Meyer EM, Tovote P, Courtin J, Herry C, Luthi A (2011) A disinhibitory microcircuit for associative fear learning in the auditory cortex. *Nature* 480:331-335.
- Li C, Sugam JA, Lowery-Gionta EG, McElligott ZA, McCall NM, Lopez AJ, McKlveen JM, Pleil KE, Kash TL (2016) Mu Opioid Receptor Modulation of Dopamine Neurons in the Periaqueductal Gray/Dorsal Raphe: A Role in Regulation of Pain. *Neuropsychopharmacology : official publication of the American College of Neuropsychopharmacology* 41:2122-2132.
- Li H, Penzo MA, Taniguchi H, Kopec CD, Huang ZJ, Li B (2013) Experience-dependent modification of a central amygdala fear circuit. *Nature neuroscience* 16:332-339.
- Likhtik E, Paz R (2015) Amygdala-prefrontal interactions in (mal)adaptive learning. *Trends in neurosciences* 38:158-166.

- Likhtik E, Popa D, Apergis-Schoute J, Fidacaro GA, Pare D (2008) Amygdala intercalated neurons are required for expression of fear extinction. *Nature* 454:642-645.
- Likhtik E, Stujenske JM, Topiwala MA, Harris AZ, Gordon JA (2014) Prefrontal entrainment of amygdala activity signals safety in learned fear and innate anxiety. *Nature neuroscience* 17:106-113.
- Lin CH, Yeh SH, Lu HY, Gean PW (2003) The similarities and diversities of signal pathways leading to consolidation of conditioning and consolidation of extinction of fear memory. *The Journal of neuroscience : the official journal of the Society for Neuroscience* 23:8310-8317.
- Livneh U, Paz R (2012) Amygdala-prefrontal synchronization underlies resistance to extinction of aversive memories. *Neuron* 75:133-142.
- Loretan K, Bissiere S, Luthi A (2004) Dopaminergic modulation of spontaneous inhibitory network activity in the lateral amygdala. *Neuropharmacology* 47:631-639.
- Lovick TA (1993) The periaqueductal gray-rostral medulla connection in the defence reaction: efferent pathways and descending control mechanisms. *Behavioural brain research* 58:19-25.
- Lu KT, Walker DL, Davis M (2001) Mitogen-activated protein kinase cascade in the basolateral nucleus of amygdala is involved in extinction of fear-potentiated startle. *The Journal of neuroscience : the official journal of the Society for Neuroscience* 21:RC162.
- Luskin MB, Price JL (1983) The laminar distribution of intracortical fibers originating in the olfactory cortex of the rat. *The Journal of comparative neurology* 216:292-302.
- MacLeod K, Backer A, Laurent G (1998) Who reads temporal information contained across synchronized and oscillatory spike trains? *Nature* 395:693-698.
- Mahanty NK, Sah P (1998) Calcium-permeable AMPA receptors mediate long-term potentiation in interneurons in the amygdala. *Nature* 394:683-687.
- Mantyh PW (1982a) Forebrain projections to the periaqueductal gray in the monkey, with observations in the cat and rat. *The Journal of comparative neurology* 206:146-158.
- Mantyh PW (1982b) The midbrain periaqueductal gray in the rat, cat, and monkey: a Nissl, Weil, and Golgi analysis. *The Journal of comparative neurology* 204:349-363.
- Maren S (2001) Neurobiology of Pavlovian fear conditioning. *Annual review of neuroscience* 24:897-931.
- Maren S, Aharonov G, Fanselow MS (1996) Retrograde abolition of conditional fear after excitotoxic lesions in the basolateral amygdala of rats: absence of a temporal gradient. *Behavioral neuroscience* 110:718-726.
- Maren S, Quirk GJ (2004) Neuronal signalling of fear memory. *Nature reviews Neuroscience* 5:844-852.
- Maren S, Yap SA, Goosens KA (2001) The amygdala is essential for the development of neuronal plasticity in the medial geniculate nucleus during auditory fear conditioning in rats. *The Journal of neuroscience : the official journal of the Society for Neuroscience* 21:RC135.

- Markram H, Lubke J, Frotscher M, Sakmann B (1997) Regulation of synaptic efficacy by coincidence of postsynaptic APs and EPSPs. *Science* 275:213-215.
- Markram H, Toledo-Rodriguez M, Wang Y, Gupta A, Silberberg G, Wu C (2004) Interneurons of the neocortical inhibitory system. *Nature reviews Neuroscience* 5:793-807.
- Maroun M, Kavushansky A, Holmes A, Wellman C, Motanis H (2012) Enhanced extinction of aversive memories by high-frequency stimulation of the rat infralimbic cortex. *PloS one* 7:e35853.
- Martinez RC, Gupta N, Lazaro-Munoz G, Sears RM, Kim S, Moscarello JM, LeDoux JE, Cain CK (2013) Active vs. reactive threat responding is associated with differential c-Fos expression in specific regions of amygdala and prefrontal cortex. *Learn Mem* 20:446-452.
- Matyas F, Lee J, Shin HS, Acsady L (2014) The fear circuit of the mouse forebrain: connections between the mediodorsal thalamus, frontal cortices and basolateral amygdala. *The European journal of neuroscience* 39:1810-1823.
- McDonald AJ (1982a) Cytoarchitecture of the central amygdaloid nucleus of the rat. *The Journal of comparative neurology* 208:401-418.
- McDonald AJ (1982b) Neurons of the lateral and basolateral amygdaloid nuclei: a Golgi study in the rat. *The Journal of comparative neurology* 212:293-312.
- McDonald AJ (1985) Immunohistochemical identification of gamma-aminobutyric acid-containing neurons in the rat basolateral amygdala. *Neuroscience letters* 53:203-207.
- McDonald AJ (1991) Organization of amygdaloid projections to the prefrontal cortex and associated striatum in the rat. *Neuroscience* 44:1-14.
- McDonald AJ (1998) Cortical pathways to the mammalian amygdala. *Progress in neurobiology* 55:257-332.
- McDonald AJ, Mascagni F (2001) Colocalization of calcium-binding proteins and GABA in neurons of the rat basolateral amygdala. *Neuroscience* 105:681-693.
- McDonald AJ, Mascagni F, Guo L (1996) Projections of the medial and lateral prefrontal cortices to the amygdala: a Phaseolus vulgaris leucoagglutinin study in the rat. *Neuroscience* 71:55-75.
- McDonald AJ, Mascagni F, Zaric V (2012) Subpopulations of somatostatin-immunoreactive non-pyramidal neurons in the amygdala and adjacent external capsule project to the basal forebrain: evidence for the existence of GABAergic projection neurons in the cortical nuclei and basolateral nuclear complex. *Frontiers in neural circuits* 6:46.
- McDonald AJ, Zaric V (2015) GABAergic somatostatin-immunoreactive neurons in the amygdala project to the entorhinal cortex. *Neuroscience* 290:227-242.
- McKernan MG, Shinnick-Gallagher P (1997) Fear conditioning induces a lasting potentiation of synaptic currents in vitro. *Nature* 390:607-611.

- McNally GP (2005) Facilitation of fear extinction by midbrain periaqueductal gray infusions of RB101(S), an inhibitor of enkephalin-degrading enzymes. *Behavioral neuroscience* 119:1672-1677.
- McNally GP, Lee BW, Chiem JY, Choi EA (2005) The midbrain periaqueductal gray and fear extinction: opioid receptor subtype and roles of cyclic AMP, protein kinase A, and mitogen-activated protein kinase. *Behavioral neuroscience* 119:1023-1033.
- McNally GP, Pigg M, Weidemann G (2004) Opioid receptors in the midbrain periaqueductal gray regulate extinction of pavlovian fear conditioning. *The Journal of neuroscience : the official journal of the Society for Neuroscience* 24:6912-6919.
- McNally GP, Westbrook RF (2006) Predicting danger: the nature, consequences, and neural mechanisms of predictive fear learning. *Learn Mem* 13:245-253.
- Menetrey D, Chaouch A, Binder D, Besson JM (1982) The origin of the spinomesencephalic tract in the rat: an anatomical study using the retrograde transport of horseradish peroxidase. *The Journal of comparative neurology* 206:193-207.
- Meyer PJ, Morgan MM, Kozell LB, Ingram SL (2009) Contribution of dopamine receptors to periaqueductal gray-mediated antinociception. *Psychopharmacology* 204:531-540.
- Milad MR, Quirk GJ (2002) Neurons in medial prefrontal cortex signal memory for fear extinction. *Nature* 420:70-74.
- Milad MR, Vidal-Gonzalez I, Quirk GJ (2004) Electrical stimulation of medial prefrontal cortex reduces conditioned fear in a temporally specific manner. *Behavioral neuroscience* 118:389-394.
- Millhouse OE (1986) The intercalated cells of the amygdala. *The Journal of comparative neurology* 247:246-271.
- Miserendino MJ, Sananes CB, Melia KR, Davis M (1990) Blocking of acquisition but not expression of conditioned fear-potentiated startle by NMDA antagonists in the amygdala. *Nature* 345:716-718.
- Mitchell IJ, Dean P, Redgrave P (1988) The projection from superior colliculus to cuneiform area in the rat. II. Defence-like responses to stimulation with glutamate in cuneiform nucleus and surrounding structures. *Experimental brain research* 72:626-639.
- Morawska MM, Fendt M (2012) The effects of muscimol and AMN082 injections into the medial prefrontal cortex on the expression and extinction of conditioned fear in mice. *The Journal of experimental biology* 215:1394-1398.
- Morgan MA, LeDoux JE (1995) Differential contribution of dorsal and ventral medial prefrontal cortex to the acquisition and extinction of conditioned fear in rats. *Behavioral neuroscience* 109:681-688.
- Morgan MA, Romanski LM, LeDoux JE (1993) Extinction of emotional learning: contribution of medial prefrontal cortex. *Neuroscience letters* 163:109-113.
- Morgan MA, Schulkin J, LeDoux JE (2003) Ventral medial prefrontal cortex and emotional perseveration: the memory for prior extinction training. *Behavioural brain research* 146:121-130.

- Morgan MM, Sohn JH, Liebeskind JC (1989) Stimulation of the periaqueductal gray matter inhibits nociception at the supraspinal as well as spinal level. *Brain research* 502:61-66.
- Morrow BA, Elsworth JD, Inglis FM, Roth RH (1999a) An antisense oligonucleotide reverses the footshock-induced expression of fos in the rat medial prefrontal cortex and the subsequent expression of conditioned fear-induced immobility. *The Journal of neuroscience : the official journal of the Society for Neuroscience* 19:5666-5673.
- Morrow BA, Elsworth JD, Rasmusson AM, Roth RH (1999b) The role of mesoprefrontal dopamine neurons in the acquisition and expression of conditioned fear in the rat. *Neuroscience* 92:553-564.
- Motta SC, Goto M, Gouveia FV, Baldo MV, Canteras NS, Swanson LW (2009) Dissecting the brain's fear system reveals the hypothalamus is critical for responding in subordinate conspecific intruders. *Proceedings of the National Academy of Sciences of the United States of America* 106:4870-4875.
- Muller JF, Mascagni F, McDonald AJ (2006) Pyramidal cells of the rat basolateral amygdala: synaptology and innervation by parvalbumin-immunoreactive interneurons. *The Journal of comparative neurology* 494:635-650.
- Muller JF, Mascagni F, McDonald AJ (2007) Postsynaptic targets of somatostatin-containing interneurons in the rat basolateral amygdala. *The Journal of comparative neurology* 500:513-529.
- Myers KM, Davis M (2002) Behavioral and neural analysis of extinction. *Neuron* 36:567-584.
- Myers KM, Davis M (2007) Mechanisms of fear extinction. *Molecular psychiatry* 12:120-150.
- Narayanan V, Heiming RS, Jansen F, Lesting J, Sachser N, Pape HC, Seidenbecher T (2011) Social defeat: impact on fear extinction and amygdala-prefrontal cortical theta synchrony in 5-HTT deficient mice. *PloS one* 6:e22600.
- Neugebauer V, Li W, Bird GC, Han JS (2004) The amygdala and persistent pain. *The Neuroscientist : a review journal bringing neurobiology, neurology and psychiatry* 10:221-234.
- Nicolelis MA, Baccala LA, Lin RC, Chapin JK (1995) Sensorimotor encoding by synchronous neural ensemble activity at multiple levels of the somatosensory system. *Science* 268:1353-1358.
- Nieuwenhuys R (1994) The neocortex. An overview of its evolutionary development, structural organization and synaptology. *Anatomy and embryology* 190:307-337.
- Orsini CA, Kim JH, Knapska E, Maren S (2011) Hippocampal and prefrontal projections to the basal amygdala mediate contextual regulation of fear after extinction. *The Journal of neuroscience : the official journal of the Society for Neuroscience* 31:17269-17277.
- Pan BX, Ito W, Morozov A (2009) Divergence between thalamic and cortical inputs to lateral amygdala during juvenile-adult transition in mice. *Biological psychiatry* 66:964-971.

- Papez HC, Pare D (2010) Plastic synaptic networks of the amygdala for the acquisition, expression, and extinction of conditioned fear. *Physiological reviews* 90:419-463.
- Pare D, Collins DR (2000) Neuronal correlates of fear in the lateral amygdala: multiple extracellular recordings in conscious cats. *The Journal of neuroscience : the official journal of the Society for Neuroscience* 20:2701-2710.
- Pare D, Gaudreau H (1996) Projection cells and interneurons of the lateral and basolateral amygdala: distinct firing patterns and differential relation to theta and delta rhythms in conscious cats. *The Journal of neuroscience : the official journal of the Society for Neuroscience* 16:3334-3350.
- Pare D, Quirk GJ, LeDoux JE (2004) New vistas on amygdala networks in conditioned fear. *Journal of neurophysiology* 92:1-9.
- Pare D, Smith Y (1993) Distribution of GABA immunoreactivity in the amygdaloid complex of the cat. *Neuroscience* 57:1061-1076.
- Pascoe JP, Kapp BS (1985) Electrophysiological characteristics of amygdaloid central nucleus neurons during Pavlovian fear conditioning in the rabbit. *Behavioural brain research* 16:117-133.
- Pelletier JG, Pare D (2004) Role of amygdala oscillations in the consolidation of emotional memories. *Biological psychiatry* 55:559-562.
- Penzo MA, Robert V, Li B (2014) Fear conditioning potentiates synaptic transmission onto long-range projection neurons in the lateral subdivision of central amygdala. *The Journal of neuroscience : the official journal of the Society for Neuroscience* 34:2432-2437.
- Petrovich GD, Canteras NS, Swanson LW (2001) Combinatorial amygdalar inputs to hippocampal domains and hypothalamic behavior systems. *Brain research Brain research reviews* 38:247-289.
- Peyrache A, Khamassi M, Benchenane K, Wiener SI, Battaglia FP (2009) Replay of rule-learning related neural patterns in the prefrontal cortex during sleep. *Nature neuroscience* 12:919-926.
- Pitkanen A, Kempainen S (2002) Comparison of the distribution of calcium-binding proteins and intrinsic connectivity in the lateral nucleus of the rat, monkey, and human amygdala. *Pharmacology, biochemistry, and behavior* 71:369-377.
- Pitkanen A, Pikkarainen M, Nurminen N, Ylinen A (2000) Reciprocal connections between the amygdala and the hippocampal formation, perirhinal cortex, and postrhinal cortex in rat. A review. *Annals of the New York Academy of Sciences* 911:369-391.
- Pitkanen A, Savander V, LeDoux JE (1997) Organization of intra-amygdaloid circuitries in the rat: an emerging framework for understanding functions of the amygdala. *Trends in neurosciences* 20:517-523.
- Pitkanen A, Stefanacci L, Farb CR, Go GG, LeDoux JE, Amaral DG (1995) Intrinsic connections of the rat amygdaloid complex: projections originating in the lateral nucleus. *The Journal of comparative neurology* 356:288-310.

- Pitman RK, Rasmusson AM, Koenen KC, Shin LM, Orr SP, Gilbertson MW, Milad MR, Liberzon I (2012) Biological studies of post-traumatic stress disorder. *Nature reviews Neuroscience* 13:769-787.
- Plendl W, Wotjak CT (2010) Dissociation of within- and between-session extinction of conditioned fear. *The Journal of neuroscience : the official journal of the Society for Neuroscience* 30:4990-4998.
- Popa D, Duvarci S, Popescu AT, Lena C, Pare D (2010) Coherent amygdalocortical theta promotes fear memory consolidation during paradoxical sleep. *Proceedings of the National Academy of Sciences of the United States of America* 107:6516-6519.
- Pouille F, Marin-Burgin A, Adesnik H, Atallah BV, Scanziani M (2009) Input normalization by global feedforward inhibition expands cortical dynamic range. *Nature neuroscience* 12:1577-1585.
- Quirk GJ (2002) Memory for extinction of conditioned fear is long-lasting and persists following spontaneous recovery. *Learn Mem* 9:402-407.
- Quirk GJ, Armony JL, LeDoux JE (1997) Fear conditioning enhances different temporal components of tone-evoked spike trains in auditory cortex and lateral amygdala. *Neuron* 19:613-624.
- Quirk GJ, Likhtik E, Pelletier JG, Pare D (2003) Stimulation of medial prefrontal cortex decreases the responsiveness of central amygdala output neurons. *The Journal of neuroscience : the official journal of the Society for Neuroscience* 23:8800-8807.
- Quirk GJ, Mueller D (2008) Neural mechanisms of extinction learning and retrieval. *Neuropsychopharmacology : official publication of the American College of Neuropsychopharmacology* 33:56-72.
- Quirk GJ, Repa C, LeDoux JE (1995) Fear conditioning enhances short-latency auditory responses of lateral amygdala neurons: parallel recordings in the freely behaving rat. *Neuron* 15:1029-1039.
- Quirk GJ, Russo GK, Barron JL, Lebron K (2000) The role of ventromedial prefrontal cortex in the recovery of extinguished fear. *The Journal of neuroscience : the official journal of the Society for Neuroscience* 20:6225-6231.
- Rajasethupathy P, Sankaran S, Marshel JH, Kim CK, Ferenczi E, Lee SY, Berndt A, Ramakrishnan C, Jaffe A, Lo M, Liston C, Deisseroth K (2015) Projections from neocortex mediate top-down control of memory retrieval. *Nature* 526:653-659.
- Ray JP, Price JL (1992) The organization of the thalamocortical connections of the mediodorsal thalamic nucleus in the rat, related to the ventral forebrain-prefrontal cortex topography. *The Journal of comparative neurology* 323:167-197.
- Rea K, Roche M, Finn DP (2011) Modulation of conditioned fear, fear-conditioned analgesia, and brain regional c-Fos expression following administration of muscimol into the rat basolateral amygdala. *The journal of pain : official journal of the American Pain Society* 12:712-721.
- Redgrave P, Dean P, Mitchell IJ, Odekunle A, Clark A (1988) The projection from superior colliculus to cuneiform area in the rat. I. Anatomical studies. *Experimental brain research* 72:611-625.

- Rescorla RA, Heth CD (1975) Reinstatement of fear to an extinguished conditioned stimulus. *Journal of experimental psychology Animal behavior processes* 1:88-96.
- Resnik J, Paz R (2015) Fear generalization in the primate amygdala. *Nature neuroscience* 18:188-190.
- Resstel LB, Joca SR, Guimaraes FG, Correa FM (2006) Involvement of medial prefrontal cortex neurons in behavioral and cardiovascular responses to contextual fear conditioning. *Neuroscience* 143:377-385.
- Reynolds DV (1969) Surgery in the rat during electrical analgesia induced by focal brain stimulation. *Science* 164:444-445.
- Rizvi TA, Ennis M, Behbehani MM, Shipley MT (1991) Connections between the central nucleus of the amygdala and the midbrain periaqueductal gray: topography and reciprocity. *The Journal of comparative neurology* 303:121-131.
- Roberts GW, Woodhams PL, Polak JM, Crow TJ (1982) Distribution of neuropeptides in the limbic system of the rat: the amygdaloid complex. *Neuroscience* 7:99-131.
- Rodrigues SM, Schafe GE, LeDoux JE (2001) Intra-amygdala blockade of the NR2B subunit of the NMDA receptor disrupts the acquisition but not the expression of fear conditioning. *The Journal of neuroscience : the official journal of the Society for Neuroscience* 21:6889-6896.
- Rodrigues SM, Schafe GE, LeDoux JE (2004) Molecular mechanisms underlying emotional learning and memory in the lateral amygdala. *Neuron* 44:75-91.
- Rogan MT, LeDoux JE (1995) LTP is accompanied by commensurate enhancement of auditory-evoked responses in a fear conditioning circuit. *Neuron* 15:127-136.
- Rogan MT, Staubli UV, LeDoux JE (1997) Fear conditioning induces associative long-term potentiation in the amygdala. *Nature* 390:604-607.
- Rosen JB, Hitchcock JM, Miserendino MJ, Falls WA, Campeau S, Davis M (1992) Lesions of the perirhinal cortex but not of the frontal, medial prefrontal, visual, or insular cortex block fear-potentiated startle using a visual conditioned stimulus. *The Journal of neuroscience : the official journal of the Society for Neuroscience* 12:4624-4633.
- Rosenkranz JA, Grace AA (2002) Dopamine-mediated modulation of odour-evoked amygdala potentials during pavlovian conditioning. *Nature* 417:282-287.
- Roux L, Buzsaki G (2015) Tasks for inhibitory interneurons in intact brain circuits. *Neuropharmacology* 88:10-23.
- Rumpel S, LeDoux J, Zador A, Malinow R (2005) Postsynaptic receptor trafficking underlying a form of associative learning. *Science* 308:83-88.
- Sacchetti B, Baldi E, Lorenzini CA, Bucherelli C (2002) Differential contribution of some cortical sites to the formation of memory traces supporting fear conditioning. *Experimental brain research* 146:223-232.

- Sah P, Faber ES, Lopez De Armentia M, Power J (2003) The amygdaloid complex: anatomy and physiology. *Physiological reviews* 83:803-834.
- Sakata S, Yamamori T, Sakurai Y (2005) 7-12 Hz cortical oscillations: behavioral context and dynamics of prefrontal neuronal ensembles. *Neuroscience* 134:1099-1111.
- Salinas E, Sejnowski TJ (2001) Correlated neuronal activity and the flow of neural information. *Nature reviews Neuroscience* 2:539-550.
- Sandkuhler J, Herdegen T (1995) Distinct patterns of activated neurons throughout the rat midbrain periaqueductal gray induced by chemical stimulation within its subdivisions. *The Journal of comparative neurology* 357:546-553.
- Sandner G, Schmitt P, Karli P (1979) Central gray and medial hypothalamic stimulation: correlation between escape behavior and unit activity. *Brain research* 170:459-474.
- Santini E, Ge H, Ren K, Pena de Ortiz S, Quirk GJ (2004) Consolidation of fear extinction requires protein synthesis in the medial prefrontal cortex. *The Journal of neuroscience : the official journal of the Society for Neuroscience* 24:5704-5710.
- Santini E, Quirk GJ, Porter JT (2008) Fear conditioning and extinction differentially modify the intrinsic excitability of infralimbic neurons. *The Journal of neuroscience : the official journal of the Society for Neuroscience* 28:4028-4036.
- Sarhan M, Freund-Mercier MJ, Veinante P (2005) Branching patterns of parabrachial neurons projecting to the central extended amygdala: single axonal reconstructions. *The Journal of comparative neurology* 491:418-442.
- Savander V, Go CG, LeDoux JE, Pitkanen A (1995) Intrinsic connections of the rat amygdaloid complex: projections originating in the basal nucleus. *The Journal of comparative neurology* 361:345-368.
- Savander V, Go CG, Ledoux JE, Pitkanen A (1996) Intrinsic connections of the rat amygdaloid complex: projections originating in the accessory basal nucleus. *The Journal of comparative neurology* 374:291-313.
- Schmitt P, Carrive P, Di Scala G, Jenck F, Brandao M, Bagri A, Moreau JL, Sandner G (1986) A neuropharmacological study of the periventricular neural substrate involved in flight. *Behavioural brain research* 22:181-190.
- Senn V, Wolff SB, Herry C, Grenier F, Ehrlich I, Grundemann J, Fadok JP, Muller C, Letzkus JJ, Luthi A (2014) Long-range connectivity defines behavioral specificity of amygdala neurons. *Neuron* 81:428-437.
- Sesack SR, Deutch AY, Roth RH, Bunney BS (1989) Topographical organization of the efferent projections of the medial prefrontal cortex in the rat: an anterograde tract-tracing study with Phaseolus vulgaris leucoagglutinin. *The Journal of comparative neurology* 290:213-242.

- Shaban H, Humeau Y, Herry C, Cassasus G, Shigemoto R, Ciochi S, Barbieri S, van der Putten H, Kaupmann K, Bettler B, Luthi A (2006) Generalization of amygdala LTP and conditioned fear in the absence of presynaptic inhibition. *Nature neuroscience* 9:1028-1035.
- Shehadi K, Maroun M (2013) Different effects of low frequency stimulation to infralimbic prefrontal cortex on extinction of aversive memories. *Brain research* 1490:111-116.
- Shi C, Davis M (1999) Pain pathways involved in fear conditioning measured with fear-potentiated startle: lesion studies. *The Journal of neuroscience : the official journal of the Society for Neuroscience* 19:420-430.
- Shi C, Davis M (2001) Visual pathways involved in fear conditioning measured with fear-potentiated startle: behavioral and anatomic studies. *The Journal of neuroscience : the official journal of the Society for Neuroscience* 21:9844-9855.
- Shin LM, Liberzon I (2010) The neurocircuitry of fear, stress, and anxiety disorders. *Neuropsychopharmacology : official publication of the American College of Neuropsychopharmacology* 35:169-191.
- Shin RM, Tsvetkov E, Bolshakov VY (2006) Spatiotemporal asymmetry of associative synaptic plasticity in fear conditioning pathways. *Neuron* 52:883-896.
- Shinonaga Y, Takada M, Mizuno N (1994) Topographic organization of collateral projections from the basolateral amygdaloid nucleus to both the prefrontal cortex and nucleus accumbens in the rat. *Neuroscience* 58:389-397.
- Shumyatsky GP, Tsvetkov E, Malleret G, Vronskaya S, Hatton M, Hampton L, Battey JF, Dulac C, Kandel ER, Bolshakov VY (2002) Identification of a signaling network in lateral nucleus of amygdala important for inhibiting memory specifically related to learned fear. *Cell* 111:905-918.
- Siapas AG, Lubenov EV, Wilson MA (2005) Prefrontal phase locking to hippocampal theta oscillations. *Neuron* 46:141-151.
- Sierra-Mercado D, Jr., Corcoran KA, Lebron-Milad K, Quirk GJ (2006) Inactivation of the ventromedial prefrontal cortex reduces expression of conditioned fear and impairs subsequent recall of extinction. *The European journal of neuroscience* 24:1751-1758.
- Sierra-Mercado D, Padilla-Coreano N, Quirk GJ (2011) Dissociable roles of prelimbic and infralimbic cortices, ventral hippocampus, and basolateral amygdala in the expression and extinction of conditioned fear. *Neuropsychopharmacology : official publication of the American College of Neuropsychopharmacology* 36:529-538.
- Silva BA, Mattucci C, Krzywkowski P, Murana E, Illarionova A, Grinevich V, Canteras NS, Ragozzino D, Gross CT (2013) Independent hypothalamic circuits for social and predator fear. *Nature neuroscience* 16:1731-1733.
- Singer W (1999) Time as coding space? *Current opinion in neurobiology* 9:189-194.

- Sirota A, Montgomery S, Fujisawa S, Isomura Y, Zugaro M, Buzsaki G (2008) Entrainment of neocortical neurons and gamma oscillations by the hippocampal theta rhythm. *Neuron* 60:683-697.
- Smith MA, Banerjee S, Gold PW, Glowa J (1992) Induction of c-fos mRNA in rat brain by conditioned and unconditioned stressors. *Brain research* 578:135-141.
- Smith Y, Pare D (1994) Intra-amygdaloid projections of the lateral nucleus in the cat: PHA-L anterograde labeling combined with postembedding GABA and glutamate immunocytochemistry. *The Journal of comparative neurology* 342:232-248.
- Sotres-Bayon F, Bush DE, LeDoux JE (2007) Acquisition of fear extinction requires activation of NR2B-containing NMDA receptors in the lateral amygdala. *Neuropsychopharmacology : official publication of the American College of Neuropsychopharmacology* 32:1929-1940.
- Sotres-Bayon F, Diaz-Mataix L, Bush DE, LeDoux JE (2009) Dissociable roles for the ventromedial prefrontal cortex and amygdala in fear extinction: NR2B contribution. *Cereb Cortex* 19:474-482.
- Sotres-Bayon F, Quirk GJ (2010) Prefrontal control of fear: more than just extinction. *Current opinion in neurobiology* 20:231-235.
- Spampanato J, Sullivan RK, Perumal MB, Sah P (2016) Development and physiology of GABAergic feedback excitation in parvalbumin expressing interneurons of the mouse basolateral amygdala. *Physiological reports* 4.
- Spruston N (2008) Pyramidal neurons: dendritic structure and synaptic integration. *Nature reviews Neuroscience* 9:206-221.
- Stevenson CW (2011) Role of amygdala-prefrontal cortex circuitry in regulating the expression of contextual fear memory. *Neurobiology of learning and memory* 96:315-323.
- Stutzmann GE, LeDoux JE (1999) GABAergic antagonists block the inhibitory effects of serotonin in the lateral amygdala: a mechanism for modulation of sensory inputs related to fear conditioning. *The Journal of neuroscience : the official journal of the Society for Neuroscience* 19:RC8.
- Swanson LW, Petrovich GD (1998) What is the amygdala? *Trends in neurosciences* 21:323-331.
- Swett JE, Woolf CJ (1985) The somatotopic organization of primary afferent terminals in the superficial laminae of the dorsal horn of the rat spinal cord. *The Journal of comparative neurology* 231:66-77.
- Szinyei C, Heinbockel T, Montagne J, Pape HC (2000) Putative cortical and thalamic inputs elicit convergent excitation in a population of GABAergic interneurons of the lateral amygdala. *The Journal of neuroscience : the official journal of the Society for Neuroscience* 20:8909-8915.
- Tang J, Ko S, Ding HK, Qiu CS, Calejesan AA, Zhuo M (2005) Pavlovian fear memory induced by activation in the anterior cingulate cortex. *Molecular pain* 1:6.
- Thierry AM, Blanc G, Sobel A, Stinus L, Glowinski J (1973) Dopaminergic terminals in the rat cortex. *Science* 182:499-501.

- Thompson BM, Baratta MV, Biedenkapp JC, Rudy JW, Watkins LR, Maier SF (2010) Activation of the infralimbic cortex in a fear context enhances extinction learning. *Learn Mem* 17:591-599.
- Tian S, Huang F, Gao J, Li P, Ouyang X, Zhou S, Deng H, Yan Y (2011) Ventrolateral prefrontal cortex is required for fear extinction in a modified delay conditioning paradigm in rats. *Neuroscience* 189:258-268.
- Tovote P, Esposito MS, Botta P, Chaudun F, Fadok JP, Markovic M, Wolff SB, Ramakrishnan C, Fenno L, Deisseroth K, Herry C, Arber S, Luthi A (2016) Midbrain circuits for defensive behaviour. *Nature* 534:206-212.
- Tovote P, Fadok JP, Luthi A (2015) Neuronal circuits for fear and anxiety. *Nature reviews Neuroscience* 16:317-331.
- Tsvetkov E, Carlezon WA, Benes FM, Kandel ER, Bolshakov VY (2002) Fear conditioning occludes LTP-induced presynaptic enhancement of synaptic transmission in the cortical pathway to the lateral amygdala. *Neuron* 34:289-300.
- Tully K, Li Y, Tsvetkov E, Bolshakov VY (2007) Norepinephrine enables the induction of associative long-term potentiation at thalamo-amygdala synapses. *Proceedings of the National Academy of Sciences of the United States of America* 104:14146-14150.
- Turner BH, Herkenham M (1991) Thalamoamygdaloid projections in the rat: a test of the amygdala's role in sensory processing. *The Journal of comparative neurology* 313:295-325.
- Uylings HB, van Eden CG (1990) Qualitative and quantitative comparison of the prefrontal cortex in rat and in primates, including humans. *Progress in brain research* 85:31-62.
- Van De Werd HJ, Rajkowska G, Evers P, Uylings HB (2010) Cytoarchitectonic and chemoarchitectonic characterization of the prefrontal cortical areas in the mouse. *Brain structure & function* 214:339-353.
- Van Eden CG, Uylings HB (1985) Cytoarchitectonic development of the prefrontal cortex in the rat. *The Journal of comparative neurology* 241:253-267.
- Varela C, Kumar S, Yang JY, Wilson MA (2014) Anatomical substrates for direct interactions between hippocampus, medial prefrontal cortex, and the thalamic nucleus reuniens. *Brain structure & function* 219:911-929.
- Varela F, Lachaux JP, Rodriguez E, Martinerie J (2001) The brainweb: phase synchronization and large-scale integration. *Nature reviews Neuroscience* 2:229-239.
- Veening JG, Swanson LW, Sawchenko PE (1984) The organization of projections from the central nucleus of the amygdala to brainstem sites involved in central autonomic regulation: a combined retrograde transport-immunohistochemical study. *Brain research* 303:337-357.
- Veinante P, Stoeckel ME, Freund-Mercier MJ (1997) GABA- and peptide-immunoreactivities co-localize in the rat central extended amygdala. *Neuroreport* 8:2985-2989.

- Verberne AJ, Guyenet PG (1992) Midbrain central gray: influence on medullary sympathoexcitatory neurons and the baroreflex in rats. *The American journal of physiology* 263:R24-33.
- Vertes RP (2004) Differential projections of the infralimbic and prelimbic cortex in the rat. *Synapse* 51:32-58.
- Vertes RP (2006) Interactions among the medial prefrontal cortex, hippocampus and midline thalamus in emotional and cognitive processing in the rat. *Neuroscience* 142:1-20.
- Vertes RP, Hoover WB, Szigeti-Buck K, Leranath C (2007) Nucleus reuniens of the midline thalamus: link between the medial prefrontal cortex and the hippocampus. *Brain research bulletin* 71:601-609.
- Vianna DM, Brandao ML (2003) Anatomical connections of the periaqueductal gray: specific neural substrates for different kinds of fear. *Brazilian journal of medical and biological research = Revista brasileira de pesquisas medicas e biologicas / Sociedade Brasileira de Biofisica* [et al] 36:557-566.
- Vianna DM, Landeira-Fernandez J, Brandao ML (2001) Dorsolateral and ventral regions of the periaqueductal gray matter are involved in distinct types of fear. *Neuroscience and biobehavioral reviews* 25:711-719.
- Vidal-Gonzalez I, Vidal-Gonzalez B, Rauch SL, Quirk GJ (2006) Microstimulation reveals opposing influences of prelimbic and infralimbic cortex on the expression of conditioned fear. *Learn Mem* 13:728-733.
- Vouimba RM, Garcia R, Baudry M, Thompson RF (2000) Potentiation of conditioned freezing following dorsomedial prefrontal cortex lesions does not interfere with fear reduction in mice. *Behavioral neuroscience* 114:720-724.
- Vouimba RM, Maroun M (2011) Learning-induced changes in mPFC-BLA connections after fear conditioning, extinction, and reinstatement of fear. *Neuropsychopharmacology : official publication of the American College of Neuropsychopharmacology* 36:2276-2285.
- Watabe AM, Ochiai T, Nagase M, Takahashi Y, Sato M, Kato F (2013) Synaptic potentiation in the nociceptive amygdala following fear learning in mice. *Molecular brain* 6:11.
- Weinberger NM (2004) Specific long-term memory traces in primary auditory cortex. *Nature reviews Neuroscience* 5:279-290.
- Weisskopf MG, Bauer EP, LeDoux JE (1999) L-type voltage-gated calcium channels mediate NMDA-independent associative long-term potentiation at thalamic input synapses to the amygdala. *The Journal of neuroscience : the official journal of the Society for Neuroscience* 19:10512-10519.
- Wilensky AE, Schafe GE, Kristensen MP, LeDoux JE (2006) Rethinking the fear circuit: the central nucleus of the amygdala is required for the acquisition, consolidation, and expression of Pavlovian fear conditioning. *The Journal of neuroscience : the official journal of the Society for Neuroscience* 26:12387-12396.

Wilson-Poe AR, Morgan MM, Aicher SA, Hegarty DM (2012) Distribution of CB1 cannabinoid receptors and their relationship with mu-opioid receptors in the rat periaqueductal gray. *Neuroscience* 213:191-200.

Wilson NR, Runyan CA, Wang FL, Sur M (2012) Division and subtraction by distinct cortical inhibitory networks in vivo. *Nature* 488:343-348.

Womelsdorf T, Fries P (2007) The role of neuronal synchronization in selective attention. *Current opinion in neurobiology* 17:154-160.

Yoder RM, Pang KC (2005) Involvement of GABAergic and cholinergic medial septal neurons in hippocampal theta rhythm. *Hippocampus* 15:381-392.

Zhang SP, Bandler R, Carrive P (1990) Flight and immobility evoked by excitatory amino acid microinjection within distinct parts of the subtentorial midbrain periaqueductal gray of the cat. *Brain research* 520:73-82.

Zhang SP, Davis PJ, Carrive P, Bandler R (1992) Vocalization and marked pressor effect evoked from the region of the nucleus retroambigualis in the caudal ventrolateral medulla of the cat. *Neuroscience letters* 140:103-107.